UNIVERSIDADE DE LISBOA
FACULDADE DE MEDICINA

DEVELOPMENT OF TRACELESS STRATEGIES FOR THE SELECTIVE RELEASE OF BET INHIBITORS IN CANCER CELLS

Rui Miguel Petrucci Albuquerque Traquete

Orientadores: Dr. Gonçalo José Lopes Bernardes
Dr. Sérgio de Almeida
Dr. Rudi Oliveira

Tese especialmente elaborada para obtenção do grau de Doutor em Ciências Biomédicas, especialidade de Bioquímica Médica

2020

UNIVERSIDADE DE LISBOA

FACULDADE DE MEDICINA

DEVELOPMENT OF TRACELESS STRATEGIES FOR THE SELECTIVE RELEASE OF BET INHIBITORS IN CANCER CELLS

Rui Miguel Petrucci Albuquerque Traquete

Orientadores: Dr. Gonçalo José Lopes Bernardes

Dr. Sérgio de Almeida

Dr. Rudi Oliveira

Tese especialmente elaborada para obtenção do grau de Doutor em Ciências Biomédicas, especialidade de Bioquímica Médica

Presidente:

- Doutor João Eurico Cortez Cabral da Fonseca, Professor Catedrático e Vice-Presidente do Conselho Científico da Faculdade de Medicina da Universidade de Lisboa

Vogais:

- Doutor Georg Winter, Investigador Principal do Research Center for Molecular Medicine of the Austrian Academy of Sciences;
- Doutora Paula Alexandra de Carvalho Gomes, Professora Associada com Agregação da Faculdade de Ciências da Universidade do Porto;
- Doutor Miguel Augusto Rico Botas Castanho, Professor Catedrático da Faculdade de Medicina da Universidade de Lisboa;
- Doutor João António Augusto Ferreira, Professor Associado da Faculdade de Medicina da Universidade de Lisboa;
- Doutor Luís António Marques da Costa, Professor Associado Convidado da Faculdade de Medicina da Universidade de Lisboa;
- Doutor Gonçalo José Lopes Bernardes, Professor Auxiliar Convidado da Faculdade de Medicina da Universidade de Lisboa (Orientador)

Projecto financiado por Hovione Farmaciência SA

2020

As opiniões expressas nesta publicação são da exclusiva responsabilidade do seu autor

A impressão desta tese foi aprovada pelo Conselho Científico da Faculdade de Medicina de Lisboa em reunião de 15 de Janeiro de 2019

O presente trabalho foi desenvolvido sob orientação do Doutor Gonçalo Bernardes do Instituto de Medicina Molecular João Lobo Antunes da Faculdade de Medicina da Universidade de Lisboa e do Departamento de Química da Universidade de Cambridge, Reino Unido e co-orientação da Doutora Angela Koehler, do David H. Koch Institute for Integrative Cancer Research, Center For Precision Cancer Medicine, Department of Biological Engineering, Massachussetts Institute of Technology, Cambridge, USA. Este trabalho foi financiado Hovione Farmaciência SA tendo como orientadores interinos o Dr. William Heggie e o Dr. Rudi Oliveira.

This work was developed under scientific supervision of Dr. Gonçalo Bernardes Instituto de Medicina Molecular João Lobo Antunes, Faculty of Medicine, University of Lisbon and Department of Chemistry, University of Cambridge, Cambridge, UK, and co-supervision of Dr Angela Koehler, from David H. Koch Institute for Integrative Cancer Research, Center For Precision Cancer Medicine, Department of Biological Engineering, Massachussetts Institute of Technology, Cambridge, USA. The work was financially supported by Hovione Farmaciência SA having Dr. William Heggie and Dr. Rudi Oliveira as internal supervisors.

Table of Contents

Page

Figure Index

Page

Table Index

Page

Scheme Index

Page

Acknowledgments

This work would not have been possible without the contribution and support of numerous individuals. To all I am sincerely thankful.

Foremost, I would like to thank to all the supervisors for the support throughout the thesis. I am particularly grateful to Dr. Gonçalo Bernardes for the endless confidence in the project and for the extensive personal and professional guidance. Your passion towards science is truly inspirational and I will carry that with me in my next endeavours. To Dr. Angela Koehler I will be forever grateful for accepting me in the lab and giving me all the conditions needed to succeed at such a critical stage of the project. To my former supervisor at Hovione Farmaciência Dr. William Heggie, I am very grateful for the extensive dedication and all the comprehensive meetings in the very early years of this work. I also acknowledge Dr. Rudi Oliveira contribution and insights given throughout the project, particularly for the important help with organic chemistry while at the Faculdade de Farmácia da Universidade de Lisboa.

I am thankful to Hovione Farmaciência for the financial support. My sincere thanks to Peter Villax for the opportunity, support and confidence in this project. To Sofia Villax for all the help establishing the scholarship. To Claudia Vaz for the professionalism and unstoppable dedication, making the academia-industry bridge smaller than ever.

I would like to acknowledge Dr Pedro Gois valuable contribution since day one by opening his lab doors every time I needed any organic chemistry expertise or any resources. To the Gois lab members I am also deeply thankful, especially to Fábio Santos for the friendship and all the help given throughout these years. I am also thankful to Professor Carlos Afonso for making available of his lab equipment for some experiments.

I would like to thank several people for their valuable technical support on this project, namely Noelia Duarte (from Faculdade de Farmácia of University of Lisbon) for making the NMR facility available and easy to access at all times; to António Temudo and Ana Nascimento (from Instituto de Medicina Molecular) for their training and help with the bioimaging experiments; to Richard Cook (from the Koch Institute for Integrative Cancer Research at MIT) for the support with the linker release assay; to Glenn Paradis (from the Koch Institute for Integrative Cancer Research at MIT) for the help running the flow cytometry equipment and data analysis; to Stuart Levine and Vincent Butty (from the Koch Institute for Integrative Cancer Research at MIT) for helping design the transcriptome analysis and the bioinformatics analysis and to Jaime Cheah (from the Koch Institute for Integrative Cancer Research at MIT) for helping with the cytotoxicity screening.

I am also deeply thankful to everyone than contributed directly to this work by running some of the experiments herein presented, namely Sarah Picaud and Panagis Filippakopoulos (from the Structural Genomics Consortium at the University of Oxford) for running the DSF, ITC and crystallography experiments; to Tiago Rodrigues and Marta Marques (from Instituto de Medicina Molecular) for their contribution with the docking studies and biophysical data analysis; to Andrew Chen (from the Koch Institute for Integrative Cancer Research at MIT) for his contribute preparing the samples for the transcriptome analysis; to Rob Wilson (from the Koch Institute for Integrative Cancer Research at MIT) for processing and analysing the transcriptome analysis data; to João Seixas and Pedro Cal (from Instituto de Medicina Molecular) for their help establishing the synthetic route towards the final drug conjugates; to Xhenti Ferhati (from *Centro de Investigacion en Sintesis Quimica of Universidad de La Rioja*) for the large scale synthesis of the DUPA-VC-linker-RT53; to Dr Francisco Corzana (from *Centro de Investigacion en Sintesis Quimica of Universidad de La Rioja*) for providing the molecular dynamics simulations and to João Conde (from Instituto de Medicina Molecular) for running the *in vivo* experiments.

To the past and present members at the GBernardes lab, this long journey is also yours. I am profoundly grateful for having shared with you all the laughs, frustrations and successes. To Ana Guerreiro, Annabel Kitowski, Inês Albuquerque, Charlotte Baker, João Conde, Marta Marques, Padma Akkapeddi, Tiago Rodrigues, Pedro Cal, João Seixas and Florian Sieglitz I will be forever thankful for your friendship and support. Hope we can share a Beernardes again anytime soon.

I would also like to thank all the people from the Koehler lab at the Koch Institute for Integrative Cancer Research at MIT, namely Andrew Chen, Becky Leifer, Shelby Doyle, Nicholas Struntz, Dave Freeman and Helen Hevans for being so welcoming and supportive. Special thanks to Andre Richters and Rob Wilson for all the good moments at Muddy.

A very special thanks to Pedro Cal that took the effort to extensively review this thesis. I would also like to thank the thesis Committee members Dr João Barata, Dr. Pedro Gois and Dr. João Seixas for taking their time to listen and give precious feedback of this work.

To all my friends, there are no words that could thank you enough. Having you on my side makes everything so much easier and fun. To my brothers in heart Vasco Ferreira, João Mendes, Francisco Santos Lima, João Garcia and João Ferreira, to Andreia Pais, Ana Silva, Eduardo Alves and Laura Dias, we will keep on rocking this life together.

To Rui Alves and Alice Alves, thank you for all the lovely family weekends and the good times we always spend together. These are always a perfect boost of energy to face a long week of work.

To my best friend and the love of my life, Filipa. You walked this path with me from day one and dealt with all the ups and downs like a rock. You know me like no one else and you always find a way to turn my bad temper into a smile. I am extremely thankful for having you on my side at all moments.

Finally, to my family. To my parents, João and Margarida and my sister Inês for all their love and endless support. You always gave me the best advices and the confidence I needed to accomplish all my goals and challenges. Most importantly, you always gave me the freedom to pursue my dreams. For that, and for everything you did and still do for me, this thesis is dedicated to you.

Abbreviations

Ac	Acetyl
ACN	Acetonitrile
AcOH	Acetic acid
ADC	Antibody-drug conjugate
ALCL	Anaplastic large cell lymphoma
Alpha Screen	Amplified luminescence proximity homogeneous assay
AML	Acute myeloid leukemia
ApoA1	Apolipoprotein A1
AR	Androgen receptor
Arg	Arginine (R)
Asn	Asparagine (N)
Asp	Aspartic Acid (D)
AURKB	Aurora B kinase
Avg	Average
BET	Bromodomain and extra-terminal domain
BL	Burkitt's lymphoma
BOC	butyloxycarbonyl protecting group
BRD	Bromodomain
BRD2(1)	First domain of bromodomain-containing protein 2
BRD2(2)	Second domain of bromodomain-containing protein 2
BRD3(1)	First domain of bromodomain-containing protein 3
BRD3(2)	Second domain of bromodomain-containing protein 3
BRD4(1)	First domain of bromodomain-containing protein 4
BRD4(2)	Second domain of bromodomain-containing protein 4
CAIX	Carbonic anhydrase IX
CETSA	Cellular thermal shift Assay
CPM	Counts per million mapped reads
CRPC	Castration-resistant prostate cancer
CTM	C-terminal motif
CuAAC	Copper-catalysed azide-alkyne cycloaddition
DAVLBH	Desacetylvinblastine hydrazide
DCE	Dichloroethane
DCM	Dichloromethane

DIC	N,N'-Diisopropylcarbodiimide
DIPEA	Diisopropylethylamine
DLBCL	Diffuse large B-cell lymphoma
DLT	Dose-limiting toxicity
DMF	Dimethylformamide
DMSO	Dimethylsulfoxide
DNMT	DNA methyltransferase
Dscores	Druggability scores
DSF	Differential scanning fluorimetry
DUPA	2-[3-(1,3-dicarboxypropyl)-ureido]pentanedioic acid
EP300	ETA binding protein
ER^+	Estrogen-receptor positive
ESI	Electrospray ionization
ET	Extra-terminal
EtOAc	Ethyl acetate
EtOH	Ethanol
FA	Folic acid
FAP	Fluorescence Anisotropy
FDA	Food and Drug Administration
FDR	False-discovery rate
FITC	Fluorescein-5-isothiocyanate
FP	Fluorescence polarization
FR	Folate receptor
FRET	Fluorescence resonance energy transfer
GI	Gastrointestinal
GSEA	Gene set enrichment analysis
HAT	Acetyltransferases
HCC	Hepatocellular carcinoma
HCl	Hydrochloric acid
HDAC	Histone deacetylase
HER2	Human epidermal growth factor receptor 2
HL	Hodgkin's lymphoma
HMT	Histone methyltransferase
HOBt	Hydroxybenzotriazole
HPLC	High-pressure liquid chromatography

HPV	Human papillomavirus
HRMS	High-resolution mass spectrometry
IC_{50}	Half-maximal inhibitory concentration
Ig	Immunoglobulin
IL	Interleukin
IL7R	Interleukin receptor 7
IPA	Isopropyl alcohol
IPTG	Isopropyl-β-D-thiogalactopyranoside
ITC	Isothermal titration calorimetry
ITDRF	Isothermal dose-response fingerprint
KAc	Acetyl-lysine
KSHV	Kaposi's sarcoma-associated herpes
LANA1	Latency-associated nuclear antigen 1
LB	Luria-Bertani medium
LC-MS	Liquid chromatography – mass spectrometry
LRMS	Low-resolution mass spectrometry
Leu	Leucine (L)
LSD1	Lysine-specific demethylase 1
Lys	Lysine (K)
MALDI	Matrix-assisted laser desorption/Ionization
MBTE	Methyl *tert*-butyl ether
MD	Molecular dynamics
MDS	Myelodysplastic syndrome
Me	Methylation
MeOH	Methanol
MLL	Mixed lineage leukemia
MS	Mass spectrometry
MTD	Maximum tolerated dose
NBD	Nitrobenzofurazan
ND	Not detected
NES	Normalized enrichment score
NHS	*N*-hydroxysuccinimide
NMC	NUT midline carcinoma
NMR	Nuclear magnetic resonance
NSCLC	Non-small cell lung cancer

NUT	Nuclear protein in testis
P-TEFb	Positive transcription elongation factor b
PABC	*p*-aminobenzylcarbamate
PABQ	*p*-aminobenzyl quaternary ammonium salt
PAMPA	Parallel membrane permeability assay
PARP	Poly-ADP-ribose polymerase
PBS	Phosphate-buffered saline
PCa	Prostate cancer
PDAC	Pancreatic ductal adenocarcinoma
Pe	Effective permeability
PEG	Polyethylene glycol
PEI	Polyethyleneimine
PFA	Paraformaldehyde
PHD	Plant homeodomain
PI	Propidium iodide
PSMA	Prostate-specific membrane antigen
pVHL	Von Hippel-Lindau tumor suppressor protein
SD	Standard deviation
shRNA	Short hairpin RNA
SMDC	Small-molecule drug conjugate
TB	Terrific Broth medium
TBAI	Tetrabutylammonium iodide
TCEP	Tris (2-carboxyethyl) phosphine
TCGA	Cancer genome atlas
TFA	Trifluoroacetic acid
THF	Tetrahydrofuran
TLC	Thin layer chromatography
T_m	Melting temperature
TNBC	Triple-negative breast cancer
TOF	Time-of-flight
Tyr	Tyrosine (Y)
Val	Valine (V)
VC	Valine-citruline
WP	Tryptophan-proline
WPF	Tryptophan-proline-phenylalanine

Abstract

Epigenome-targeting drugs are an emerging class of therapeutic agents against a variety of human cancers. This results from the increasingly clear understanding of histone post-translational modifications and their role in tumorigenesis and tumor progression. Proteins of the bromodomain and extraterminal (BET) family, in particular, are epigenetic regulators of great interest as biological targets. These family of proteins is comprised of BRD2, BRD3, BRD4 and BRDT, which bind to chromatin through recognition of acetylated lysine residues (KAc) on histone tails, leading to the recruitment and co-activation of master regulatory transcription factors including the oncogene MYC. Preclinical modulation of BET protein function in malignant models through small molecule inhibition has therefore resulted in marked phenotypic changes and promising therapeutic benefits, driving multiple effectors into clinical evaluation. However, early clinical trials have had modest results with only a few, short-lived, responses in both hematologic and solid tumors. Relevant toxicities were observed in many patients, including severe thrombocytopenia, fatigue, gastrointestinal (GI)-side effects, nausea, vomiting, and which significantly limited compliance to treatment.

The targeted delivery of BET inhibitors to cancer cells can, on the other hand, markedly improve their therapeutic index and overall efficacy. Through the conjugation of the therapeutic agent to a tumor-cell-specific ligand via a cleavable linker, it is possible to enhance the accumulation of drug at the tumor site while sparing healthy cells and the associated collateral toxicity. This project describes the engineering of a conditionally stable construct for the efficient, targeted and traceless release of a BET-bromodomain protein effector in cancer cells.

Based on published evidence and organic chemistry methodologies, a BET inhibitor was designed to retain high binding efficacy to target proteins and potent antitumor activity, while enabling targeted delivery approaches. The derivatised compound, featuring a tertiary amine suitable to accommodate a self-immolative release mechanism, engaged BET protein targets with great affinity as determined by different biophysical assays. Crystallography studies and molecular modeling of compounds in complex with target proteins provided further mechanistic insights into their mode of binding, revealing unprecedented bond formation and establishing a rationale for the exquisite binding observed.

At the cellular level the tertiary-amine containing BET inhibitor exhibited potent antitumor activity against several human cancer cell lines from different tissues. Particularly in the context of prostate cancer, cellular target engagement strategies have shown successful binding of compounds to BET bromodomain proteins, while flow cytometry analysis displayed potent perturbations of cell cycle progression. Concomitantly, a substantial suppression of Myc protein levels was observed following

compound treatment in a dose- and time-dependent manner, further corroborated by transcriptome analysis data showing a significant down-regulation of MYC and MYC-related gene signatures. Additional transcriptional perturbations were found in several growth-promoting gene signatures and known downstream effectors of BET bromodomain protein activity, further supporting the antitumoral efficacy and therapeutic potential of the tertiary-amine containing BET inhibitor.

Finally, the derivatised BET bromodomain effector was assembled in a unique ligand-targeted conjugate for its selective delivery in prostate cancer cells. The tertiary-amine functionality of the drug was used to tether a self-immolating motif, which allows for intracellular release upon an enzymatic trigger, further conjugated to a ligand that specifically targets prostate cancer cells. The data observed confirmed the labile nature of the release mechanism and selective liberation of the tertiary-amine derivative in the presence of a triggering event. Furthermore, in a mice model of prostate cancer it is shown that the unique ligand-linker-BET inhibitor conjugate has a remarkably superior therapeutic activity than that of the BET inhibitor alone, thus suggesting a therapeutic advantage over the non-targeted counterparts.

Keywords: Epigenetic cancer therapy, BET bromodomain inhibitors, prostate cancer, drug delivery, drug conjugates

Resumo

Fármacos direcionados para marcadores epigenéticos são uma classe emergente de agentes terapêuticos para o tratamento de cancro. Isto resulta do facto de haver um crescente avanço científico acerca dos mecanismos pós-traducionais em histonas e o respetivo impacto na carcinogénese e progressão tumoral. As proteínas da família bromodomain e extraterminal (BET) constituem reguladores epigenéticos de particular interesse como alvo biológico para o desenvolvimento de novas terapias anticancerígenas. Estas proteínas (BRD2-4 e BRDT) ligam-se à cromatina através do reconhecimento de lisinas acetiladas (KAc) presentes na cauda das histonas. Este reconhecimento por sua vez desencadeia o recrutamento e co-activação de fatores de transcrição fundamentais para o desenvolvimento de neoplasias malignas, como por exemplo o oncogene MYC. A manipulação pré-clínica da actividade das proteínas BET em diversos modelos cancerígenos, através da inibição com compostos de baixo peso molecular, tem revelado alterações fenotípicas significativas e benefícios terapêuticos promissores. Por este motivo existe um grande número de inibidores de proteínas BET que têm sido analisados em ensaios clínicos para o tratamento de diversos tumores, incluindo tumores sólidos e hematológicos. Contudo, resultados preliminares dos primeiros ensaios clínicos têm revelado um efeito modesto destes compostos, com poucos pacientes a responder ao tratamento e respostas de curta-duração a serem observadas. Simultaneamente, efeitos secundários adversos significativos foram observados em diversos pacientes, e que incluíram por exemplo trombocitopenia persistente (baixa contagem de plaquetas no sangue), fadiga, problemas do trato gastrointestinal, náusea e vómitos, que limitam fortemente a adesão de pacientes ao tratamento.

Por outro lado, a entrega seletiva de inibidores das proteínas BET em tecidos cancerígenos pode melhorar significativamente a eficácia destes compostos e o seu índice terapêutico. Através da conjugação destes agentes terapêuticos com um ligando específico para células tumorais, unidos por uma ligação clivável que permite a libertação do fármaco após um determinado estímulo celular, é possível aumentar a acumulação seletiva dos fármacos em tecidos malignos limitando assim a sua actividade em células saudáveis e diminuindo os efeitos tóxicos colaterais daí resultantes. Este projeto descreve o desenvolvimento de um sistema conjugado que permite a entrega seletiva e direcionada de inibidores de proteínas BET em tecidos malignos.

Com base em literatura publicada e tirando partido de metodologias de química orgânica, foi desenvolvido um novo inibidor de proteínas BET com alta afinidade para as proteínas alvo e subsequente eficácia anti tumoral, ao mesmo tempo que possibilita a instalação de estratégias de entrega seletiva de fármacos. O novo análogo, funcionalizado com uma amina terciária terminal que

permite acomodar um mecanismo de libertação controlada, mostrou grande afinidade para as proteínas BET em diversos ensaios biofísicos. Ademais, a aplicação de técnicas como cristalografia de raios-X e simulações computacionais de dinâmica molecular permitiram compreender com grande detalhe os mecanismos de distribuição dos compostos em complexo com as proteínas alvo. Estes resultados revelaram a formação de ligações químicas sem precedentes entre interações semelhantes, e que sugerem indicar uma explicação para a elevada eficácia de ligação às proteínas BET observada no composto modificado.

A nível celular o inibidor modificado com uma amina terciária terminal mostrou elevada actividade anti tumoral em diversas linhas celulares humanas provenientes de tecidos com origens distintas, incluindo cancro da mama, próstata, cérebro e tumores hematológicos. Em particular no contexto de cancro da próstata, e de acordo com os ensaios biofísicos, diferentes estratégias celulares permitiram confirmar a ligação eficaz do inibidor às proteínas alvo também em sistemas vivos. Por sua vez, a análise por citometria de fluxo demonstrou uma forte perturbação na normal progressão ciclo celular após tratamento com o inibidor, nomeadamente ao nível da transição da fase G1 para a fase S do ciclo celular. Um estudo mais profundo do mecanismo de actividade antitumoral do novo composto indicou uma supressão substancial dos níveis de proteína oncogénica Myc após tratamento, numa resposta dependente da dose administrada e do tempo de incubação. Estes resultados foram corroborados através de uma análise transcriptómica a todo o genoma celular após incubação com o novo inibidor, onde se verificou uma supressão significativa do oncogene Myc e de diversas assinaturas genéticas relacionadas com o mesmo. Foram ainda observadas perturbações significativas da transcrição de diversas assinaturas genéticas envolvidas no crescimento celular e também de conhecidos efetores modulados pela actividade de proteínas BET. Estes resultados *in vitro* em modelos de cancro da próstata demonstram claramente a eficácia anti tumoral do inibidor após funcionalização química e dão enfâse ao seu potencial terapêutico.

Por fim, procedeu-se à construção de um conjugado fármaco-ligando único para a entrega seletiva do inibidor de proteínas BET em modelos de cancro da próstata. A funcionalização do inibidor com a amina terciária terminal permitiu a conjugação química através deste grupo com um sistema de libertação controlada, que permite a libertação intracelular do fármaco após um evento enzimático que ocorre com maior extensão no ambiente tumoral. Este foi de seguida conjugado a um ligando específico para recetores PSMA que se encontram sobre expressos à superfície de células de cancro da próstata, mas apenas marginalmente encontrados em tecidos saudáveis. Esta seletividade permite assim evitar efeitos tóxicos colaterais por ação indiscriminada do composto em células sãs e células malignas. A síntese dos conjugados finais foi estabelecida através de metodologias de química

orgânica e estes foram posteriormente caracterizados na sua estabilidade, seletividade e eficácia. Os resultados obtidos comprovaram a natureza clivável dos conjugados, uma vez que na presença de um estímulo enzimático o fármaco foi eficientemente libertado, enquanto que na ausência do mesmo o conjugado fármaco-ligando permaneceu intacto. Por fim, o sucesso da estratégia aqui apresentada foi comprovado através da seletividade e eficácia demonstrada pelo conjugado, primeiro em células e à posteriori em modelos animais de cancro da próstata. Nestes ensaios o conjugado fármaco-ligando demonstrou uma actividade terapêutica muito superior quando comparada com os agentes terapêuticos não direcionados, sugerindo assim que o sistema de entrega aqui desenvolvido promoveu uma maior acumulação do fármaco no ambiente tumoral.

Palavras-Chave: Terapêutica cancerígena epigenética, inibidores de proteínas BET, cancro da próstata, entrega seletiva de fármacos, fármacos conjugados

Chapter I

State of the Art

Rui Traquete[1], Gonçalo J. L. Bernardes[1,2]

[1] Instituto de Medicina Molecular João Lobo Antunes, Faculdade de Medicina, Universidade de Lisboa, Avenida Professor Egas Moniz, 1649-028 Lisboa, Portugal

[2] Department of Chemistry, University of Cambridge, Lensfield Road, CD2 1EW Cambridge, UK

Author Contributions

R.T. wrote the chapter, G.J.L.B. directed the research and revised the text.

Chapter I.
State of the Art

I.1. Targeting the epigenome

The interaction between genome and epigenome is fundamental for the development and function of any multicellular organism. While chromatin describes the complex of DNA and histone proteins that provide the scaffold for the packaging of the entire genome, the epigenome is characterized by covalent modifications of histone proteins and DNA that can fundamentally alter the organization of chromatin.[1] This interplay between covalent modifications of chromatin components and chromatin structure has a crucial role in the regulation of all DNA-based processes, such as transcription, DNA repair and replication.[1,2] The post-translational modifications are dynamic processes established by chromatin-modifying enzymes in a highly regulated manner. These include enzymes that apply (*writers*) or remove (*erasers*) the covalent modifications to specific aminoacids in histone proteins (H2A, H2B, H3 and H4) and enzymes that recognize and interpret those chemical modifications and subsequently translate them in the context of chromatin reorganization and transcriptional control (*readers*) (Figure 1).[3] Examples of writer proteins include histone acetyltransferases (HATs) specifically for histone acetyl (Ac) modification, histone methyltransferases (HMTs) in methylation (Me) of histone lysines or kinases in the phosphorylation of serine, threonine and tyrosine, among others (Figure 1). Reader proteins include modules such as bromodomains or chromodomains for histone acetyl modifications, plant homeodomains, tumor domains, PWWP domains and malignant brain tumor domains for the methylation of histone lysines or 14-3-3 proteins and BRCT domains for covalent phosphorylation. In turn, histone deacetylases (HDACs), demethylases and phosphatases are examples of eraser proteins for histone acetylation, methylation and phosphorylation, respectively (Figure 1).[3]

The majority of the histone modifications are found on the histone amino *N*-terminal tails that protrude from their own nucleosome and contact adjacent nucleosomes. Thus, covalent modifications at these tails will affect inter-nucleosomal interactions and influence the overall chromatin structure.[4] Together with the acetylation, methylation and phosphorylation marks mentioned above, post-translational modifications can also include ribosylation, biotinilation, citrullination and SUMOylation[5], and it is their combination that ultimately modulates the expression of genes controlling cell cycle progression, DNA repair and mitosis. Consequently, abnormal expression patterns or genomic alterations in chromatin regulators can have profound results including the induction and maintenance of various cancers.[6]

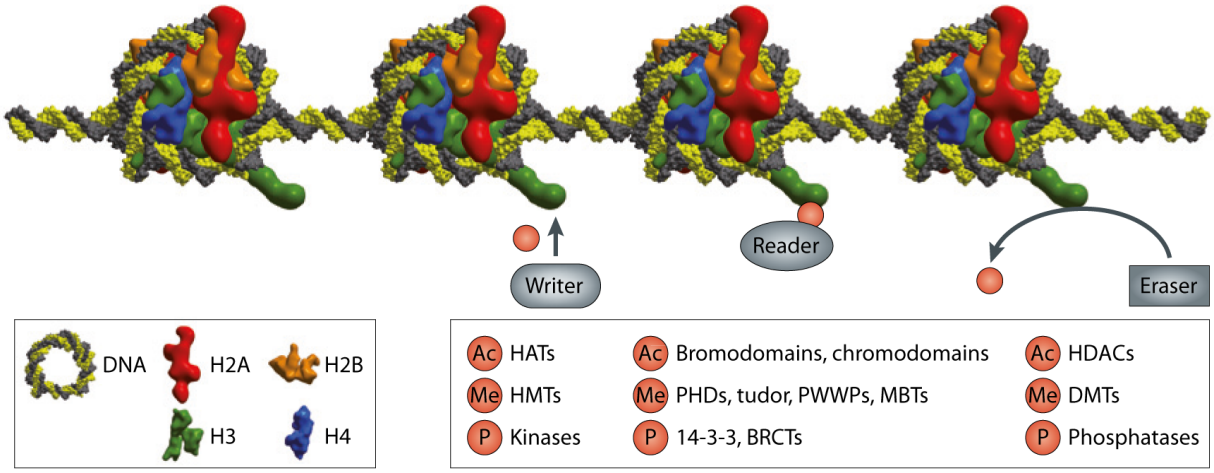

Figure 1. Histone modifications and their readout in the context of chromatin. Post-translational modifications in histone proteins (H2A, H2B, H3 and H4) are found at the core of nucleosomes. Examples of enzymes that apply (writers), remove (erasers) or interpret (readers) the covalent marks are shown. Chemical modifications include acetylation (Ac), methylation (Me) of lysine as well as phosphorylation of serine, threonine and tyrosine, among others. Adapted from reference [3]

The numerous mapping studies that were performed in many fetal and adult normal and cancerous tissues enhanced immensely our understanding of chromatin basic biology and biochemistry by defining the genome-wide localization of chromatin modifications.[7-10] In particular, the genome sequencing efforts in a vast array of tumors has revealed the frequent existence of mutations in writers, readers and erasers, thus establishing a causative role for an altered epigenome in cancer. The compilation of the epigenetic regulators mutated in various cancers highlighted histone acetylation and methylation as the most widely affected epigenetic pathways.[6] For instance, the analysis of various cancer genomes have demonstrated recurrent translocations and coding mutations in a large number of histone lysine methyltransferases including *MMSET*, *EZH2* and *MLL* family members.[6] These mutations have been observed in malignancies such as acute myeloid leukemia (AML), acute lymphocytic leukemia, medulloblastoma, breast cancer, among others. Particularly in the latter, recurrent mutations of the histone methyltransferase *MLL2* were found in close to 90 % of cases.[11] Importantly, a growing number of evidence is revealing the profound effects of these mutations on the epigenome. For example, mutations in the isocitrate dehydrogenase-encoding genes *IDH1* and *IDH2* in gliomas and AML inhibit the activity of histone demethylases and DNA demethylases, resulting in altered methylation patterns that drive the disease phenotype.[12-14] In addition, chimeric fusion proteins that are seen in leukemia, such as PML-RARα, PLZF-RARα, and AML1-ETO, have been shown to recruit the chromatin eraser proteins HDACs to mediate aberrant gene silencing, contributing to leukemogenesis.[15]

Many other observations showing chromatin-controlling genes mutated in cancer have created an opportunity to develop first-in-class molecules that disrupt these altered transcriptional pathways. Importantly, the enzymatic nature of epigenetic writers, readers and erasers poses them as ideal drug targets for the development of pharmacological molecules affecting transcriptional pathways[16]. Such enzymatic nature is extremely relevant, especially if considering the arduous development of small molecule modulators against transcription factors like p53, *MYC* and *MYB,* among others, which has proven challenging due to the absence of binding pockets and their involvement in a large number of co-factors to form a transcriptional complex. Currently, several drug classes harness epigenetics for cancer therapy including DNA methyltransferases inhibitors, HDAC inhibitors, lysine-specific demethylase 1 (LSD1) inhibitors, enhancer of zeste homolog 2 (EZH2) inhibitors and bromodomain and extra-terminal (BET) motif inhibitors.[16,17] The most successful modulators of epigenetic processes have been the Food and Drug Administration (FDA)-approved DNA methyltransferase inhibitors such as azacitadine® from Celgene and decitabine® from Eisai, which are used to treat myelodysplastic syndrome (MDS) and a range of other malignancies by inhibiting DNA methyltransferases (DNMTs).[16,18,19] These enzymes are responsible for the methylation of DNA wrapped around histone proteins, and have been recognized as causing global hypomethylation and ultimately DNA damage and cell death[20]. Additional FDA-approved epigenetic effectors include vorinostat® from Merck, romidepsin® from Celgene and belinostat® from Spectrum Pharmaceuticals for the treatment of cutaneous or peripheral T cell lymphomas.[16,17,21-23] These drugs act by inhibiting the epigenetic eraser HDAC and appear to halt tumor progression though the induction of apoptosis, cell cycle arrest and by altering the DNA damage pathway. Panobinostat® from Novartis has been recently approved for the treatment of drug-resistant multiple myeloma when used in combination with the proteasome inhibitor bortezomib® from Millenium Pharmaceuticals.[2]

An important class of epigenetic targets are the reader proteins that, in contrast to the inhibition of the catalytic domains of epigenetic writers and erasers described above, involves the disruption of protein-protein interactions.[16] This is evidenced by the development of bromodomain inhibitors that specifically target the BET proteins, and which have shown great promise for potential clinical applications, as presented below.

I.2. BET bromodomain proteins and their role in homeostasis and cancer

The bromodomain-containing family of proteins represents an important class of readers of epigenetic marks. These proteins specifically recognize and bind to acetylated lysine residues and are involved in the maintenance of epigenetic memory and gene transcription.[24] The bromodomain (BRD) modules are components of multidomain proteins, in which these are linked *via* flexible sequences to diverse interaction or catalytic domains.[25] This conformational flexibility allows BRDs to combine protein-protein interaction domains, as those of PHD or PWWP, with catalytic domains such as HAT and helicase domains. This complex combination of functional modules within each protein facilitates their interaction with other proteins inside complexes, but also the recruitment to specific sites and directed catalytic activity.[25]

I.2.1. Bromodomain module architecture and organization

The bromodomain motif consists of an evolutionary conserved domain of 110 aminoacids that fold into a four helix motif and is present in several proteins in humans, fruit flies and yeast.[26] The human genome encodes for 42 different proteins that contain a total of 61 unique BRDs, where differences in the amino acid residues around the acetyl-lysine binding site impart binding specificit.y[27] Despite the large sequence variation, the BRD module has a distinctive architecture comprising four α-helices (αZ, αA, αB and αC) that are linked by two loop regions of variable length (ZA and BC loops) surrounding the acetyl-lysine (KAc) binding site (Figure 2). These are stabilized by a number of conserved residues that are found within the module, including a PxY motif at the carboxyl terminus of the ZA loop region and a Tyrosine (Tyr) residue in the AB loop that forms a salt bridge to a residue on αB. Docking of the neutralized side chain of the KAc peptide occurs in a central deep hydrophobic cavity, anchored by a conserved Asparagine (Asn) residue at the amino terminus of the BC loop (Figure 2A). In addition, the binding of the entire acetylated peptide is mainly driven by the large charged interface at the surface surrounding the KAc-binding pocket (Figure 2B).[25] Interestingly, different BRD modules present a distinct charge distribution on their surface. Considering that acetylated histone peptides are typically rich in positively charged Lysine (Lys) and Arginine (Arg) residues, it is likely that BRD modules exhibiting highly positively charged surfaces accommodate other targets.

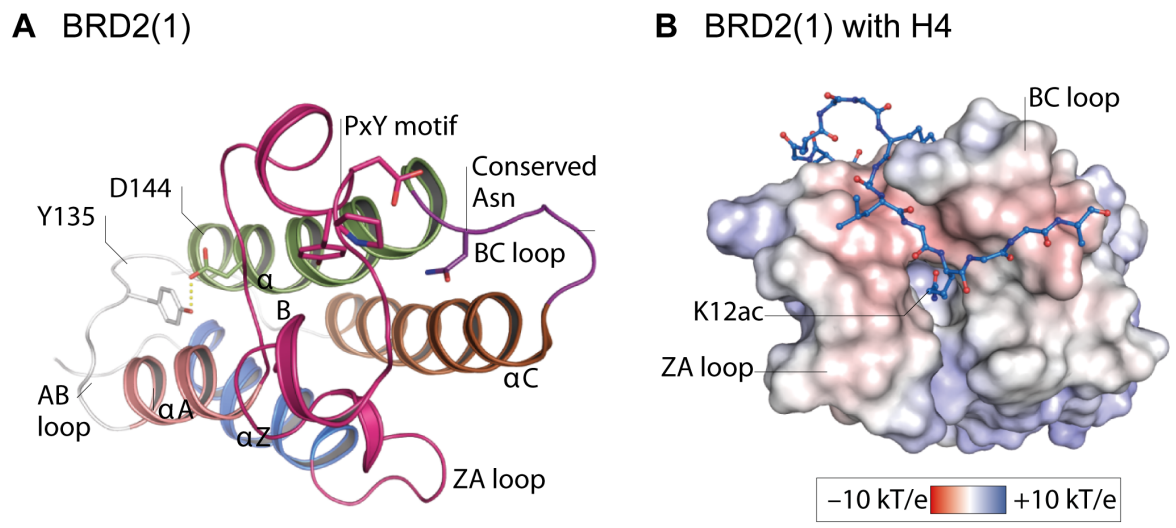

Figure 2. Bromodomain overall fold and substrate binding. (A) Structure of the first bromodomain (BRD) module of bromodomain-containing protein 2 (BRD2(1)). The conserved structural elements are colored including the four α-helices (αZ, αA, αB and αC) linked by flexible loop regions (AB, BC and ZA loops). A salt bridge is formed between the conserved Tyr (Y135 in BRD2) of the AB loop and an aspartic acid (Asp) residue (D144), stabilizing αA and αB helices. It is also shown the conserved Asparagine (Asn) residue in the BC loop and which is responsible for docking of acetylated KAc peptides. (B) Surface charge of BRD2(1) colored according to its electrostatic potential as indicated in the inset (e, electron charge; k, Boltzmann constant; T, temperature), demonstrating the surface that lines the KAc-binding cavity where the K12Ac inserts. Adapted from reference [25]

Based on their structural topology and sequence similarity, the 61 available human BRD modules were clustered into eight families. These include, for instance, the family containing the HAT enzymes *CREB binding protein* and *ETA binding protein p300* whose BRDs have been extensively studied in the context of histone binding and nucleosome remodelling.[27-29] Another BRD family comprises the transcriptional repressor *tripartite motif-containing 66*, the *tripartite motif-containing 33* and the transcriptional regulator *transcriptional intermediary factor 1*, whose main characteristic is the existence of a PHD/BRD tandem module and which seems a necessary structural motif for peptide recognition and protein stability.[27]

The BET proteins belong to other BRD family. Their architecture is shared across family members and consists of two *N*-terminal BRDs that exhibit high levels of sequence conservation as well as an extra-terminal (ET) domain and a more divergent *C*-terminal motif (Figure 3). The BET family of proteins comprises four members including the ubiquitously expressed BRD2, BRD3, BRD4 and *bromodomain testis-specific protein* BRDT, the latter of which is expressed in germ cells.[17] These proteins engage onto acetylated chromatin *via* their BRD modules and recruit components of the transcriptional machinery *via* their ET domain (Figure 3). The conserved ET domain performs an effector role in transcriptional activation and chromatin remodelling by interacting with several different cofactors.

These include the demethylase protein JMJD6, the methyltransferase/adaptor protein NSD3, and the chromatin remodelling ATPase CH4 and BRG1.[30] Indeed, evidence suggests that BRD4 relies on a unique subset of these ET-interacting proteins for transcriptional activation in particular cell types, however this context-specific function of ET domains is currently not well understood.[31,32] In addition, it is also worth noting that the two *N*-terminal BRDs of BET proteins are mutually related and arranged in tandem, exhibiting high affinity for histone H3 and H4 peptides with single or multiple acetylations.[27,30]

BET proteins have multiple mechanisms of action and, depending on the context, can either function as co-activators or co-repressors of gene expression. Given the key roles of BET proteins in initiation and maintenance of transcription these have been studied extensively in the context of homeostasis and disease, and will be the focus of our studies.

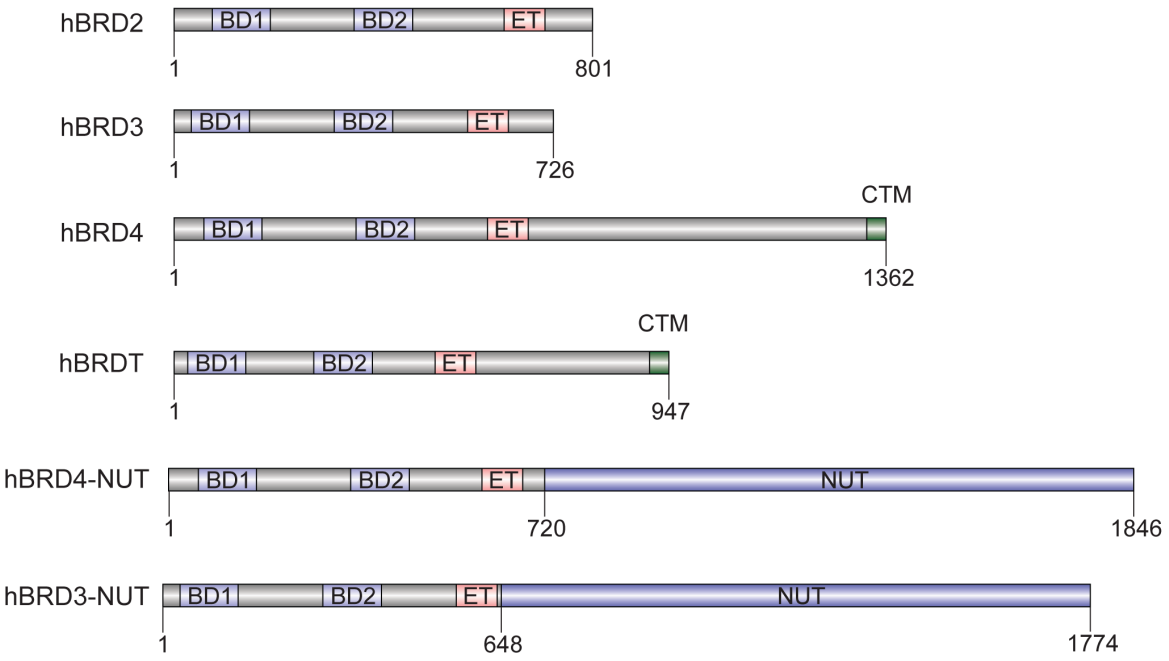

Figure 3. Domain architecture of human bromodomain and extraterminal (BET) protein family and BET-NUT fusion proteins. BET proteins contain two bromodomains (BD1 and BD2) and an extraterminal (ET) domain. BRD4 and BRDT have an additional carboxy-terminal motif (CTM). BRD3/BRD4 – NUT fusion proteins are found in NUT midline carcinoma (NMC) patients, and fuse the amino terminus of BRD2/3 with almost the entire NUT protein. Adapted from reference [30].

I.2.2. BET bromodomains as co-regulators of transcriptional networks

BET proteins have a crucial role in regulating gene transcription through the recruitment of proteins to form complexes that modify chromatin. BRD2 was the first BET protein to be functionally characterized and was found recruiting transcription factors, transcriptional co-activators and

transcriptional co-repressors upon binding to acetyl-histone H4.[33,34] In particular, BRD2 was found recruiting elements from the Mediator complex, which is a large multiprotein complex that regulates transcription from a diverse set of RNA polymerase II-controlled promoters,[35,36] together with other proteins involved in chromatin remodelling such as SWI/SNF subunits.[35] Furthermore, BRD2 provided a scaffold in chromatin to recruit other epigenetic modulators including HDACs and HAT enzymes.[33,37] BRD2 also participates in cell cycle control by forming complexes with RNA Polymerase II and E2F transcription factors, guiding the latter to the Cyclin A promoter.[17]

Similarly to BRD2, BRD4 was first identified as a component of the murine Mediator coactivator complex and a MED1-interacting protein.[36] Consistent with this interaction, BRD4 and Mediator co-occupy similar sites across the genome and can stabilize one another's occupancy at certain regions, including thousands of enhancers and promoters associated with active genes.[38] Loven *et a*l. have shown that exceptionally high levels of these cofactors occur at a small set of large enhancer regions, called super-enhancers.[38] These large enhancer regions stimulate the transcription of growth-promoting and lineage-specific survival genes and also play key roles in driving the expression of oncogenes during cancer development and progression.[24] BRD4 is also a crucial regulator of the transcription elongation through the recruitment of the positive transcription elongation factor b (P-TEFb), a heterodimer of cyclin-dependent kinase 9 and cyclin T that phosphorylates the carboxy-terminal domain of RNA polymerase II.[30] BRD4 interaction with P-TEFb is mediated by its unique CTM motif, also found in BRDT but not in other BET family members (Figure 3), and followed by several phosphorylation events that will ultimately promote transcription elongation. In particular, it is likely that the M phase to G1 phase transition in cell cycle progression is partially controlled by BRD4 recruitment of P-TEFb to target post mitotic genes for transcription.[35] Furthermore, BRD4 also contributes to the recruitment of P-TEFb to hyper acetylated enhancer and promoter regions across the genome, thus promoting P-TEFb accumulation near docking sites harbouring target transcriptional activators.[30] The presence of the CTM region in BRD4 and subsequent interaction with P-TEFb, which is not found in BRD2 or BRD3, may explain why BRD4 has a broader nonredundant role in transcriptional activation than the other BET proteins despite having 80% identity at the aminoacid level in both mice and human.[35] As an example, BRD4 genetic inactivation led to slow growth phenotypes in numerous mammalian cell lines, whereas BRD2 and BRD3 ablation results in more subtle phenotypes.[30]

As exemplified above for BRD2, BET proteins also play key roles in cell cycle regulation. Evidence shows that unlike non-BET bromodomain proteins, both BRD2 and BRD4 remain bound to chromosomes during mitosis,[39] which might be important for the maintenance of epigenetic memory.[35,40] These mechanisms consist on BET proteins bookmarking genes, which will be transcribed in late mitosis and early G1.[41] Furthermore, different reports have showed that BRD4 knockdown results in cell

cycle arrest, further highlighting its importance in cell cycle progression.[42,43] The elemental role of BET proteins in the normal cell cycle may be in part due to BRD4 regulation of Aurora B expression (AURKB), which is a member of the Aurora family of serine/threonine protein kinases and is a key player in chromosome segregation during mitosis.[44]

Given their role in the co-activation or co-repression of several transcriptional networks (Figure 4), it is not surprising that perturbations of BET-mediated processes have a significant impact in the development of disease, namely in inflammation, viral infections and cancer. For instance, BRD4 has been linked to increased expression of inflammatory genes *via* the transcriptional activation of NF-κB[45] and BRD2 can co-activate pro-inflammatory genes that depend on NF-κB transcription.[35] Furthermore, BRD2 gene disruption in mice has led to a broad range of inflammatory responses and protection of animals from inflammatory complications of obesity-induced insulin resistance.[35] Consistent with these findings, inhibition of BET proteins has shown anti-inflammatory potential through the suppression of several crucial pro-inflammatory cytokines and chemokines such as interleukin(IL)-1β, IL-6, IL-12α, CXCL9 and CCL12,[46] or through blockage of tumor necrosis factor production.[47] Also in certain virus infections, host-encoded BET proteins have been shown to be crucial for both transcriptional activation and transcriptional repression of virus promoters. For instance, BRD4 interacts with E2 protein of human papillomavirus (HPV) *via* its CTM domain to enable transcriptional activation of E2-target genes and E2-repression of oncogenic E6 and E7 genes.[48-50] Similarly, BET proteins contribute to the latency-associated nuclear antigen (LANA1)-regulated transcription, which is a Kaposi's sarcoma-associated herpes virus (KSHV) latent protein, thus leading to cell cycle progression.[51] As observed in BRD4-E2 interaction, LANA1 transcriptionally activates some genes, such as E2F-dependent cell cycle genes, while repressing others, such as p53-dependent pro-apoptotic genes, to promote the proliferation of KSHV-infected cells.[52,53]

Altogether these findings further highlight the role of BET proteins as either transcription co-activators or co-repressors in homeostasis, thus corroborating the possibility for context-dependent functions (Figure 4). It is therefore not surprising that these dual roles of certain BRD-containing proteins are also found in cancer, with their aberrant expression either stimulating or supressing malignant phenotypes. Indeed in recent years the BET family of bromodomains has emerged as one of the most prominent transcriptional vulnerabilities in human cancer, corroborated by the numerous malignant processes that have recently been identified that are BET protein-dependent.

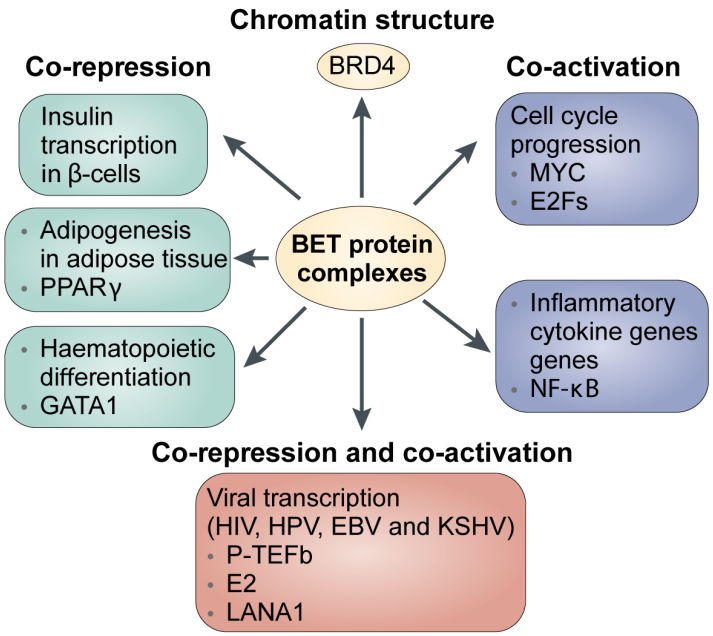

Figure 4. BET proteins and their role in the co-regulation of transcriptional networks. While some interactions involve transcriptional co-repression, as as insulin transcription and GATA-1-controlled hematopoietic differentiation, others involve transcriptional co-activation, such as those involving genes that promote cell-cycle progression (Myc and E2F proteins). Adapted from reference [35].

I.2.3. BET bromodomain proteins in cancer

BRD-containing proteins have been found highly deregulated in cancer, either by forming fusion proteins that result in aberrant function or as a result of mutations that lead to malfunctioning protein phenotypes. For instance, in 21 different pediatric cancer subtypes, 21 out of 42 BRD-containing proteins had recurrent mutations, including the BET family of bromodomains.[54] Similar findings have been extended to a wide range of tumors, including in hepatocellular carcinoma,[55] squamous cell lung cancers,[56] lung adenocarcinomas,[57-59] small-cell lung cancers,[60] non-small-cell lung cancers,[61] T cell lymphoma,[62] follicular lymphomas,[63] cervical carcinomas,[64] colorectal cancer and gastric cancers,[65] among others.[25] Although these studies did not include the mutation load in BRD modules and subsequent impact on KAc recognition, Fujisawa *et al.* have mapped the mutations annotated in the cancer genome atlas (TCGA), and found in BRD modules, that could indicate a potential loss of function to each structure of human BRDs. In brief, point mutations in BET bromodomain proteins were mostly identified in the large intestine (4.88% point mutations in BRD4 out of 1229 samples tested), skin cancer (3.82% point mutations in BRD4 out of 864 samples tested) and stomach cancer (3.60% point mutations in BRD4 out of 555 samples tested). The mapping pattern observed for BRD4 was shared across other BET family members, although to a minor extent.[25] Thus, considering the importance of the charged

interface surrounding KAc binding cavity for the binding affinity, it is likely that most of these mutations will negatively affect the binding of BRD-containing proteins to their targets.

Misexpression of BET-bromodomains has also been shown to drive various malignant phenotypes. For example, BRD2 is found highly expressed in melanoma[66] whereas BRDT is found over activated in non-small-cell lung cancer.[61] BRD4 was also shown to have increased expression in hepatocellular carcinoma (HCC),[67] melanoma,[66] glioblastoma[68] and malignant peripheral nerve sheath tumors.[69] Furthermore, using an *in vivo* short-hairpin RNA (shRNA) screen, Baratta *et al*. identified BRD4 as being necessary for the proliferation of high-grade serous ovarian carcinoma models by contributing to *MYC* overexpression.[70] Regulation of *MYC* transcription by BRD4 proteins was also found in experimental models of multiple myeloma, corroborated by chromatin immunoprecipitation studies showing a strong enrichment of BRD4 immunoglobulin (Ig) heavy-chain enhancers bearing rearrangement at the *MYC* locus.[71] Indeed, in models of *MYC*-addicted hematologic cancers, BRD4 localizes with *MYC* throughout the active genome and contributes to elevated transcriptional elongation.[38,72] The role of BRD4 in oncogenesis is further highlighted by the BRD4-Twist interaction in basal-like breast cancer. Twist is a key transcription activator of the epithelial-mesenchymal transition, a biological process that allows a polarized epithelial cell to assume a mesenchymal cell phenotype, and which was found using a unique mechanism to recruit BRD4 *via* an H4 mimic motif that becomes diacetylated. This interaction ultimately leads to tumorigenicity through BRD4-mediated activation of P-TEFb followed by phosphorylation of RNA polymerase II and enhanced *WNT5A* transcription.[73] Furthermore, Roe *et a*l. have shown that BRD4 chromatin occupancy in AML closely correlates with the hematopoietic transcription factors *PU.1*, *FLI1*, *ERG*, *C/EBPα*, *C/EBPβ* and *MYB* at nucleosome depleted enhancer and promoter regions. In addition, their findings have demonstrated that, together with hematopoietic transcription factors and p300/CBP, BRD4 acts to promote transcriptional activation and leukemia maintenance.[74]

As mentioned above BRD-containing proteins have also been found to form fusion proteins, which results from chromosomal translocation between genes encoding these proteins and other genomic regions. These events can lead to protein's native function inactivation and/or confer a completely new function to the proteins[25]. In BET-bromodomain proteins this is evidenced by BRD3 and BRD4 fusions with the nuclear protein in testis (NUT) gene, which encodes a nuclear protein that is predominantly expressed in testis (Figure 3). BRD3 and BRD4 have been identified as a component of the recurrent t(15; 19)(q14: p13.1) chromosomal translocation, with the resulting fusion protein blocking differentiation and driving the growth of NUT midline carcinoma (NMC) cells, a subtype of squamous cell cancer which is one of the most aggressive human solid malignancies known.[75] The BRD4-NUT fusion protein contains the amino terminus of BRD4 or, in rare cases, of BRD3. The bromodomain fragment containing both bromodomains and essentially the entire coding region for NUT.[3] Furthermore, BRD4-NUT fusion

protein has been shown to rely on BRD4 bromodomains for its oncogenic function. BRD4-NUT recruits a number of factors that stimulate local chromatin hyper acetylation, thus promoting further recruitment of BRD and ultimately leading to transcriptional activation and increased expression of pro-survival genes.[25] Importantly, BET inhibition with thienodiazepine compounds could selectively target the BRD4-NUT fusion protein by displacing BRD4 from chromatin and inducing differentiation, which led to therapeutically relevant phenotypes in mice xenograft models.[76] Concomitantly, due to the key roles BET bromodomain proteins have in cellular homeostasis and driving malignant phenotypes herein demonstrated, several new chemical entities have been developed to interfere with the BRD-mediated recognition of KAc. As discussed below, current efforts suggest that there is a therapeutic window for controlling and modulating the activity of these proteins and which can lead to novel, improved cancer therapeutics.

I.3. BET bromodomain proteins as cancer therapeutic targets

The largely hydrophobic nature of the KAc binding cavity of BRDs, which is necessary to accommodate the charge-neutralized acetylated lysine, makes these modules highly amenable for the development of small molecule inhibitors targeting BRD acetyl-lysine protein-protein interactions.[3] Furthermore, considering that BET proteins exhibit multiple mechanisms of action, including the involvement in transcriptional stimulation and control of lineage specific genes that are linked to cell cycle control, their inhibition has led to very strong phenotypes.[25] Together these observations make BET bromodomain proteins very attractive for the development of small molecule effectors that can attenuate their function. This was further evidenced in a report that explored the druggability of the entire family of bromodomains.[77] Therein druggability scores (Dscores) were attributed to different BRD modules, which consisted of numerical quantities calculated from experimental structural data to assess the likelihood of proteins binding to drug-like molecules. For these simulations it was taken into account the contributions from the volume, the level of enclosure and the degree of hydrophobicity of a pocket towards the binding of small molecules. Based on the calculated Dscores, the BET bromodomains were predicted by the analysis as having higher druggability than other bromodomains, thus suggesting that in screening efforts higher hit rates are observed.[77] Subsequent publication of two potent ligands for the BET bromodomains demonstrating effective inhibition of bromodomain-acetyl-lysine protein-protein interactions and associated strong phenotypic effects in relevant models of disease, stimulated further the interest in the development of BET bromodomain modulators.

I.3.1. BET bromodomain inhibitor development

Potent inhibitors of BET bromodomain proteins were not described until 2010, when two diazepine-based potent pan-BET ligands, (+)-JQ1 and I-BET762, were reported for successfully targeting BET-mediated protein-protein interactions in the context of human squamous carcinoma ((+)-JQ1) and inflammation (I-BET762).[46,76] The structural disclosure of these compounds and their powerful cellular effects has then ignited great interest in BET bromodomain inhibition, with a large number of new chemical scaffolds being developed that aim to modulate the epigenetic function of the KAc reading process. Interestingly, the lead molecules for both ligands were discovered using a phenotypic screening approach, whose targets were initially unknown. The patent literature on compounds with the general triazolothienodiazepine core of (+)-JQ1 can be traced back to 1998, when these were described as potential therapeutics for the treatment of inflammatory intestinal diseases, including ulcerative colitis and Chrohn's disease.[3,78,79] Only later in 2009 these were identified as BET bromodomain ligands, leading to suppression of cellular proliferation in tumor models.[80] In turn, I-BET762 emerged from phenotypic screening approaches to discover small molecule upregulators of apolipoprotein A1 (ApoA1), which is involved in protection from atherosclerosis progression and immunomodulation.[46,81] Upon successful identification of BET bromodomain proteins as their molecular targets, the chemical scaffold of the lead compounds was optimized and ultimately led to the highly potent I-BET762 and (+)-JQ1 compounds. Both have been extensively characterized showing high selectivity for all BET bromodomains, but not for BRD members outside of the BET family, along with strong binding affinities as determined by different biophysical techniques. For example, (+)-JQ1 displayed an *in vitro* IC_{50} of 77 nM (determined by AlphaScreen)[76] while I-BET762 displaced a tetra-acetylated histone H4 peptide from BRD4 with an IC_{50} of 36 nM (determined by fluorescence resonance energy transfer) (Figure 5).[46,82]

Crystallographic studies highlighted that both (+)-JQ1 and I-BET762 bind to BET protein module by forming hydrogen bonds with the conserved Asn residue in a way that mimics the binding mode of acetylated lysine. Other small molecule inhibitors of BET proteins, such as MS436, engage the bromodomain module within the acetylated-lysine binding pocket but without forming a canonical hydrogen bond with the conserved asparagine. Based on this evidence Filippakopoulos *et al.* have categorized known bromodomain inhibitors into two main classes, depending on the presence of absence of moieties that act as acetylated lysine mimetics.[3] Importantly, the formation of hydrogen bonds with the conserved asparagine as is observed in KAc-binding mimetic scaffolds results in the binding of the inhibitor deeper within the module cavity, usually resulting in stronger interactions.

Nevertheless, both classes of compounds bind to BET bromodomains in a competitive manner with acetyl lysine to displace BET-containing protein complexes from chromatin.[30]

In the last few years many different chemical scaffold templates have been developed to engage the BET bromodomain KAc binding cavity, including triazolothienodiazepines ((+)-JQ1,[76] OXT015,[83] MS417),[84] triazolobenzodiazepines (I-BET762),[46,81] quinazolones (RVX-208),[85] quinazolines (PFI-1),[86] 3,5-dimethyl-isoxazoles (OXFBD02 and OXFBD03,[87] I-BET151),[47] tetrahydroquinolines (I-BET726)[88,89] and 4-acylpyrroles (XD14),[90] among others.[3,78] In Figure 5 the KAc mimicking component responsible for the compound binding, as determined by X-ray crystallography, is highlighted for each BET inhibitor represented. For example in (+)-JQ1, high-resolution crystal structures have shown that it is the triazolo ring of the molecule that inserts deep into the KAc pocket and occupies the same position as the acetyl head group of the KAc peptides present in histone tail peptides.[3] The triazolo motif establishes a direct hydrogen bond with a conserved asparagine (N140 in the first bromodomain of BRD4, BRD4(1)), while the chlorophenyl substituent of the diazepine ring engages the shelf between the BC loop and the Tryptophan-Proline (WP) motif (W81 and P82 in BRD4(1)), thus occupying the same location of a second KAc in peptide complexes. Furthermore, (+)-JQ1 occupancy of the KAc binding cavity is completed by the engagement of the dimethyl-substituted thieno ring between the WP motif and the ZA loop shelf (Figure 6).[76] The triazolobenzodiazepine I-BET762 follows the same binding mode and affinities as (+)-JQ1, and together these two chemical scaffolds have been widely used to guide the development of novel classes of inhibitors. Among these are the diazepine-based BET bromodomain ligands MS417 and OTX015, which are structurally similar to (+)-JQ1, or compound **(3)**, that Bayer researchers have recently developed to optimize the pharmacokinetic properties and solubility of I-BET762 by replacing the ethylamide group.[91] Therein, analysis of a number of substituents in this position revealed compound **(3)** with a 2-methyl-1,3,4-oxadiazole replacement and which has shown an IC_{50} value of 20 nM against BRD4(1) (as determined by AlphaScreen).[78]

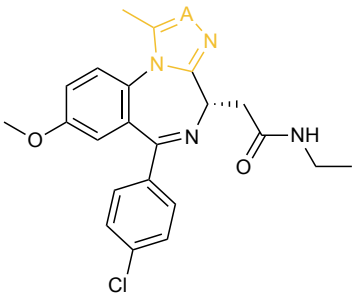

I-BET762 (1)
BRD4(1/2) IC_{50} = 36 nM (*FRET*)

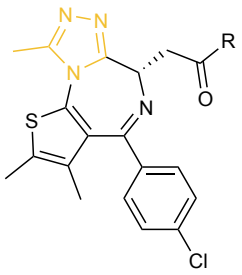

(+)JQ1; R = O^{t}Bu
BRD4(1) IC_{50} = 77 nM
(AlphaScreen)
MS417; R = OMe
BRD4(1) IC_{50} = 30 nM *(FAP)*
OTX015; R =
NH-(4-hydroxy)phenyl

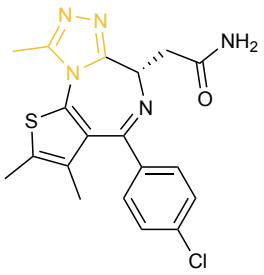

(2)
BRD4(1) IC_{50} = 26 nM
(AlphaScreen)

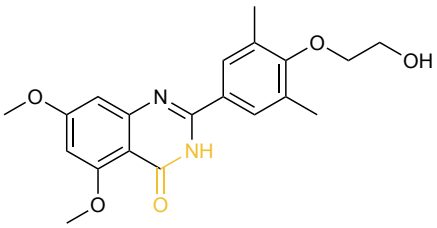

RVX-208
BRD4(1) IC_{50} = 1800 nM *(FRET)*
BRD4(1) K_D = 1100 nM *(ITC)*
BRD4(2) IC_{50} = 40 nM *(FRET)*
BRD4(1) K_D = 140 nM *(ITC)*

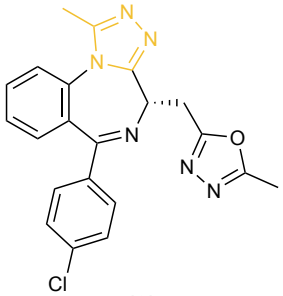

(3)
BRD4(1/2) IC_{50} = 20 nM *(FRET)*

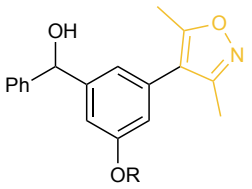

OFXBD02; R = H
BRD4(1) IC_{50} = 382 nM
(AlphaScreen)
OXFBD03; R = Ac
BRD4(1) IC_{50} = 371 nM
(AlphaScreen)

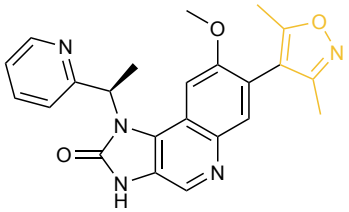

I-BET151
BRD2(1/2) IC_{50} = 36 nM *(FAP)*
BRD4(1/2) K_D = 100 nM (*SPR*)

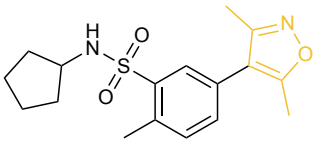

(4)
BRD2(1) IC_{50} = 500 nM *(FRET)*

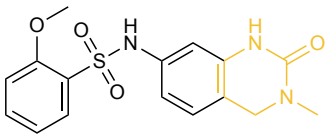

PFI-1
BRD4(1) IC_{50} = 220 nM
(AlphaScreen)

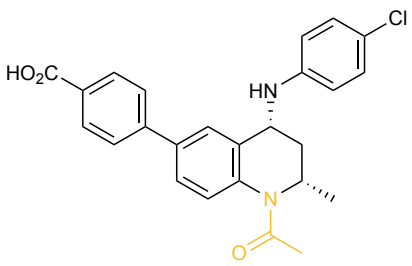

I-BET726
BRD4(1/2) IC_{50} = 22 nM *(FRET)*

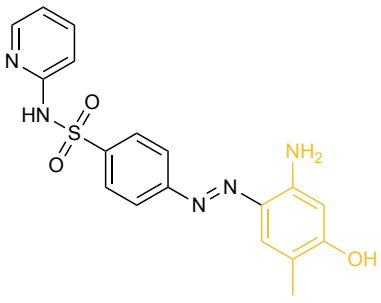

MS436
BRD4(1) K_D < 85 nM *(FAP)*
BRD4(2) K_D = 340 nM (FAP)

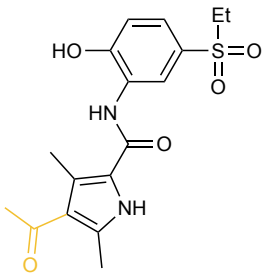

XD14
BRD4(1) K_D = 160 nM
(BROMOscan)
BRD4(1) K_D = 237 nM (FAP)

Figure 5. Structures of key BET bromodomain inhibitors and their IC_{50}/K_D values and the respective method. In orange is labeled the KAc-mimicking component of the molecule, as determined by high-resolution

crystallography, except for MS436. This compound engages the BET bromodomain KAc binding cavity through the highlighted region though not establishing a canonical hydrogen bond with a conserved asparagine residue, thus representing a type of inhibitor that is not KAc-binding mimetic. Adapted from reference [78].

Other chemical scaffolds, such as the quinazolone template, have shown modest selectivity for the second over the first bromodomain of BET proteins. In particular, ITC experiments carried out by Picaud *et al*. for RVX-208 gave a K_D of 140 nM for BRD4(2), but 1.1 μM for BRD4(1). A 20-fold higher selectivity was also observed for BRD3(2) (K_D = 0.194 μM) in comparison with BRD3(1) (K_D = 4.06 μM).[92] High-resolution crystal structures suggested that the enhanced affinity of RVX-208 towards the second bromodomain modules resulted from rearrangement of the binding surface upon ligand engagement onto the KAc binding cavity. Yet it remains unclear whether this selectivity significantly affects the physiological action of the compounds. In addition, recent efforts to identify potent BET bromodomain effectors have focused on fragment-based drug discovery approaches and *in silico* methodologies.[3,78] These enable the identification of low molecular-weight lead hits which, although showing weak affinities, are further optimized through structure-guided methodologies.[93] For lead optimization of fragment libraries high-resolution crystal structures of BRDs and computational techniques such as molecular dynamics, docking, or quantum mechanical calculations have been widely used. The success of this approach is evidenced by the development of the 4-acyl pyrrole XD14 (Figure 5), which was identified upon virtual screening of over 9 million compounds from the Dictionary of Natural Products, the ChEMBL database and the ZINC library. XD14 was the most active hit, displaying a K_D of 237 nM against BRD4(1) by ITC and a K_D value of 160 nM in the BROMOscan ligand displacement assay.[90] Bamborough *et al.* at GlaxoSmithKline have also taken a structure-based design to optimize a phenyl dimethyl isoxazole chemotype into a series of sulfonamide derivatives such as compound **(4).** This compound was shown to be effective at occupying the tryptophan-proline-phenylalanine (WPF) shelf and having reasonable affinity for the BET bromodomains (BRD2(1) IC_{50}= 500 nM by FRET).[47] Using a similar approach, researchers at Constellation Pharmaceuticals have developed a BET inhibitor using hits from fragment-based screens.[94] Structure-guided lead optimization with BRD4(1) led to the development of the carboxamide **(2)** with an IC_{50} value of 26 nM against BRD4(1) as determined by Alphascreen, and which compares favourably with the affinity observed with (+)-JQ1 and I-BET762 using the same methodology. This compound was proven effective in cellular assays and pharmacokinetic profiling in rat and dog demonstrated suitable characteristics for further *in vivo* experiments, further validating fragment-based hit discovery approaches towards the BET family of bromodomains.[94]

Together with the examples above a substantial number of new chemical scaffolds have been established during the last years that bind to BET bromodomain proteins with high potency and

selectivity.[2,3,24,78] Potent inhibitors targeting non-BET bromodomains as CREB binding protein or BAZ2B have also emerged, which demonstrates that specific targeting of other bromodomain families is also achievable. Importantly this work has been strongly structure-guided, as the knowledge gained in BET-bromodomains crystallization has proved transferable to over half of the other human bromodomains.[78] Of particular interest, recent studies suggest that the BET family of bromodomains can be potentially targeted by small molecules that were specifically designed against kinases, thus offering novel opportunities to explore poly-pharmacology strategies to simultaneously target both protein classes.[95-98] Altogether the new compounds targeting distinct subsets of BRD modules will be critical for the validation of molecular targets and activities of BRD-containing proteins. However, it is fundamental to understand the cellular changes that these compounds evoke, particularly in therapeutic areas where bromodomain's function is implicated such as oncology, inflammation and viral infections. In this regard, the exciting development of numerous chemical scaffolds leading to BET inhibition were followed by many reports disclosing a rich body of data demonstrating their anti-proliferative activity against cancer cell lines.

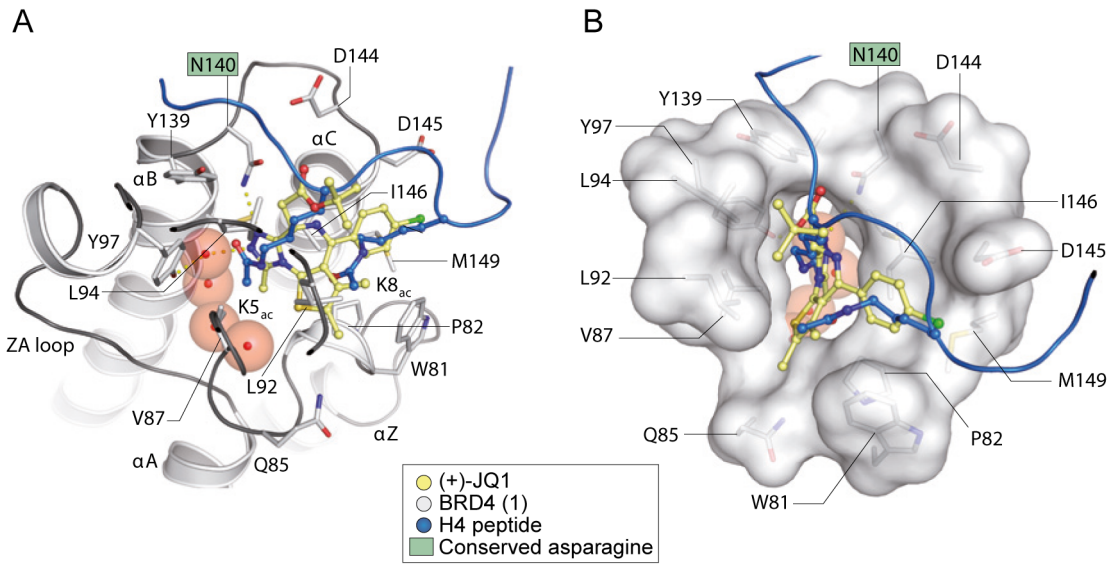

Figure 6. (+)-JQ1 engagement in BRD4(1) KAc binding cavity. (A) and (B) show the overlay of the de-acetylated H4 histone peptide (H4K5Ac/K8Ac) in complex with BRD4(1) (PDB ID: 3UVW) and (+)-JQ1 in complex with BRD4(1) (PBD ID: 3MXF). (+)-JQ1 binds to the conserved asparagine residue (N140) via its triazolo moiety, while the chlorophenyl substituent packs between the D145 of the BC loop and the WP shelf (W81/P82) and the dimethyl-substituted thieno ring between the W81/P82 motif and L92 of the ZA loop. Peptides are shown as cartoons (H4 in blue) with acetylated lysine residues shown as sticks. (+)-JQ1 is shown in ball and stick representation. Adapted from reference [3].

I.3.2. BET bromodomain inhibitors as antitumor agents

Given the above description of BET protein function in the regulation of transcriptional control, it would be expected that inhibition of these important genome-associated proteins would adversely affect global gene expression in healthy cells, especially because BET proteins are ubiquitously expressed and acetylated histones are found at all active promoters and enhancers in the genomes. On the contrary, there is only a modest reduction in global gene expression and mRNA levels, with BRD4 inhibition leading to significant reduction of the transcript levels of only a few hundred genes.[99] Furthermore a number of reports have shown that small molecules targeting BET bromodomain proteins preferentially supress the transcription of cancer-promoting genes.[99] For instance, in the myeloma cell line MM1.S Delmore and colleagues have shown a significant transcriptional downregulation of the *MYC* gene and *MYC*-dependent genes after treatment with (+)-JQ1, while other transcription factors important for the biology of myeloma were not affected.[71] The molecular basis of the transcriptional selectivity towards the *MYC* oncogene exhibited by BET inhibitors was further exploited by Loven *et al*.[38] In this study, also using models of multiple myeloma Lovén and colleagues have found that (+)-JQ1 treatment caused a preferential loss of BRD4, Mediator and P-TEFb at super-enhancers, leading to transcription elongation defects that preferentially implicated super-enhancer-associated genes, including the *MYC* oncogene. These observations suggest that key oncogene drivers of tumor cells are regulated by super-enhancers, which can thus confer high sensitivity to the loss of BRD4 coactivator leading to rather selective inhibition of transcription by BET inhibitors.[3,38] Concomitantly Chapuy *et al*. corroborated this asymmetric BRD4 occupancy at super-enhancer-associated dependencies in models of diffuse large B cell lymphoma (DLBCL), showing that 33 % of the total BRD4 localizes at super-enhancers which are predicted to regulate just 1.6 % of all active genes. Along with *MYC*, other key transcription factors implicated in lymphomagenesis are associated with super-enhancers, including *BCLF6*, *IRF8*, *PAX5*, *OCA-B.*[72] In line with these findings a number of reports have also shown that BET inhibition can repress the expression of oncogenic transcription factors beyond *MYC*, further expanding the potential clinical application of BET inhibitors to several solid tumors. These include colorectal cancer, castration-resistant prostate cancer (CRPC), glioblastoma, breast cancer, non-small cell lung cancer (NSCLC), among others as described below.[24,100,101] Taken together these data offers an explanation for the specific repression of the transcription of tumor-promoting and lineage specific genes by BET bromodomain inhibitors. Subsequently it is possible that this mechanism protects differentiated tissues from the actions of BET inhibitors, resulting in reasonably well-tolerated inhibition of BET bromodomains in mouse tumor models.[3]

An emerging example of direct inhibition of an oncogenic transcriptional factor is bromodomain inhibition in carcinomas harbouring fusions of BET bromodomain coactivators. As described earlier in chapter I.2.3, the BET bromodomomain members BRD3 and BRD4 have been detected in oncogenic

rearrangements that lead to highly tumorigenic fusion proteins. Indeed, among the most aggressive subtypes of lung, head and neck cancer are tumors expressing the chimeric, oncogenic cofactors BRD4-NUT or BRD3-NUT. NMC is a poorly differentiated, chemoresistant and aggressive malignancy that lacks effective FDA-approved therapy.[102] However, the BET inhibitor (+)-JQ1 has been shown to displace BRD4 from chromatin in preclinical models of NMC, thus resulting in potent and irreversible squamous differentiation.[76] In addition, (+)-JQ1 induced a robust pro-differentiation and antiproliferative response, associated with durable responses by PET-CT imaging, in murine models harbouring primary human NMC xenografts. This provided compelling evidence for targeting BRD4-NUT in an aggressive form of cancer, leading other BET inhibitors to transition to clinical investigation.[103]

Several reports have been published where BET inhibitors show potent therapeutic effects in diverse genetic contexts of haematological malignancy, with effects comparable to observations in NMC models. [71,104-107] In human MLL-fusion driven leukemia cell lines I-BET151 induced rapid induction of cell cycle arrest, apoptosis and complete ablation of clonogenic potential.[104] More recently, the same inhibitor has also shown potent antitumor activity across different AML subtypes, including those associated with NPM1c mutation. The wild-type nuclear NPM1 protein colocalizes with BRD4 and represses its transcriptional functions. The mutated form lifts this repressive effect and upregulates a transcriptional programme, thus leading to increased sensitivity to I-BET151 both *in vitro* and *in vivo.*[108] Compelling preclinical evidence of BET-inhibitor-mediated antitumor activity against both B- and T-cell ALL has also emerged from a number of studies.[106,109-111] Treatment of B-ALL cells with (+)-JQ1 was shown to induce a clear antiproliferative and pro-apoptotic effect *in vitro* and in xenotransplantation models, followed by depletion of MYC and interleukin 7 receptor gene (*IL7R*) transcripts.[106] Consistent with these findings, (+)-JQ1 supressed c-*MYC* expression and inhibited the growth of relapsed and pediatric T-ALL samples *in vitro.*[110] Furthermore, Picaud *et al*. have reported PFI-1-mediated antiproliferative effects on several leukemia cell lines. Those that were responsive to PFI-1 treatment showed G1 cell-cycle arrest, induction of apoptosis and substantial downregulation of protein levels of AURKB.[109] The BET inhibitors I-BET762 and I-BET151 have also been shown to induce cell cycle arrest and apoptosis in myeloma cells, which were associated with *MYC* downregulation and *HEXIM1* upregulation. Both inhibitors were found active *in vivo* in subcutaneous and systemic myeloma xenograft models.[111] Interestingly, and in contrast to *MYC* suppression, *HEXIM1* upregulation in response to BET protein inhibitors was not BRD4 mediated. Yet, it led to reduced active P-TEFb availability and contributed to the overall antitumor activity of these compounds in myeloma models.[111] In agreement with previous observations in different models of haematological malignancies, BET inhibition was also proven effective against lymphoma tumors. On a comprehensive panel of 34 human lymphoma cell lines, including 21 DLBCL, 6 Burkitt's lymphoma (BL) and 7 Hodgkin's lymphoma (HL), the inhibitors

(+)-JQ1, I-BET151, OTX015 and I-BET762 demonstrated comparable potency with concomitant induction of G1 cell cycle arrest. Furthermore, highly significant transcriptional downregulation of *MYC* and *E2F1* target genes and the selective depletion of BRD4-loaded promoters and enhancers were identified for all subtypes of DLBCLs studied.[72] Despite the evidenced efficacy of the HDAC inhibitors vorinostat and panabinostat in mature T-cell lymphomas, the preclinical evidence for BET inhibitors activity in this malignancy is limited. In this regard, OTX015 has been reported to show anti-proliferative active by inducing cell cycle arrest, but not apoptosis, in five out of seven anaplastic large-cell T-cell lymphoma cell lines tested, with concomitant down-regulation of the *MYC* gene.[112]

Over the past 6 years the efficacy of BET inhibitors has also been shown in numerous preclinical solid tumor models including breast, prostate, colon, intestine, pancreas, liver and brain malignancies.[24,101] For instance in breast cancer, (+)-JQ1 supressed estrogen-induced growth and transcription in MCF7 and T47D estrogen-receptor-positive (ER+) breast cancer cell lines. In this study Nagarajan *et al*. established a rationale for the observed antitumor effect by showing that BRD4 activity is required for the proliferation of ER^+ breast and endometrial cancer cells and for uterine growth in mice.[113] Furthermore, a number of studies have investigated the use of BET inhibitors in endocrine-resistant tumors, including in tamoxifen-resistant breast cancer. Importantly, BET proteins contribute to tamoxifen resistance by recruiting WHSC1, a histone H3K6 methyltransferase, to the *ERα* gene with inappropriate modulation of expression. Persistent suppression of *ERα* and c-*MYC* signalling was observed in tamoxifen-resistant cell lines following (+)-JQ1 treatment, while in parent cells both pathways were re-expressed in the same conditions. Concomitantly it was observed an enhanced sensitivity to the BET inhibitor (+)-JQ1 in tamoxifen-resistant cell lines rather than in the parental cell lines.[114] BET inhibitors were also shown to overcome breast cancer resistance to treatments with everolimus,[115] an allosteric inhibitor of mTOR complex 1, and lapatinib,[116] a FDA-approved small molecule inhibitor of the HER2/neu pathway. The potential of BET inhibitors for the treatment of breast cancer was further highlighted by the studies of Shu and colleagues.[117] Therein a large panel of breast cancer cells reflecting luminal, $HER2^+$ and triple-negative (TNBC) subtypes was screened against the BET inhibitors (+)-JQ1, Y803, PFI-1, I-BET762 and I-BET151, with potent inhibitory effects observed preferentially in TNBC cells. TNBC are negative for ER, PR and HER2 and are currently the only major breast tumor subtype that lacks targeted therapies.[118] In line with the role of BRD4 in transcription, (+)-JQ1 treatment induced G1 cell cycle arrest, apoptosis and senescence in TNBC cells. The growth of established xenografts derived from TNBC cell lines and from primary patient TNBC samples was also efficiently inhibited by (+)-JQ1 treatment.[24,117] Recently, the growth of TNBC cells was additionally inhibited by OTX015, both as a single agent and in combination with everolimus.[119]

Apart from breast cancer, other non-hematological malignancies have been target of BET inhibition. In CRPC cells, (+)-JQ1 blocked the proliferation, induced apoptosis and repressed the expression of anti-apoptotic factors.[120] In fact, (+)-JQ1 was more effective in blocking tumor growth in mice than enzalutamide, the currently FDA-approved therapeutic for the treatment of CRPC both following and prior to docetaxel chemotherapy.[120] In a more recent report, Asangani and colleagues extended previous studies and have observed that (+)-JQ1 and OTX015 effectively inhibited the growth of prostate cancer cell lines that become resistant to enzalutamide.[121] In addition, androgen receptor antagonists, enzalutamide and ARN509, a FDA-approved therapeutic for the treatment of CRPC, exhibited enhanced prostate tumor growth inhibition when combined with BET inhibitors. This data thus provided compelling preclinical rationale for the combination of BET inhibitors and androgen receptor (AR) antagonists to subvert resistance mechanisms in prostate cancer.[121] Also in NSCLC cell lines (+)-JQ1 treatment led to decreased proliferation, cell cycle arrest and induction of apoptosis mediated by the repression of *FOSL1*, a component of the FOS-JUN transcription factor complex. Importantly, these studies have shown that (+)-JQ1 inhibited NSCLC cells through a mechanism independent of c-*MYC* downregulation, supporting the rationale for cell-lineage-specific differences in transcriptional targets of BET proteins and their influence in the activity of BET inhibitors.[100] Still in the context of NSCLC, both (+)-JQ1[122] and a recently discovered BET inhibitor - BAY 1238097[123] - displayed potent antitumor activity in NSCLC models harbouring *RAS* mutations both *in vitro* and *in vivo.* Treatment of *KRAS*-driven malignancies is an unsolved challenge, despite the fact that 30 % of lung adenocarcinomas harbour these mutations,[124] reinforcing the antitumor impact of BET inhibition. Also, OTX015 has been recently shown to exhibit antitumor activity in NSCLC models harbouring different oncogenic mutations. Cell proliferation inhibition and cell cycle arrest, followed by *MYC* and *MYCN* downregulation, were observed in sensitive NSCLC cells.[83] In patient-derived xenograft models of pancreatic ductal adenocarcinoma (PDAC), which presents the lowest survival rates among all cancers, (+)-JQ1 supressed tumor growth but induced no consistent change in expression of c-MYC protein. Instead, inhibition of tumor progression was more closely related to decreased expression of nuclear CDC25B, a regulator of cell cycle progression.[125] The potential for BET inhibition as treatment for PDAC was further highlighted in the studies of Mazur *et al.*, where it was reported a potent synergistic tumor-supressive effect between a (+)-JQ1 and vorinostat in transgenic Kras/p53 PDAC mouse model.[126] Potent inhibitory effects of BET inhibitors were also observed in relevant models of colon,[127] hepatocellular[128] and brain tumors such as glioblastoma[129] or medulloblastoma.[130]

Altogether, it becomes clear from the numerous reports above in different genetic contexts that there is compelling preclinical evidence of the antitumor efficacy of BET inhibitors in both haematological malignancies and solid tumors. In addition the triazolobenzodiazepines and triazolothienodiazepines

showed good stability in human, mouse, and rat liver microsomes, with bioavailabilities above 30 %, permitting oral or intravenous administration.[3] As a result, the tremendous success of BET inhibitors in preclinical tumor models led to a rapid translation to clinical evaluation.

I.4. Clinical translation of BET bromodomain inhibition in cancer

Several BET inhibitor compounds have entered clinical development in phase I or II studies for patients with hematological malignancies and solid tumors (Table 1). The results of most of these studies are still preliminary, though signals of clinical relevance have been observed.

The first clinical activity reported was for a phase I dose escalation study of the thienotriazolodiazepine OTX015 in two parallel cohorts of patients with advanced hematologic malignancies. This consisted of one cohort of patients with AML[131] and one cohort of patients with nonleukemic hematologic malignancies, including lymphoma and multiple myeloma.[132] Particularly, of the total 45 patients comprising the nonleukemia cohort 33 patients had relapsed or refractory lymphoma and 12 patients had relapsed or refractory multiple myeloma that, on average, had received three prior therapies. Two patients with DLBCL achieved complete remissions lasting 4.5 and 13.7 months, respectively, and another patient with DLBCL achieve partial remission lasting 6 months. Additionally, 6 patients (2 with DLBCL, 2 with follicular lymphoma, 1 with extranodal marginal zone lymphoma, and 1 with lymphoplasmacytic lymphoma) had tumor reductions not meeting the criteria for objective response. No responses were observed in the 12 myeloma patients. Interestingly, in a retrospective subgroup analysis 11 out of the 12 DLBCL patients underwent Myc immunohistochemical testing and 5 were positive. However, only 1 of these patients responded to the drug.[132] In the acute leukemia cohort among 41 patients, 36 of whom had AML, 2 patients achieved complete remission lasting 3 and 5 months, 1 patient had achieved complete remission for 2 months but with incomplete recovery of platelets, and 2 patients experienced partial blast clearance. However, no correlation was found between somatic mutations in 42 genes, including *MYC*, *BCL2*, *CCND1* or *NF-κB*, and response to OTX015, even in the 5 patients that responded to therapy.[131]

Preliminary phase I results have also been reported in hematologic malignancies with CPI-0610, a new benzoisoxazoloazepine BET inhibitor. This compound was evaluated in a dose escalation study in 44 patients with relapsed or refractory lymphoma, half of whom had received four or more prior lines of therapy. Two patients with DLBCL achieved a complete response, 1 patient with follicular lymphoma achieved a partial response, while 5 patients experienced smaller decreases in tumor volume not

meeting the criteria for objective responses and 5 showed stable disease. The expression of the BET target gene *CCR1* was found supressed in patients subjected to higher doses of treatment (170 mg once-daily and 230 mg dose levels).[133]

As observed in Table 1, multiple early phase clinical trials of BET inhibitors are also ongoing in solid tumors. Particularly in NMC, Stathis *et al*. presented the first clinical proof-of-concept that targeting BRD4-NUT with a BET inhibitor results in impressive and rapid antitumor activity.[103] Four patients with advanced-stage, previously treated, NUT carcinoma and confirmed BRD4-NUT fusions received OTX015 treatment on a compassionate-use context, based on the dose that was declared safe in the phase I hematologic[132] Among the 4 treated patients, 2 responded rapidly with tumor regression and a third had meaningful disease stabilization with a minor metabolic response. Responses were rapid with symptomatic relief and were confirmed by PET-CT after two cycles of treatment. The duration of response was 13 cycles in 1 patient and 3 cycles in the second patient.[103,134] As part of a phase Ib trial which included 47 patients with advanced solid tumors, out of the 10 patients with NUT carcinoma 3 patients achieved a partial response following treatment with OTX015.[135] Additional studies of NMC patients have been limited but revealing, as they have shown evidences of clinical activity. An open label, dose escalation substudy of TEN-1010 in 3 patients with NMC reported 2 patients with clinical responses after 2-3 weeks of treatment. The patient having rapid tumor progression was treated at a lower dose (0.1 mg/kg), while the clinical responsive patients both received the same dose (0.45 mg/kg) and had 30 and 50 % tumor regression after 1 and 2 cycles of treatment, respectively. The TEN-1010 compound tested in this study is particularly interesting as it is structurally related with (+)-JQ1 while having longer half-life.[136] Preliminary results from a phase I/II open label single-agent in patients with NMC and other cancers have also been published for GSK52762 (I-BET762) treatment. A total of 70 patients, including 17 with NMC, have been treated with different doses of I-BET762 while showing good tolerability. Preliminary responses have been evaluated for 10 patients with 2 patients showing partial-responses and 4 stable disease.[137] Only a few preliminary results have been reported for clinical trials of BET inhibitors in solid tumors other than NMC. Preliminary results of the phase I study for OTX015, indicated above in the context of NMC, also included patients from castration-resistant CRPC), *KRAS*-mutated or *ALK*-positive NSCLC. Among these, clinical activity was only observed in NMC and CRPC. From the 47 patients with advanced solid tumors, 4 patients had a partial response, including the 3 patients reported above with NMC and 1 patient with CRPC. In addition, prolonged stable disease was observed in 5 patients with CRPC (4-8 months) and 2 patients with *KRAS*-mutated NSCLC.[135] Furthermore, no clinical activity was observed in a small phase IIa study in 12 patients with glioblastoma, and which led to the termination of the trial.[138]

Based on the data available and herein presented it is not possible to estimate what can be the clinical impact of BET inhibitors as monotherapy. Several BET inhibitors have entered clinical evaluation and clinical activity has been observed in NUT carcinoma and in hematologic malignancies however, for instance in NUT carcinoma, only 30 % of the patients responded in the phase I trial of OTX015 in solid tumors and 20 % in the phase I trial of GSK525762. Among those patients who achieved a response and for which follow-up data is available, all patients relapsed during treatment.[134] Thus, preliminary results of BET inhibitors have been modest, in that responses are few and short-lived. Furthermore, the adverse events observed in the preliminary trials raise concerns on the toxicity profile of these inhibitors for clinical application. For instance, the development of BAY 1238097 was prematurely interrupted due to severed adverse events that occurred at doses below the predicted therapeutic dose (Table 2).[139] Along with this, many other observations suggest that the safety of these compounds must be better defined, as outlined below.

Table 1. BET inhibitors in clinical development. Data from ClinicalTrials.gov (http://clinicaltrials.gov/). Last accessed on July 2018

Drug	***Phase***	***Start Date***	***Reference***	***Status***	***Indication in Development***
GSK525762 (GlaxoSmithKline)	I	03/2012	NCT01587703	Ongoing/not recruiting	Solid tumors, NUT carcinoma
	I	05/2014	NCT01943851	Ongoing/ recruiting	Hematologic malignancies
	I	05/2017	NCT03150056	Ongoing/ recruiting	Castrate-resistant Prostate Cancer
	I/II	11/2017	NCT03266159	Withdrawn	Small Cell Lung Cancer *RAS*-mutated solid tumors
	II	02/2017	NCT02964507	Ongoing/ recruiting	ER^+ Breast Cancer
OTX015/MK-8628 (Oncoethix GmbH)	I	12/2012	NCT01713582	Completed	Hematologic malignancies
	I	10/2014	NCT02259114	Completed	Solid tumors
	I	10/2014	NCT02296476	Terminated	Glioblastoma
	I	10/2016	NCT02698176	Terminated	Solid Tumors
OTX015/Vidaza	I/II	11/2014	NCT02303782	Withdrawn	Acute Myeloid Leukemia

(Oncoethix GmbH)					
CPI-0610 (Constellation Pharmaceuticals)	I	09/2013	NCT01949883	Ongoing/not recruiting	Non-Hodgkin lymphoma
	I	07/2014	NCT02157636	Completed	Multiple myeloma
	I	06/2014	NCT02158858	Ongoing/ recruiting	Myelodysplastic syndrome, leukemia
RO6870810/TEN-010 (Hoffmann-La Roche)	I	10/2013	NCT01987362	Completed	Solid tumors
	I	11/2014	NCT02308761	Completed	Acute myeloid leukemia, Myelodysplastic syndrome
	I	06/2017	NCT03068351	Ongoing/ recruiting	Multiple myeloma
	I	08/2017	NCT03255096	Ongoing/ recruiting	Diffuse Large B-cell lymphoma
	I	11/2017	NCT03292172	Ongoing/ recruiting	Ovarian cancer, Triple Negative Breast Cancer
BAY1238097 (Bayer)	I	02/2015	NCT02369029	Terminated	Neoplasms
GS-5829 (Gilead Sciences)	I	03/2015	NCT02392611	Completed	Solid tumors, lymphomas
	I/II	12/2015	NCT02607228	Ongoing/not recruiting	Castrate-resistant Prostate Cancer
	I/II	01/2017	NCT02983604	Ongoing/not recruiting	ER^+ Breast Cancer
ABBV-075 (AbbVie)	I	04/2015	NCT02391480	Ongoing/ recruiting	Solid tumors and hematologic malignancies
FT-1101 (Forma Therapeutics, Inc.)	I	09/2015	NCT02543879	Ongoing/ recruiting	Hematologic malignancies
INCB054329 (Incyte Corporation)	I/II	05/2015	NCT02431260	Completed	Solid tumors, hematologic malignancies
BMS-986158 (Brystol-Meyers	I/II	06/2015	NCT02419417	Ongoing/ recruiting	Solid tumors

Squibb)					
BI 894999 (Boehringer Ingelheim)	I	07/2015	NCT02516553	Ongoing/ recruiting	Solid tumors, non-Hodgkin lymphoma
PLX51107 (Plexxikon)	I	03/2016	NCT02683395	Ongoing/ recruiting	Solid tumors, hematologic malignancies
GSK2820151 (GlaxoSmithKline)	I	04/2016	NCT02630251	Ongoing/not recruiting	Solid tumors
ZEN-3694 (Zenith Epigenetics)	I	04/2016	NCT02705469	Completed	Castrate-resistant Prostate Cancer
	I	12/2016	NCT02711956	Ongoing/ recruiting	Castrate-resistant Prostate Cancer
INCB057643 (Incyte Corporation)	I/II	05/2016	NCT02711137	Ongoing/not recruiting	Solid tumors, hematologic malignancies
ODM-207 (Orion Corporation, Orion Pharma)	I/II	12/2016	NCT03035591	Ongoing/ recruiting	Solid tumors

I.4.1. Adverse events following treatment with BET inhibitors

The excitement emerging from the preclinical success of several BET inhibitors, supported on potent antitumor activities in a range of different genetic contexts, led to rapid clinical translation of these molecules. As observed in Table 1, an impressive amount of 16 different BET bromodomain inhibitors are being already tested in dose escalation clinical trials to investigate safety, tolerability, pharmacokinetics, pharmacodynamics, and clinical activity for a number of cancers. Furthermore, besides NMC which has a clear justification considering the urgent need for therapy, clinical studies are ongoing in tumors as diverse as treatment-refractory AML and myelodysplastic syndrome, lymphoma, multiple myeloma, TNBC and ER^+ breast cancers, small cell and NSCLC, CRPC, PDAC, colorectal cancer, neuroblastoma and *MYCN*-driven tumors Table 1.[134,140] In most of these trials the rationale for BET inhibition application does not involve translocations of BET BRD proteins, and Myc inhibition by itself will likely have little advantage over traditional antimetabolite chemotherapeutic approaches. Furthermore, as indicated in Chapter I.2.2, BET proteins can regulate transcriptional networks both as co-activators and co-repressors depending on the cellular context, and whose impact seems not to be

covered in current clinical trials. As a result, substantial setbacks are being detected in the preliminary results from the initial clinical studies.

The main toxicities observed for OTX015 in phase I trials in patients with hematologic malignancies were thrombocytopenia, anemia, neutropenia, GI symptoms which included nausea, diarrhea and dysguesia), fatigue and bilirubin elevation (Table 2).[103,131,132,135,138] Although the results are yet preliminary, thrombocytopenia, fatigue, GI symptoms and hyperbilirubinemia are also among the side effects reported for other BET inhibitors in both hematologic malignancies and solid tumors.[133,136,137] Furthermore, the development of BAY 1238097 was prematurely interrupted while performing the first-in-human dose-escalation phase I studies due to severe adverse events as dose-limiting toxicities (DLTs) were observed at subtherapeutic doses of drug.[139] Additional results from the ongoing studies should elucidate further on the safety profile of these compounds, but the adverse events observed so far promise to create a significant impact on BET inhibitor treatment compliance.

Also, reports based on preclinical data have been published that alert for potential safety concerns and further side effects involving BET inhibition. BET proteins, and particularly BRD4, are responsible to supress the Human Immunodeficiency Virus (HIV) transcription in infected cells by disrupting the interaction between HIV transactivator Tat and P-TEFb.[141] In fact there are published warnings showing that (+)-JQ1 and OTX015 can reactivate HIV-1 transcription in latent infected human T cells through that same mechanism.[142,143] Along with this, there is preclinical evidence of BRD2/4-mediated activation of DNA replication in HPV,[49,144] human herpes simplex virus 1 and 2,[145] and hepatitis B virus.[146] Reactivation of these viral infections can thus arise as adverse events following BET inhibition and should be closely monitored. Furthermore, recent reports in animal models revealed that strong suppression of BRD4 has dramatic effects in multiple tissues, including epidermal hyperplasia, alopecia, and decreased cellular diversity and stem cell depletion in the small intestine.[147] BRD4 has also been strongly implicated in the maintenance of embryonic stem cell renewal and in the control of cell fate decisions by positively regulating the expression of pluripotency genes.[148] Indications of memory deficits in mice following treatment with (+)-JQ1,[149] and development of an autism-like syndrome following treatment I-BET858[150] have also raised concerns, suggesting potential neurologic symptoms following BET treatment.

Collectively, these results indicate that BET inhibitors can be toxic and that better molecules as well as better understanding of the precise biological functions of these proteins are urgently needed. Significant efforts are being made to circumvent BET inhibition risks for toxicity that can lead to poor translation to the clinics. A better understanding of the mechanisms underlying BET inhibition has been pursued through the development of small-molecules with a better selectivity towards each protein

member.[109,151] Because of their lack of selectivity, current pan-BET bromodomain inhibitors constitute a major limiting issue for the elucidation of specific functions of BRD2, BRD3 or BRD4.[140] Others are exploring the use of synergistic therapies to enhance the potency and avoid toxicity of BET inhibitors. These have been tested in different cancers in combination with a wide range of drugs including HDAC inhibitors, kinase inhibitors, Bcl-2 inhibitors, immunomodulatory drugs and chemotherapeutic agents.[119,152-155] Finally, BET inhibition may be transformed by newer research with proteolysis targeting chimera (PROTAC) technology, with preliminary data suggesting that it can be more cytotoxic than pharmacologic BET inhibition in multiple tumor types.[156-159] Alternatively though, overcoming the non-specific actions by targeting tumor cells more selectively than healthy cells remains, to the best of our knowledge, an unmet need for BET inhibitors.

Table 2. Available clinical data including preliminary antitumor activity and main toxicities observed with BET inhibitors.

Drug	***Author***	***Tumor type(s)***	***Responses Observed***	***Adverse events***
OTX015	*Berthon, et al.*[131]	AML[i]	N[d]=41: CR[e]=2; PR[f]=3	• Thrombocytopenia • Anemia • Neutropenia • Hyponatremia • GI[c] toxicities • Fatigue • Bilirubin increase • Rash limited compliance
	Amorim, et al.[132]	Non-Hodgkin lymphoma	N=33: CR=2; PR=1	
		Multiple Myeloma	N=12: NR[g]	
	Stathis, et al.[103]	NMC	N=4: PR=2	
	Massard, et al.[135]	NMC	N=10: PR=3	
		CRPC[a]	N=36: PR=1	
		NSCLC[b]	N=9: NR	
	Hottinger, et al.[138]	GBM	N=12: NR	
CPI-0610	*Abramson, et al.*[133]	Non-Hodgkin lymphoma	N=44: CR=2; PR=1	• Thrombocytopenia • Diarrhea
GSK525762	*O'Dwyer, et al.*[137]	NMC[j]	N=10: PR=2	• Thrombocytopenia • GI[c] toxicities • Anemia • Fatigue • Bilirubin increase
TEN-010	*Shapiro, et al.*[136]	NMC	N=3: PR=2	• Irritation at the injection site • Indirect bilirubin increase

				• Anorexia
BAY 1238097	*Postel-Vinay, et al.*[139]	Solid tumors	N=8: NR	• Recurrent headaches • Vomiting • Low back pain *(Development halted as DLTs[h] occurred at subtherapeutic doses)*

[a] CRCP, castrate-resistant prostate cancer; [b] NSCLC, non-small cell lung cancer; [c] GI, gastrointestinal; [d] N, number of patients; [e] CR, complete remission; [f] PR, partial remission; [g] NR, no response; [h] DLT, dose-limiting toxicity; [i] AML, acute myeloid leukemia; [j] NMC, NUT Midline Carcinoma.

I.5. Ligand-targeted drug delivery

One attractive approach to overcome the aforementioned adverse events following treatment with BET inhibitors is to promote their selective accumulation at the tumor microenvironment while sparing healthy cells. Targeted drug delivery has been applied to many chemotherapeutic agents in clinical use and consists on the linkage of the established therapeutics to a targeting ligand that can deliver the attached motif selectively to the pathologic cell. This strategy shows great promise to maximize the safety and efficacy of a given therapeutic drug, as their selective delivery into diseased cells permits avoiding the nonspecific uptake and associated toxicities to healthy cells,[160] that can result in higher maximum tolerated doses (MTD). Most anticancer drugs need to be used near their MTD to achieve a clinically meaningful therapeutic effect, which significantly impairs the therapeutic window of these compounds.[161] For example, the FDA-approved antibody-drug conjugate trastuzumab emtansine (T-DM1) has a reported maximum tolerated dose (MTD) of 40 mg/kg in rats and 30 mg/kg in monkeys, whereas the free drug, DM1, has an MTD of 0.2 mg/kg.[162] Concomitantly, the MTD of FDA-approved monomethylauristatin E – brentuximab is 100 mg/kg in mice, whereas the free drug is only 1 mg/kg.[163,164] Ideally, targeted drugs can even be administered at lower doses than their nontargeted counterparts, since receptor binding and internalization can promote the concentration of the conjugates in the tumors microenvironment bearing receptor-positive pathologic cells.[165]

Over the last years many antigens that are highly expressed on the surface of malignant cells were identified, giving the momentum to exploit the unique binding properties of monoclonal antibodies as a mechanism for the selective delivery of cytotoxic drugs to cancer cells. The early success of this strategy sparked rigorous research in the field, with four FDA-approved antibody-drug conjugates (ADCs) currently available on the market for cancer therapy applications. Brentuximab vedotin (Adcetris®) was approved in 2011 for the treatment of relapsed HL and systemic anaplastic large cell lymphoma (ALCL), [164] while trastuzumab emtansine (Kadcyla®) was approved in 2013 for $HER2^+$ metastatic breast cancer.[166,167] In 2017 two additional ADCs were approved by the FDA, namely

inotuzumab ozogamicin (Besponsa®) for the treatment of relapsed or refractory B-cell precursor ALL,[168,169] and gemtuzumab ozogamicin (Mylotarg®) which was again approved for the treatment of CD33-positive AML after gaining its approval in 2000 and being voluntarily withdrawn in 2010 after subsequent confirmatory trials failed to verify clinical benefit and demonstrated safety concerns.[170] More than 65 ADCs are currently under clinical evaluation.[171]

Although the selective delivery of cytotoxic agents to tumor cells by means of ADCs is an attractively simple concept, it proved challenging to translate into clinical practice. There are a number of limitations to the performance of ADCs, namely related to their ability to reach cells within the tumor mass. Tumors are not homogenous masses and loss of antigen expression has been reported.[172] Furthermore, the size of the antibodies exerts a significant impact on the pharmacokinetics of an ADC, as bigger molecules (Mr > 40 000) circulate in the blood for several days. For example, Adcetris (Mr ≈ 150 000) has a half-life of 4-6 days.[173] This slower clearance kinetics can result in premature drug release, greater accumulation in excretory organs and potential adverse events. Moreover, large molecules do not exit blood vessels efficiently which results in poor diffusion into tissues, significantly compromising the bioavailability of ADCs near tumor cells that are located further away from blood cells.[174] Along with this, antibodies can be immunogenic even when they are humanized or fully human.[174] Thus, the limitations of antibodies as targeting vehicles provide a strong rationale to explore alternative strategies, including the use of low molecular weight ligands as delivery vehicles.

I.5.1. Small molecule drug conjugates

Low molecular weight ligands targeting a specific deregulated pathway show great promise as vehicles of drug delivery into cancer cells, and may overcome some of the limitations observed for ADCs. The use of smaller molecules allows prompt diffusion out of blood vessels in a matter of seconds, while also rapidly penetrating deep into tissues.[174] Their pharmacokinetics is also more favourable in comparison with ADCs, as small molecule drug conjugates (SMDC) can be quickly excreted from the body thus avoiding unwanted toxicities due to prolonged exposure. For example, the low molecular weight cancer agent etarfolatide, consisting of a folate-^{99m}Tc conjugate (Mr ≈ 856), has a half-life of only 27 min.[160] Moreover, small organic ligands can be chemically synthesized and specifically tailored for enhanced affinity and specificity towards an overexpressed receptor in the surface of tumor cells.

A number of studies validate the use of small molecular weight ligands as vehicles for selective drug delivery.[174-178] The vitamin folic acid (FA) has been successfully explored to deliver drugs more

effectively to cancer cells. Folic acid has high affinity towards the folate receptor, whose expression is largely absent in normal tissues and abundant in many tumors.[179] Up to date five folate-based small-molecule drug conjugates have been evaluated in clinical trials, including vintafolide (EC145). EC145 consists on a folic acid molecule conjugated to desacetylvinblastine hydrazide (DAVLBH) drug *via* a hydrophilic peptide spacer and a disulfide-containing self-immolative linker, and is currently undergoing phase 2 trials for several types of cancer.[180,181] Interestingly the folic acid/folate receptor mediated targeting is also being explored to develop folic-acid-targeted imaging agents. A first-in-human study was recently published, where a folate-FITC (fluorescein isothiocyanate) conjugate is used for real-time surgical visualization of tumor tissue in patients undergoing an exploratory laparotomy for suspected ovarian cancer.[182]

The conjugation of small ligands targeting the prostate-specific membrane antigen (PSMA) with imaging tools and anticancer agents has also been widely explored. PSMA is an ideal target and well-established marker of prostate cancer (PCa), as it is overexpressed on almost all PCa cells while being largely absent in healthy cells. Furthermore the levels of PCa overexpression were found to become increasingly higher as the disease progresses.[177] One of the PSMA-targeting ligands that have been developed to favor the accumulation of drugs and imaging tools near the PSMA-positive-malignant tissues is 2-[3-(1,3-dicarboxypropyl)-ureido]pentanedioic acid (DUPA). A series of PSMA-targeted ^{99m}Tc-chelate complexes were designed and synthesized for imaging PSMA-expressing human prostate cancer (LNCaP) cells. In *in vitro* assays these were found to effectively bind LNCaP cells in the nanomolar range (K_D = 14 nM), whereas *in vivo* a strong accumulation in LNCaP tumor xenografted mice (11.2 % ID g^{-1}) was observed.[177] DUPA has also been studied in conjugation with several potent cytotoxic drugs, as discussed with greater detail in Chapter V.1.2.

Recently a small-molecule drug conjugate for the treatment of tumors expressing Carbonic Anhydrase IX (CAIX) was also developed. CAIX is membrane bound-enzyme that is also a very attractive target for the selective delivery of drugs since its expression is highly enhanced in many different solid tumors in response to hypoxia or when the von Hippel-Lindau tumor suppressor protein (pVHL) is inactivated.[175] Particularly in renal carcinoma CAIX is constitutively expressed and is well established as a surface marker of this disease. In these studies, the best ligand for selectively targeting CAIX, a derivative of acetazolamide, was obtained from a DNA-encoded chemical library followed by a number of structure-activity relationships to establish high-affinity CAIX ligand-linker-payload conjugates. These consisted of either duocarmycin or DM1 cytotoxic drugs attached to the selective CAIX ligand by a disulfide linker and a peptide spacer. The duocarmicyn conjugates only indicated modest tumor growth inhibition in mice bearing subcutaneous SKRC52 tumors, while a potent antitumor effect was observed for the DM1 conjugate. Most importantly these conjugates exhibited a greater

antitumor effect when comparing with the clinically used treatment for kidney cancer, namely the kinase inhibitors sorafenib and sunitinib (standard doses of 30 mg/kg).[174,175]

The use of small-molecule ligands for the targeted delivery of cytotoxic drugs into malignant tissues is less well established in comparison with antibody-drug conjugates. However, as shown by the examples above this novel approach promises to dramatically improve the kinetics, selectivity and tissue penetration of established and less effective chemotherapeutic agents, overcoming the increasingly clear limitations of current ADCs. Thus, we proposed to systematically investigate the hypothesis of using small molecule ligands for the selective delivery of BET inhibitors into cancer cells.

General Objectives of the Thesis

In the last few years BET proteins have been strongly implicated in cancer, and modulation of their activity with small molecular weight effectors has displayed strong phenotypic responses and therapeutic benefits in various malignant preclinical models. The enthusiasm for the anti-proliferative potential of these BET inhibitors led to several cancer clinical trials against hematologic and solid tumors. However, preliminary data from those early clinical trials have raised concerns, mainly due to severe adverse side effects and limited compliance following treatment. On the other hand, the reversible attachment of a small-molecule drug to a tumor-specific ligand for targeted delivery can markedly improve pharmacokinetics and the therapeutic index of these drugs.

The aim of this project is to develop a strategy for the selective delivery of a BET inhibitor to malignant cells, while sparing healthy tissues and its collateral toxicity profile. To accomplish this, we rationally engineered a construct that allows an efficient and traceless targeted release of a BET-inhibitor in a given cancer indication.

Considering the advantages of SMDCs over ADCs, we focus on the design of this class of drugs for the delivery of a BET inhibitor. In Chapter II. we start by exploring how a non-specific therapeutic agent needs to meet certain requirements to be selectively delivered in target cells. Therein the first objective is to identify and validate an ideal BET inhibitor candidate suitable for drug delivery approaches.

Having selected and validated an ideal BET inhibitor candidate our second goal is to chemically functionalize this compound so that it can accommodate a cleavable bond. Tertiary amine-containing bioactive molecules connected to carrier antibodies using bioreversible linkages have been successfully applied to deliver antibiotics to target cells. Bearing this in mind, in Chapter III. we will base our synthetic design on the derivatization of the BET inhibitor candidate to include a tertiary amine suitable to be exploited in traceless releasing strategies. The new BET-protein effectors will be thoroughly characterized in their binding modes and affinities to BET protein targets. In Chapter IV. we aim to extensively profile the new compounds for their antitumoral activity and therapeutic potential, particularly in a given responsive tumor tissue that can be exploited for targeted delivery approaches.

Finally, in Chapter V. we aim to assemble a unique targeted-BET inhibitor conjugate by tethering the designed BET effectors to a cleavable linker technology and to a ligand conferring specificity to a particular tumor model.

Chapter II

Selection and validation of a BET effector for conjugation

Rui Traquete,[1] João D. Seixas,[1] Tiago Rodrigues,[1] Inês S. Albuquerque,[1] Florian Sieglitz,[1] Pedro M.P. Gois,[3] Gonçalo J. L. Bernardes,[1,2]

[1] Instituto de Medicina Molecular João Lobo Antunes, Faculdade de Medicina, Universidade de Lisboa, Avenida Professor Egas Moniz, 1649-028 Lisboa, Portugal

[2] Department of Chemistry, University of Cambridge, Lensfield Road, CD2 1EW Cambridge, UK

[3] Research Institute for Medicines (iMed.ULisboa), Faculty of Pharmacy, Universidade de Lisboa, Av. Prof. Gama Pinto, 1649-003, Lisboa, Portugal

Author Contributions

R.T. and G.J.L.B. designed the experiments. R.T. performed the synthesis, biochemical and cellular characterization of the compounds. J.D.S. and P.M.P.G. helped in the organic synthesis, T.R. helped with the docking simulations, I.S.A. helped with the flow cytometry analysis and F.S. helped with the confocal imaging studies. R.T. wrote the chapter, G.J.L.B. directed the research and revised the text.

Chapter II. Selection and validation of a BET effector for conjugation

II.1. Introduction

In the targeted delivery of drugs, it is the activity of the payload that primarily determines the therapeutic efficacy of the conjugate. The main criteria to be considered are the potency and specificity of the drug towards the molecular target. Highly potent drugs are preferred, with an IC_{50} of < 10^{-8} M usually found sufficient.[165] As mentioned earlier in Chapter I.3.1 several effectors of BET bromodomain protein-protein interactions have been developed. These successfully displace BET BRD proteins such as BRD4 from chromatin, leading to strong antitumor phenotypes through the inhibition of oncogenic transcriptional programs.[17,71,76,104] The hydrophobic nature of the KAc binding cavity in BET proteins together with high druggability scores[77] found for BET family members ignited significant interest in the development of such strong inhibitors with marked phenotypic changes. Among these are I-BET762 (BRD4(1/2) IC_{50} = 36 nM, FRET), (+)-JQ1 (IC_{50} = 77 nM, AlphaScreen), I-BET151 (BRD4(1/2) IC_{50} = 36 nM, FAP) or PFI-1 (BRD4(1) IC_{50} = 220 nM, AlphaScreen), among others as outlined in (Figure 5).[78]

In addition, adequate membrane permeability should also be contemplated. Most targeted conjugates enter cells by endocytosis, and therefore drugs must be able to escape the endosome compartments in order to be therapeutically active. Along with this, aqueous solubility, intracellular stability and lack of immunogenicity also influence significantly the outcome of ligand-conjugates performance and consequently the selection of a potential drug candidate.[165] In this regard, despite being a prime tool for a large body of preclinical work on BET inhibition, (+)-JQ1 has select pharmacologic characteristics including a short half-life of one h, and that preclude its clinical use and limit the ability to translate preclinical success into clinical benefit.[17]

In conjunction with the potency of a drug, it is its amenability for conjugation that ultimately drives the therapeutic success of a targeted approach. Without the possibility to successfully attach additional substituents to the therapeutic warheads a ligand-drug conjugate cannot be developed. Thus, it is critical that the selected payload has sites that can be used for derivatisation without affecting potency. The most common groups used for functionalization are hydroxyls, carboxyls, amines, carbonyls and thiols.[160] Considering all the criteria mentioned above the ligand I-BET762 stood out among its counterparts, as it will be explained further. Thus, I-BET762 was used in this study as model drug candidate for the targeted delivery of a BET-bromodomain effector.

II.1.1. I-BET762 as a candidate for targeted delivery

The discovery of I-BET762 and other triazolobenzodiazepine scaffolds was established by a phenotypic screening to ApoA1 expression, followed by lead compound optimization.[183] These compounds upregulated ApoA1 expression through mechanisms then unknown, however structure activity relationship studies suggested a defined protein target for the molecule. The benzodiazepine core was essential for activity, as was the aryl group extending from the 6-position, along with a significant influence of the C(4) stereochemistry on the effector potency.[78] Further experiments using a chemoproteomic approach identified the targets as being BET bromodomain proteins. From here a number of reports demonstrated I-BET762 excellent profile as a drug candidate. Not only it showed a high affinity to target proteins as discriminated above, but also high solubility in physiological relevant media, low plasma protein binding, good passive permeability, excellent metabolic stability and lack of immunogenicity.[46,184] More importantly for the goal of this project, high-resolution crystal structures suggest compound tolerability for derivatization. Indeed, it is now well established that binding of I-BET762 to BET bromodomain proteins occurs mainly through hydrogen bridges between the nitrogen atoms in the triazole ring and the conserved asparagine and tyrosine residues (N156 and Y113 in BRD2(1), N140 and Y139 in BRD4(1)).[183] The fused phenyl ring and the phenyl group at the 6-position of the benzodiazepine core bind into the lipophilic pocket (ZA channel) and the hydrophobic region (WPF channel) respectively (Figure 7).[183] These data suggest that derivatization of the amide group in I-BET762 should be possible while preserving the putative ligand–receptor interactions. In fact, this position was already functionalized with the fluorophore Alexafluor 488 in order to determine molecule binding kinetics through fluorescent polarization assays.[183] In addition, medicinal chemistry optimization by Mirguet *et al.* focusing on the improvement of I-BET762 lipophilicity and solubility introduced derivatives in the same region of the molecule,[185] further suggesting that at this position functionalization is tolerable and should not impair significant binding interactions. Concomitantly, the synthesis of the carboxamide **(2)** (Figure 5) by Constellation Pharmaceuticals using structure-guided lead-optimization approaches against BRD4(1) strengthened this rationale. This chapter is focused on the validation of I-BET762 as a candidate for the selective delivery of a BET-inhibitor to cancer cells and, in particular, its potential for chemical functionalization.

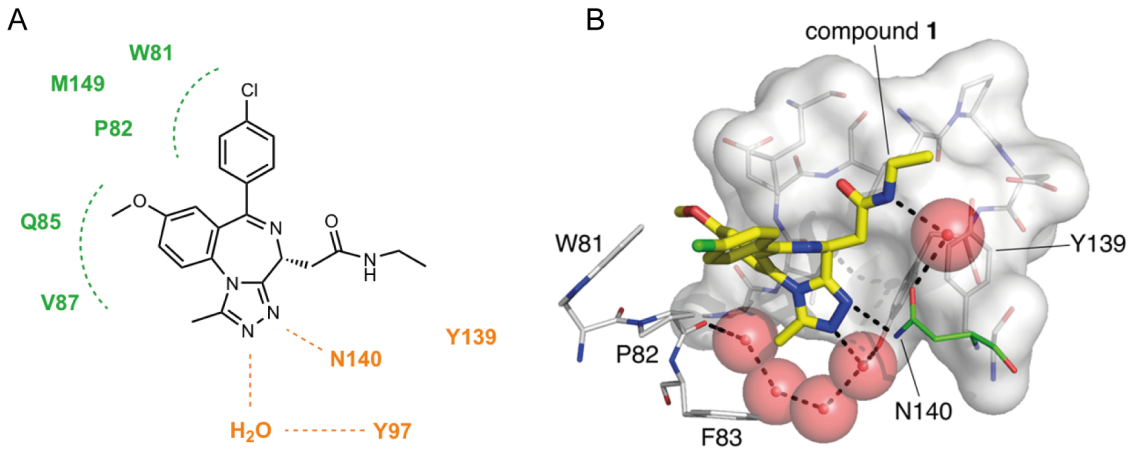

Figure 7. I-BET762 binding mode to BET-bromodomain proteins. (A) Identification on I-BET762 backbone of the residues critical for acetyl-lysine recognition (orange) and the residues stabilized by the WPF shelf (green); (B) Docking of **I-BET762** (**1**) in the pocket of BRD4(1) and representation of Kac binding mimicking groups. Adapted from reference [78].

II.2. Goals

In this chapter, the small molecule ligand towards BET-bromodomain proteins, I-BET762, will be evaluated in its potential to accommodate traceless release and targeted delivery approaches.

To achieve this the large-scale organic synthesis of I-BET762 will be implemented *in house* and the BET effector will be characterized in terms of binding affinity to molecular targets and cellular activity against relevant models of malignancy.

The validation of I-BET762 has potential therapeutic payload for targeted delivery strategies will be performed through its derivatization with bulky substituents *via* different spacer chemistries. The binding affinity of the functionalized molecules against molecular targets will be compared with the unmodified I-BET762.

Finally, the attached fluorophores will be used to exploit membrane permeability and intracellular localization of the new derivatives.

II.3. Analysis of I-BET762 as a BET-inhibitor candidate for tumor traceless release

II.3.1. Synthesis and characterization of I-BET762

The synthetic route leading to **I-BET762** was applied using established literature procedures[185] and is depicted in Scheme 1. We followed the methodology developed by Mirguet *et al*. as this led to the formation of a pure (S)-enantiomer, while the original synthetic route originated a racemate mixture of final compound.[183] This resulted from the thionation step involving Lawesson's reagent and which led to the epimerization of compound **10**. Considering that the activity of I-BET762 is critically dependent on the stereochemistry at the 4-position, with the original reaction conditions the enantiomers had to be separated by preparative chiral HPLC, a procedure that was considered arduous and time-consuming.[183] Conversely, running the thionation step in the presence of phosphorous pentasulfide and sodium carbonate rendered the final compound **I-BET762 (1)**.

After establishing the synthetic route for **I-BET762**, its affinity against BET bromodomain targets was characterized using Amplified Luminescence Proximity Homogenous Assay (Alpha) screen as the detection method. This technique is a bead-based proximity assay where a singlet oxygen generated by high-energy irradiation donor beads, travels to acceptor beads when a biological interaction brings the beads together. The generation of a cascade of chemical reactions ultimately leads to the generation of a chemiluminescent signal.[186] The data obtained showed a strong binding affinity of **I-BET762** against BRD4(1) (IC_{50} = 0.42 µM ± 0.13 log units) and BRD4(2) (IC_{50} = 0.30 µM ± 0.14 log units), suggesting that the compound was active against its target proteins (Figure 8). Interestingly, the efficacy was decreased considerably against the targets BRD2(1) (IC_{50} = 3.8 µM ± 0.13 log units) and BRD3(1) (IC_{50} = 12.3 µM ± 0.14 log units), though still displaying IC_{50} values in the low micro molar range (Figure 8).

Given that the **I-BET762** molecule synthesized is key for the development of new derivatives in the entire project, it was analysed whether it was also functional in a cellular context. For this purpose, we evaluated its ability to inhibit the growth of a prostate cancer cell line (LNCaP) in comparison with a commercially available version (Selleckchem, S7189). LNCaP cells are well established in literature as being responsive to the inhibition of BET bromodomains and particularly to **I-BET762**,[89,120] and was thus used as an *in vitro* model system for this exploratory assay. As observed in Figure 9, both compounds decreased cellular growth significantly at very low doses and in an equivalent manner **(I-BET762** gIC_{50} = 0.13 µM; commercial **I-BET762** gIC_{50} = 0.25 µM), further validating the activity of the synthesized **I-BET762**.

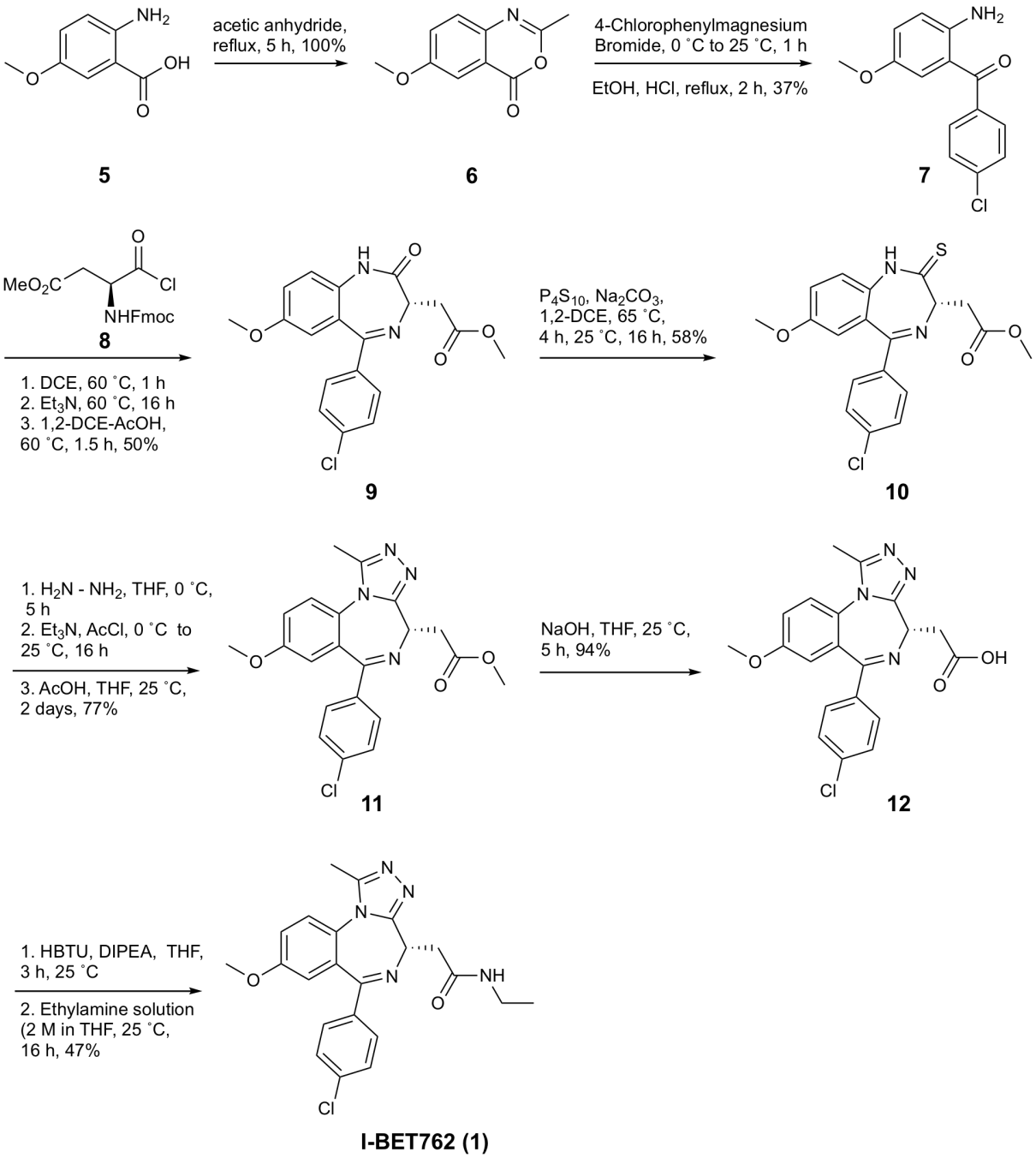

Scheme 1. Synthesis of I-BET762. Abbreviations: EtOH, ethanol; HCl, hydrochloric acid; DCE, dichloroethane; AcOH, acetic acid; P_4S_{10}, phosphorus pentasulfide; Na_2CO_3, sodium carbonate; $H_2N\text{-}NH_2$, hydrazine hydrate; THF, tetrahydrofuran; NaOH, sodium hydroxide; HBTU, *N,N,N',N'*-Tetramethyl-*O*-(1*H*-benzotriazol-1-yl)uranium hexafluorophosphate; DIPEA, *N,N*-Diisopropylethylamine.

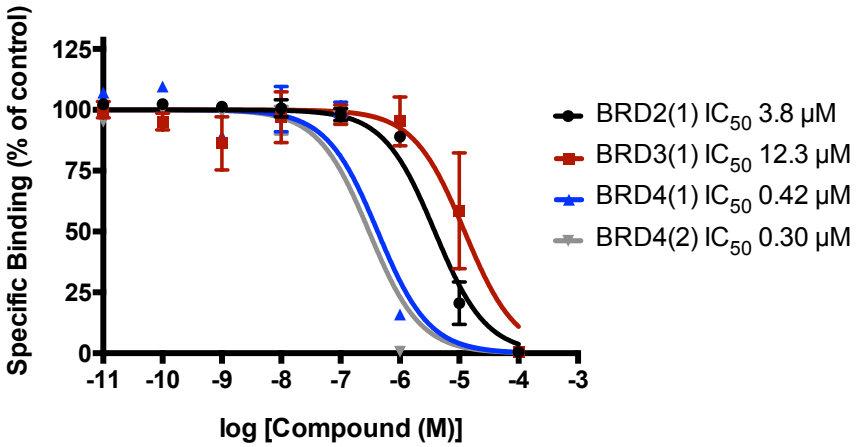

Figure 8. Binding affinity of synthesized I-BET762 (1) against BET-bromodomain protein targets.

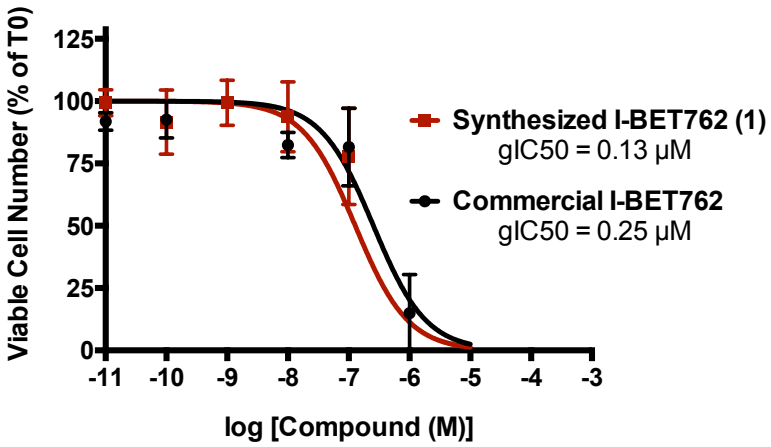

Figure 9. LNCaP growth inhibition after treatment with the synthesized I-BET762 (1) and its commercial version.

II.3.2. Conjugation site validation with I-BET762 – fluorescein derivatives

After establishing its organic synthesis, the binding affinity and cellular activity, **I-BET762** was chemically functionalized with bulky substituents to confirm whether the conjugation site could be derivatised while retaining putative ligand-receptor interactions. Fluorescein was used as a model cargo and tethered to **I-BET762** through spacers with different lengths (Scheme 2). Ranging from a simple propyl chain (**13**), a 5-atom PEG **(14)** and 8-atom PEG (**15**) these moieties were considered for their distinct properties in modulating the activity of the construct. In general, longer linkers are preferred for bulky substituents, while PEGs in different sizes can contribute to the overall hydrophilicity of the conjugate.[165] The synthetic route leading to three different fluorescent-labelled **I-BET762**-based ligands is depicted in Scheme 3. Briefly, the diamine spacers were protected in one of their primary amines with *t*-butyloxycarbonyl (Boc) protecting group, leaving the free amine for conjugation with the carboxylic acid

in intermediate **12**. HBTU was used as coupling reagent in the presence of diisopropylethylamine (DIPEA). Upon conjugation and purification of the Boc intermediate, this was deprotected using trifluoroacetic acid (TFA) in dichloromethane (DCM). The amine-reactive group was then conjugated with a fluorescein motif bearing a *N*-hydroxysuccinimide ester (NHS-ester). For negative control in biological studies, it was also synthesized a probe without ligand (compound **22**), as depicted in Scheme 4.

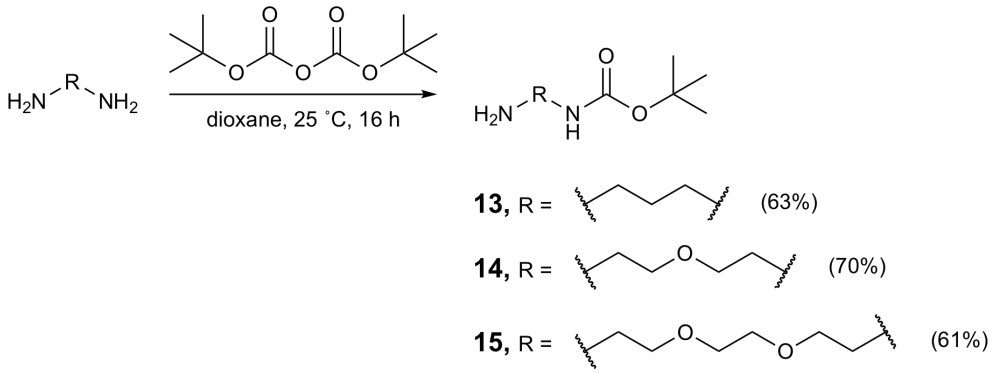

Scheme 2. Preparation of diamine spacers for conjugation, *via* single-protection with Boc.

Once the fluorescent probes were synthesized, purified and characterized, they were evaluated for their affinity towards BET-bromodomain proteins. As in the binding of **I-BET762** (Figure 8), these included establishing compound affinity towards BRD2(1), BRD3(1), BRD4(1) and BRD4(2) BET modules using AlphaScreen technology as the detection method. The retrieved data suggested that overall the compounds were able to bind efficiently to the target proteins despite the presence of a bulky substituent as fluorescein. Among all of them it was found a higher consistency in the binding data for BRD4(1) and BRD4(2) proteins. Against both of these proteins though, there was a clear decrease in the binding potency. This was evident for all compounds in BRD4(2) with a 6- to 10-fold decrease in comparison with **I-BET762** (IC_{50} = 0.3 μM), and for the PEGylated probes **21** (IC_{50} = 2.77 μM, 7-fold decrease) and **20** (IC_{50} = 5.22 μM, 12-fold decrease) in BRD4(1) (Figure 10). Interestingly, compound **19** comprising a simple propyl chain as spacer was found binding with high affinity to BRD4(1) (IC_{50} = 0.85 μM). Yet when analysing the affinity of compounds across the different proteins no correlation between spacer chemistry and binding potency was observed. While the latter compound was 16 times more potent (IC_{50} = 0.24 μM) than **I-BET762** (IC_{50} = 3.9 μM) against BRD2(1), the same compound was unable to induce competitive peptide displacement in BRD3(1) at concentrations as high as 100 μM (Figure 10). If not assay-dependent, these data might suggest different binding requirements to the active site of each domain.

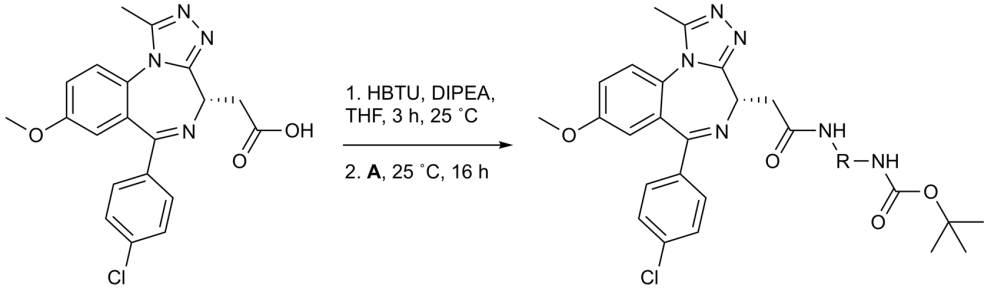

16, A = compound **13** (45%)
17, A = compound **14** (75%)
18, A = compound **15** (56%)

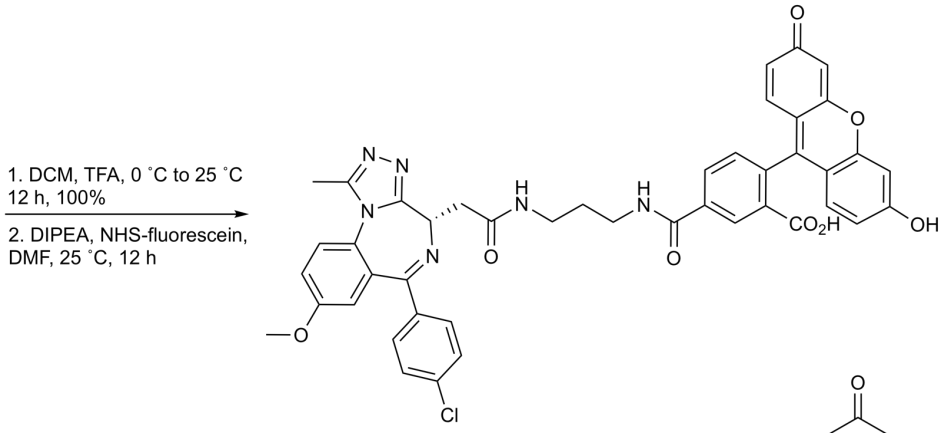

19 (23%)

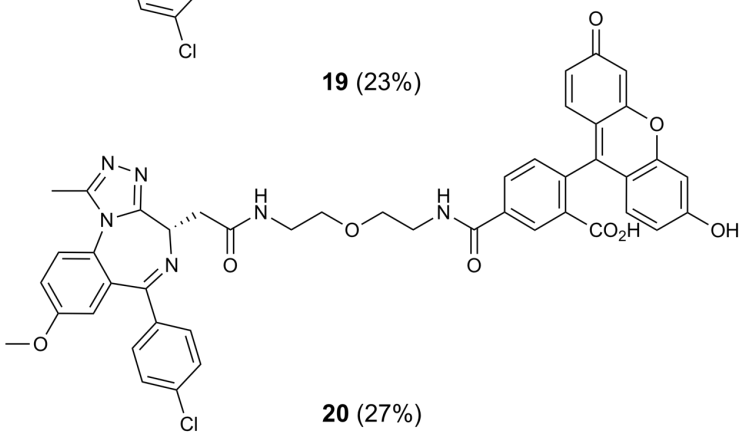

20 (27%)

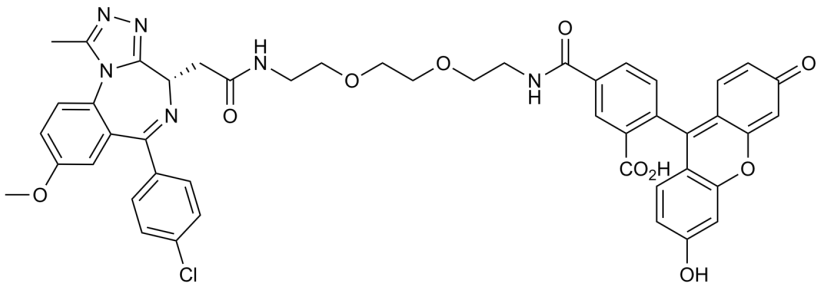

21 (76%)

Scheme 3. Synthesis of several I-BET762 – fluorescein conjugates with different spacer chemistries. Abbreviations: HBTU, *N,N,N',N'*-Tetramethyl-*O*-(1*H*-benzotriazol-1-yl)uranium hexafluorophosphate; DIPEA, *N,N*-Diisopropylethylamine; THF, tetrahydrofuran; DCM, dichloromethane; TFA, trifluoroacetic acid; NHS, *N*-hydroxysuccinimide; DMF, dimethylformamide.

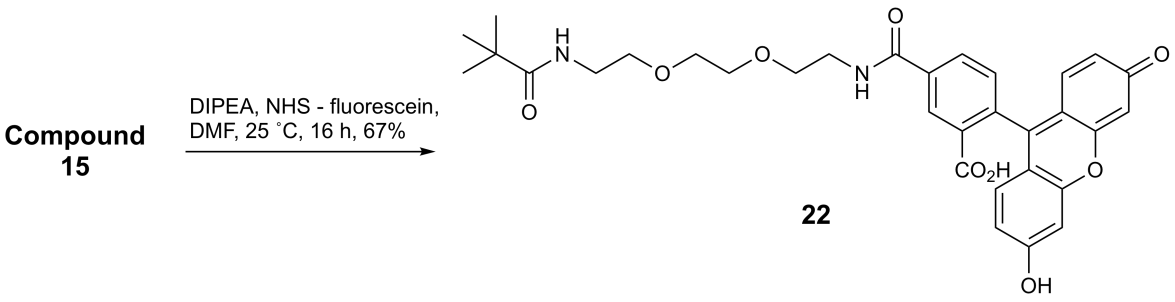

Scheme 4. Synthesis of a fluorescent probe without a BET ligand. Abbreviations: DIPEA, *N,N*-Diisopropylethylamine; NHS, *N*-hydroxysuccinimide; DMF, dimethylformamide.

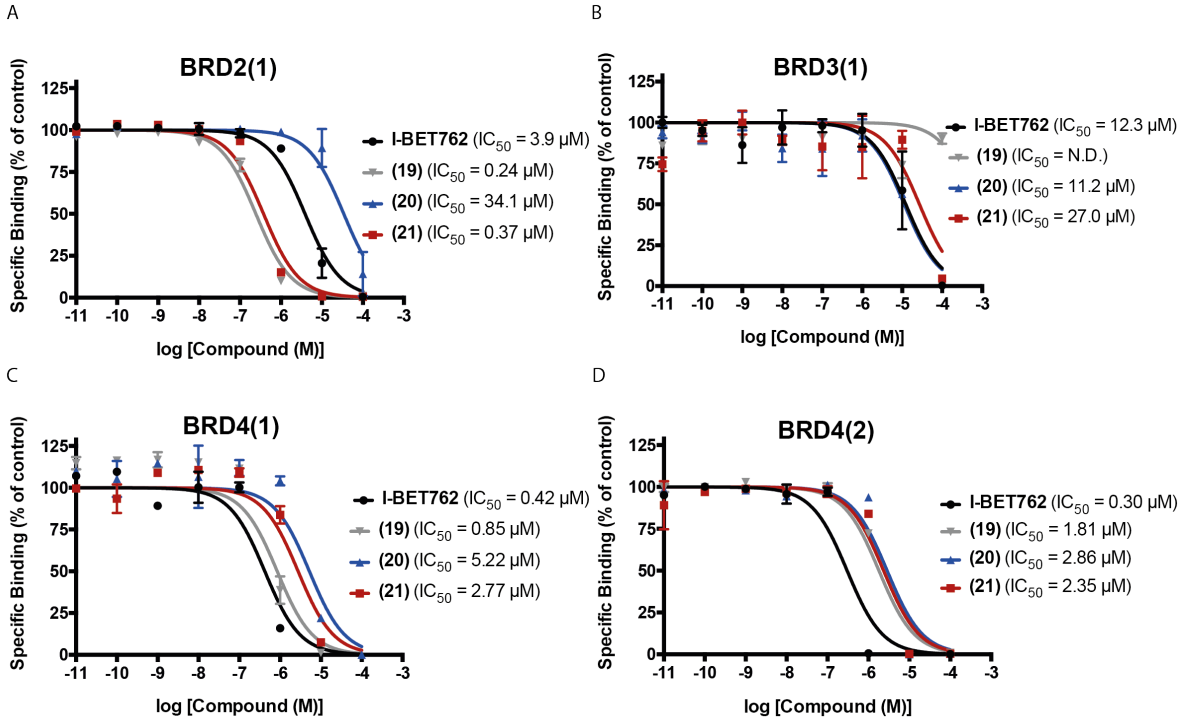

Figure 10. Binding affinity of fluorescent-labelled probes towards the BET-proteins BRD2(1), BRD3(1), BRD4(1) and BRD4(2).

The protein-ligand interaction mode of the fluorescent-labelled molecules was then simulated in docking studies using PyMOL software. The target BRD4(1) was used as template. These simulations confirmed that despite the bulky attachment of spacers and fluorescein, both **20** and **19** maintained a binding mode equivalent to the one in parent compound I-BET762 (Figure 11). This involved the triazolyl ring as the main interaction in the BRD4(1) pocket, leaving the appended spacer and fluorescein moieties exposed to the solvent. Interestingly the docking simulation of compound **21** suggests a slightly different engagement with the binding pocket, yet no detailed conclusions can be drawn without additional investigations. Altogether this data indicates that, regardless of the spacer size, functionalization is well tolerated at this conjugation site.

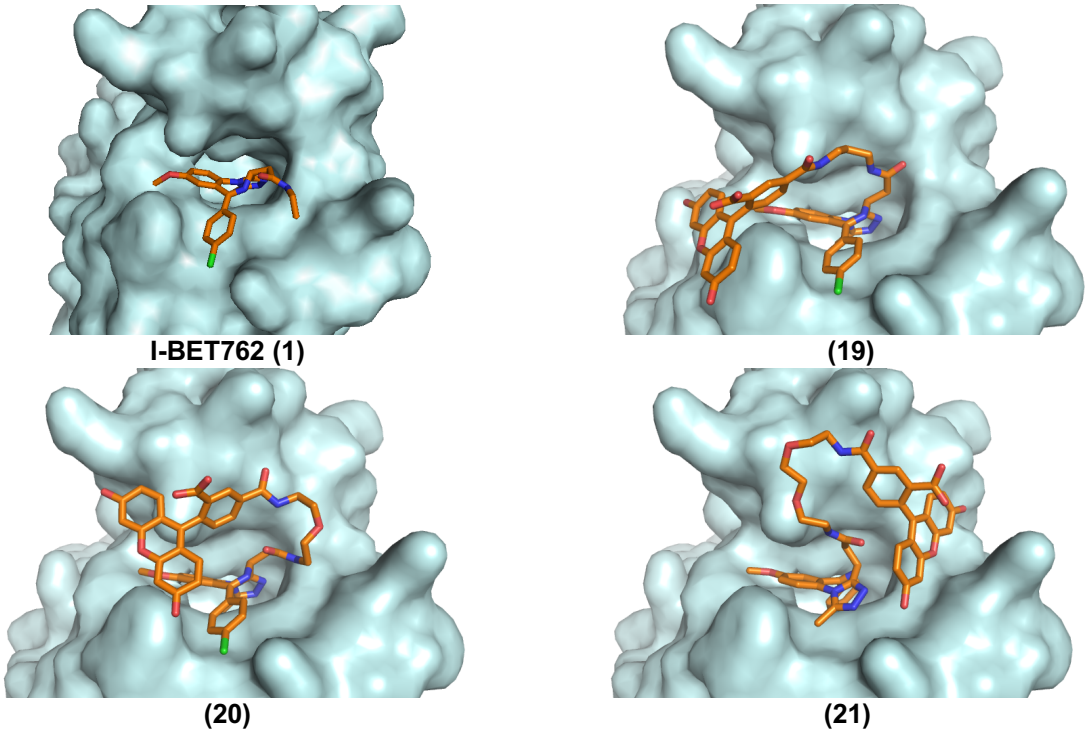

Figure 11. Docking simulations of fluorescent-labelled ligands against BRD4(1).

II.3.3. Cellular internalization and trafficking of fluorescein-based derivatives

Fluorescence-based techniques are important research tools for probing intermolecular interactions. These have been used extensively in biology for quantitative ligand-binding assays including fluorescence polarization (FP) assays and fluorescence resonance energy transfer (FRET). However, the potential of ligand-fluorophore conjugates goes beyond their application in ligand binding kinetics. Indeed, by retaining most of the pharmacological profile of the parent unlabeled counterpart, a fluorescent probe can be useful in an array of pharmacological experiments including cellular localization, trafficking and signaling processes.[187]

With this in mind, the intracellular localization of the fluorescein-labelled conjugates was evaluated. As in our earlier study (depicted in Figure 9) LNCaP cells were used as *in vitro* model. In a preliminary experiment using flow cytometry the rate of compound internalization was measured as the total number of cells incorporating fluorescein. After 2 h treatment with 10 μM of compound **21,** only 0.8% of the total cells were positive for fluorescein (Figure 12A). When the doses were increased to 50 μM, 36.6% of the population of cells was fluorescent-labelled (Figure 12B). Yet, at these concentrations the treatment with compound **22**, which does not have a BET-targeting ligand (Scheme 4), also resulted in 12.6% of fluorescein-positive cells. This data suggested that most of the probe internalization at 50 μM doses

was non-specific. Non-functionalized **I-BET762** (with no fluorescein) was used for normalization to account for possible effects in cells induced by compound treatment.

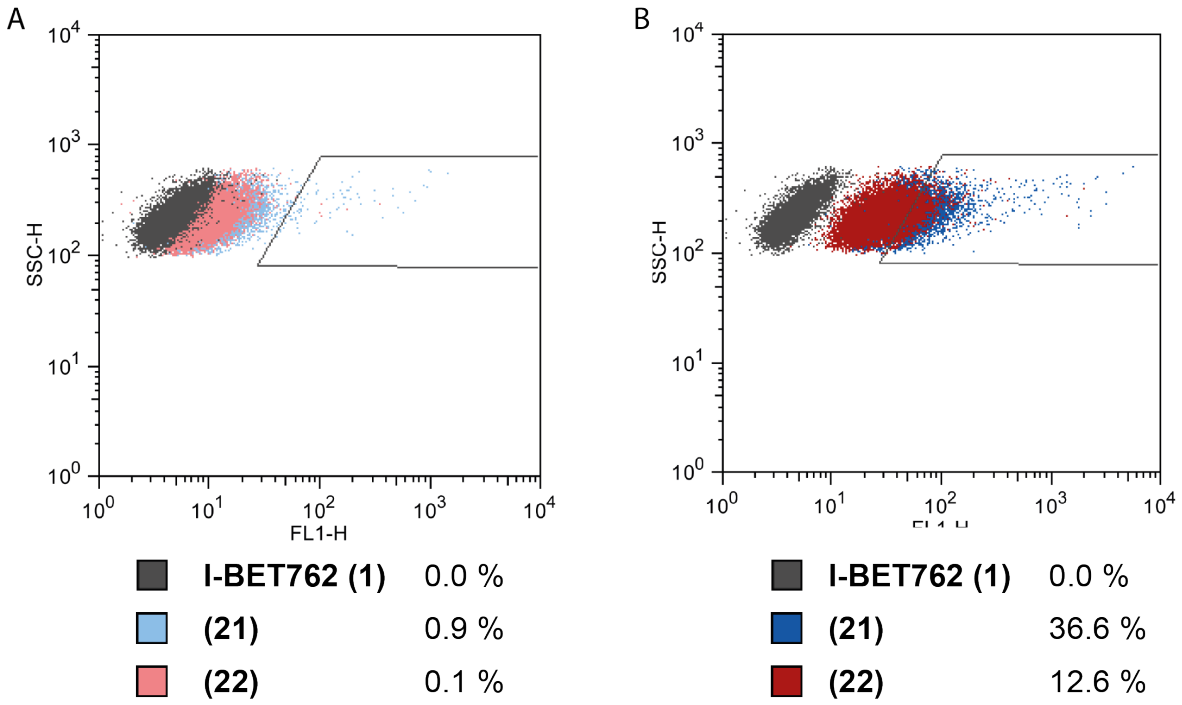

Figure 12. Flow cytometry analysis of fluorescein-positive cells after treatment with (A) 10 µM and (B) 50 µM of labelled conjugates (data represented as percentage of FITC+ cells).

Imaging experiments using confocal microscopy confirmed previous findings. LNCaP cells were incubated in the presence of 10 µM of compounds **21** and **22** for 2 h before images were captured. As observed in Figure 13F the amount of internalized dye was minimal in **21**-treated cells, yet greater than the control **22** without the BET-bromodomain ligand (Figure 13B).

It is reported that fluorescein has a high rate of fluorescence quenching and low photostability, which could explain the poor signal observed.[188] To investigate this further, the cellular membrane was disrupted with Triton X-100 detergent prior incubation with both conjugates. In these conditions all cells treated with compound **21** (Figure 13H) showed a pronounced fluorescent signal, whereas in samples treated with **22** still no staining was observed (Figure 13D). In addition, the fluorescent signal of **21** was much stronger in the nuclei where the BET-bromodomain proteins are localized, suggesting an efficient targeting in cells. Importantly, cells treated with the non-targeted fluorescent probe **22** were not stained even when the membrane is disrupted, emphasizing the role of the BET-based effector.

The same trend was observed when incubating cells with the fluorescent conjugate **19**, comprising only a 3-atom spacer. When disrupting the cellular membrane with a detergent, nuclei co-localization of

the BET-targeted fluorescent probes was observed (Figure 14D). However, internalization in live LNCaP cells with an intact cellular membrane was only modest (Figure 14F,H). Single-time point confocal images were taken after 1 and 4 h incubation with 10 μM doses, with no differences being observed.

Altogether, the data of **19** and **21** excluded the possibility for fluorescein photo quenching. Moreover, it also showed that similarly to what was observed in the biophysical assays for binding affinity (Figure 10), there is no correlation between spacer chemistry and the rate of cellular internalization. In order to understand why the fluorescent-labelled probes were effective when the membrane is disrupted but not in live cells, their diffusion across the cell membrane was studied with Parallel Membrane Permeability Assay (PAMPA). As observed in Table 3, the Pe values for the derivatised compounds **21** (0.22), **20** (0.36), **19** (0.4) and **22** (0.20) were close to the detection limit in the acceptor compartment. This indicated that the results for these compounds were comparable to the detection limit of low permeable standard atenolol. Conversely the parent molecule **I-BET762** alone was highly permeable. In summary, this data demonstrated that the diffusion across cellular membranes of the fluorescein derivatives is strongly impaired.

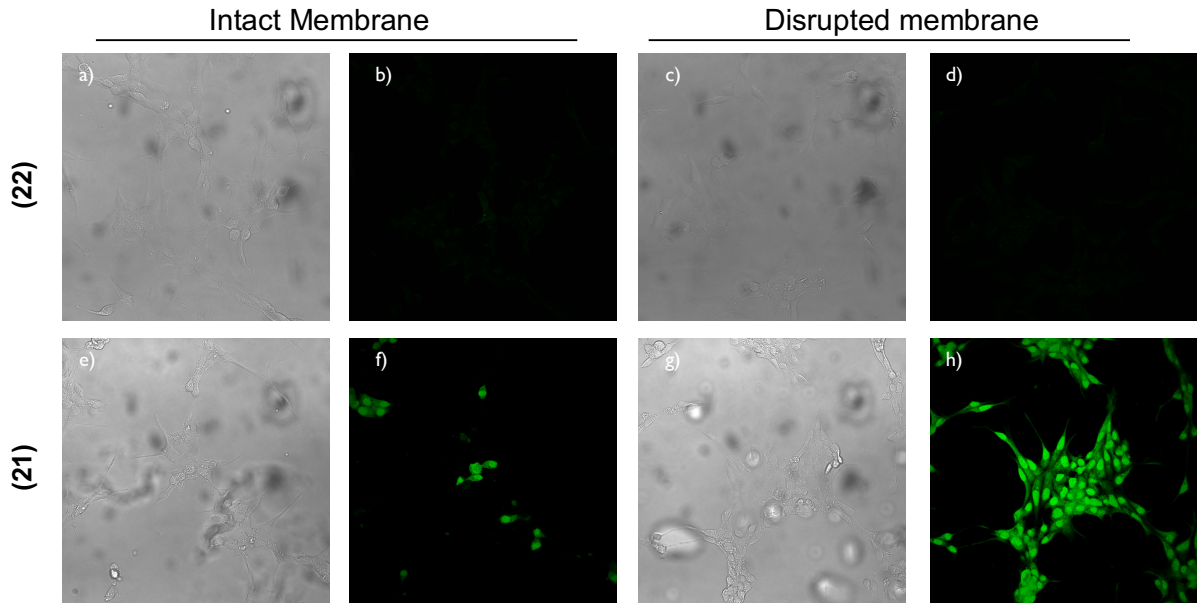

Figure 13. Confocal microscopy analysis on the internalization rate of **21** (e-h) and **22** (a-d) with and without membrane disruption. (40x magnification; Green: fluorescein; grey: transmitted light)

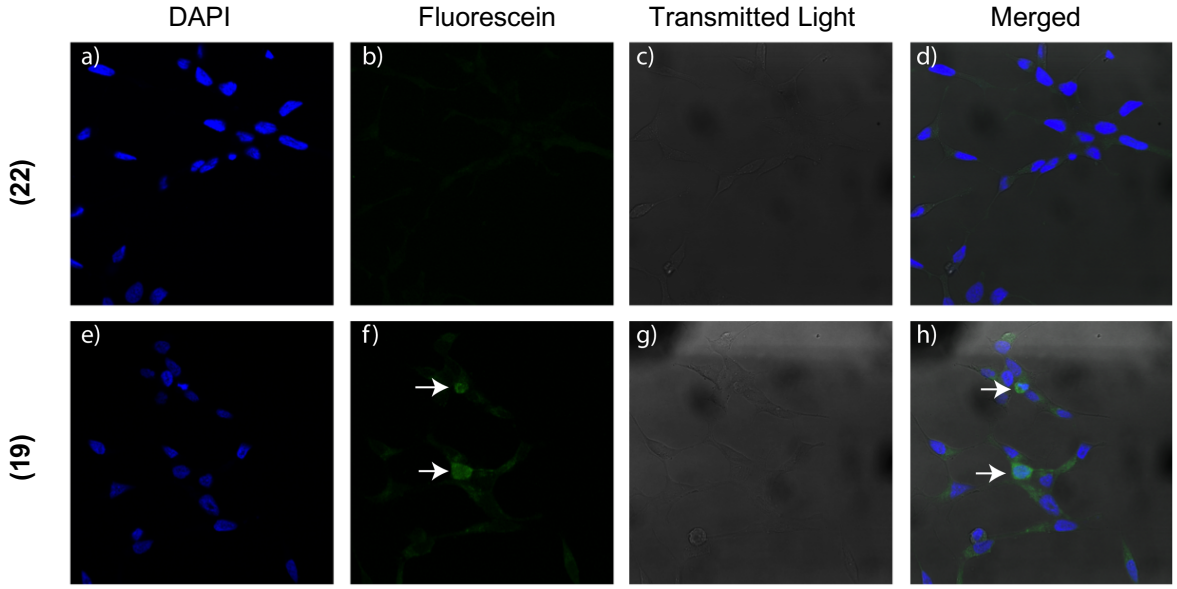

Figure 14. Confocal microscopy analysis on the internalization rate of **22** (a-d) and **19** (e –h) in live cells after 1 h incubation with compounds (40 x magnification; blue: DAPI, Green: fluorescein; grey: transmitted light).

Table 3. Permeability of compounds by PAMPA assay.

Compound	pH	Avg. Pe[a]	SD Pe	Avg. % R[b]	SD[e] % R	Avg.[c] logPe	SD logPe
I-BET762	6.8	51	5	14	10	-4.29	0.03
(19)	6.8	0.40	0.15	3	1	-6.42	0.17
(20)	6.8	0.36	0.06	7	1	-6.45	0.07
(21)	6.8	0.22	0.13	6	1	-6.72	0.26
(22)	6.8	0.20	0.07	5	1	-6.73	0.18
Propranolol	6.8	74	11	27	2	-4.14	0.06
Atenolol	6.8	<0.31	ND[d]	4	2	ND	ND

[a] Pe, effective permeability (x10^{-6} cm/sec); [b] % R, membrane retention; [c] Avg, the value is reported as average of quadruplicates; [d] ND, undetected due to weak UV absorbance of compound caused by low solubility; [e] SD, Standard deviation.

II.3.4. Synthesis and bioimaging of nitrobenzofurazan-labelled conjugates

Given the limited efficacy of the fluorescein-based probes to enter cells by diffusion, a new strategy was envisaged with nitrobenzofurazan (NBD) derivatives in place of fluorescein. In the absence of an extracellular receptor aiding in internalization, the use of a smaller and more neutral dye like NBD could be beneficial. For this the nitrobenzofurazan motif **23** was modified with bromoethylamine and subsequently reacted with **18** after a deprotection step to remove Boc (Scheme 5).

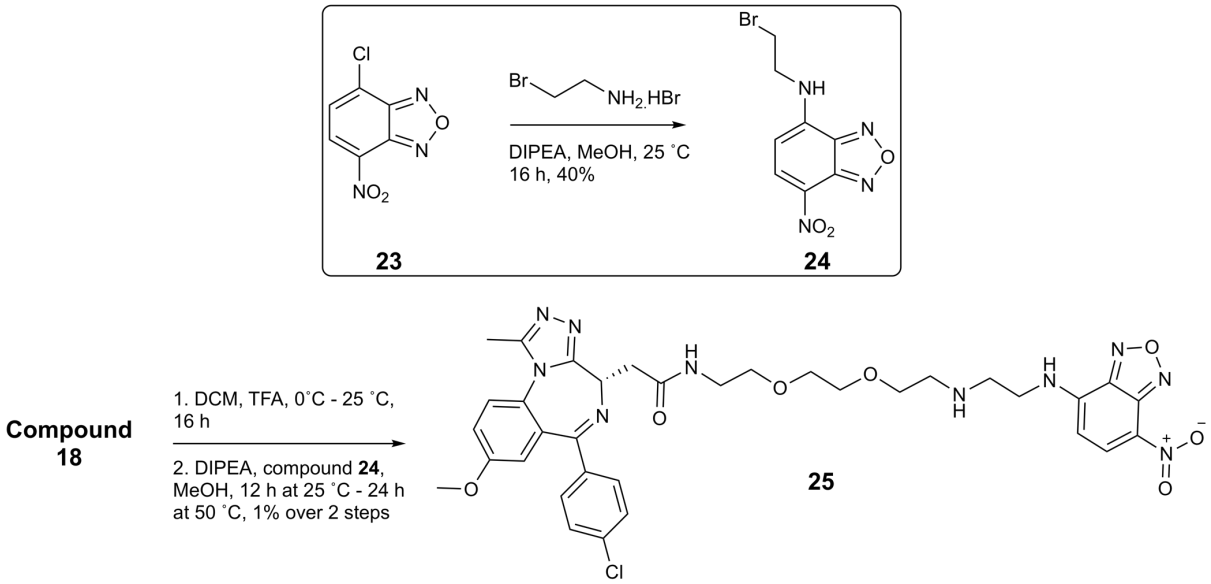

Scheme 5. Synthesis of nitrobenzofurazan-labelled I-BET762 conjugates. Abbreviations: DIPEA, *N,N*-Diisopropylethylamine; MeOH, methanol.

Compound **25** internalization in LNCaP cells was then evaluated. Confocal images were taken after 1 h, 2 h and 4 h incubation and compared with compound **21** bearing a fluorescein derivative. The retrieved images indicated that the fluorescent signal was modest, suggesting a poor internalization of the NDB-labelled probes (Figure 15). Moreover, no improvements in the fluorescence intensity were observed when comparing with that of **21**. The use of NBD in place of fluorescein was therefore an unsuccessful strategy to enhance dye diffusion and accumulation in cells. Altogether, these results highlight the need for a receptor to mediate the internalization process.

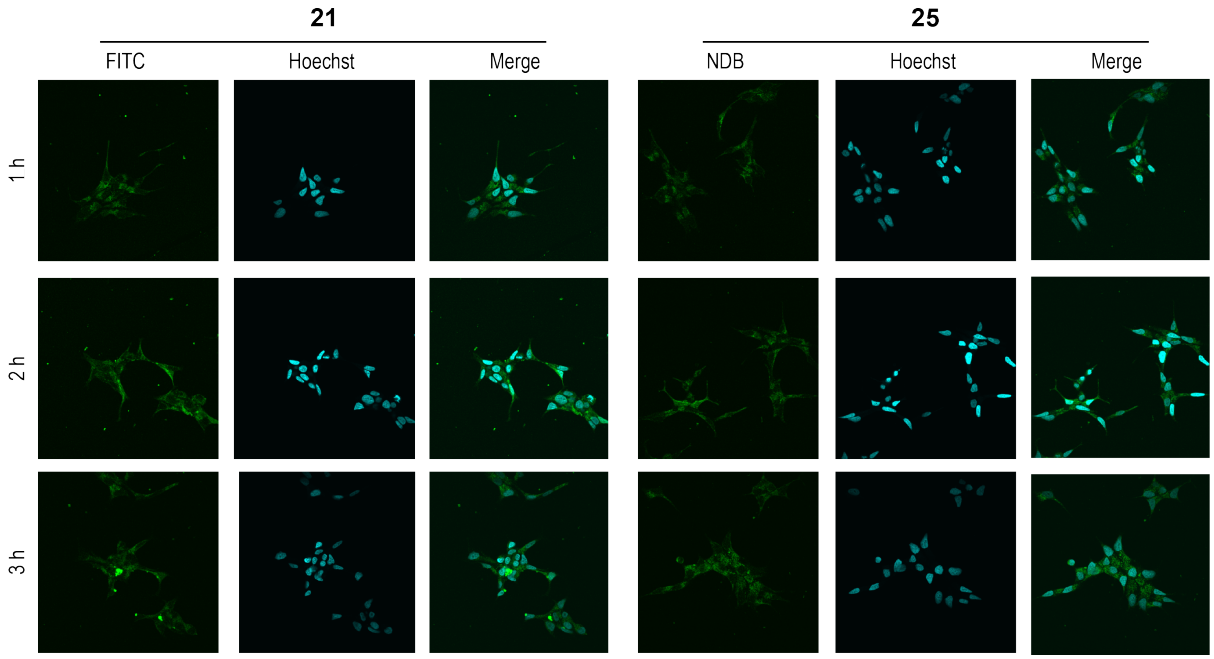

Figure 15. Confocal microscopy analysis of the rate of internalization in LNCaP cells of compound **25**. Nuclei were stained with Hoechst; Merge images represent fluorescein (FITC) and Hoechst channels over imposed.

II.4. Conclusion

In this chapter it was validated that **I-BET762** is a suitable BET inhibitor for targeted delivery approaches.

Through the introduction of bulky substituents via alkyl or PEG spacers to the putative conjugation site in **I-BET762**, it was examined whether its pharmacological properties were retained. Gratifyingly, potent binding affinities towards the target BET bromodomains BRD2-4 were still observed in the **I-BET762** derivatives. Docking simulations further validated these findings by suggesting engagement in the BRD4 cavity in a similar mode to the unmodified compound, despite the chemical modifications introduced.

Although not being the main goal of this chapter, we failed to take full advantage of **I-BET762**-based fluorophore derivatives and their potential in studying membrane permeability and intracellular localisation. Poor membrane diffusion was observed, despite an efficient co-localization in the nuclei after membrane disruption.

Chapter III

Tailoring I-BET762 for targeted delivery

Rui Traquete[1], Marta C. Marques[1], Tiago Rodrigues[1], Sarah Picaud[3,4], Francisco Corzana[5], Panagis Filippakopoulos[3,4], Gonçalo J. L. Bernardes[1,2]

[1] Instituto de Medicina Molecular João Lobo Antunes, Faculdade de Medicina, Universidade de Lisboa, Avenida Professor Egas Moniz, 1649-028 Lisboa, Portugal

[2] Department of Chemistry, University of Cambridge, Lensfield Road, CD2 1EW Cambridge, UK

[3] *Nuffield Department of Clinical Medicine, University of Oxford, Old Road Campus Research Building, Roosevelt Drive, Oxford OX3 7DQ, UK*

[4] *Ludwig Institute for Cancer Research, Nuffield Department of Clinical Medicine, University of Oxford, Old Road Campus Research Building Roosevelt Drive, Oxford OX3 7DQ, UK*

[5] *Departamento de Quimica, Universidad de La Rioja, Centro de Investigacion en Sintesis Quimica, 26006 Logroño (Spain)*

Author Contributions

R.T. and G.J.L.B. designed the experiments. R.T. performed the synthesis and characterization of the compounds. M.C.M. and T.R. helped with data analysis and interpretation, S.P. and P.F. collected and processed ICT and DSF data and crystallized the compounds, F.C. performed molecular dynamic simulations. R.T. wrote the chapter, G.J.L.B. directed the research and revised the text.

.

Chapter III. Tailoring I-BET762 for targeted delivery

III.1. Introduction

After selecting and validating in Chapter II. I-BET762 as the model BET inhibitor for targeted delivery, a key element in the design of an optimal ligand-targeted drug is the linker technology. This is in fact critical since an injudicious design can significantly compromise target receptor affinity or payload therapeutic efficacy. In brief, an optimally designed cleavable linker should be stable whilst the conjugate is in circulation, but allowing the controlled release of the therapeutic warhead upon internalization into the targeted cell.[160] Different technologies have been engineered towards this aim, including linkages undergoing pH-dependent, reductive and enzyme-catalysed cleavage. The various linker cleavage strategies will be discussed with greater detail in Chapter V.

Moreover, linker cleavage should release a therapeutic warhead without any fragments or modifications from the connecting spacer that may affect its activity. Often though, due to the absence of functional groups in the payload and/or targeting ligand, cleavable linkers are used as adaptors to connect the two chemical entities. As a result the drug is released with covalent modifications that impair their pharmacodynamics and may trigger immune responses.[174]

III.1.1. Self-cleaving release chemistries

When suitable functional groups are present directly in both the targeting ligand and therapeutic warhead a linkerless attachment is possible, leading to a traceless conjugate where only the free drug and targeting ligand are released. This strategy has been successfully applied by Bernardes *et al.,* where they have generated an antibody conjugate targeting the tumor vasculature based on a potent thiol-containing drug and mixed disulfides[189]. Furthermore, Casi *et al.* have also successfully generated linkerless conjugates by attaching potent aldehyde drugs with *N*-terminal cysteine residues of recombinant antibodies[190].

Alternatively, a traceless release of the therapeutic payload can be achieved through the introduction of self-immolative linkers. In this approach, a specific triggering event in the target cell generates a series of cascading reactions in the linkers that, ultimately, liberate the tethered drug in its unmodified form. To enable the attachment of such systems, the therapeutic payload must have suitable functional groups prone for derivatization that include hydroxyl, carboxyl, amine, carbonyl or thiol functions. Given the structural diversity amongst potential drugs that could be used in targeted approaches, recently

other self-immolative linkers have been developed to accommodate drugs containing broader functionalities as indole[191] or phenol moieties[192].

Nonetheless, amine-containing drugs have been the most explored therapeutics for traceless release strategies, particularly through the attachment with the self-immolative spacer *p*-aminobenzylcarbamate (PABC). Indeed, this has become the standard linker to construct an antibody-drug conjugate with approximately half of the 65 conjugates currently undergoing clinical studies using this approach.[193] The pinnacle of this release mechanism is the ADC Adcetris which, as mentioned in Chapter I.5, is approved by FDA for relapsed or refractory Hodgkin lymphoma, and where the immolation of PABC releases the natural product analogue monomethyl auristatin E through a azaquinone methide following protease dependent cleavage.[164] (Scheme 6).

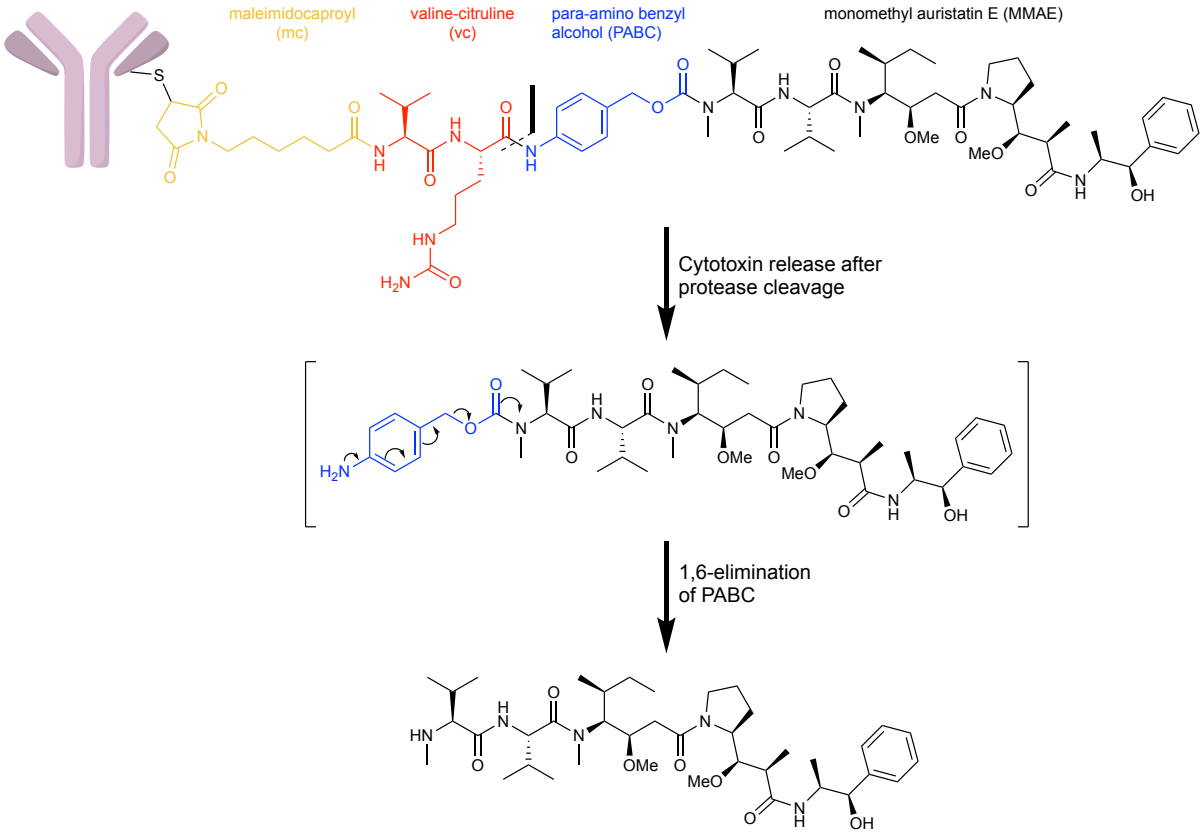

Scheme 6. Structure and mechanism of drug release in the ADC Adcetris with a protease recognition sequence of valine-citruline tethered to a para-amino benzyl alcohol (PABC) self immolative moiety.

However, due to the hydrophobicity of these constructs the use of PABC linker chemistry is limited, leading to enhanced aggregation and poor solubility which subsequently impacts the therapeutic activity of the conjugate.[194] The introduction of charge through quaternary ammonium motifs has been explored

as a means to enhance solubility and decrease aggregation of small molecule-peptide or protein constructs. In this regard Zhao *et al.*, through the development of negatively charged cross-linkers, have synthesized antibody-maytansinoid conjugates with superior solubility and without triggering aggregation.[195] In a different study, the *N*-terminal attachment of a betaine molecule bearing a quaternary ammonium markedly decreased the aggregation and increased the solubility of model polypeptides that are prone for aggregation.[196]

In line with these studies, tertiary and heteroaryl amine-containing bioactive molecules connected to carrier antibodies using a bioreversible linkage based on a quaternary ammonium[197-199] have also been successfully used in antibody-mediated intracellular delivery of antibiotics.[200] In this approach, the use of a self-immolative *p*-aminobenzyl quaternary (PABQ) ammonium salt provided appropriate stability and release characteristics, as well as an improvement in the therapeutic activity over conjugates with the standard carbamate (PABC) connection.[199] Importantly, the charged nature of the PABQ motif and resulting hydrophilicity also resulted in significantly less aggregation of the targeted conjugate.[201] Bearing all this in mind we sought to explore a PABQ-based self-immolative mechanism for the traceless release of I-BET762 in cancer cells. In order to enable the installation of such a system in I-BET762, the BET-inhibitor was chemically derivatised to include a terminal tertiary and heteroaryl amine-containing groups suitable to accomodate the self-immolative PABQ substituent.

III.2. Goals

In this chapter tertiary amine functionalities will be introduced in I-BET762 that, if successful, can later enable the accommodation of a self-immolative *p*-aminobenzyl quaternary ammonium salt for traceless release of the new molecule.

After synthesizing the new I-BET762-based effectors, this chapter will be centred in unravelling the affinity and binding mechanisms of the new compounds towards the target BRD proteins.

At first, the impact of the chemical substitutions in putative ligand-receptor binding interactions will be extensively studied using complementary biophysical methodologies.

The binding mechanism of the new compounds to BET proteins will then be thoroughly studied through crystallography studies of compounds in complex with target BRD proteins, and further complemented with computational molecular dynamic simulations.

By focusing on the efficiency of binding interactions we expect to gather comprehensive information on whether the functionalization of I-BET762 to accommodate a self-immolative linker was a successful strategy.

III.3. Design and characterization of a functionalisable BET inhibitor

III.3.1. Synthetic modifications to accommodate traceless release strategies

As validated in Chapter II. the derivatization of the amide group in **I-BET762** is possible while preserving putative ligand-receptor interactions. Therefore, this position was used to include terminal tertiary amines, which in turn enable the accommodation of traceless release strategies. **I-BET762** precursor **12**, bearing a free carboxylic acid, allowed subsequent installation of different synthetic modifications. These modifications included a piperidine ring bearing a terminal tertiary amine with (compound **27**, hereafter **RT48**) or without (compound **26**, hereafter **RT53**) a phenyl ring between this motif and the amide bond formed with the **I-BET762** scaffold (Scheme 7). An analogue bearing a quaternary ammonium (compound **28**, hereafter **RT56**) instead of the tertiary amine was also synthesized and used as a control since the terminal positively charged group should impair membrane permeability and thus most cellular effects (Scheme 8). The installation of these modifications is detailed below.

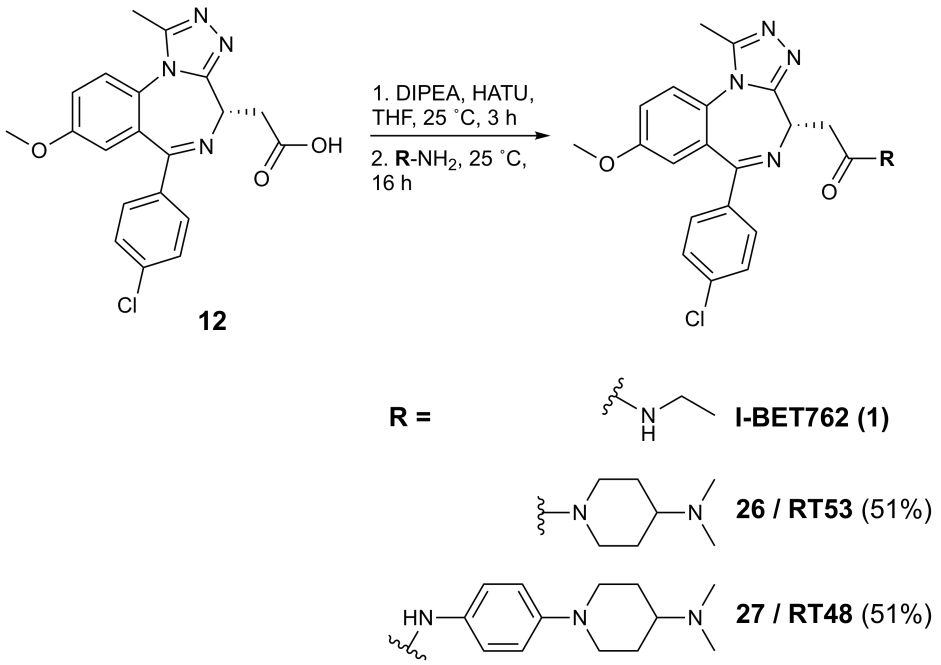

Scheme 7. Chemical modification of I-BET762 affording terminal tertiary amine analogues. Abbreviations: DIPEA, *N, N*-Diisopropylethylamine; HATU, 1-[Bis(dimethylamino)methylene]-1*H*-1,2,3-triazolo[4,5-*b*]pyridinium 3-oxid hexafluorophosphate; THF, tetrahydrofuran.

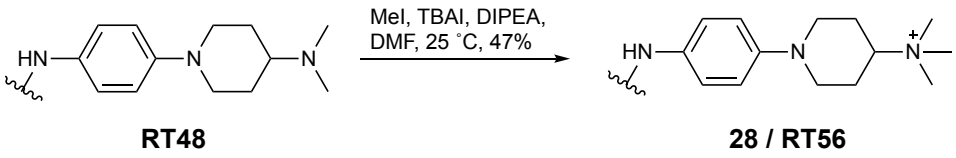

Scheme 8. Chemical modification of I-BET762 affording a quaternary amine analogue. Abbreviations: MeI, iodomethane; TBAI, tetrabutylammonium iodide; DIPEA, *N, N*-Diisopropylethylamine; DMF, dimethylformamide.

Having a series of fuctionalisable, tertiary and quaternary-amine containing **I-BET762** analogues in hand, it was then evaluated if these modifications did not impaired putative ligand-receptor interactions. For this a series of biophysical assays were performed, including differential scanning fluorimetry (DSF), AlphaScreen and Isothermal Titration Calorimetry (ITC).

DSF is a rapid screening method that monitors the thermal unfolding of proteins in the presence of a fluorescent dye. If a compound binds to the purified protein its thermal stability may increase, which is proportional to the concentration and affinity of the ligand on ligand-receptor interactions.[202] With the exception of BRDT(1), all compounds led to enhanced melting temperatures, in some cases even when compared to the parent I-BET762 molecule, which suggests a specific and strong binding interaction to a panel of BET proteins (Figure 16). Outside the BET family (BAZ2BA, CREBP, PB1(5) and PCAF) no

melting temperature shifts were identified, confirming that these ligands are tailored for the BET family of bromodomain proteins.

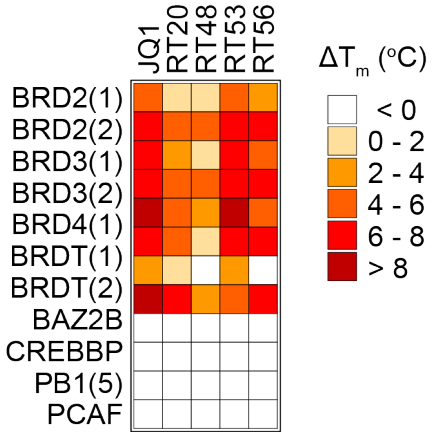

Figure 16. Protein Stability Shift Assay (Differential Scanning Fluorimetry, DSF) assessing binding efficacy and selectivity across different bromodomain families. Shown are average temperature shifts (ΔT_m^{obs}) in degrees Celsius upon binding of compounds at a final concentration of 10 µM.

Target binding affinity was further studied using Alpha Screen technology. As performed in chapter II.3.1 and chapter II.3.2, AlphaScreen was run against the BRD2(1), BRD3(1), BRD4(1) and BRD4(2) (Figure 17). The data obtained suggested that the RT compounds possess binding affinities to BRD domains as good or even better when compared to **I-BET762**. In particular, **RT53** showed an increase of 4-fold against BRD2(1) (IC_{50} = 19.3 nM) and BRD4(1) (IC_{50} = 18.2 nM) in comparison with the parent molecule **I-BET762** (IC_{50} BRD2(1) = 84.9 nM; IC_{50} BRD4(1) = 68.1 nM) (Figure 17A,C). Also, against BRD3(1) an IC_{50} increase of 3-fold was observed for **RT53** (IC_{50} = 67.1 nM) in comparison with **I-BET762** (IC_{50} = 214.8 nM) (Figure 17B), whereas no significant changes were observed against BRD4(2) (**RT53** IC_{50} = 25.9 nM ; **I-BET762** IC_{50} = 21.3 nM) (Figure 17D). Furthermore, the presence of a positive charge in **RT56** did not impair binding. In fact, **RT56** also showed a potent binding against BRD4(1) (IC_{50} = 6.6 nM) (Figure 17C) and BRD4(2) (IC_{50} = 2.4 nM) (Figure 17D).

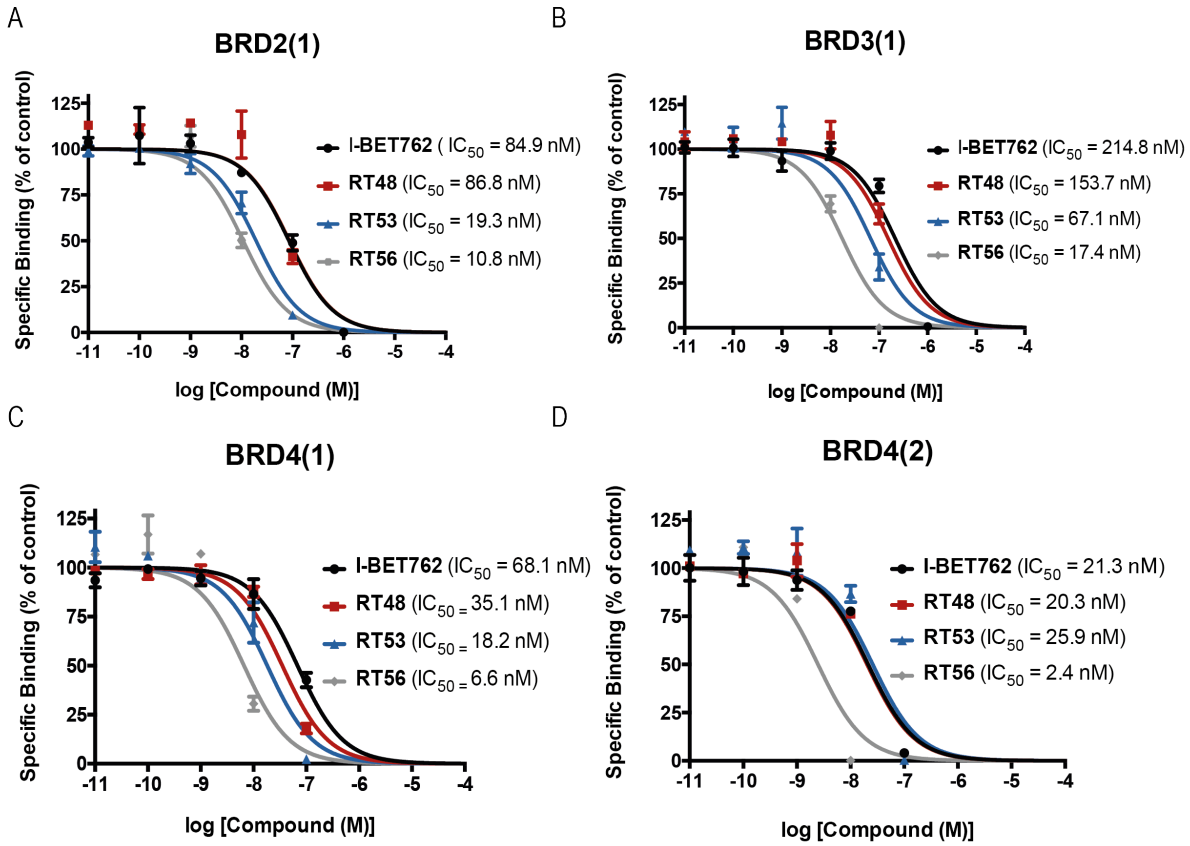

Figure 17. AlphaScreen of compound binding to (A) BRD2(1); (B) BRD3(1); (C) BRD4(1) and (D) BRD4(2).

The binding affinity of compounds was further characterized in solution through ITC. Conversely to AlphaScreen, ITC allows measuring the affinity of binding partners in their native state. The K_D values and thermodynamic parameters obtained confirmed that derivatization of BET inhibitors to contain terminal tertiary amine (**RT53**) or quaternary ammonium (**RT56**) motifs does not impair binding and can, in fact, lead to more potent BET inhibition. In addition, it was observed that **RT53** and **RT56** bind to isolated BRD4(1) and BRD4(2) in a similar range of K_D values (14 and 21 nM for BRD4(1) and 21 and 18 nM for BRD4(2), respectively) (Figure 18, Table 4). Interestingly the interaction of both inhibitors with the second domain of BRD2 and BRD4 is characterized by favourable positive entropy change ($T\Delta S$ ~ +2 to +3 kcal/mol), while in BRD4(1) a negative $T\Delta S$ is observed (~ -0.4 to ~ -1 kcal/mol), suggesting that the essential mechanisms of molecular recognition and engagement may be distinctive (Table 4). Together this data shows that the synthetic design to convert **I-BET762** into a tertiary amine-containing BET inhibitor was successful in that **RT53** shows a potent inhibition of BET proteins even when compared to the parent molecule.

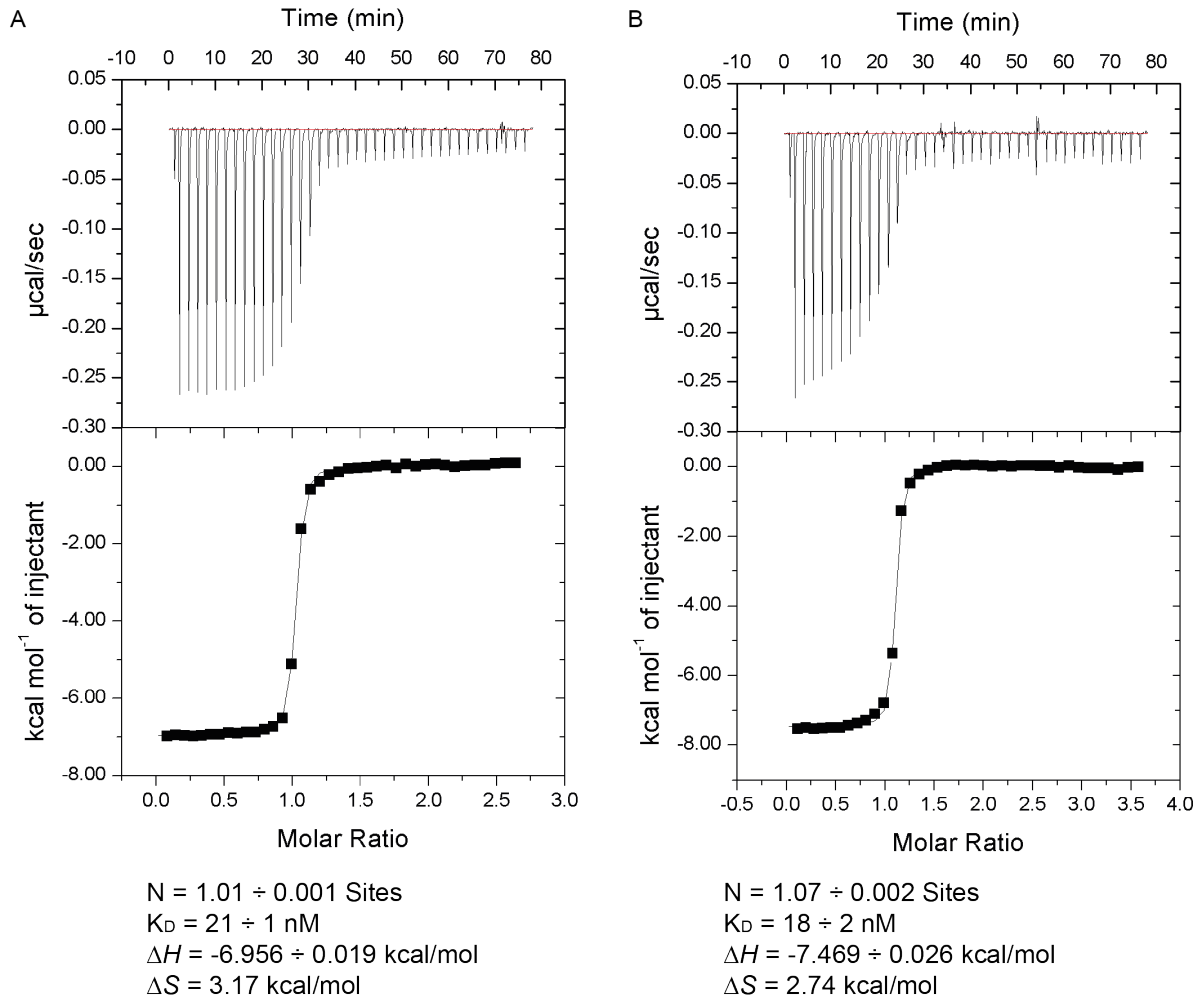

Figure 18. Isothermal Titration Calorimetry analysis of (A) **RT53** and (B) **RT56** against BRD4(2). Time courses of raw injection heats (upper panel) and normalized binding enthalpies are shown.

Table 4. Thermodynamic characterization and K_D values from Isothermal Titration Calorimetry.

Protein	Compound	[P][a] (µM)	[C][b] (µM)	K_D[c] (µM)	ΔH^{obs}[d] (kcal/mol)	N[e]	$T\Delta S$[f] (kcal/mol)	ΔG[g] (kcal/mol)
BRD2(2)	I-BET762	392.0	25.0	0.129 ± 0.007	-6.210 ± 0.023	0.98 ± 0.002	2.87	-9.08
	RT53	392.0	30.0	0.350 ± 0.003	-5.549 ± 0.052	1.00 ± 0.006	2.96	-8.51
	RT56	392.0	25.0	0.101 ± 0.007	-5.843 ± 0.025	-0.94 ± 0.002	3.37	-9.21
BRD4(1)	I-BET762	371.0	20.0	0.042 ± 0.002	-10.55 ± 0.026	1.10 ± 0.001	-0.82	-9.72
	RT53	371.0	25.0	0.014 ± 0.001	-10.77 ± 0.030	0.951 ± 0.01	-0.39	-10.38
	RT56	368.0	20.0	0.021 ± 0.001	-11.34 ± 0.019	1.02 ± 0.007	-1.20	-10.134
BRD4(2)	I-BET762	397.7	25.0	0.062 ±	-7.398 ±	1.04 ±	2.10	-9.50

			0.006	0.037	0.003		
RT53	386.0	30.0	0.021 ± 0.001	-6.956 ± 0.019	1.01 ± 0.001	3.17	-10.12
RT56	341.0	20.0	0.018 ± 0.002	-7.469 ± 0.026	1.07 ± 0.002	2.74	-10.21

[a] [P], concentration of protein sample solution in ITC Buffer; [b] [C], amount of protein in the calorimetric cell; [c] [K_D], dissociation constant; [d] ΔH^{obs}, changes in enthalpy of binding; [e] N, reaction stoichiometry; [f] $T\Delta S$, changes in entropy of binding; [g] ΔG, changes in the free energy of binding.

III.3.2. Structural characterization of the new BET bromodomain effectors

III.3.2.1. Crystallography studies

To obtain insight into the gain of binding of the new molecules as observed in biophysical assays, the crystal structures of recombinant BRD2(2) and BRD4(1) were solved in complex with **RT53** (Figure 19A,C) and **RT56** (Figure 19B,D). The high-resolution co-crystal structures revealed that these inhibitors engage the BET acetyl-lysine recognition pocket similarly, and in a competitive manner with the acetylated peptide binding. In brief, **RT53** and **RT56** directly engage the conserved asparagine residue (N140 in BRD4(1), N429 in BRD2(2)) *via* their triazolo moiety, as well as with the side chain of the conserved residues of tyrosine as was already described extensively.[76,183,185,203,204] The inhibitor-protein complexes were further stabilized by inserting the chlorophenyl substituent between the WPF shelf (W81/P82 in BRD4(1); W370/P371 in BRD2(2)) and an aspartic acid residue of the BC loop (D145 in BRD4(1); D434 in BRD2(2)). In line with previous work characterizing unmodified thienotriazolodiazepines in complex with BRD4(1), we also found the fused phenyl ring of **RT53** and **RT56** packing between the conserved L92 of the ZA loop and the WPF shelf (W81/P82) in BRD4(1).[185] The same interaction was conserved in BRD2(2), with the fused-phenyl rings engaging with L381 residue (Figure 19).

It was also determined the electrostatic potential of the BRD modules in complex with **RT53**. As observed in Figure 20, the surface surrounding the acetyl-lysine binding pocket presents a large charged interface, though the charge distribution varied dramatically between the two modules. This has been previously described in literature for different BRD proteins, suggesting that the ones exhibiting highly positively charged surfaces may engage other targets than acetylated histone peptides, which are rich in positively charged Lys and Arg.[25] Furthermore, **RT53** was found being further stabilized by structural water molecules at the bottom of the pocket module (Figure 20B,D). These are depicted within the acetyl-lysine binding cavity as small spheres with their Van der Walls radii highlighted as semi-transparent red-spheres.

Interestingly, the **RT56** NH–group in the acetamide linker is available to make an unprecedented hydrogen bond with the polar side-chain of N429, suggesting a possible role for the binding improvement of this compound to BRD2(2) (Figure 21). We were also able to identify an interaction between **RT53** and H433, which may also account for the improved stability.

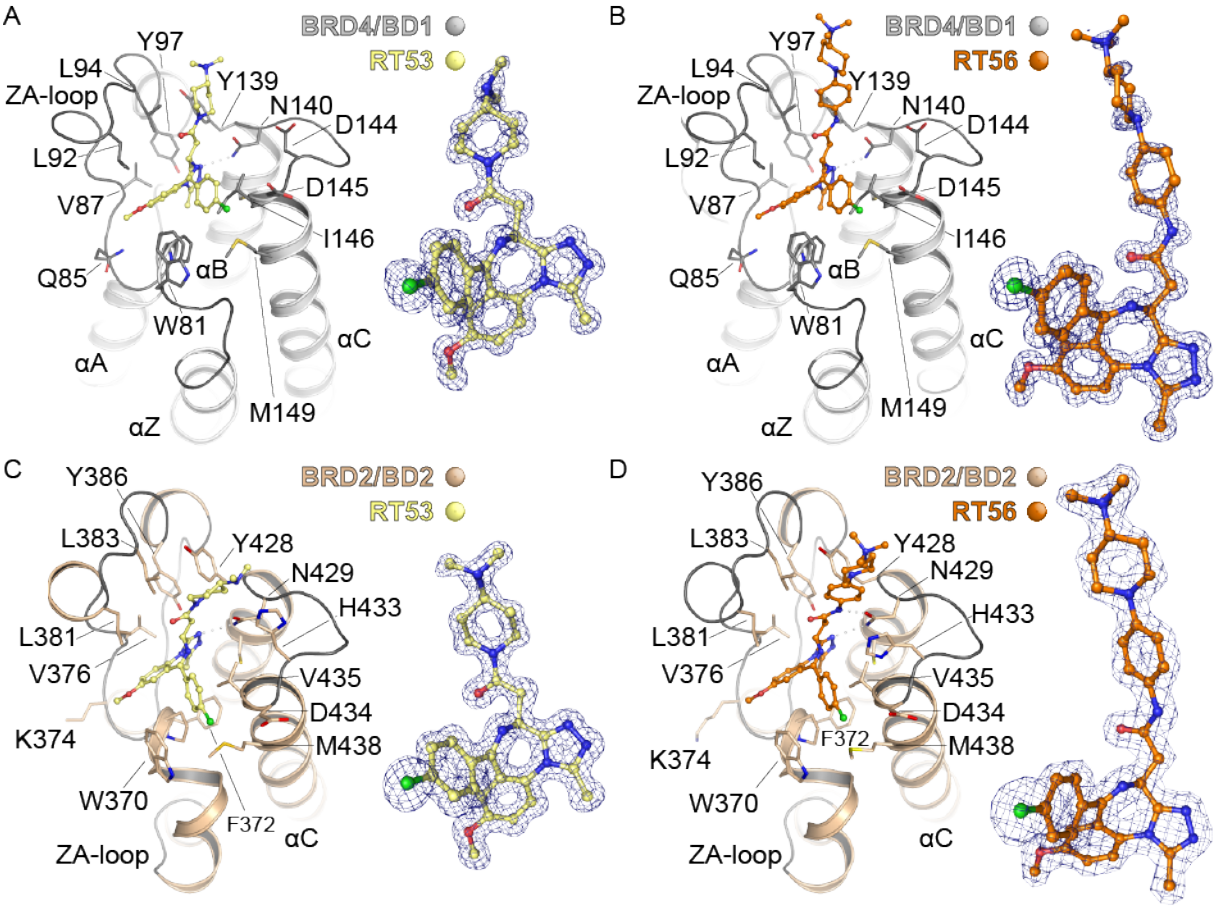

Figure 19. X-ray crystal structure of **RT53** and **RT56** in complex with BRD4(1) and BRD2(2).

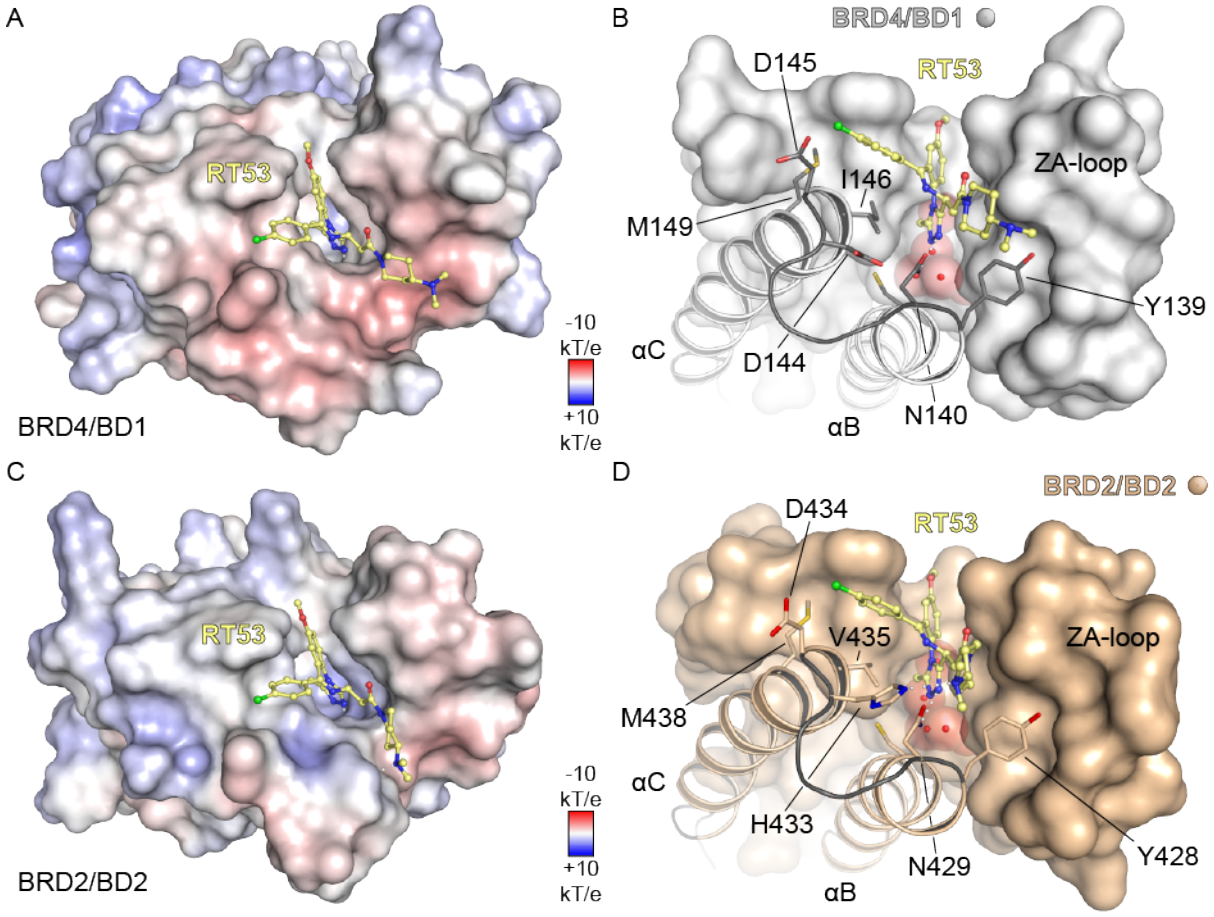

Figure 20. (A,C) Electrostatic surface potential of BRD4(1) and BRD2(2) in complex with **RT53**, between -10kTe (red) and +10kTe (blue) (e: electron charge; k: Boltzmann constant; T: Temperature); (B,D) conserved binding of **RT53** to BRD4(1) and BRD2(2) with water molecules interactions depicted as red spheres

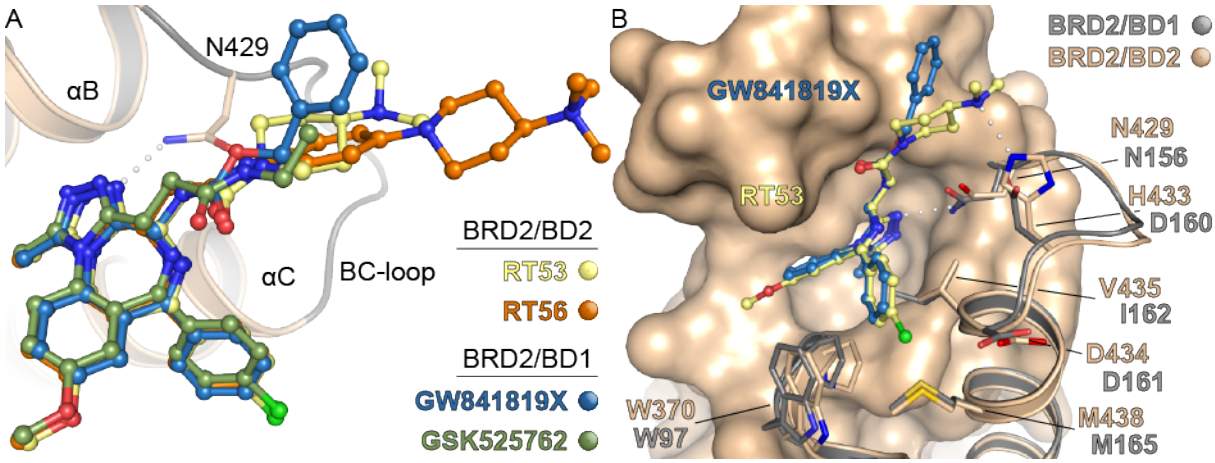

Figure 21. Binding mode of I-BET762 versus **RT53** and **RT56** in BRD2(2).

III.3.2.2. Molecular Dynamics simulations

The ligand-binding interactions of **RT53** and **RT56** compounds with BRD4(1) and BRD2(2) where further characterized through molecular dynamics (MD) simulations. This computational methodology allowed studying the conformational rearrangement of the molecules observed during ligand binding, thus accounting for the structural flexibility of the overall drug-target model system.[205] For this, 200 ns MD simulations in explicit water were conducted.

According to these simulations the complexes were stable, with most of the functionalized motif in **RT53** and **RT56** being exposed to the solvent. These corroborated previous observations of X-ray studies suggesting that the synthetic modifications were not involved in significant ligand-binding interactions (Figure 22). Notably, the inhibitors did not establish significant hydrogen bonds with the receptors in solution. In fact, the population of these hydrogen bonds was very low in all cases (population < 20%).

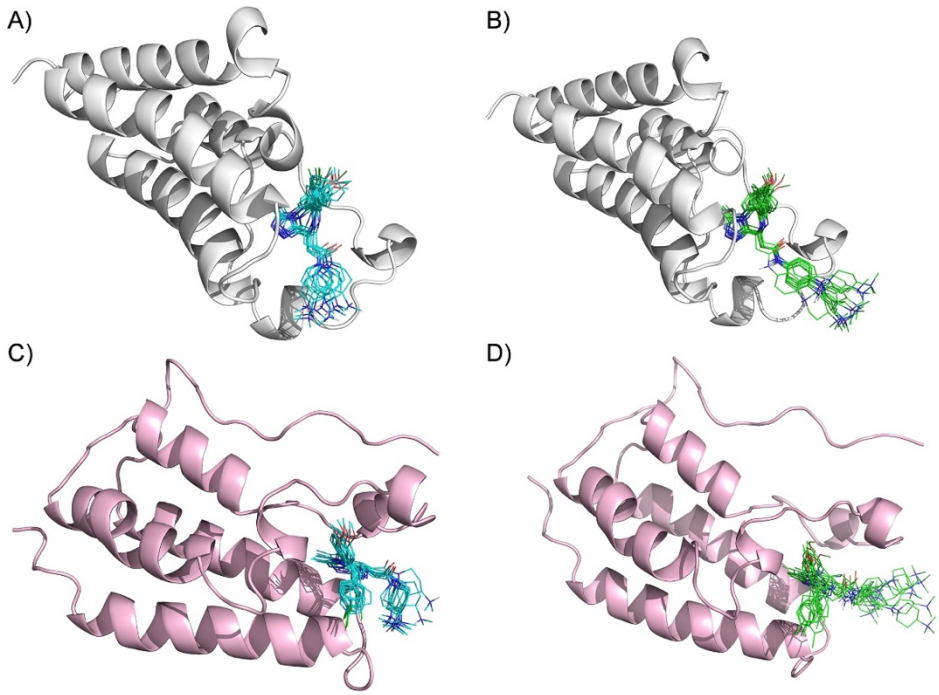

Figure 22. Ensembles obtained from 200 ns molecular dynamics simulations in explicit solvent of (A) BRD2(2)/**RT53**; (B) BRD2(2)/**RT56**; (C) BRD4(1)/**RT53**; (D) BRD4(2)/**RT56**

An electrostatic interaction, a classical salt-bridge, was actually found in complex BRD4(1)/**RT53** between the side chain of N144 and the positive charge at the functionalized dimethyl amine of the inhibitor (Figure 23A), population around 73%, whereas in complex BRD4(1)/**RT56** the functionalized motif and the side chain N96 were implicated, with a population close to 32% (Figure 23B).

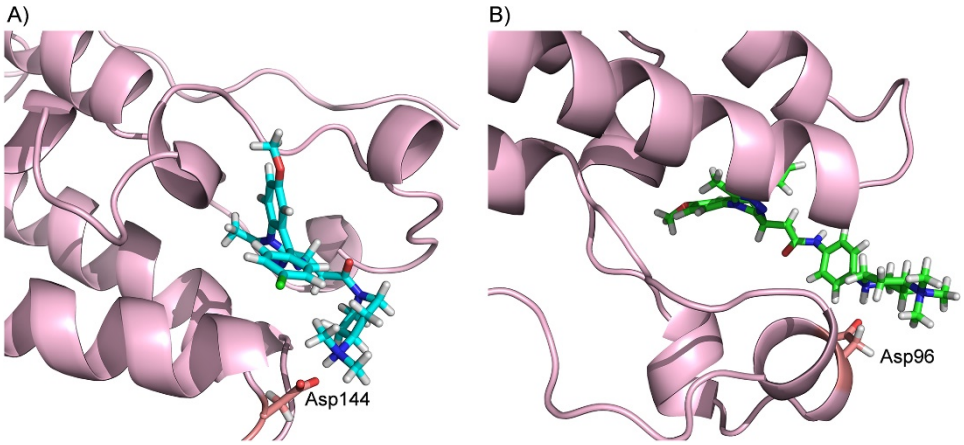

Figure 23. Electrostatic interactions between (A) N144 in BRD4(1) and **RT53**; (B) N96 in BRD4(1) and **RT56**.

Furthermore, the MD simulations showed that all complexes were stabilized by key CH-π interactions. Thus, while the chlorophenyl substituent of inhibitors **RT53** and **RT56** was engaged in an interaction with V435 of BRD2(2), the fused phenyl ring of the benzodiazepine core was involved in an interaction with P371. For both compounds was found a π-stacking interaction between the pendent chlorophenyl substituent and W370. A further CH-π interaction between the fused phenyl ring and the side chain of L381 was established in complex BRD2(2)/**RT53**. In BRD4(1), the CH-π interactions were conserved and displayed between the chlorophenyl substituent and the side chains of I145 and the fused phenyl ring and P82. Again, an extra interaction was observed for **RT53** between the fused phenyl ring and the hydrophobic L92.

Finally, the existence of persistent water pockets between the ligand/protein complexes was found through normalized two-dimensional RDF functions (2D-RDF). These functions calculate the probability of finding a water molecule close to two selected atoms in comparison to the one obtained in bulk and quantify the magnitude of localized water density. The calculated pairwise values of shared water density were high (>5 g/mL) in all cases, demonstrating the presence of persistent water pockets and the active role of solvent in binding. The highest shared water density (≈ 32 g/ml) was obtained between the carbonyl group of the side-chain of N429 of BRD2(2) and the NH of the amide group of **RT56** (Figure 24). Thus, this data indicate that the hydrogen bonding found in solid state (Figure 22) is water-mediated in solution. For compound **RT53** in complex with BRD4(1), a significant shared water density was observed between the triazole ring and the OH group of Y97.

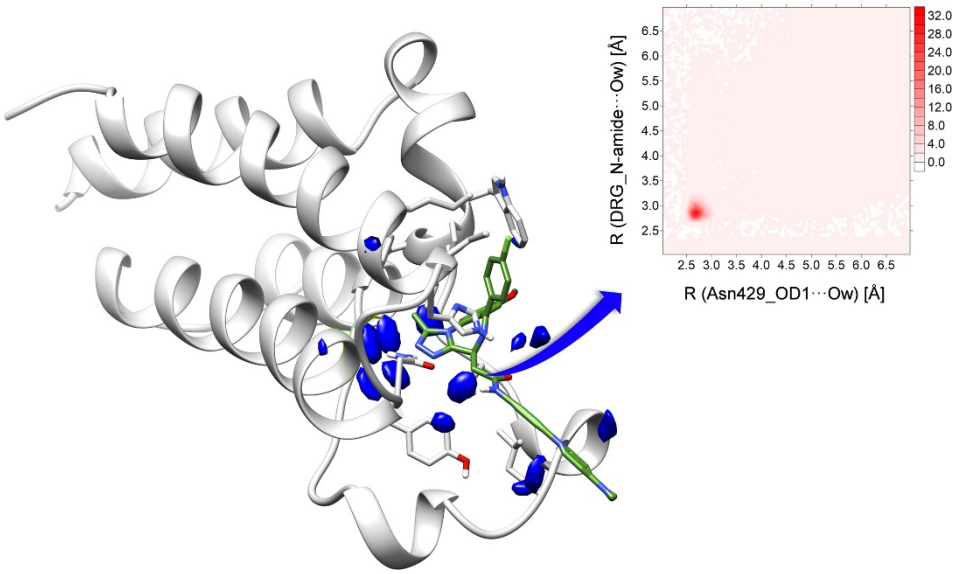

Figure 24. Water oxygen density over 200 nanoseconds calculated for the complex BRD2(2)/**RT56** through MD simulations, together with 2D-RDF functions for the side-chain of N429 and the amide group of **RT56**.

III.4. Conclusion

In this chapter **I-BET762** was derivatised to include terminal tertiary amine motifs suitable to be exploited in traceless release strategies, particularly through their attachment to a self-immolative linker based on an aminobenzyl quaternary ammonium salt.

Upon synthesis of the new BET effectors, different biophysical assays were used to study their binding affinities towards the target BET BRD2-4 proteins in comparison with the parent molecule **I-BET762**. The methodologies applied included differential scanning fluorimetry, Alpha Screen technology and isothermal titration calorimetry, and altogether strongly suggested that functionalization was a successful strategy. In all assays the synthesized BET effectors successfully stabilized (DSF) or engaged (AlphaScreen and ITC) their bromodomain targets at very low concentrations, having in some cases better affinity profiles than the parent molecule.

Furthermore, crystallography studies and molecular modelling of compounds in complex with BRD2(1) and BRD4(1) provided mechanistic insights into binding. In general, the new BET effectors engaged the BET cavity in a manner competitive with the acetylated peptide binding. However unprecedented hydrogen bonds were observed between the NH-group in the acetamide linker of **RT53** and the side-chain of H433 and in the acetamide linker of **RT56** and the side-chain of N429. In addition, molecular dynamics simulations in explicit water suggested the presence of stabilizing electrostatic interactions in complex BRD4(1)/**RT53** through the tertiary amine group of the inhibitor and N144.

Together these findings provided compelling evidence for a strong binding affinity of the new BET-effectors against their protein targets, further suggesting that in terms of putative ligand-receptor interactions functionalization of I-BET762 with tertiary amine motifs was a successful strategy.

Chapter IV

Biological evaluation of the new BET effectors

Rui Traquete[1,3], Jaime H. Cheah[3], Rob Wilson[3], Andrew Chen[3], Helen L. Evans[3], Angela N. Koehler[3], Gonçalo J. L. Bernardes[1,2]

[1] Instituto de Medicina Molecular João Lobo Antunes, Faculdade de Medicina, Universidade de Lisboa, Avenida Professor Egas Moniz, 1649-028 Lisboa, Portugal

[2] Department of Chemistry, University of Cambridge, Lensfield Road, CD2 1EW Cambridge, UK

[3] David H. Koch Institute for Integrative Cancer Research, Center For Precision Cancer Medicine, Department of Biological Engineering, Massachusetts Institute of Technology, Cambridge, MA, USA

Author Contributions

R.T., A.N.K. and G.J.L.B. designed the experiments. R.T. performed all experiments. J.H.C helped in the design and execution of cell line viability profiling, A.C. helped in preparing samples for RNA sequencing, R.W. analysed sequencing data, H.L.E. helped with affinity-based chemoproteomics assays, R.T. wrote the chapter, G.J.L.B. directed the research and revised the text.

Chapter IV. Biological evaluation of the new BET effectors

IV.1. Introduction

Given the critical role of bromodomain-containing proteins in homeostasis and disease, as described earlier in chapter I.2 the modulation of BET proteins with selective inhibitors such as (+)-JQ1 and I-BET762 results in marked phenotype changes. This has shown benefits not only in cancer but also inflammation and viral infections.[3,46,143,206,207] BET bromodomain inhibitors have supressed tumor growth in several mouse models of tumors such as multiple myeloma,[71,111] Burkitt's lymphoma,[105] AML and mixed-lineage leukemia (MLL)[104,107,208] as well in acute lymphoblastic leukemia.[106,209] Recently, a growing number of evidence shows that BET inhibitors can also block progression of non-hematologic malignancies including tumors from the brain,[129,130] breast,[117] colon,[127] pancreas,[126,210] liver,[128,211] prostate[89,120] and lung.[100,122,212] Yet, despite such widespread sensitivity of cancer cells to BET inhibitors in some tumor types their growth can also remain largely unaffected.[3]

Based on the reports above that have uncovered the mechanism of action in responsive cancer cell lines, BET inhibitors are expected to induce generalized transcriptional repression and cell cycle arrest upon treatment. BRD4 was previously reported to be essential for progression to G1 phase of the cell cycle,[41,43] and indeed several inhibitors have been observed to induce G1 cell cycle arrest in models of hematologic and solid tumors.[72,76,89,100,105,109,210] For example, in MLL models, BET inhibition with I-BET151 repressed the transcription of *BCL2*, *MYC* and *CDK6*, all of which are critical to cell cycle progression,[104] whereas in melanoma cell lines the critical cell cycle genes *MYC*, *ERK1* and *SKP2* were found downregulated after treatment with MS417.[66] Furthermore, in TNBC (+)-JQ1 treatment prevented cell cycle re-entry and arrested cells in early G1, as well as inducing cellular senescence. In addition genome-wide studies with ChIP-seq and RNA-seq also lead to a coordinated suppression of transcriptional pathways involved in cell proliferation, invasion and survival.[117] Wyce *et al*. also found I-BET762 strongly reducing *MYC* expression in prostate cancer cell lines with subsequent inhibition of cell growth through cell cycle arrest.[89]

It also becomes evident from the studies above that Myc regulation is a recurrent event after treatment of tumor cells with BET bromodomain inhibitors. Indeed, the repression of the *MYC* oncogene has been considered a hallmark of BET bromodomain inhibition. The Myc protein is well established to promote cell growth, differentiation and survival in several cancer types.[213] As observed in chapter I.3.2., *MYC* is transcriptionally regulated by large stretches of super-enhancers and inhibition of BET

bromodomains effectively displaces BRD4 from these super-enhancer regions, leading to a rather selective suppression of *MYC* transcription. Interestingly there is generally a lack of consistent gene-expression alterations following BET inhibitor treatment, suggesting cell-dependent transcriptional effects. Furthermore, while some studies suggested that suppression of the *MYC* oncogene was intensified in *MYC*-amplified tumors,[130] current results do not clarify whether the extent of transcript downregulation is necessarily correlated with response to BET inhibition.[89,214] In fact, recent studies by Donato *et al*. in Myc-driven tumors have shown a number of instances where, despite showing robust anti-growth activity, BET inhibition did not lead to Myc downregulation.[215] In line with these findings, in a recent screen of 83 lung tumor cell lines, Myc levels were unaffected despite the great sensitivity of SCLC lines to BET inhibitors in a cell proliferation assay.[212] In addition, recent observations have shown that BET inhibitors can modulate the expression of oncogenic transcription factors beyond *MYC*. These include the repression of *FOSL1* in non-small lung cancer[100] and pancreatic dual adenocarcinoma[216] after treatment with (+)-JQ1, or repression of *E2F*-regulated genes in cell models of gastric[217] and ovarian cancer.[218] All of these observations clearly demonstrate that there is a complex relationship between Myc regulation and sensitivity to BET inhibition and a remarkably heterogeneous response across tumor types. Furthermore, these also display how widespread are the effects of BET inhibitors across different cancer cell lines as well as their disperse mechanisms of action in different cellular contexts. As a result, and considering the structural modifications introduced onto the well-studied I-BET762 effector, this chapter is focused on the characterization of the antitumor activity of the new compounds and their underlying mechanism of action.

IV.2. Goals

This chapter aims at providing insights on the therapeutic potential of the new BET effectors in comparison with the parent molecule, thus validating their use as warhead for targeted delivery approaches.

The new compounds will be profiled against several cancer tissues and the most responsive cell lines will be identified and considered for further biological studies. Cellular viability and proliferation after compound treatment will be established for the new derivatives in a dose-dependent manner and compared with the parent molecule I-BET762.

Different strategies will be applied to monitor whether the new effectors engage BET proteins inside living cells. In affinity-based studies, chemical modifications will be introduced in the BET ligand to accommodate *in situ* labelling and target engagement profiling.

The underlying mechanisms leading to anti-proliferative effect of the new effectors will be analysed, namely in terms of cell cycle progression, induction of apoptotic processes and modulation of key downstream effectors of BET bromodomain activity.

Finally, widespread modulation of transcriptional programs will be studied and the gene signatures affected by compound treatment will be identified in order to establish a strong rationale for the overall mechanism of action.

IV.3. Cellular response and mechanisms of action

IV.3.1. Cancer cell killing activity

Given that cellular activity is critical for the demonstration of therapeutic potential, the new BET bromodomain effectors were profiled against several cancer cell lines to find the most responsive models. A semi-automated small-molecule sensitivity profiling of 26 cancer cell lines was established and their response evaluated after 96 h incubation with compounds in comparison with the parent molecule **I-BET762**. Cellular response was determined in cell lines deriving from a wide range of tissues including prostate, lung, brain, pancreas, breast, ovary, colon, as well as haematological and bone marrow tumors (Figure 25). In the solid tumors tested, potent inhibitory effects were observed mostly in prostate cancer cell lines, particularly in those dependent on AR signalling (LNCaP, VCaP and 22RV1, IC_{50} = 0.2 – 2.6 μM). In contrast, AR negative cells (DU145 and PC3) were overall more resistant to treatment. Interestingly though, PC3 cells were responsive only to **RT53** (IC_{50} = 3.1 μM), whilst neither **RT48** nor **I-BET762** affected cellular viability up to the maximum dose tested (10 μM). In AR-positive cell lines the response to **RT53** and **RT48** treatment was comparable to that of the parent molecule, **I-BET762**, although **RT53** was clearly the most effective amongst the three (**RT53** IC_{50} = 0.2 – 0.7 μM; **RT48** IC_{50} = 0.3 – 2.6 μM; **I-BET762** IC_{50} = 0.2 – 1.5 μM). Conversely, **RT56** was ineffective across all cell lines (IC_{50} > 10 μM), likely due to the quaternary ammonium salt motif impairing compound internalization. This was further confirmed by PAMPA that showed that **RT56** does not diffuse across cellular membranes (Table 5). In regard to membrane permeability, it was also interesting to note the modest diffusion observed for **RT53** (logPe = -5.92) in comparison with **I-BET762** (logPe = -4.32), despite **RT53** showing equivalent and in some cases even more cancer cell killing activity than the parent molecule (Table 5). Nevertheless, drug sensitive phenotypes were also partially observed in cell lines from breast (MDA-MB-453, IC_{50} = 1.3 – 5.0 μM), ovary (CAOV3, IC_{50} = 0.5 -1.9 μM) and brain tissues (U87-MG, IC_{50} = 1.72 – 7.93 μM), as well as in all blood cancer cells tested, namely those from

acute T cell leukemia (Jurkat, IC_{50} = 0.3 – 1.2 μM), acute myeloblastic leukemia (Kasumi-1, IC_{50} = 0.1 – 0.3 μM), and Burkitt's lymphoma (DAUDI, IC_{50} = 0.4 – 1.3 μM). Moreover, cancer cell lines derived from lung, pancreas and colon tissues were entirely unresponsive to all compounds (IC_{50} > 10 μM).

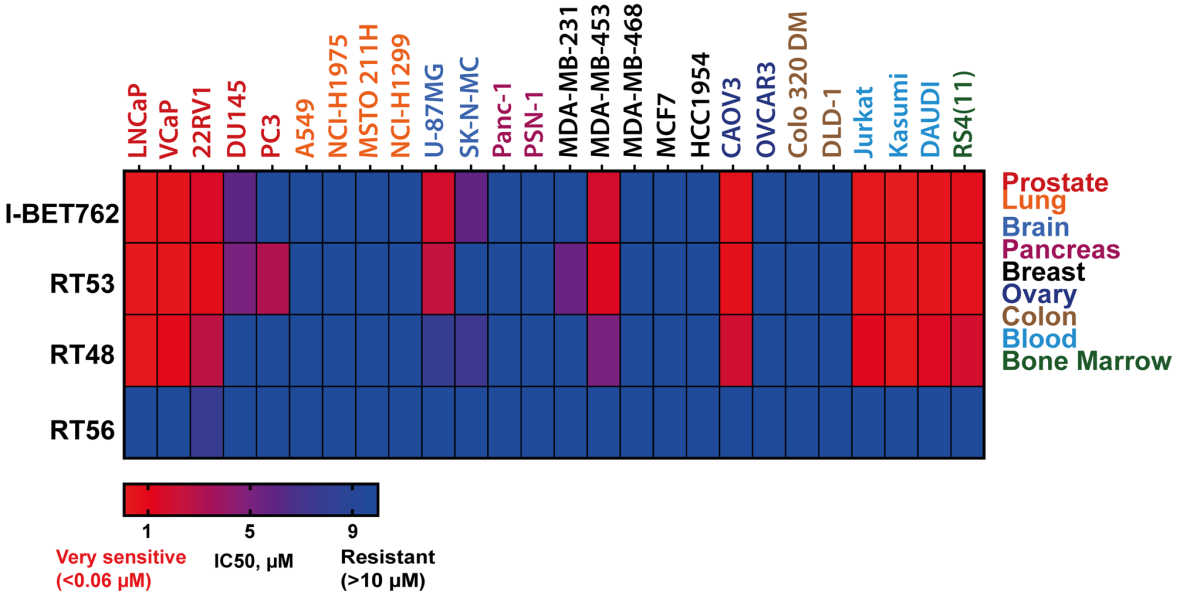

Figure 25. Heat map of IC_{50} values obtained for **I-BET762**, **RT53**, **RT48** and **RT56** against cancer cell lines derived from different tissues. Red represents sensitivity to compounds, blue indicates resistance.

Table 5. PAMPA of the new BET-based effectors.

Compound	pH	Avg. Pe[a]	SD Pe	Avg.%R[b]	SD % R	Avg.[c] logPe	SD[d] logPe
I-BET762	6.8	48	3	17	5	-4.32	0.03
RT48	6.8	1.8	0.2	69	1	-5.75	0.05
RT53	6.8	1.2	0.1	52	1	-5.92	0.03
RT56	6.8	<0.01	-	7	1	-	-
Propranolol	6.8	53	4	27	3	-4.28	0.04
Atenolol	6.8	<0.01	-	8	1	-	-

[a] Pe, effective permeability (x10^{-6} cm/sec); [b] % R, membrane retention; [c] Avg, the value is reported as average of quadruplicates; [d] SD, standard deviation

For proof of concept we pursued our studies using prostate cancer as a model disease. Preclinical data from a number of reports demonstrated BET bromodomain inhibition as a promising therapeutic option for castration-resistant prostate cancer,[89,120] and clinical trials are being actively pursued with multiple BET inhibitors. In addition, the established overexpression of PSMA[219] offers an opportunity for targeted delivery of a BET inhibitor, as it will be discussed in greater detail in Chapter V.1.2. Further examination of cellular response corroborated the high sensitivity of LNCaP cells to **RT48** (IC_{50} = 0.37 μM) and particularly **RT53** (IC_{50} = 0.26 μM) inhibitors (Figure 26A). In agreement with the cellular

profiling only **RT53** (IC_{50} = 2.9 μM) was effective against PC3 cells, whereas **RT56** was ineffective against both cell lines as expected (Figure 26B).

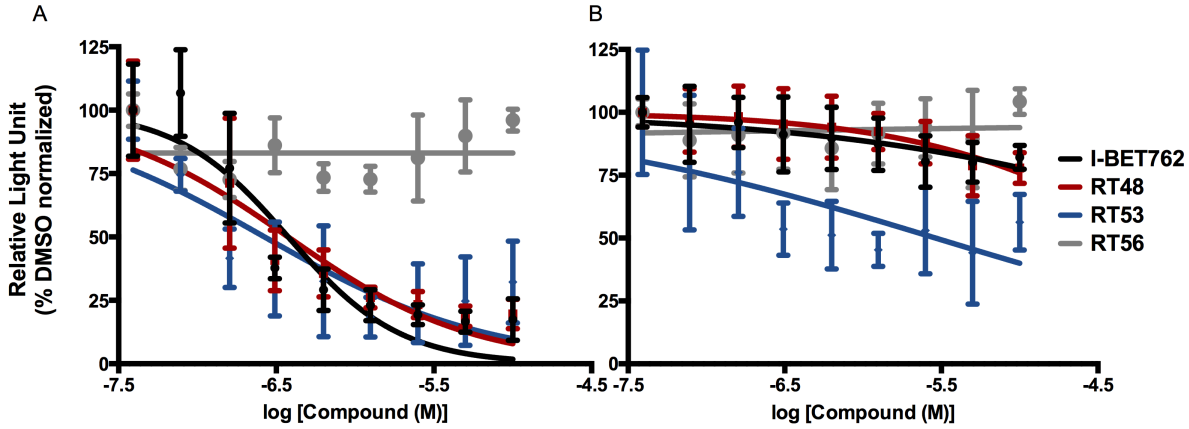

Figure 26. Cellular viability of (A) LNCaP and (B) PC3 cells after treatment with **I-BET762**, **RT53**, **RT48** and **RT56** compounds (96 h incubation, triplicate means ± SD).

Considering LNCaP response to compounds in terms of viability, these were also evaluated in their proliferation capacity after drug treatment. For that it was used Incucyte ZOOM™ technology and its confluence processing analysis tool, which provide cell confluence metrics in real-time by analysing the occupied area of cell images over time. LNCaP proliferation was greatly impaired with **RT53** and **RT48** treatment at low doses (0.25 μM) during 7 days (Figure 27A). **I-BET762** treated samples showed higher variability, but overall a milder growth inhibition comparing to **RT53** was observed at 0.25 μM and 1.0 μM whilst at higher doses (2.5 μM and 10.0 μM) proliferation of LNCaP was strongly supressed (Figure 27C,D). On the other hand, as expected given the viability data LNCaP were unresponsive to **RT56** treatment as cells proliferated linearly even at high doses (10 μM, Figure 27D).

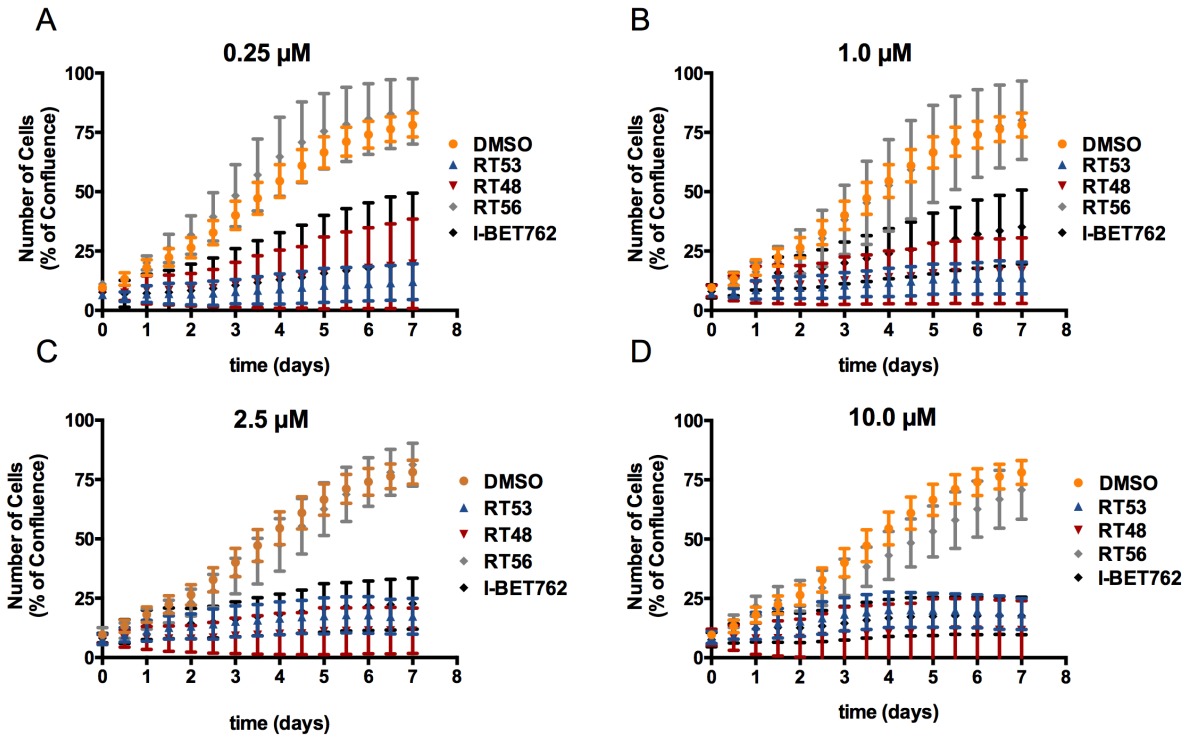

Figure 27. Incucyte ZOOM™ proliferation assay for LNCaP cells after compound treatment at (A) 0.25 µM, (B) 1.0 µM, (C) 2.5 µM and (D) 10.0 µM for 7 days. Data is presented as percentage of confluence over time, as given by the Incucyte confluence analysis tool through the determination of occupied area by cells per well.

IV.3.2. BET BRD target engagement in living systems

IV.3.2.1. Cellular Thermal Shift Assay (CETSA)

While previous experiments have used cellular viability and proliferation assays as a surrogate for BET inhibition in cells, direct evaluation of compound binding to target proteins in living systems is critical for the pharmacological validation of the new compounds.

With this in mind, compound engagement of BET proteins in LNCaP cells was initially evaluated using cellular thermal shift assay (CETSA). As with traditional melting temperature (T_m) shift, this technique relies on protein stabilization upon ligand binding, allowing the quantification of the stabilized soluble protein fraction whereas the denatured material irreversible aggregates and precipitates.[220,221] The greatest advantage of CETSA for small-molecule target engagement in cells over other techniques is that it is a modification-free approach, since it relies in the employment of the biologically active compound without any chemical modifications or linker attachments.[222] To assess drug target engagement with CETSA usually two different experimental formats are used. Most often CETSA is executed based on a temperature gradient and subsequent comparison of the apparent aggregation

temperature curves for a target protein in the presence of a ligand. Conversely, the second format relies on the generation of an isothermal dose-response fingerprint ($ITDRF_{CETSA}$), meaning that it is based on a single temperature and the measuring of protein stabilization as a function of increasing ligand concentration. Considering previous work by Tanaka *et al*. in which the temperature for protein aggregation was established for the bromodomains BRD2, BRD3 and BRD4, assay development could be bypassed and direct application of $ITDRF_{CETSA}$ was performed.[223] Thus, it was generated an $ITDRF_{CETSA}$ at 48.5 ˚C for the measurement of BRD2 and BRD4 stabilization after incubating LNCaP cells for 1 h with increasing concentrations of **RT53** and **RT56**. As given by the immunoblot analysis against BRD4 and in comparison with DMSO, in **RT53** treated samples an increasing amount of protein was detected in a dose-dependent manner, suggesting that BRD4 was successfully stabilized with this inhibitor (Figure 28). The same pattern, although to a minor extent, was observed to BRD2 (Figure 29**,** as indicated by the black arrows). Conversely, in the samples treated with the positively charged quaternary ammonium derivative **RT56**, neither BRD2 nor BRD4 were identified by immunoblotting, suggesting protein denaturation and inefficient binding in cells which, considering the lack of membrane permeability of **RT56** was not surprising. Altogether, these data suggested that ligand **RT53** successfully engaged BRD2 and BRD4 in live cells in a dose-dependent manner.

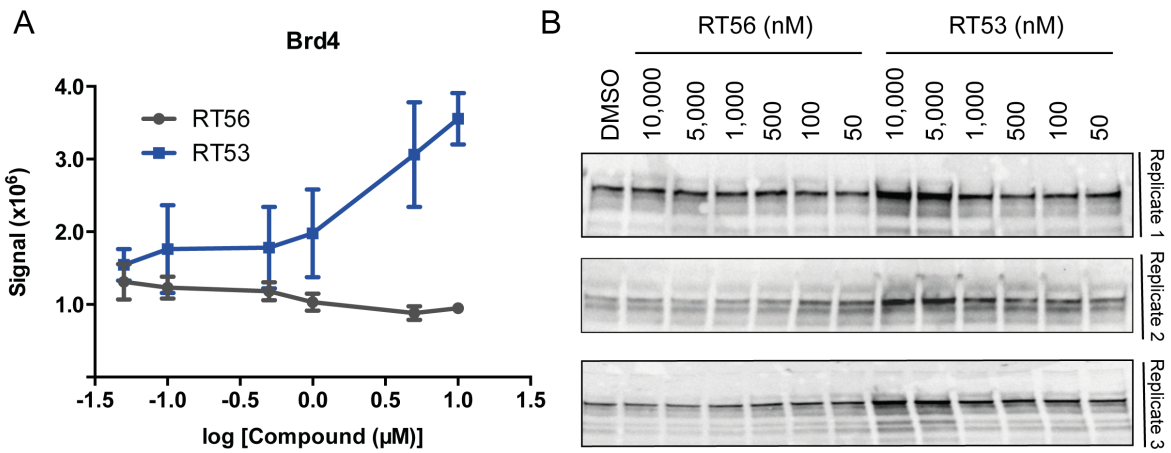

Figure 28. Isothermal dose-response fingerprint CETSA of BRD4 after 1-h incubation of LNCaP cells with increasing concentrations of **RT53** and **RT56**. (A) Data represents immunoblot signal quantification as mean ± SD of biological triplicates; (B) gel source data of each biological replicate with an anti-BRD4 antibody.

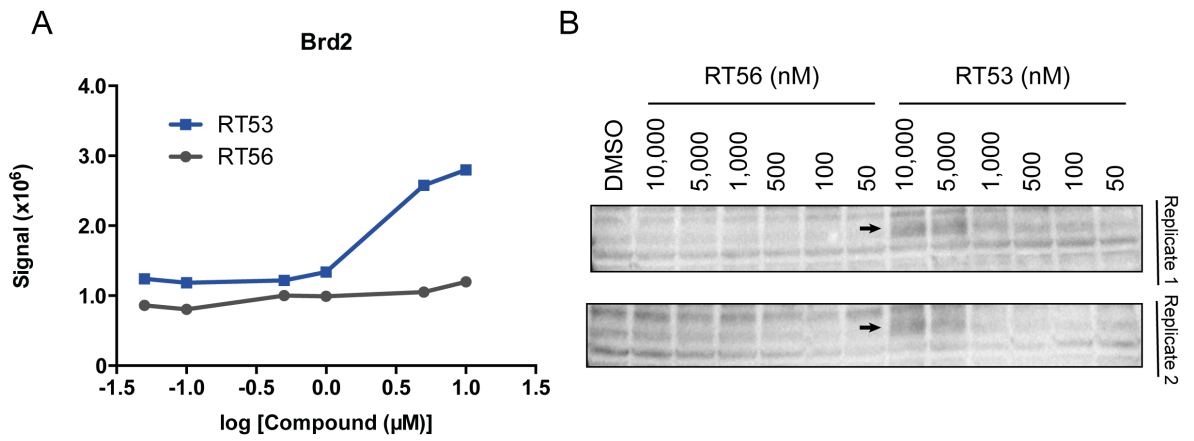

Figure 29. Isothermal dose-response fingerprint CETSA of BRD2 after 1-h incubation of LNCaP cells with increasing concentrations of **RT53** and **RT56**. (A) Data represents immunoblot signal quantification as mean ± SD of biological duplicates; (B) Gel source data of each biological replicate with an anti-BRD2 antibody. Arrows indicate enhanced immunoblot signal in RT53-treated samples.

IV.3.2.2. Affinity-based photoreactive chemoproteomics

Contrary to CETSA, affinity based chemoproteomic approaches require the modification of the ligand to accommodate chemical handles in order to enable compound binding to proteins. Alkyne or azide groups can therefore be introduced in the compounds and, through bioorthogonal reaction using copper-catalysed azide-alkyne cycloaddition (CuAAC) chemistry, a functional tag is appended to the handle allowing affinity purification of covalently bound proteins. The biotin-streptavidin interaction is a clear example of functional tags introduced to ligands *in situ* for protein identification, but this methodology can also be extended to UV light-induced trapping of probe-protein interaction in cells.[222] Scheme 9 depicts the workflow applied in these studies for the covalent binding of compounds to BET bromodomain proteins. The new **RT53** ligand was chemically modified to accommodate a diazirine photoreactive cross-linking and an alkyne handle for CuAAC chemistry. The diazirine serves as a photoreactive group that, upon activation with long-wave UV light (330 to 370 nm), generates carbine intermediates that will covalently cross-link the probe with the macromolecular binding partner based on the close proximity of the two constructs.[224] Thus, following treatment of cells with the chemical probe their exposure to UV light leads to covalent ligand-protein interactions, after which cell lysis is performed and a reporter group is covalently attached *via* bioorthogonal reaction. Target engagement is monitored by SDS-PAGE. Here two different reporter groups were used, an azide-bearing Alexa Fluor fluorescent probe for in gel fluorescence detection and a biotin-based tag for immunoblotting detection and streptavidin pull down assays.

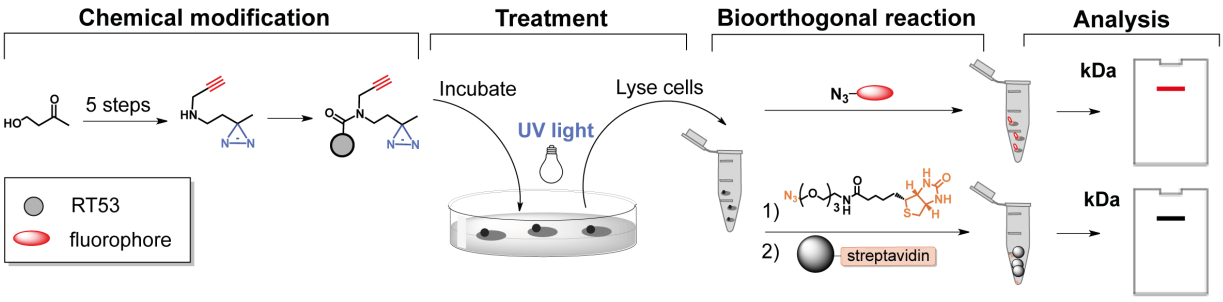

Scheme 9. Workflow for ligand target engagement in cells through affinity-based chemical proteomics and covalent interactions

Before pursuing binding studies, it was critical establishing a synthesis route and structure activity relationships to enable the derivatisation of the compounds with the chemical handle. As depicted in Scheme 9, again the **I-BET762** precursor **12** bearing a free carboxylic acid was derivatised with a piperidine motif as in **RT53**, followed by introduction of the diazirine photoreactive substituent to afford **32**. LNCaP cellular viability was used as a surrogate for compound activity after the introduction of the chemical handle. A 10-fold decrease in the IC_{50} value of **32** (IC_{50} = 1.5 µM) was observed in comparison with **RT53** (IC_{50} = 0.3 µM), though still presenting excellent cell killing activity and suggesting that the efficacy of the compound was not compromised by the introduction of the photoreactive probe (Figure 30).

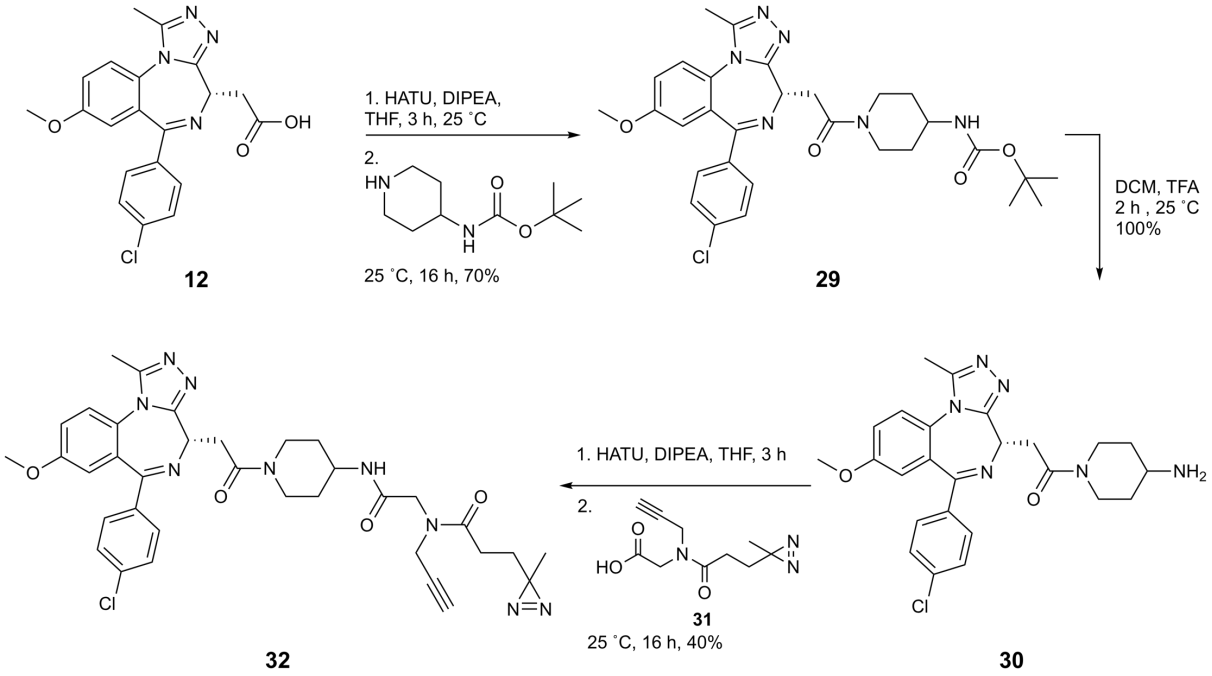

Scheme 10. Synthesis route for a **RT53**-based photoreactive probe. Abbreviations: HATU, 1-[Bis(dimethylamino)methylene]-1*H*-1,2,3-triazolo[4,5-*b*]pyridinium 3-oxid hexafluorophosphate; DIPEA, *N, N*-Diisopropylethylamine; THF, tetrahydrofuran; DCM, dimethylformamide; TFA, trifluoroacetic acid.

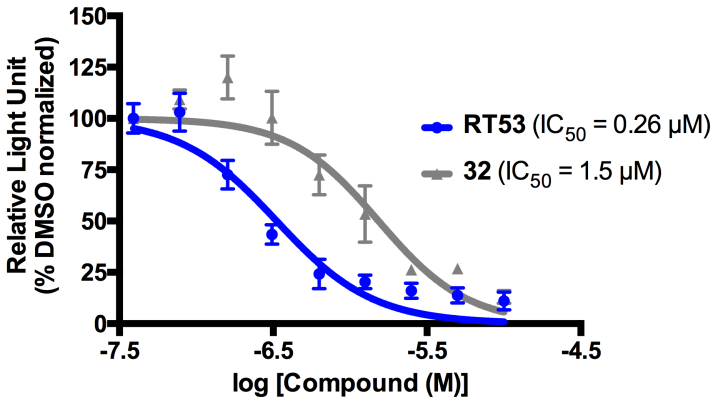

Figure 30. Cellular viability of LNCaP cells after treatment with compound **32** and **RT53** (96 h incubation, technical triplicate means ± SD).

After establishing the synthesis route and the activity of the photoreactive probe cells were exposed to increasing concentrations of compound for 1 h, followed by the photoactivation of the diazirine motif through UV light exposure for 15 min. An Alexa Fluor™ 647 Azide was used as a tag and was incubated with cell lysates for 1 h before analysing the in gel fluorescence. A dose-dependent response was observed as indicated by the increasing fluorescence intensity with enhanced concentrations of compound **32** (Figure 31). Importantly, in the absence of UV exposure or $CuSO_4$ no fluorescent signal was observed. While the absence of UV disables diazirine photoactivation and subsequent covalent binding of **32** to proteins, $CuSO_4$ is a limiting component of bioorthogonal CuAAC chemistry and without this catalyst the reaction does not occur. Thus, these data confirm that the fluorescence observed in the gel results from established covalent interactions between **32** and the proteins in its close proximity, as well as indicating a successful bioorthogonal reaction between the Alexa Fluor azide tag and alkyne handle of **32**. However, despite a dose-dependent response being observed, the targets to which the probe was bound seemed mostly unspecific, with a great extent of band smears across the entire molecular weight spectra. As for bromodomain engagement BRD4 was not identified as one of the bound targets since no fluorescence signal was observed at 150 kDa, and despite the identification of a band at 100 kDa that could suggest BRD2 or BRD3 engagement, these were also unspecific as verified in the soluble completion sample. In this competitive analysis, cells were firstly incubated with free **RT53** for 1 h before adding **32** (50:10 µM ratio), which should abrogate probe engagement in case of BET bromodomain specificity. The opposite has been observed though, with the fluorescence signal being alike the one of **32** at the same concentration but without **RT53** (Figure 31, 10 µM sample).

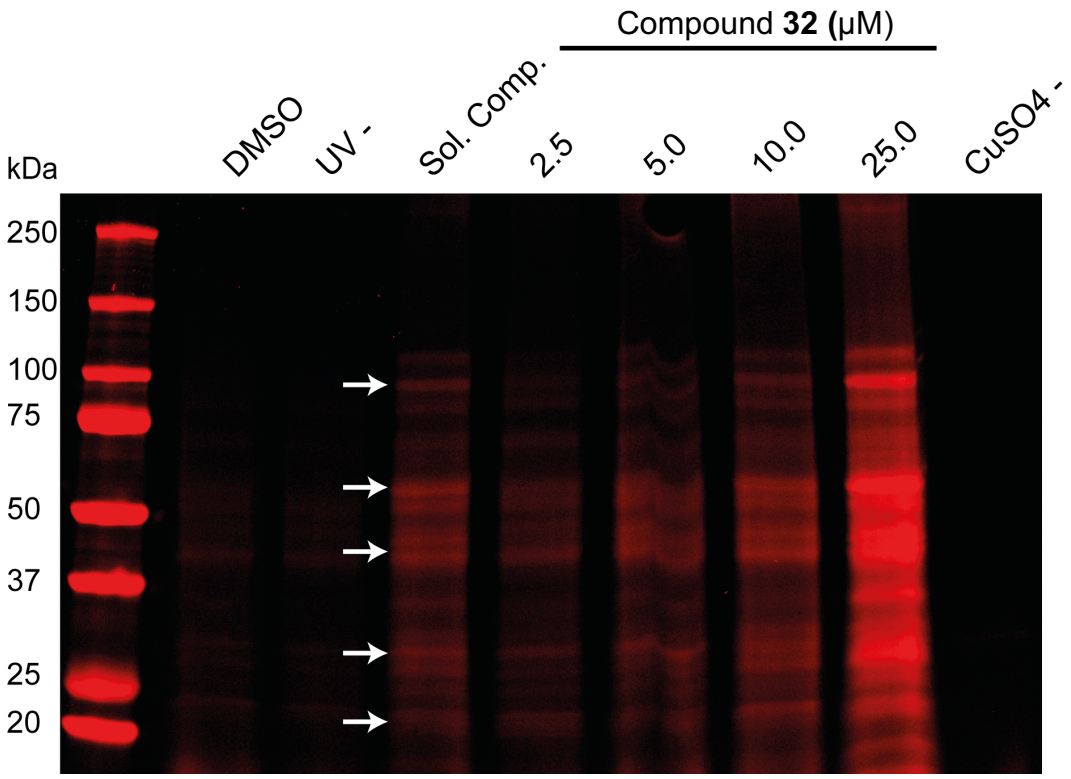

Figure 31. Affinity-based target engagement of photoreactive probe **32** after incubation of LNCaP cells with 1 h, followed UV activation and reaction with AlexaFluor™ 647 azide.

To confirm whether the chemical probe was failing to engage BET proteins, the functional tag was changed from Alexa Fluor™ 647 azide to a PEG-Biotin-azide. The entire procedure except the reporter motif was performed as above. As indicated by Figure 32 when blotting for biotin, only non-specific binding interactions were detected since the same pattern was identified in all samples including in those treated with vehicle. In this experiment a control for the bioorthogonal reaction was not performed so one cannot tell for sure whether compound **32** was successfully functionalized with the biotin-azide reporter or not. In addition, based on the strong affinity between biotin and streptavidin, streptavidin beads were then used to pull down the proteins covalently bound to the biotinilated **RT53**-based probe, but further labelling with anti-BRD4 (Figure 33A) and anti-BRD2 (Figure 33B) antibodies failed to identify any traces of these proteins. Silver staining was used for protein detection in the polyacrylamide gels so that it could be determined the molecular weight of the proteins recovered by the pull down with streptavidin. As observed in Figure 33C, only unspecific proteins were rescued since again these were detected in all samples, including the vehicle control and UV negative sample.

Altogether the data obtained clearly showed that this strategy, as it was applied, was unsuccessful in determining BET bromodomain engagement in cells. From previous experience in the laboratory when studying different ligand-receptor interactions, optimization of this assay has proven

arduous, time-consuming and often unsuccessful. For these reasons, to further confirm target engagement of the new BET-effector in LNCaP cells a different approach was pursued and is described in the following section (IV.3.2.1).

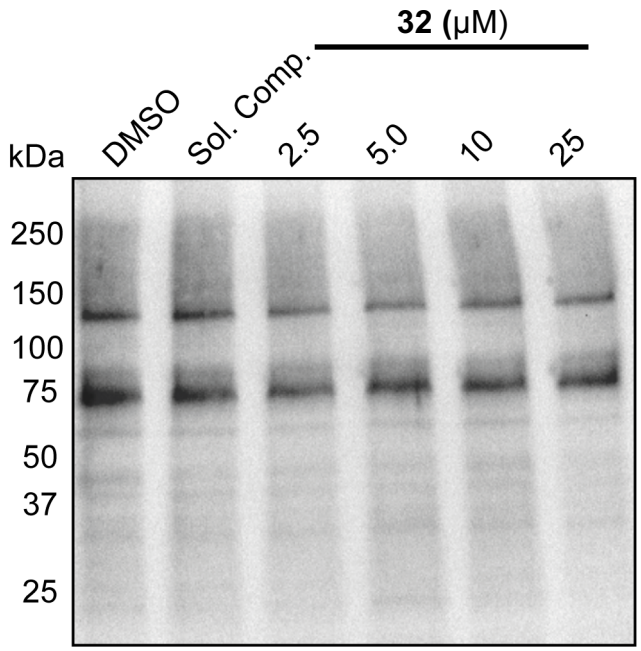

Figure 32. Affinity-based target engagement of probe **32** after incubation of LNCaP cells with 10 mM compound for 1 h, followed UV activation and reaction with a PEG-Biotin-azide reporter. Soluble competition sample is UV + pre-incubated with 50 μM of **RT53** for 1 h.

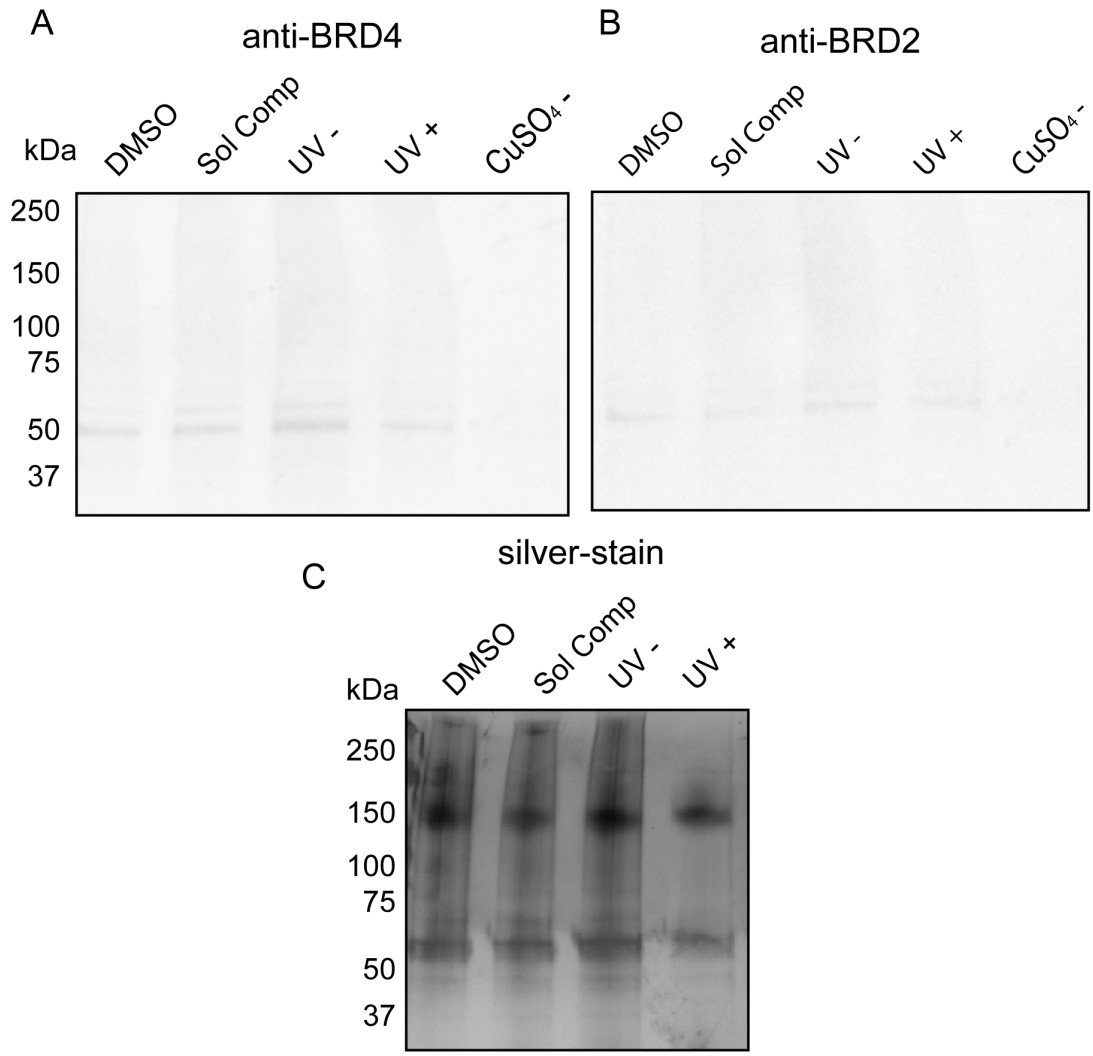

Figure 33. Streptavidin pull-down assays to rescue proteins covalently bound to biotinilated compounds after LNCaP incubation with 10 µM of compound **32**, in the presence (UV +) or absence (UV -) of UV irradiation. A $CuSO_4$-free control was used in an otherwise UV + sample, as well as a soluble competition assay which is UV + pre-incubated with 50 µM **RT53**.

IV.3.2.1. Affinity-based compound-anchored agarose beads

As observed above and despite the potential for strong and irreversible binding, target engagement assessment with the photo reactive probe **32** was not achieved. This could have been due to potential crosslinking with non-specific proteins, or even due to a differential behaviour in cells from the chemical modifications installed in the parent molecule. Furthermore, the introduction of a diazirine motif in close proximity with the alkyne handle followed by the introduction of bulky reporter tags may have also led to an ineffective binding into the cavity of target proteins. Thus, considering the fine-tuning and optimization required, a more efficient methodology was applied in which an affinity matrix was used as a tool to capture ligand-bound proteins from cellular lysates. To achieve this an affinity media based on

agarose beads and comprising a reactive NHS group (AffiGel® 10) was cross-linked with compound **30**, along with capping the non-reacted sections of the resin with ethanolamine and assembling ethanolamide-coupled agarose beads for negative control (Scheme 11). After establishing both affinity matrixes LNCaP cells were then lysed and incubated in the presence of the compound-anchored beads with end-over-end rotation for 12-14 h, followed by bead sedimentation and detection of target proteins by immunoblotting.

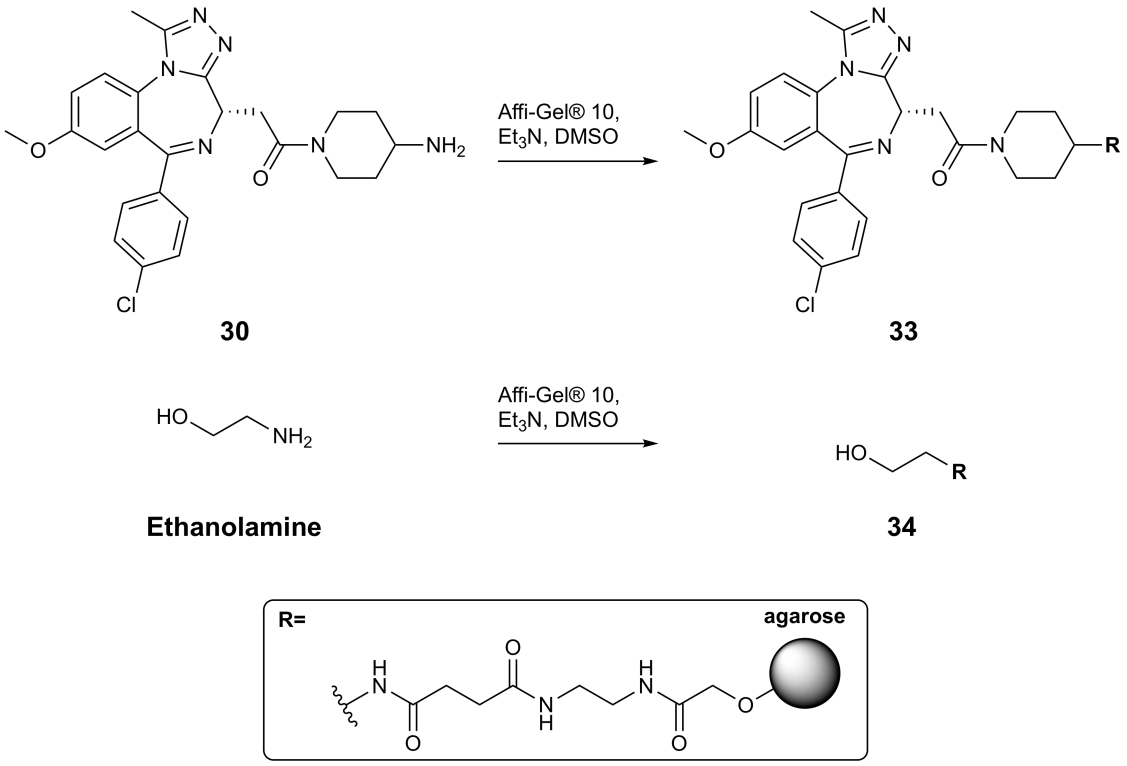

Scheme 11. Synthesis of a chemical affinity matrix with Affi-Gel® 10 and the target ligand. Ethanolamine was used as negative control. Abbreviations: Et_3N, *N, N*-Diethylethanamine; DMSO, dimethyl sulfoxide.

Both BRD4 and BRD2 proteins were identified in the compound-anchored fraction (compound **33**), but not in the ethanolamide-linked resin (compound **34**), therefore suggesting that the resins bearing the **RT53** ligand successfully engaged to these target proteins in cellular lysates (Figure 34 and Figure 35). Furthermore, this effect became more evident in the soluble competition fraction, and in the experiments where free **RT53** was pre-incubated with the lysates for 1 h before adding the **RT53**-coupled beads (**RT53** + compound **33** fraction in the immunoblot). By saturating their binding sites, BRD4 or BRD2 proteins were no longer recovered from **RT53**-anchored agarose beads. It is also worth noting that when analysing the flow through, *i.e.* the fraction of proteins not sedimented with the agarose beads, BRD4 content (Figure 34) was greatly diminished in the samples treated with the affinity matrix

33. This suggests that the proteins successfully engaged with the **RT53**-anchored beads but not with the control beads based on ethanolamide. Thus, the data herein observed together with CETSA observations strongly suggest that the inhibitor **RT53** is capable of engaging both BRD2 and BRD4 proteins in a cellular context.

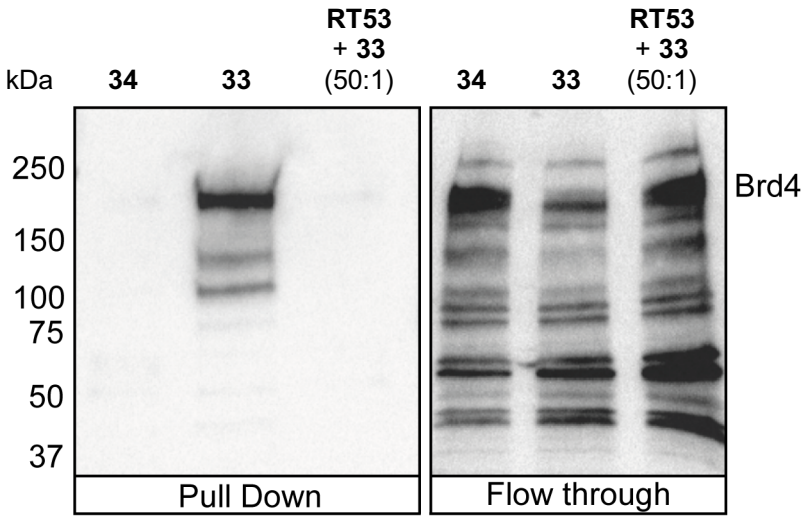

Figure 34. BRD4 affinity-based binding assay with compound anchored agarose beads, in the presence (pull down) or absence (flow-through) of bead sedimentation and immunoblotted with an anti-BRD4 antibody.

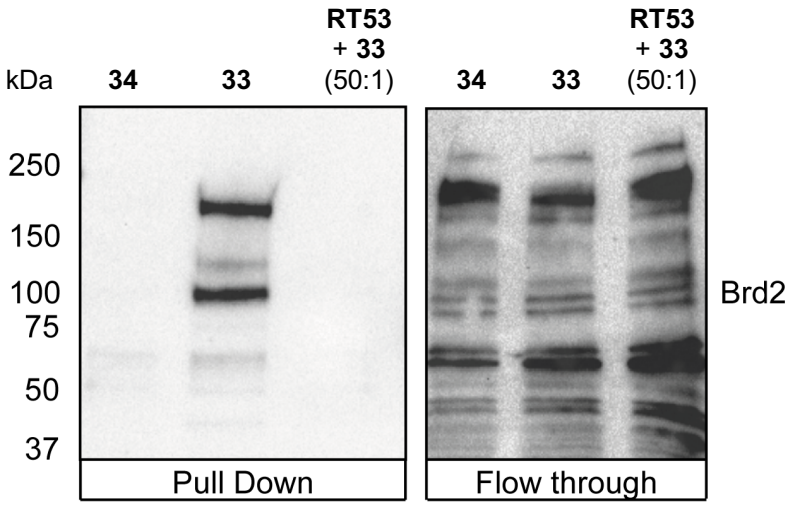

Figure 35. BRD2 affinity-based binding assay with compound anchored agarose beads, in the presence (pull down) or absence (flow-through) of bead sedimentation and immunoblotted with an anti-BRD2 antibody.

IV.3.3. Mechanism of action

It was seen so far that the new IBET-762 based effectors and in particular the ligand **RT53** strongly impair the viability and proliferation of LNCaP prostate cancer cell lines through BET bromodomain

inhibition. In this section and in section IV.3.4 it will be evaluated with greater detail what are the underlying mechanisms involved in these cellular effects.

As highlighted in chapter I.3.2, BET inhibitors show a remarkably heterogeneous response among different cancer cell lines, with some having their cell cycle progression blocked while others undergo apoptosis. To evaluate the mechanism of **RT53** in this particular scenario detection of cleaved poly-ADP-ribose-polymerase (PARP) was used as surrogate for apoptotic events. PARP proteins play a significant role in DNA repair and upon their cleavage by caspases generate a signature 89-kDa fragment, which has been widely used as an hallmark of apoptotic processes.[225] After incubation of compounds in LNCaP cells these were lysed and the proteins immunoblotted for full length and cleaved PARP fragments. Cleaved PARP was not detected after **RT53** treatment neither on a dose-dependent manner up to 2.5 μM for 48 h (Figure 36) neither on a time-dependent manner up to 96 h (Figure 37), thus suggesting that viability of LNCaP was possibly affected by other means than through the induction of apoptotic mechanisms.

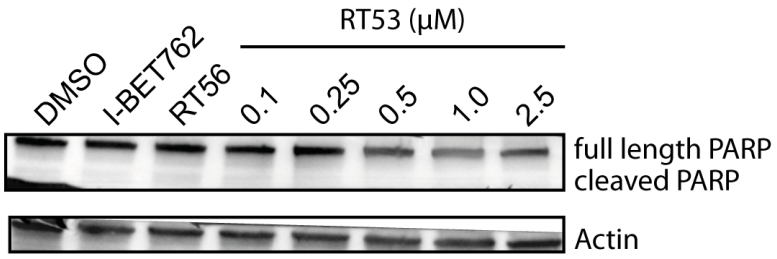

Figure 36. PARP protein content in LNCaP cells after treatment with 2.5 μM of **I-BET762** and **RT56**, and increasing concentrations of **RT53** for 48 h.

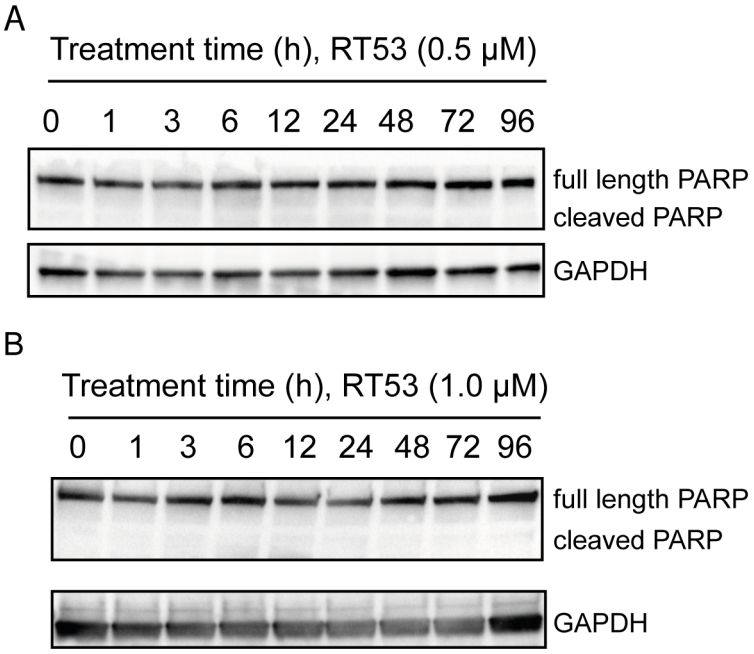

Figure 37. PARP protein content in LNCaP cells at different time points after treatment with either (A) 0.5 μM or (B) 1.0 μM concentrations of **RT53**.

Simultaneously with cleaved PARP detection, cell cycle arrest was determined with propidium iodide (PI) staining and flow cytometry. PI is a DNA binding dye that, based on the premise that it binds in proportion to the amount of DNA present in the cell, allows for subsequent DNA content quantitation and analysis of the cell population in each phase of the cell cycle.[226] G1 cell cycle arrest was observed for **RT53** treated samples (87 % population versus 70 % in vehicle) at low concentrations (0.5 μM) and at a minor extent for **I-BET762** (74 % cell population in G1) (Figure 38). Cell-cycle response to **RT48** was only observed at 1.0 μM (75 % population in G1) and no growth inhibition was observed for **RT56**, as expected due to the inefficient diffusion across cellular membranes. It is also important noting that when at 1.0 μM of **RT53**, a substantial cell cycle arrest was observed with 94.2 % of the cell population observed being in the G1 phase, whereas only 82.5 % were observed in **I-BET762** treated samples (Figure 39). Together this data suggested that the derivatised analogue **RT53** acts in LNCaP cells mostly through a strong impairment of the cellular growth and cell cycle progression. These observations are consistent with the studies of Wyce *et al*., in which they observed similar mechanism of action for **I-BET762** in LNCaP cells.[89]

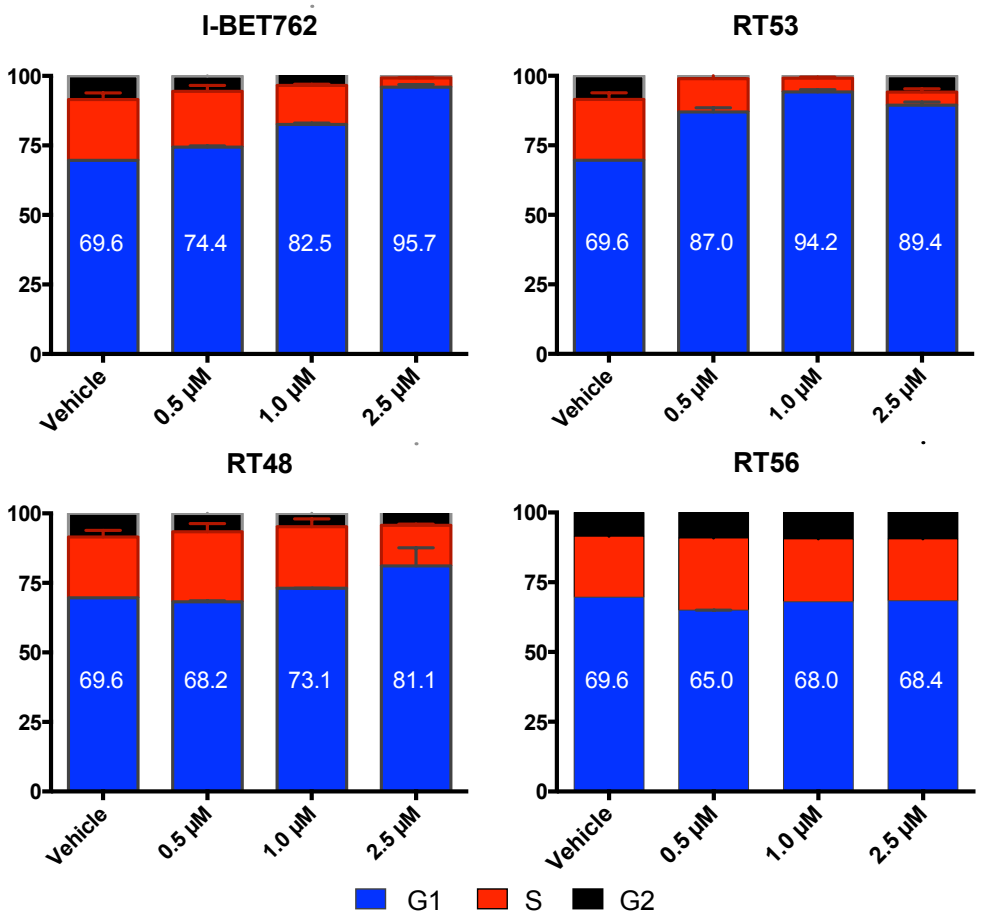

Figure 38. Cell cycle distribution after compound treatment in LNCaP cells for 48 h. DNA content was determined by PI staining and cell population measured by flow cytometry. Data is percentage of cells in each phase represented as mean ± SD of biological duplicates.

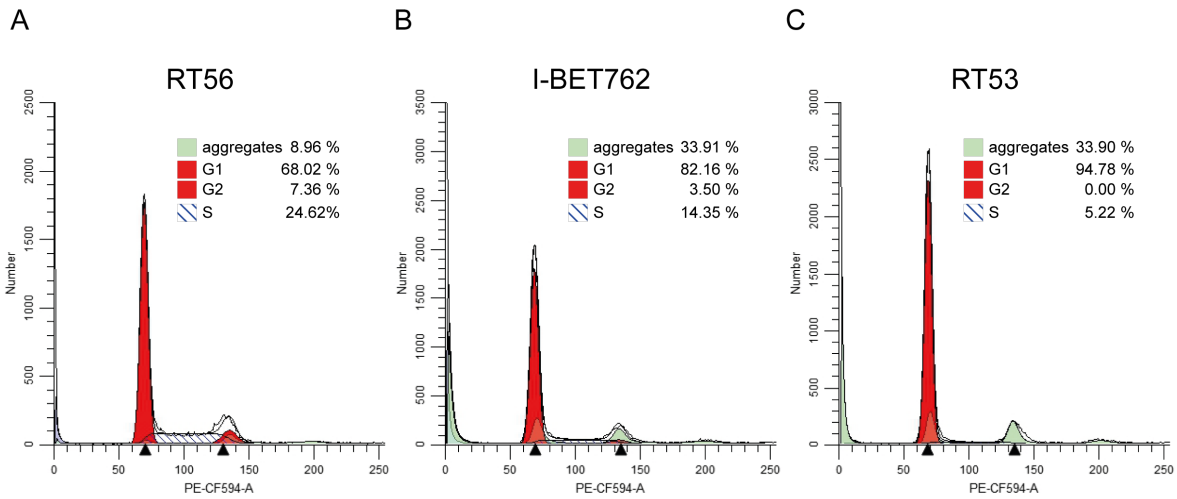

Figure 39. Histogram plots for cell cycle profile after treatment of LNCaP cells with 1.0 µM for 48 h.

To further explore the underlying mechanisms for the anti-proliferative activity of **RT53**, Myc protein content after drug treatment was also analysed. Deregulated Myc protein levels are frequently found in human oncogenesis and a number of observations suggest that Myc regulation might be implicated in BET protein function. In fact, down-regulation of *MYC* transcription has been described in several tumors as a hallmark of BET inhibition,[71,105] and particularly in prostate cancer.[89,120] Although the relationship between Myc levels and sensitivity to BET inhibition is quite complex and is not yet fully understood, **I-BET762** was found to inhibit cell growth of several prostate cancer models by potently decreasing MYC gene expression and Myc protein levels.[89] Thus, it was studied whether **RT53** induction of LNCaP cellular growth arrest had an associated response in Myc protein as well.

Indeed, immunoblot analysis suggested that **RT53** acts through similar mechanisms as observed by Wyce *et al*. for **I-BET762** in LNCaP cells, since Myc protein levels were down-regulated in a dose- (Figure 40) and time-dependent manner (Figure 41). Myc protein content was depleted at concentrations as low as 0.25 μM and with a maximum effect observed at 3 h. In line with previous observations,[223] Myc down-regulation was reversible at lower concentrations (0.5 μM) of **RT53**. Conversely, the BRD4 content increased up to 96 h upon **RT53** treatment, though it is not possible to infer if this is actually being promoted directly by BET inhibition.

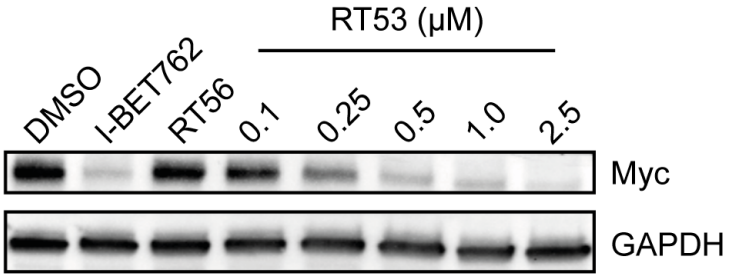

Figure 40. Myc protein levels after treatment with **I-BET762** and **RT56** at 2.5 μM, and increasing concentrations of **RT53** (0.1- 2.5 μM) for 48 h.

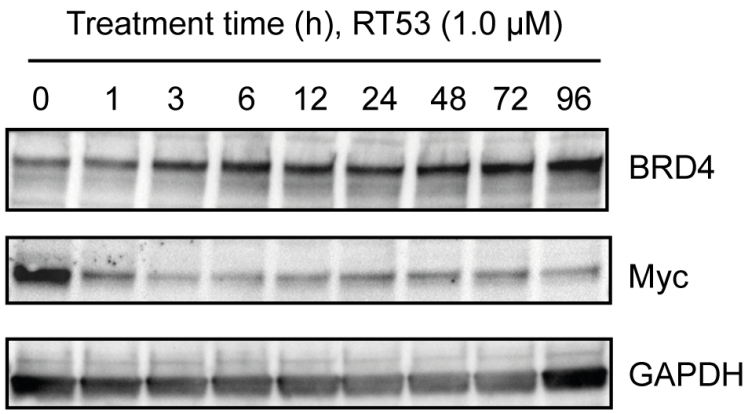

Figure 41. Myc and BRD4 protein content at different time points after LNCaP cell incubation with 1.0 μM of **RT53**.

IV.3.4. Transcriptome analysis

To gain additional insights on the underlying mechanism of action of **RT53** in comparison with I-BET762, changes in transcription were examined by RNA sequencing. LNCaP and PC3 cells were treated with 1.0 μM concentrations of compounds or a DMSO vehicle for 24 h prior to mRNA sequencing. Differential gene expression analysis was conducted for each cell line against the corresponding vehicle control. Both **I-BET762** and **RT53** induced widespread transcriptional perturbations, with **I-BET762** significantly affecting mRNA levels of 12 % and 4 % of all observed transcripts for LNCaP and PC3, respectively, while **RT53** affected 25 % and 15 % of observed transcripts (defined as $q<0.01$). Within these, global repressive effects were observed in LNCaP but not in PC3. In LNCaP following **RT53** treatment 58 % out of the 25 % affected transcripts had their mRNA levels down-regulated while **I-BET762** suppressed the mRNA levels of 67 % out of the 12 % affected transcripts. Conversely, in PC3 only 33 % of the affected transcripts were down-regulated for both **I-BET762** and **RT53**. The transcriptional effects of **I-BET762** and **RT53** were highly correlated though, with the vast majority of genes being affected by both drugs (Figure 42). This is further highlighted by the computed logFC of all observed transcripts, which had Pearson coefficients of 0.82 in LNCaP and 0.84 in PC3, suggesting that the cellular effects of the two compounds at 24 h are largely identical, although differences in potency may exist.

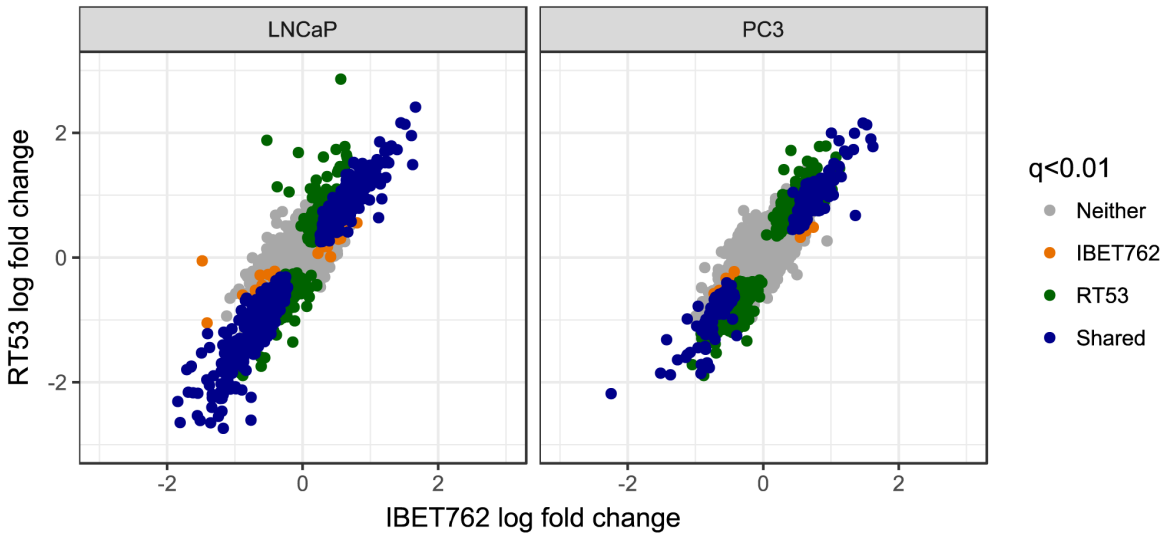

Figure 42. Scatter plot of transcript mRNA fold change (log_2FC) after incubation of LNCaP and PC3 cells with 1.0 μM of **I-BET762**, **RT53** or DMSO vehicle for 24 h. Colored dots represent transcripts affected by I-BET762 (orange), RT53 (green), both (blue) or neither (grey). Data is log_2FC of quadruplicates.

Subsequently it was performed gene set enrichment analysis (GSEA) to identify transcriptional programs modulated by **I-BET762** or **RT53**, checking for enrichment against the Hallmarks and C2 curated collections in the molecular signatures database. In line with previous observations on cellular growth or cell cycle progression, both compounds induced significant repression of several growth-promoting signatures, notably including G2/M checkpoint progression and targets of the E2F family of transcription factors, previously demonstrated to be key downstream effectors of BRD4 activity (Figure 43**,** Table 6). Importantly, *MYC* was also associated with several suppressed gene sets in line with the findings of Wyce *et al*. for **I-BET762** in prostate cancer cell lines.[89] Other curated gene sets as those related to the tumor suppressor p53 and N-Ras signaling were also found enriched significantly among genes down-regulated by **RT53** in LNCaP cells (Table 6), further highlighting **RT53** transcriptional perturbations in a broad set of networks critical for the regulation of tumor growth and cell cycle regulation.

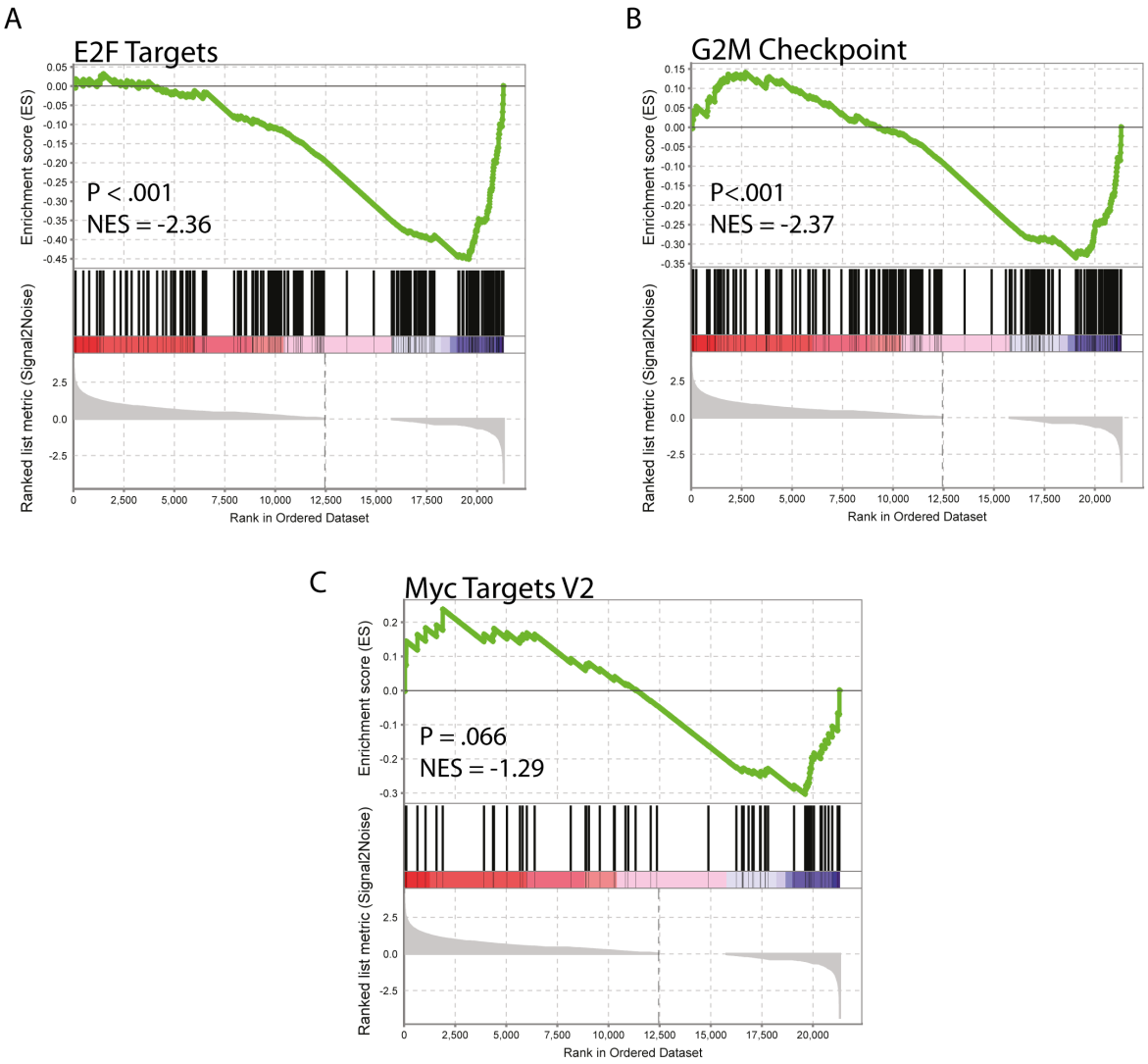

Figure 43. Gene set enrichment analysis (GSEA) of gene signatures down-regulated by **RT53** in LNCaP (NES represents the normalized enrichment score while P represents data significance).

Table 6. Gene signatures enriched among genes down-regulated by **RT53** in LNCaP cells.

Gene set	**N[a]**	**NES[b]**	**FDR-q-val[c]**
ISHIDA_E2F_TARGETS	53	-2.89	< 0.0001
TANG_SENESCENCE_TP53_TARGETS_DN	57	-2.44	< 0.0001
KONG_E2F3_TARGETS	97	-2.42	0.0001
KOBAYASHI_EGFR_SIGNALING_24HR_DN	251	-2.37	0.0006
CROONQUIST_NRAS_SIGNALING_DN	72	-2.32	0.0007
EGUSHI_CELL_CYCLE_RB1_TARGETS	23	-2.27	0.0009
WHITFIELD_CELL_CYCLE_LITERATURE	44	-2.11	0.0017
YU_MYC_TARGETS_UP	42	-2.08	0.0021

[a] N, number of genes in each set; [b] NES, normalized enrichment score; [c] FDR q-value, test of statistical significance

IV.4. Conclusions

In this chapter the new BET bromodomain effectors were profiled for their therapeutic potential and in their capacity to be used as therapeutic warheads in targeted delivery approaches. For this their biological activity and mechanisms of action were comprehensively studied.

Against a panel of cancer cell lines comprising 9 different tissues, potent growth inhibitory effects were observed mostly in a subset of AR-positive prostate cancer. In LNCaP cells these were driven by perturbations of the cell cycle progression with an arrest in the G1 to S phase transition. These observations are consistent with the studies of Wyce *et al*. for **I-BET762,**[89] therefore suggesting similar mechanisms of action for the tertiary amine derivatives in comparison with the parent molecule.

Importantly, target engagement studies revealed that **RT53** successfully engaged BRD2 and BRD4 inside living cells as confirmed by cellular thermal shift assays and also in lysates as monitored by affinity-based pull downs with compound-anchored agarose beads, demonstrating compound efficacy and confirmation of the mode of action.

Furthermore, the observations provided herein seem to corroborate the existing rationale of Myc protein downregulation as a hallmark of the antitumoral activity of BET inhibitors. A substantial suppression of Myc protein levels was observed after **RT53** treatment both in a dose- and time-dependent manner. The transcriptional output following drug treatment sustained these observations with a significant down-regulation of *MYC* and *MYC*-related gene signatures being determined by gene set enrichment analysis studies. In addition, **RT53** strongly supressed mRNA levels of known BRD4 downstream effectors involved in cell cycle checkpoint progression and targets of the E2F family of transcription factors. Altogether, the retrieved data suggests that **RT53** exerts its antitumoral activity in LNCaP cells through the modulation of transcriptional networks critically involved in cellular growth and cell cycle progression.

Therefore, although slight differences in potency may exist, **RT53** and **I-BET762** had identical cellular effects in LNCaP, further supporting the antitumoral efficacy and therapeutic potential of the new tertiary amine derivative. In addition, this data favoured the use of **RT53** as a payload for targeted delivery strategies and, importantly, established prostate cancer as a potential target disease.

Chapter V

Targeted delivery of a BET effector in prostate cancer

Rui Traquete[1,3], Pedro M. S. D. Cal[1], João Conde[1], Richard F. Cook[3], Xhenti Ferhati[4], Francisco Corzana[4], Angela N. Koehler[3], Gonçalo J. L. Bernardes[1,2]

[1] Instituto de Medicina Molecular João Lobo Antunes, Faculdade de Medicina, Universidade de Lisboa, Avenida Professor Egas Moniz, 1649-028 Lisboa, Portugal

[2] Department of Chemistry, University of Cambridge, Lensfield Road, CD2 1EW Cambridge, UK

[3] David H. Koch Institute for Integrative Cancer Research, Center for Precision Cancer Medicine, Department of Biological Engineering, Massachusetts Institute of Technology, Cambridge, MA, USA

[4] Departamento de Quimica, Universidad de La Rioja, Centro de Investigacion en Sintesis Quimica, 26006 Logroño (Spain)

Author Contributions

R.T., A.N.K. and G.J.L.B. designed the experiments. R.T. performed the synthesis, linker stability studies and cellular characterization of compounds. P.M.S.D.C. helped with the synthesis of the final conjugates, J.C analysed therapeutic activity in tumor bearing mice, R.F.C. helped in linker-drug stability and release studies, X.F. and F.C. performed large scale synthesis of final conjugate, R.T. wrote the chapter, G.J.L.B. directed the research and revised the text.

Chapter V. Targeted delivery of a BET effector in prostate cancer

V.1. Introduction

In the previous chapters it were extensively studied the resulting effects of **I-BET762** functionalization to make it suitable for traceless release strategies in cancer tissues. Given that the efficacy of a ligand-targeted drug conjugate is primarily determined by the activity of the payload, biophysical and cellular assessments assuredly validated the therapeutic potential of the tertiary amine derivative **RT53**. Finally, a link must be established between **RT53**, the cleavable bridge and a targeting ligand in order to promote preferential localization followed by traceless release of the new BET effector in diseased tissues.

V.1.1. Cleavability of the linker

As described in Chapter III. the synthetic design on the derivatisation of **I-BET762** aimed at including a tertiary amine that could enable the accommodation of a self-immolative aminobenzyl quaternary ammonium salt (PABQ). Enhanced pharmacokinetic properties of targeted conjugates have been observed when using these quaternary ammonium self-immolative motifs instead of the more frequently applied carbamates (PABC), namely by showing superior solubility, decreased aggregation and appropriate stability as well as absence of immune responses that can hamper conjugate's therapeutic index.[195,196,199] Staben *et al*. addressed those challenges and envisioned that self-immolation of a PABQ could lead to the traceless release of the appended drug through the fragmentation of radical anions in the nitrobenzyl quaternary ammonium salt.[199] However, an intracellular chemical or enzymatic event specific to cancer cells is needed to trigger the start of the reaction and allow for the controlled stability and drug release.

It is critical for the success of targeted conjugates that these triggering events occur only at the site of the disease and not while in circulation, which can lead to premature drug release and subsequent toxicitiy. For SMDCs, this means that the linker needs to be stable for only a few min. to an h, as within this time frame the conjugates should either be captured by their targeted receptors or cleared from the body.[160] Thus, considering the importance of the biochemical properties of these cleavable motifs to the efficacy of the conjugates, a variety of releasing mechanisms have been engineered for activation by different intracellular processes. In the study of Staben *et al*. two different cleavable moieties were

introduced into the linkers, a protease-cleavable valine-citruline dipeptide or a reductive cleavage of a disulfide bridge (Scheme 12).

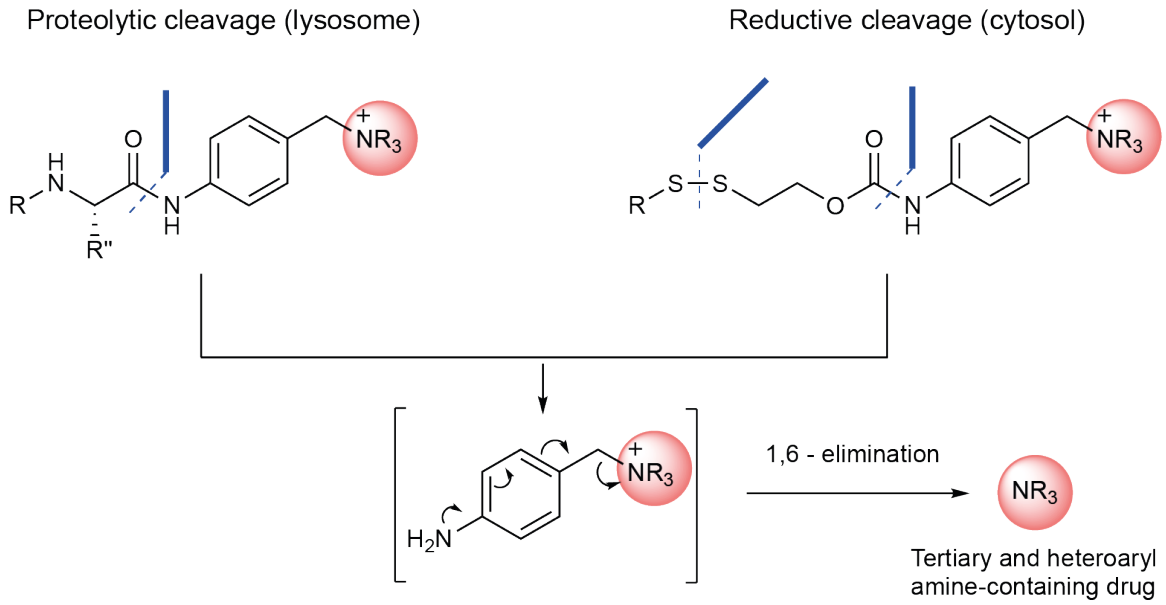

Scheme 12. Targeted delivery of tertiary and heteroaryl amine-containing drugs, with the self-immolation of the *p*-aminobenzyl moiety leading to the corresponding free drug.

Reductively cleavable linker chemistries take advantage of the elevated reducing potential that is usually much greater in the cell cytoplasm than in the extracellular milleu, mostly due to an enhanced glutathione concentration inside cells. This leads to proper stability of the disulfide linkers while in the bloodstream and interstitial fluids, followed by a fast release kinetics due to glutathione reduction upon internalization of a conjugate into an endosome.[165,174] The release of a therapeutic payload through disulfide reduction is usually favoured when peptides or small molecules like folate are used as targeting agents, since these are processed through the endosome or translocated directly to the cytosol.

Conversely, self-immolation of linkers triggered by proteolytic cleavage is usually the preferred mechanism of drug release when the targeting motifs are processed through lysosomal pathways.[227,228] These linkers exploit the differential expression of hydrolytic enzymes inside diseased cells in comparison with healthy cells, which confers the controlled release nature to the cleavable bridge. The dipeptide valine-citruline (VC) has been widely used as one such releasing mechanism, since it is well known to cleave on exposure to lysosomal proteases and particularly to cathepsin B, a cysteine protease highly upregulated in a wide variety of cancers.[229] Indeed, the VC linker often accompanies the PABC self-immolative spacer and both constitute the most commonly applied cleavable linker

technology among ADCs currently undergoing clinical studies.[193] One of the reasons why these are so attractive is that in comparison with other cleavable chemistries, VC linkers have a significantly longer half-life in plasma. This enhanced stability is partially because the VC dipeptide is a substrate of proteases that are primarily located in acidic lysosomes, so a fast cleavage rate and efficient payload release requires the internalization of the conjugate.[163,230]

Interestingly it has been demonstrated recently that extracellular proteolytic cleavage of the VC linker can also occur, while still maintaining efficient drug release and potent anti-tumor activity,[231,232] therefore suggesting that the internalization of drug conjugates may not be such a critical requirement. In support of these findings, Caculitan and colleagues have recently shown that suppression of cathepsin B through CRISPR-Cas9 gene deletion or shRNA knockdown had no effect on the anti-tumor activity of ADCs bearing a cleavable VC linker.[233] These observations suggest the existence of functional redundancy within the cathepsin protease family, further confirmed by data showing efficient cleavage of the VC-linker by other cysteine cathepsins with varying degrees of efficiency.[233] These broader possibilities for linker processing are not entirely surprising, as it is well established that the distribution of cathepsins varies depending on cell type and often their localization changes during neoplastic progression.[229] However, these also accentuate the need for further understanding on how protease-cleavable linkers operate in each particular scenario.

Together, many other observations suggest that cleavable linkers per se are unlikely to increase the therapeutic index of ligand-drug conjugates,[175,189,234,235] whereas the nature of a ligand-receptor interaction can indeed significantly influence the potency and metabolism of targeted drug conjugates.

V.1.2. Disease-specific receptor and targeting ligand

Without doubt a major determinant for selective delivery of drugs lies in the differential expression of a targeted receptor in diseased versus normal tissues. A threefold or higher overexpression of the targeted receptor on the cancer cells is generally considered sufficient to avoid unacceptable toxicities in healthy cells.[165] Indeed, the two more prominent receptors targeted by drugs in the clinic have only twofold or threefold overexpression in malignant versus normal tissues. These include HER2, targeted with Kadcyla (Trastuzumab-SMCC-DM1) in HER2-positive breast cancer patients,[236] and also the CD30 antigen targeted by Adcetris (brentuximab vedotin) in Hodgkin's lymphoma and anaplastic large cells lymphoma.[237,238] In addition, to be useful for targeted delivery a minimal absolute level of receptor expression in the malignant cell is required. This means that if to achieve a therapeutic effect a certain concentration of drug is required inside cells, enough receptor density must be present to mediate drug

internalization into the target cell. Examples of often exploited tumor-enriched antigens that are expressed in vast excess include FR, PSMA and glucose transporter 1 (GLUT1).[165]

Concomitantly to receptor expression profile in malignant versus healthy tissues, their location and accessibility must also be considered. Generally, a receptor expressed on the surface of cancer cells is preferred since intracellular targets imply non-specific membrane diffusion and therefore indiscriminate targeting of malignant and healthy cells. Thus, different classes of overexpressed cell-surface exposed receptors have been exploited for drug delivery. These include, for example, proteins that are normally only expressed inside healthy cells but become exposed upon disease transformation,[239,240] or receptors that are normally expressed on the apical surfaces of epithelial cells and that become readily accessible upon malignant transformation.[241-243] In addition, receptors whose accessibility in normal tissues is either limited or absent are also promising targets for drug delivery. Among the latter is the cell surface enzyme PSMA, which is prominently expressed in healthy brain tissue including astrocytes and Schwann cells but with a distinct overexpression on prostate tumor cells.[160,244]

The cellular trafficking of targeted-drug conjugates upon internalization is also determined by the cell-surface receptors. Most of the commonly targeted receptors traffic through various intracellular compartments such as early endosomes, late endosomes or lysosomes. If the therapeutic payload is membrane permeable and is tethered to the targeting ligand *via* a cleavable bridge, it can be released from the linker and diffuse out of these intracellular compartments and into the cell cytoplasm where it can perform its function.[160,165,174] While in most cases endocytosis of the targeted-drug conjugate has been exploited, the therapeutic payload can also be released by an extracellular triggering event specific to the diseased tissue microenvironment, as recently observed for targeted drugs tethered by dipeptide valine-citruline linkers.[231,232] Concomitantly to this scenario the therapeutic warhead must be capable of passively diffusing across the malignant cell membrane and into the cytoplasm. Finally, the internalization rate in some cell-surface receptors is enhanced by the binding of a ligand, which can be advantageous for targeted therapeutics due to the recycling of receptors to the cell surface. Again, the PSMA proteins in prostate cancer cells is one such example as its internalization rate was found to be increased up to threefold after binding of specific ligands.[244] In addition, some of the PSMA proteins are rapidly recycled back to the cell surface through the recycling endosomal compartment, rendering them available for additional internalization of compounds.[245]

Once established the criteria for the identification of a disease-specific receptor, a targeting-ligand that is also suitable to be a drug delivery vehicle must be found. The ligand size by itself has a great influence on the conjugate pharmacokinetics as previously described in chapter I.5. Given the longer circulation times, poor extravasation from blood vessels and extent of penetration into solid tissues of

their larger counterparts, SMDCs were preferably exploited in this study. All targeting ligands currently in clinical development are characterized by a high affinity and high specificity towards their receptor. Ligands having a target affinity in the low nanomolar range are usually preferred (K_D < 10 nM)[160], though in certain cases the lack of receptor avidity is compensated with multiple ligands[246]. As for ligand specificity, it is important to avoid compounds that bind promiscuously to many different proteins, thus leading to nonspecific interactions.

A common concern in the development of targeted-drug conjugates is the availability of conjugation site chemistries that enable the attachment of substituents while preserving the biological properties of the different elements. This was taken in consideration for payload selection (Chapter II.1) and upon the installation of tertiary amine derivatives on **I-BET762** (Chapter III.3). Likewise, derivatization of the targeting ligand should not interfere with the affinity for its receptor to other elements. Furthermore, alike in payload selection the most used functionalities to tether ligands to spacers or cleavable bridges have included carboxylic acid, amine, alcohol, thiol and aldehyde functionalities.[160]

The search for smaller vehicles that meet the criteria above-outlined has mainly focused on naturally occurring molecules such as small peptides[247,248] or vitamins.[249,250] Conjugates of potent cytotoxic drugs with peptide ligands have shown promising results in several cancer cell models, particularly those using as ligands derivatives of the luteinizing hormone-releasing hormone.[251,252] Due to very rapid cell-division cycles, tumor cells and enhanced requirements for vitamins as folate, biotin and cobalamine, the corresponding cell-surface uptake transporter proteins are often overexpressed and have been widely explored for drug delivery applications. The hallmark of this strategy is the folate-targeted desacetylvinblastine hydrazide conjugate EC145, which uses the FA/FR system and is currently undergoing phase 2 clinical trials for several types of cancer.[180,181] Substrate analogues that target tumor-associated enzymes have also been widely used as targeting ligands, namely those that target the PSMA protein.[177,244] Particularly using DUPA as the targeting ligand several motifs have been delivered to prostate cancer cells including imaging agents and cytotoxics.[176,177,253] As introduced in Chapter I.5.1, DUPA-^{99m}Tc was investigated as a radio-imaging agent (K_D= 14 nm towards LNCaP *in vitro*)[176] and potent activity against LNCaP cells has been observed for DUPA-drug conjugates including desacetylvinblastine (IC_{50} = 31 nM), camptotecin (IC_{50} = 115 nM), verrucarin A (IC_{50} > 1 μM), tubulysins H I, II and III (IC_{50} = 5-24 nM) and didemnin B (107 nM).[174] Another ligand-drug conjugate targeting PSMA, EC1169, is in phase 1 clinical trials for the treatment of metastatic CRPC.[254] This has been well tolerated and showing evidences of anti-tumor activity, therefore suggesting that a PSMA-targeted therapeutic is viable.[255] Considering all the key elements involving the selection of ideal cleavable bridges and targeting ligands, in this chapter it will be assembled a unique targeted-BET-inhibitor

conjugate specific for prostate cancer cells and which enables **RT53** traceless release based on a self-immolative quaternary ammonium salt.

V.2. Goals

The aim of this chapter is to design, develop and characterize a novel SMDC for the selective delivery of the new BET effector into cancer cells.

The synthesis route will be designed and **RT53** chemically tethered to a dipeptide VC linker through an aminobenzyl quaternary ammonium salt. Controllable payload release upon a triggered enzymatic event will be studied in the presence of an enzymatic trigger and biological studies will be performed as surrogate for payload release in a cellular context.

The linker-drug conjugate will then be attached to a ligand that specifically targets an overexpressed receptor on the surface of prostate cancer cells. Therapeutic efficacy of the final conjugate through the selective liberation of **RT53** will be studied first in cells and then in mouse models of prostate cancer, in comparison with unconjugated derivatives and the unmodified **I-BET762**.

V.3. Development and validation of a targeted BET inhibitor

V.3.1. Traceless release of RT53

Taking advantage of the installed tertiary-amine functionalities, the **RT53** derivative was attached to a bioreversible bridge consisting of a dipeptide VC linker through an PABQ salt. While the findings of Staben *et al.* discussed in Chapter V.1.1 extended PABQ application to both disulfide and proteolytic release mechanisms, the VC linker was selected as the candidate to test our traceless release hypothesis. Importantly, the VC triggering mechanism can be found in various ligand-drug conjugates processing through the endosomal and/or lysosomal pathways,[199] which makes it suitable for conjugation with the targeting ligand exploited in the next section.

The model linker motif and subsequent attachment to **RT53** was prepared *via* a multistep route and is depicted in Scheme 13. In brief solid-phase peptide synthesis was used to synthesize the VC dipeptide through a 2-chlorotrityl resin followed by the sequential addition and deprotection of Fmoc-Cit-OH and Fmoc-Val-OH. The VC dipeptide was then functionalized with an aminophenyl group

for derivatization with the new BET effector **RT53**, affording compound **38** (hereafter **VC-PABQ-RT53**) conjugate that should enable the traceless release of **RT53**.

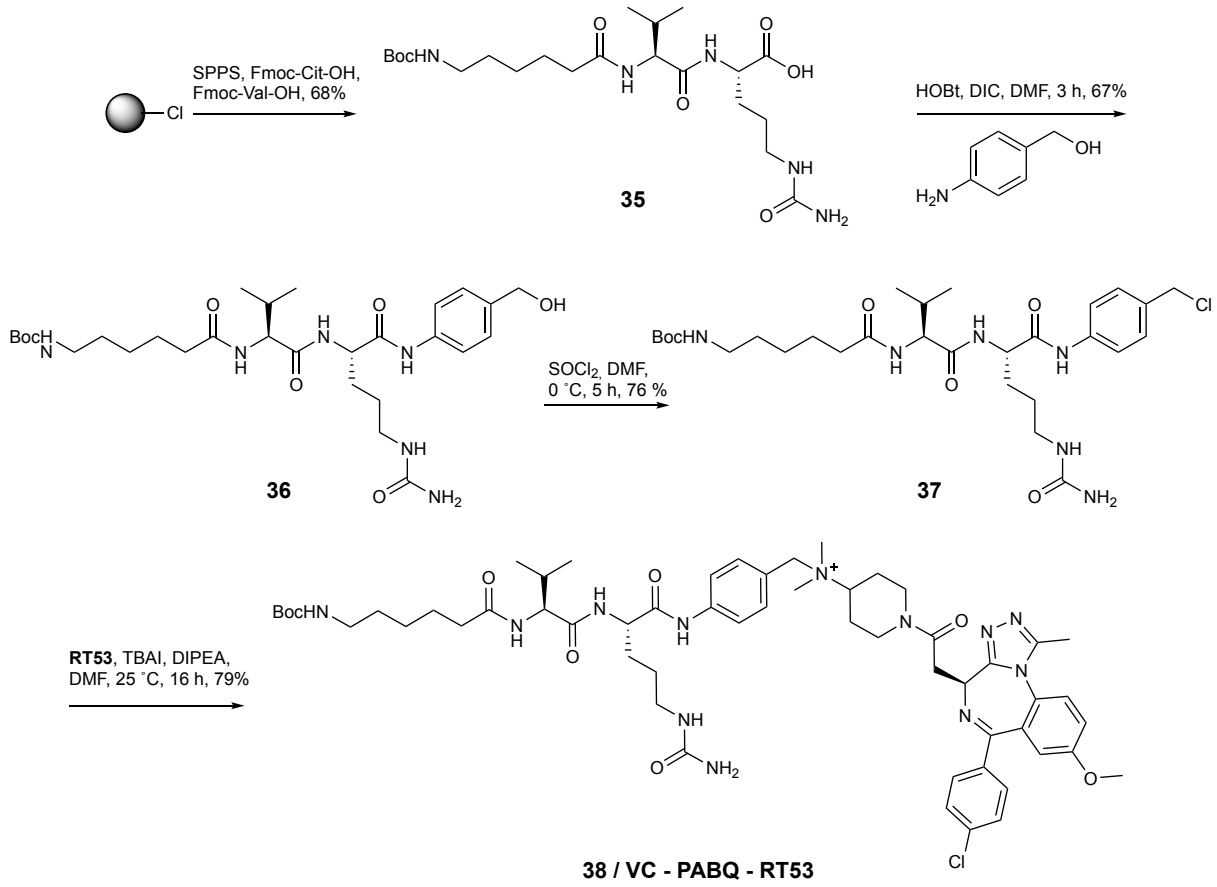

Scheme 13. Synthesis of the traceless linker conjugated to a BET effector affording **VC-PABQ-RT53** construct. Abbreviations: SPPS, solid-phase peptide synthesis; HOBt, *N*-Hydroxybenzotriazole; DIC, *N,N'*-Diisopropylcarbodiimide; DMF, dimethylformamide; $SOCl_2$, thionyl chloride; DMF, dimethylformamide; TBAI, tetrabutylammonium iodide; DIPEA, *N,N*-Diisopropylethylamine; DMF, dimethylformamide.

As described above (Chapter V.1.1) VC linkers were designed to be cleaved by lysosomal proteases such as the cysteine protease cathepsin B,[256] an enzyme found up-regulated in cancers and metastatic tumors.[229] Thus, for proof-of-concept it was evaluated if **RT53** could be released from the linker technology and whether this linker would be stable and only revert to the unmodified BET effector on a designed triggering event. In a buffered medium containing cathepsin B (pH 5.5, 37 ˚C) it was observed complete liberation of **RT53** in 18 h (0% of **VC-PABQ-RT53**) (Figure 44, Figure 45), whereas in the absence of the proteolysis enzyme negligible decomposition of **VC-PABQ-RT53** was observed during the same period of time (90% of **VC-PABQ-RT53**) (Figure 45), thus providing preliminary support for the controlled release nature of the construct. As noted in the HPLC analysis (Figure 45) it was also

observed a slight increase in a third species throughout time, which was identified as having an *m/z* $(M+H)^+$ of 388.43 corresponding to the VC spacer, further corroborating the complete self-immolation of the benzylic ammonium motif. Furthermore, at each time point the aliquots taken were immediately quenched with the protease inhibitor E-64 at a 1:1 (enzyme to inhibitor) ratio, thus assuring that the data output reflects the conversion rate at each specific time point.

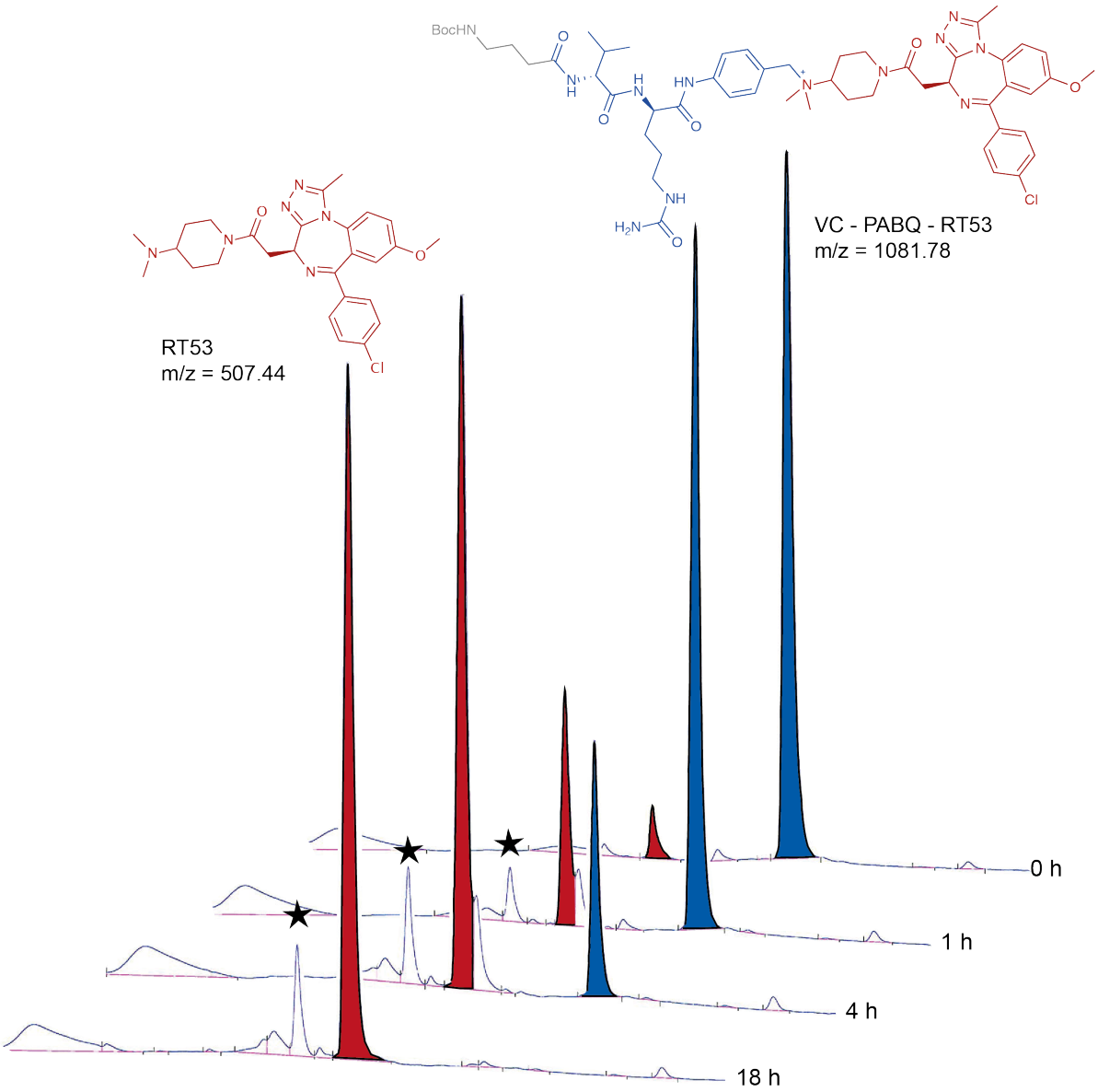

Figure 44. Controlled release of **RT53** from **VC-PABQ-RT53** in the presence of cathepsin B up to 18 h. Traces were detected with HPLC and compounds confirmed by LC-MS and co-injection with a pure standard. Star indicates VC peak.

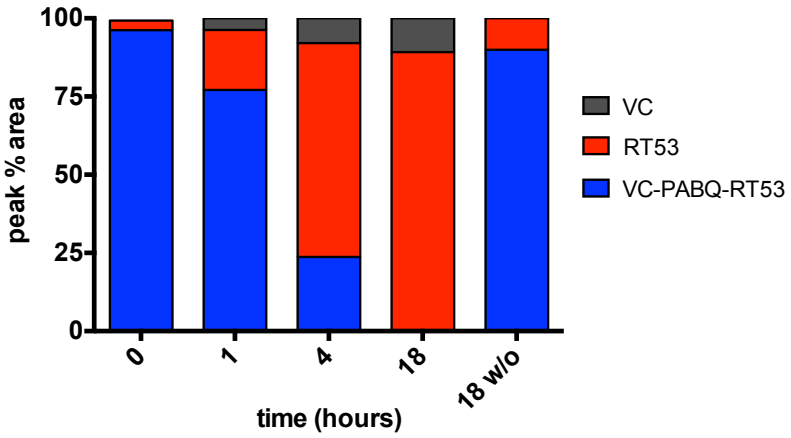

Figure 45. Rate of **RT53** drug release in the presence of cathepsin B, estimated from peak area (mAU*s) divided by the sum of free drug and linker-drug conjugates.

To elucidate if the success of **RT53** traceless release was also extended to a cellular context, LNCaP viability and down-regulation of Myc protein content were used as a surrogate for linker self-immolation in comparison with the free **RT53** drug. The rationale was that in the case of an unsuccessful payload release the quaternary ammonium motif in **VC-PABQ-RT53** construct could also impair the antitumoral activity as it has been previously observed for **RT56**. Despite showing lower potency than **RT53** alone, a potent inhibitory effect was still observed in LNCaP upon treatment with **VC-PABQ-RT53** (IC_{50} = 1.7 μM; IC_{50} = 0.26 μM for **RT53**) (Figure 46). Furthermore, although Myc protein levels were not affected in a time-dependent manner at 2.5 μM single doses of **VC-PABQ-RT53** up to 24 h (Figure 47A), a dose-dependent response was observed after 48 h incubation with the linker-drug conjugate (Figure 47B).

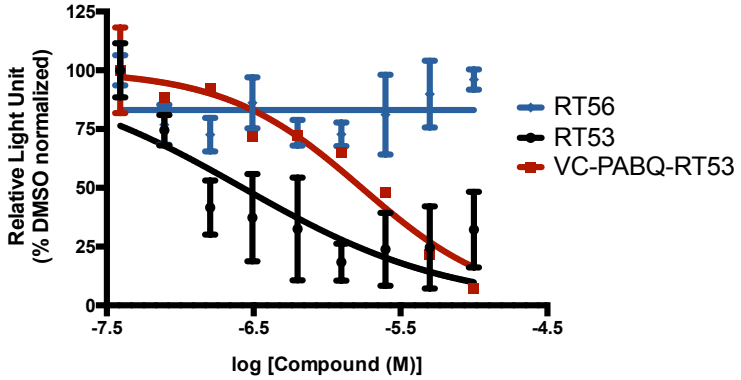

Figure 46. Antitumoral activity of **VC-PABQ-RT53** as surrogate for **RT53** release in LNCaP cells. Cellular viability was normalized to DMSO after compound treatment in LNCaP cells (96 h incubation, triplicate means ± SD).

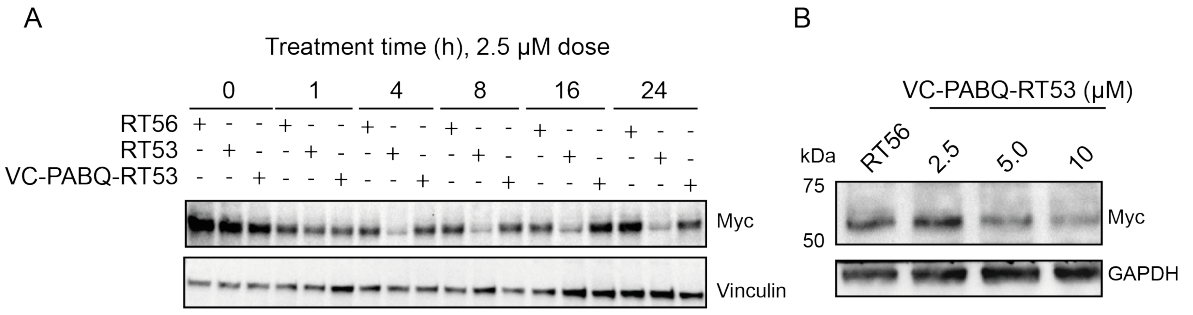

Figure 47. Myc protein levels after (A) treatment with **RT56**, **RT53** and **VC-PABQ-RT53** at 2.5 μM at different time points, and (B) increasing concentrations of **VC-PABQ-RT53** (2.5 - 10 μM) for 48 h.

V.3.2. Targeting prostate cancer

With promising preliminary data in hand, and considering the efficacy of **RT53** towards LNCaP, it was then engineered a unique ligand-BET inhibitor conjugate to specifically target prostate cancer cells. Through appropriate conjugation chemistry the linker-drug conjugate **VC-PABQ-RT53** was tethered to the PSMA ligand – DUPA. This ligand is well established as having high affinity towards PSMA (K_i = 8 nM), a type two transmembrane protein which is up to 1000-fold overexpressed in prostate cancer cells and minimally detected in normal cells.[257,258] This differential expression in malignant cells along with other key properties evidenced earlier in this chapter turn PSMA a prime biomarker for tumor targeting, further corroborated by the numerous strategies using this receptor in drug delivery applications.[176,177,244] Importantly, PSMA-bound ligands are known to internalize by endocytosis through clathrin-coated pits then being either retained in lysosomal compartments along with the degrading PSMA receptor or released to distribute within the cell,[245] which is compatible with the VC-PABQ release mechanism tethered to the BET effector **RT53**.

DUPA ligand was synthesized as previously described by Kularatne *et al*.,[177] and is shown in Scheme 14. In brief, a solution of *α,γ,-Di-tert*-butyl glutamate **39** was treated with triphosgene in the presence of triethylamine to afford an isocyanate intermediate, that upon the addition of glutamate **40** bearing benzyl and *tert*-butyl protection groups provided the urea **41**. Atmospheric hydrogenation of the latter for two days in the presence of Pd/C afforded the pure DUPA precursor **42**. Deprotection of BOC in **VC-PABQ-RT53** with trifluoroacetic acid provided the functional amine for HBTU-mediated coupling with the DUPA precursor **42** bearing a free carboxylic acid and providing compound **43**, which upon *tert*-butyl deprotection with trifluoroacetic acid for 1.5 h at room temperature afforded the final conjugate **44** hereafter **DUPA-VC-PABQ-RT53 (**Scheme 15**)**.

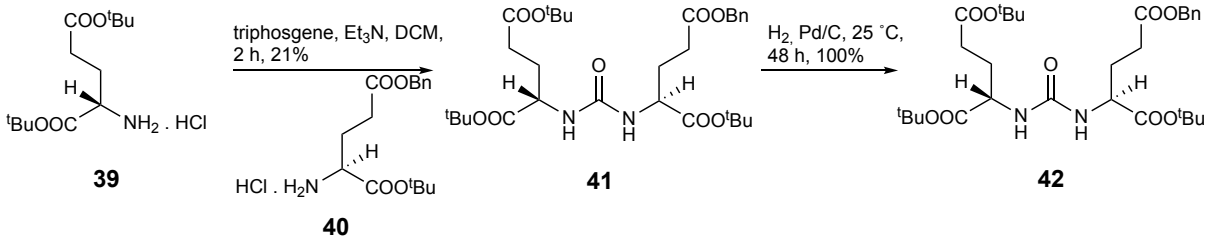

Scheme 14. Synthesis route to afford DUPA intermediate. Abbreviations: Et_3N, *N,N* -diethylethanamine; DCM, dichloromethane; Pd/C, palladium on carbon.

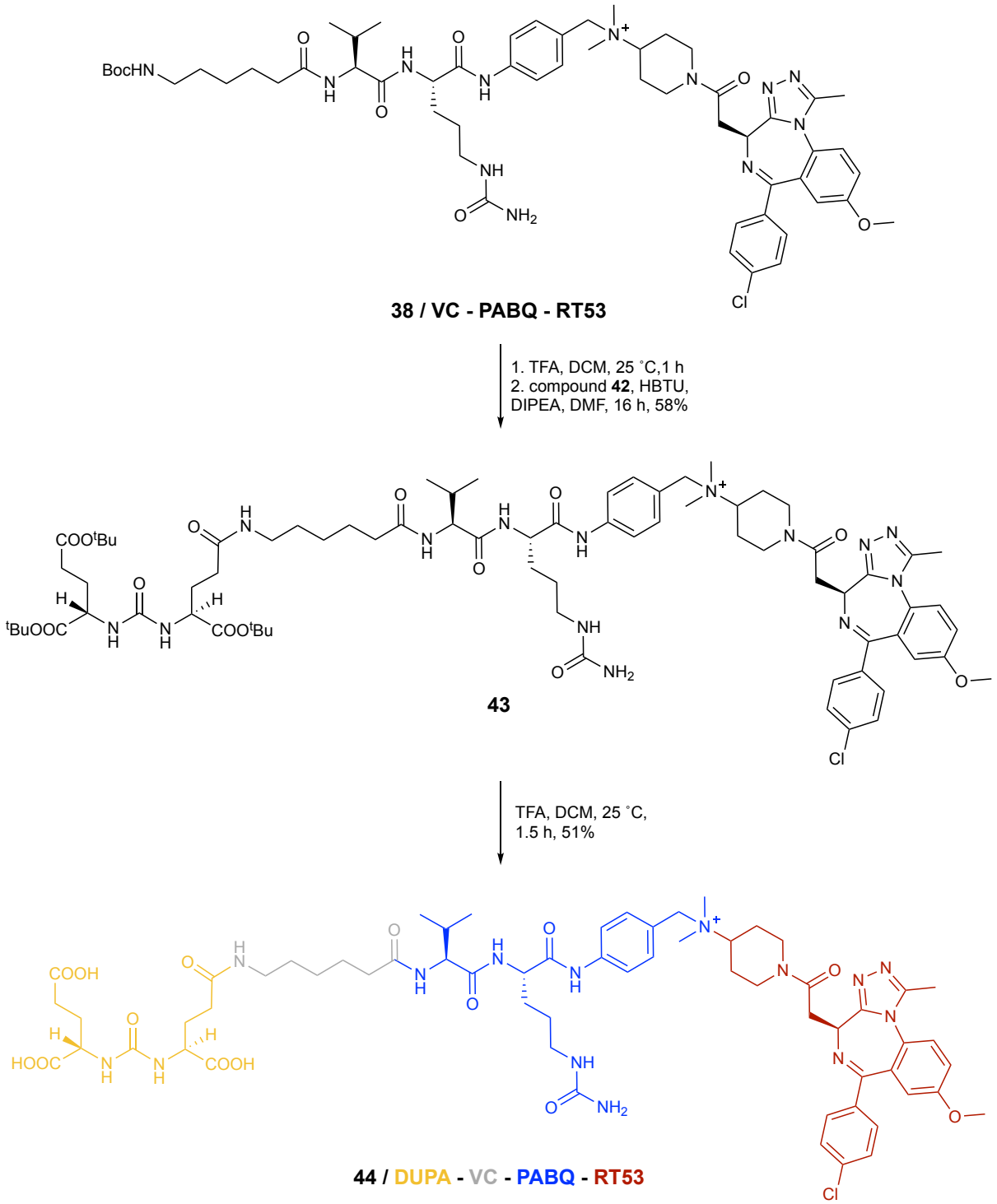

Scheme 15. Synthesis of prostate cancer targeting conjugate DUPA-VC-PABQ-RT53. Abbreviations: TFA, trifluoroacetic acid; DCM, dichloromethane; HBTU, *N,N,N',N'*-Tetramethyl-*O*-(1*H*-benzotriazol-1-yl)uranium hexafluorophosphate; DIPEA, *N,N'*-Diisopropylethylamine; DMF, dimethylformamide.

Upon establishing the synthetic route affording **DUPA-VC-PABQ-RT53,** and before embarking on the *in vivo* experiment, its antitumoral activity was examined in cells expressing the PSMA receptor (LNCaP) versus cells that do not express it (PC3).[244] Gratifyingly, the obtained results indicated a strong cellular response to conjugate treatment in PSMA-positive cells (IC_{50} = 4.9 μM), but not in PSMA-negative (IC_{50} > 10 μM) (Figure 48).

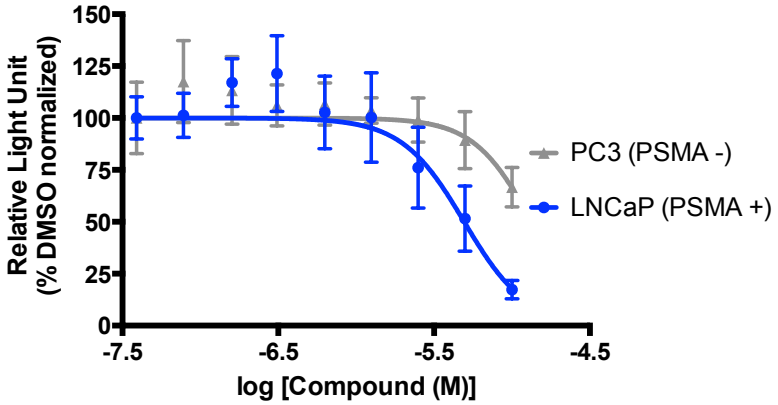

Figure 48. Cellular viability of PSMA – positive (LNCaP) versus PSMA – negative (PC3) cells after treatment with DUPA-VC-PABQ-RT53 for 96 h (data is means ± SD of biological triplicates, normalized to DMSO).

The therapeutic activity of the conjugates was then tested in mice bearing subcutaneous LNCaP tumors. The animals were randomized and then received (n=5 per group) vehicle or drugs at 12 mg/kg for 7 consecutive days. Strikingly, treatment with **DUPA-VC-PABQ-RT53** conjugate led to a significant reduction in tumor volume (93%, p=0.0001) (Figure 49A) and tumor weight (92%, p=0.0001) (Figure 49B) in comparison with vehicle, whereas the single drugs **RT53** and **I-BET762** had a much less pronounced effect (approximately 40 and 50% reduction of tumor volume and weight, respectively (Figure 49). The targeted conjugate **DUPA-VC-PAQB-RT53** has also shown a stronger tumor growth inhibition in comparison with the linker-drug-conjugate **VC-PAQB-RT53** (68%), which suggests a successful DUPA-mediated accumulation of drugs in the PSMA-positive LNCaP tumors. Importantly all drugs were well tolerated in the mice models at the dose tested and up to the 15 days post drug exposure as indicated by the maintenance of stable body weight (Figure 50). The safety of the drugs is currently being confirmed by routine pathological analysis of major organs.

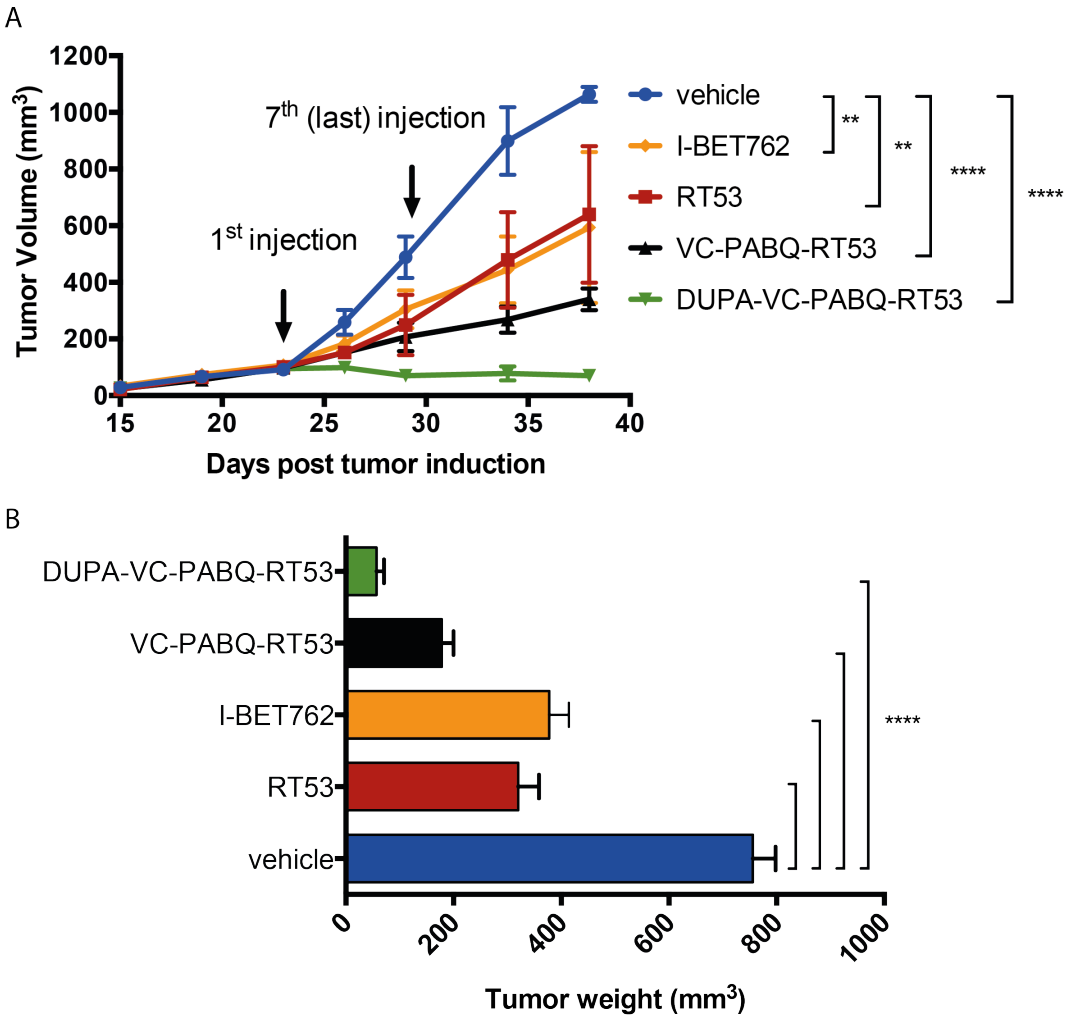

Figure 49. Therapeutic efficacy of conjugates *in vivo*. LNCaP cells were implanted subcutaneously in mice and vehicle or compounds were injected intravenously at 12 mg/kg. Mean tumor volume ± SD (A) and mean tumor weight ± SD (B) is shown. Statistical significance was determined by one way ANOVA followed by Dunnet's multiple comparisons test. **adjusted p-value < 0.01; **** adjusted p-value < 0.0001.

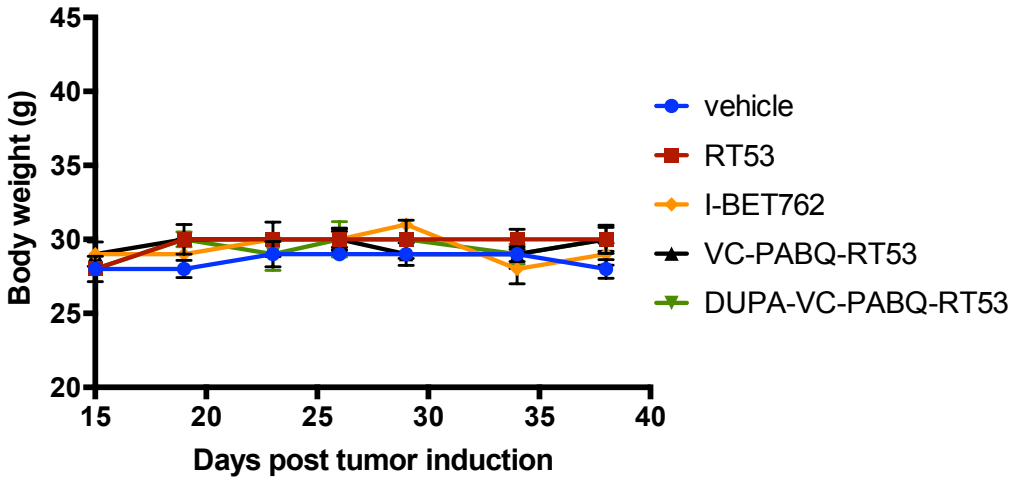

Figure 50. Change of average weight of mice treated with compounds.

V.4. Conclusion

In this chapter we successfully designed and synthesized the first ligand-drug conjugate that enables the selective targeted and traceless release of a BET inhibitor, particularly in prostate cancer.

Here it was demonstrated the controlled release nature of the construct. The linker technology consisting on a PABQ self-immolative motif tethered to a VC cleavable bridge and RT53 was proven stable in the absence of an enzymatic event, though allowing the intracellular release of RT53 when triggered.

Based on the potent activity of RT53 against prostate cancer cells, we then identified a targeting ligand capable of delivering therapeutic agents specifically to prostate cancer. DUPA was selected as an ideal vehicle to confer selectivity to RT53, and was successfully installed in the VC-PABQ-RT53 linker-drug technology synthesized before. The final drug conjugate, DUPA-VC-PABQ-RT53 was shown to affect the viability of prostate cancer cells positive for the DUPA ligand receptor PSMA, but not in PSMA-negative cells, thus suggesting an efficient DUPA-mediated targeting of RT53.

Finally, the therapeutic activity and safety of the final ligand-drug conjugate was demonstrated in mice bearing prostate cancer xenografts. In comparison with the non-targeted BET-inhibitors the final ligand-drug conjugate DUPA-VC-PABQ-RT53 has shown a significant improvement in efficacy at decreasing tumor volume and tumor weight, thus suggesting a therapeutic advantage over the single agents.

General Conclusions

The BET bromodomain family of proteins are rapidly emerging as a target class amenable to inhibition by small molecules. These bromodomain modules are responsible for reading acetylated lysine marks on histone tails, which are key post-translational modifications that modulate chromatin structure and are involved in a multitude of fundamental cellular functions. We have extensively described herein the critical role BET proteins play in the maintenance of cellular homeostasis, and how their dysregulation has been linked to the development of cancer. For example, these proteins are involved in the regulation of transcriptional programmes and have been identified in oncogenic rearrangements that lead to highly oncogenic fusion proteins. Furthermore, BET proteins can also lead to the recruitment and co-activation of master regulatory transcription factors including the oncogene *MYC*, just to name a few of their active roles in tumorigenesis. Several inhibitors that displace BET bromodomain proteins from chromatin by competing with their acetyl-lysine recognition modules have been developed as anticancer agents in the last few years, and many of them are currently being evaluated in numerous oncology-related clinical trials. Results from these clinical trials, however, showed limited single-agent activity and severe adverse events that may limit their approval for treatment. Thus, the main goal of this project was to tailor a BET inhibitor for selective delivery in cancer cells. Given the current evidence retrieved from early clinical trials, we hypothesized that the safety and efficacy of a BET inhibitor with antitumor potential could be substantially improved when tethering it to a targeting ligand and a self-immolative traceless releasing mechanism. We thoroughly evaluated the individual building blocks that participate in the assembly of a ligand-drug conjugate, and ultimately provided compelling evidence for the targeted and traceless release of a BET inhibitor in prostate cancer.

The study of our hypothesis has commenced with the selection of a proper therapeutic payload to be delivered to cancer cells. I-BET762 was selected as a model candidate among several other BET inhibitors due to its favourable pharmacokinetic properties, excellent binding affinities and, according to published evidence, amenability for conjugation with other chemical substituents without interfering with putative ligand-receptor interactions. We were able to validate this information in chapter II through the attachment of bulky fluorophores in I-BET762, which retained potent binding affinities to BET bromodomain targets after derivatization.

This led us to the selection of the cleavable bridge to be attached to I-BET762. We based our synthetic design on the derivatization of I-BET762 to include a terminal tertiary amine, which ultimately would enable the attachment of the self-immolative linker based on an aminobenzyl quaternary

ammonium salt (PABQ). Biophysical experiments showed that the chemical motifs introduced on I-BET762 did not interfere with native binding interactions, and in some cases actually shown better affinity profiles than the parent molecule. The crystal structures of the new inhibitors in complex with BRD2 and BRD4 confirmed their ability to engage the binding pocket in a manner conserved with I-BET762 and competitive with acetyl-lysine peptide, in agreement with previous studies.[3,183] More importantly for the purpose of our studies, the biophysical analysis of the new BET effectors has shown excellent tolerability to the installation of linker motifs.

Potent growth inhibitory effects were observed preferentially in a subset of AR-positive human prostate cancer cell lines including LNCaP and VCaP cell lines. In LNCaP cells these effects were mostly driven by cell cycle alterations, namely by an arrest in G1 phase, rather than by the induction of apoptotic mechanisms. These observations are consistent with the studies of Wyce *et al.*, in which they observed similar mechanisms of action for I-BET762.[89] Furthermore we have shown that the inhibitor RT53 successfully engaged BRD2 and BRD4 in a cellular context as confirmed by CETSA and affinity-based pull down assays. The synthesized BET effector thus combined excellent binding to BET targets with an effective cellular response.

The efficacy of BET inhibitors in haematological malignancies and some solid tumors has been strongly attributed to the control of *MYC* expression. Indeed, not disregarding the role of AR signalling, the findings of Wyce *et al*. support Myc as a key target of BET inhibition in prostate cancer. Our data is consistent with this report by showing a substantial suppression of Myc protein levels in a dose- and time-dependent manner upon treatment with RT53. Altogether, the data seems to corroborate a rationale for antitumoral activity through *MYC* down-regulation. The transcriptional output following drug treatment sustained these findings as we observed a significant suppression of *MYC* and *MYC*-related gene subsets. Importantly, we have also shown a pronounced suppression of *E2F*-dependent transcriptional signatures. Similar observations have been made for other BET inhibitors against multiple myeloma,[71] acute myeloid leukemia,[107] glioblastoma,[259] among others.[218,260]

Finally, we constructed for the first time a ligand-drug conjugate based on a BET inhibitor. We have shown cleavage of the VC linker by cathepsin B and subsequent release of the free drug RT53. Moreover we found the VC-PABQ-RT53 conjugate stable in the absence of such proteolytic stimuli. Cellular viability data and MYC protein down-regulation further suggested RT53 release in cells. Given the efficacy of RT53 in human prostate cancer cell lines we then successfully installed a PSMA-specific ligand, thus establishing a unique ligand-BET inhibitor conjugate. *In vivo* studies in mice bearing prostate cancer xenografs have shown a remarkable improvement of therapeutic efficacy upon DUPA-

VC-PABQ-RT53 treatment over the non-targeted counterparts, RT53 and I-BET762. These findings strongly suggest that the instalment of a targeting moiety and a self-immolative traceless releasing mechanism to a BET inhibitor as RT53 was a successful strategy to overcome the limited efficacy of the current standard of care using this class of antitumor agents.

Chapter VII

Materials and Methods

Chapter VI. Materials and Methods

VI.1. General Remarks

All solvents and reagents were purchased from Sigma Aldrich, Merck, Alfa Aesar or Acros and used as supplied without further purification. All reactions using anhydrous conditions were performed under an argon atmosphere in oven-dried glassware.

Reactions were followed by thin layer chromatography (TLC) using coated silica gel plates (Merck, aluminum sheets, silica gel 60 coated with fluorescent indicator F254) and visualized by UV light, potassium permanganate and ninhydrin staining. Flash column chromatography was performed using Merck silica gel 60 (230-400 mesh ASTM) eluting with various solvent mixtures

NMR spectra were obtained on a Bruker Fourier 300 (300 MHz), Bruker Avance 400 (400 MHz) or Varian Inova 500 (500 MHz) using deuterated chloroform, methanol or dimethylsulfoxide as solvents and $(CH_3)_4Si$ (^1H) as internal standard; chemical shifts, δ, are expressed in ppm, and coupling constants, *J*, are expressed in Hz. Multiplicities are given as: s (singlet), d (doublet), dd (double doublet), dt (double triplet), t (triplet), td (triple doublet), tt (triple triplet), q (quartet), quint (quintuplet) and m (multiplet).

Low-resolution mass spectrometry (LRMS) analysis was recorded on a Waters Quattro micro API and High-Resolution mass spectrometry (HRMS) on a Bruker Daltonics microTOF ESI-TOF mass spectrometer. Calculated and exact m/z values are indicated in Daltons.

For the synthesis of **I-BET762**, their precursors and all fluorescent derivatives, analytical reversed-phase high pressure liquid chromatography (HPLC) was performed on a Waters Separations Module with a Dual Absorbance Detector using a VDspher 100 C18 5 µm, 250 x 4.6 mm column at a flow rate of 1 mL/min with linear gradients of 97 % A/ 3 % B to 100 % B over 15 min (A = Millipore water, B = ACN). For compound **RT56** HPLC was run on a Luna 100 C18 10 µm, 250 x 10 mm column at a flow rate of 1 mL/min with linear gradients of 97 % A/ 3 % B to 5 % A / 95 % B over 15 min and 5 min. rest at 5 % A / 95 % B (A = Millipore water, B = ACN). Compound **DUPA-VC-PABQ-RT53** HPLC was performed on a Phenomenex Luna C18 10 µm, 250 × 21.2 mm column at a flow rate of 10 mL/min using linear gradients of 80 % A/ 20 % B to 60 % A/ 40% B over 40 min. (A = Milipore water + 0.1% TFA, B = ACN).

VI.2. Experimental Section of Chapter II

VI.2.1. Experimental details of the synthesis of compounds

VI.2.1.1. Synthesis of I-BET762 (Scheme 1, p41)

Literature basis – Mirguet, O.; Gosmini, R.; Toum, J.; Clément, C.A.; Barnathan, M.; Brusq, J.M.; Mordaunt, J.E.; Grimes, R.M.; Crowe, M.; Pineau, O.; Ajakane, M.; Daugan, A.; Jeffrey, P.; Cutler, L.; Haynes, A.C.; Smithers, N.N.; Chung, C.W.; Bamborough, P.; Uings, I.J.; Lewis, A.; Witherington, J.; Parr, N.; Prinjha, R.K.; Nicodeme, E. *J. Med. Chem*. **2013**. *56(19):*7501

- Synthesis of 2**-**methyl-6-(methyloxy)-4H-3,1-benzoaxazin-4-one **(**compound **6)**.

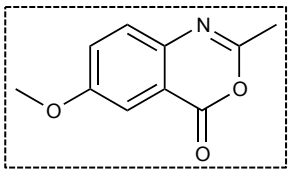

A solution of 2-amino-5-methoxybenzoic acid **5** (2 g, 12 mmol) was refluxed in acetic anhydride (11 mL) for 5 h. The reaction mixture was then concentrated twice in the presence of toluene. The crude compound was washed with diethyl ether to afford the product **6** as a brown solid (2.32 g, 100%).

^{1}H NMR (300 MHz, Chloroform-*d*) δ 7.56 (d, *J* = 2.9 Hz, 1H), 7.48 (d, *J* = 8.9 Hz, 1H), 7.35 (dd, *J* = 8.9, 2.8 Hz, 1H), 3.90 (s, 3H), 2.45 (s, 3H).

- Synthesis of 2-amino-5-(methyloxy)phenyl](4-chlorophenyl)methanone (compound **7**)

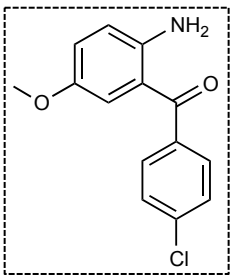

To a solution of **6** (2.32 g, 12 mmol, 1.24 eq) in a toluene/ether mixture (2/1, 45 mL anhydrous) at -80 ˚C was added dropwise a solution of 4-chlorophenylmagnesium bromide (9.7 mL, 9.7 mmol of 1 M solution in Et_2O, 1 eq). The reaction mixture was left at -80 ˚C for 30 min. and then allowed to warm up to room temperature. The mixture was stirred at room temperature for 1 h before being quenched with 1 N HCl (12 mL). The aqueous layer was extracted with EtOAc (3 times) and the combined organics were washed with brine, dried over magnesium sulfate, filtered and concentrated under reduced pressure to afford the intermediate amide. The crude compound was then dissolved in ethanol (25 mL) and 6 N HCl (9 mL) was added. The mixture was refluxed for 2 h before being concentrated under reduced pressure. EtOAc was added and the mixture neutralized with 1 N NaOH. The aqueous layer was extracted with EtOAc (3x) and the combined organics washed with brine, dried over magnesium sulfate, filtered and concentrated under reduced pressure. The crude mixture was

purified by chromatography on silica gel with a gradient of hexane:EtOAc (20:80 to 100 % EtOAc) to afford compound **7** as yellow solid. (1.16 g, 37%)

^{1}H NMR (300 MHz, DMSO-*d6*) δ 7.66 – 7.54 (m, 4H), 7.05 (dd, *J* = 9.0, 3.0 Hz, 1H), 6.84 (d, *J* = 9.0 Hz, 1H), 6.72 (d, *J* = 2.9 Hz, 1H), 3.56 (s, 3H). **LRMS**: (m/z) $[M+H]^+$ calcd for $C_{14}H_{12}ClNO_2Na$, 284.0; found 284.0.

- Synthesis of Methyl[5-(4-chlorophenyl)-7-methyloxy)-2-oxo-2,3-dihydro-1*H*-1,4-benzodiazepin-3-yl]acetate (compound **9**)

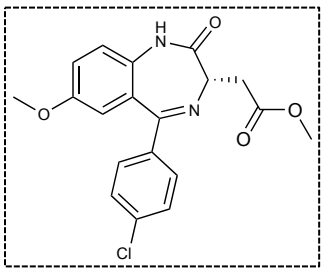

N-Fmoc-L-aspartic acid 4-methyl ester (1.63 g, 4.5 mmol, 1.02 eq) was dissolved in anhydrous DCM (30 mL) and $SOCl_2$ (4.8 mL, 66 mmol, 15 eq) was added to the reaction mixture dropwise at 0 ˚C. The mixture was refluxed for 2 h before being concentrated under reduced pressure to afford intermediate **8**. The crude compound was dissolved in anhydrous 1,2-DCE (20 mL) and **7** (1.16 g, 4.4 mmol, 1 eq) was added. The resulting mixture was refluxed for 2 h and cooled to room temperature before adding Et_3N (2.45 mL, 17.6 mmol, 4 eq). The reaction was refluxed for 16 h. The resulting mixture was concentrated to dryness and the crude dissolved in 1,2-DCE (50 mL). AcOH (2.8 mL, 48.4 mmol, 11 eq) was added carefully and the reaction stirred for 2 h at 60 ˚C before being concentrated in vacuum and dissolved in DCM. The organic layer was washed with 1 N HCl and the aqueous layer extracted with DCM (3 times). The combined organic layers were washed with water, brine, dried over $MgSO_4$, filtered and concentrated under reduced pressure. The crude was recrystallized in CH_3CN to afford **9** as an off-white colored solid (0.83 g, 50%).

^{1}H NMR (300 MHz, DMSO-*d6*) δ 10.52 (s, 1H), 7.50 (s, 4H), 7.23 (s, 2H), 6.75 (d, *J* = 2.4 Hz, 1H), 3.92 (d, *J* = 7.1 Hz, 1H), 3.70 (s, 3H), 3.61 (s, 3H), 3.27 – 3.14 (m, 1H), 3.03 (dd, *J* = 16.6, 6.6 Hz, 1H). **LRMS**: (m/z) $[M+H]^+$ calcd for $C_{19}H_{18}ClN_2O_4$, 373.1; found 373.0

- Synthesis of Methyl-[5-(4-chlorophenyl)-7-(methyloxy)-2-oxo-2,3-dihydro-1*H*-benzodiazepin-3-yl]acetate (compound **10**)

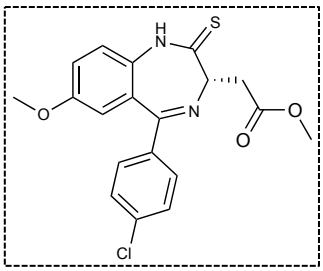

P_4S_{10} (3 g, 13.7 mmol, 1.8 eq) and Na_2CO_3 (1.5 g, 13.7 mmol, 1.8 eq) were dissolved in 1,2-DCE (50 mL) and stirred at room temperature for 2 h. The amide **9** (2.83 g, 7.6 mmol, 1.0 eq) was dissolved in 1,2-DCE (50 mL) and added to the P_4S_{10} and Na_2CO_3 suspension. The resulting reaction was stirred for 4 h at 65˚C followed by 16 h at room temperature. The obtained residue was taken in a saturated $NaHCO_3$ solution and extracted with DCM (3 times). The combined organics were dried over $MgSO_4$, filtered and concentrated under reduced pressure. The

crude compound was then recrystallized with DCM/*i*-Pr_2O for 12 h to yield compound **10** as a yellow solid (1.7 g, 58%).

^{1}H NMR (300 MHz, Chloroform-*d*) δ 7.49 (d, *J* = 8.6 Hz, 2H), 7.36 (d, *J* = 2.0 Hz, 2H), 7.20 (d, *J* = 8.9 Hz, 1H), 7.12 (dd, *J* = 8.8, 2.8 Hz, 1H), 6.77 (d, *J* = 2.8 Hz, 1H), 4.38 (t, *J* = 6.8 Hz, 1H), 3.75 (s, 3H), 3.73 (s, 3H), 3.63 (dd, *J* = 16.8, 6.5 Hz, 1H), 3.38 (dd, *J* = 16.9, 7.1 Hz, 1H). **LRMS**: (m/z) $[M+H]^+$ calcd for $C_{29}H_{18}ClN_2O_3S$, 389.1; found 388.8.

- Synthesis of Methyl-2-((4S)-6-(4-Chlorophenyl)-8-methoxy-1-methyl-4H-benzol[f][1,2,4]triazolo[4,3-a][1,4]diazepin-4-yl)acetate (compound **11**)

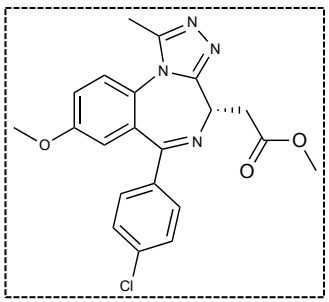

The thioamide **10** (1.7 g, 4.4 mmol, 1 eq) was suspended in THF (65 mL) and hydrazine monohydrate added (0.64 mL, 13.2 mmol, 3 eq) at 0 ˚C dropwise. The mixture was stirred for 5 h at 0 ˚C followed by the addition of Et_3N (1.84 mL, 13.2 mmol, 3 eq) and AcCl (0.94 mL, 13.2 mmol, 3 eq) dropwise. The reaction mixture was then allowed to warm to room temperature and stirred for 16 h before being concentrated under reduced pressure. The crude compound was dissolved in DCM and washed with water. The organic layer was dried over $MgSO_4$, filtered and concentrated under reduced pressure to afford the intermediate hydrazone. The intermediate was dissolved in THF (65 mL) and AcOH (10 mL) was added. The reaction mixture stirred for 2 days before being concentrated under reduced pressure. The crude solid was triturated in *i*-Pr_2O and decanted to give compound **11** (1.4 g, 77%).

^{1}H NMR (300 MHz, Chloroform-*d*) δ 7.53 – 7.45 (m, 2H), 7.39 (d, *J* = 9.0 Hz, 1H), 7.36 – 7.29 (m, 2H), 7.20 (dd, *J* = 8.9, 3.0 Hz, 1H), 6.88 (d, *J* = 2.9 Hz, 1H), 4.59 (dd, *J* = 7.7, 6.4 Hz, 1H), 3.80 (s, 3H), 3.62 (d, *J* = 2.8 Hz, 1H), 3.60 (d, *J* = 1.6 Hz, 1H), 2.60 (s, 3H). **LRMS**: (m/z) $[M+H]^+$ calcd for $C_{21}H_{20}ClN_4O_3$, 411.1; found 411.0

- Synthesis of 6-(4-Chlorophenyl)-1-methyl-8-(methyloxy)-4*H*-[1,2,4]triazolo[4,3-a)[1,4]benzodiazepin-4-yl]acetic acid (compound **12**)

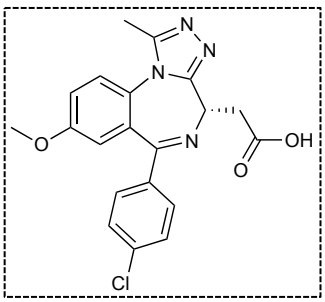

Compound **11** (1.4 g, 3.4 mmol) was dissolved in THF (40 mL) and a solution of 1 N NaOH (7 mL) was added. The reaction mixture was stirred for 5 h at room temperature before being quenched with 0.5 N HCl (14.3 mL) and concentrated under reduced pressure. Water was added to the residue and the aqueous layer was extracted with DCM (3 times). The combined organic layers were dried over $MgSO_4$, filtered and concentrated under reduced pressure to afford compound **12** as a yellow solid (1.3 g, 94%).

^{1}H NMR (300 MHz, Chloroform-*d*) δ 7.51 (d, *J* = 8.6 Hz, 2H), 7.44 (d, *J* = 8.9 Hz, 1H), 7.33 (d, *J* = 8.6 Hz, 2H), 7.24 – 7.20 (m, 1H), 6.89 (d, *J* = 2.8 Hz, 1H), 4.58 (t, *J* = 6.9 Hz, 1H), 3.81 (s, 3H), 3.63 (dd, *J* = 9.9, 7.0 Hz, 2H), 2.64 (s, 3H). **LRMS**: (m/z) $[M+H]^+$ calcd for $C_{20}H_{18}ClN_4O_3$, 396.8; found 396.9.

- Synthesis of *S*)-2-(6-(4-chlorophenyl)-8-methoxy-1-methyl-4*H*-benzo[*f*][1,2,4]triazolo[4,3-*a*][1,4]diazepin-4-yl)-*N*-ethylacetamide (**I-BET762 / 1**)

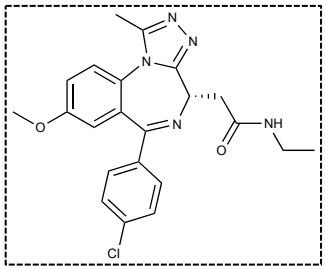

To a solution of acid **12** (0.09 g, 0.23 mmol) in THF (10 mL) at room temperature was added DIPEA (0.08 mL, 0.46 mmol, 2 eq) followed by HTBU (0.174 g, 0.46 mmol). The reaction mixture was stirred for 3 h at this temperature and ethylamine (0.23 mL, 2 M in THF, 0.46 mmol) was added dropwise. The mixture was stirred for 12 h before being concentrated under reduced pressure. The crude material was dissolved in DCM and washed successively with water, 1 N NaOH and 1 N HCl. The organic layer was dried over $NaHCO_3$, filtered and concentrated under reduced pressure. The crude product was then purified by chromatography on silica gel to give compound **I-BET762 (1)** as a yellow solid (50 mg, 47%).

^{1}H NMR (300 MHz, Chloroform-*d*) δ 7.51 – 7.45 (m, 2H), 7.39 (d, *J* = 8.9 Hz, 1H), 7.32 (d, *J* = 8.5 Hz, 2H), 7.20 (dd, *J* = 8.9, 2.9 Hz, 1H), 6.85 (d, *J* = 2.9 Hz, 1H), 6.59 (s, 1H), 4.62 (t, *J* = 7.0 Hz, 1H), 3.79 (s, 3H), 3.53 – 3.42 (m, 1H), 3.38 – 3.22 (m, 3H), 2.61 (s, 3H), 1.16 (t, *J* = 7.3 Hz, 3H). **LRMS**: (m/z) $[M+H]^+$ calcd for $C_{22}H_{22}ClN_5O_2$, 424.2; found 423.9

VI.2.1.2. Synthesis of fluorescein-labelled conjugates

VI.2.1.2.1. *Diamine protection (Scheme 2, p43)*

Literature basis: Zuckermann, R.N.; Martin, E.J.; Spellmeyer, D.C.; Stauber, G.B.; Shoemaker, K.R.; Kerr, J.M.; Figliozzi, G.M.; Goff, D.A.; Siani, M.A.; Simon, R.J.; Banville, S.C.; Brown, E.G.; Wang, L.; Ritcher, L.S.; Moos, W.H. *J. Med. Chem.* **1994**. *37:*2678

- Synthesis of *tert*-butyl-(3-aminopropyl)carbamate (compound **13**)

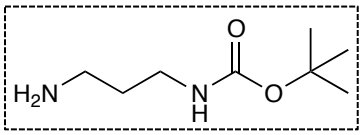

1,3-diaminopropane (1.14 mL, 13.7 mmol) was dissolved in dry dioxane (3 mL) and stirred at room temperature. Di-*tert*-butylcarbonate (0.52 mL, 2.3 mmol) was added in dioxane (2 mL) dropwise to the

reaction mixture. This was stirred for 12 h and concentrated under reduced pressure. The residue was dissolved in water and rinsed with DCM (3 times). The combined organics were rinsed with brine, dried over $MgSO_4$, filtered and concentrated in vacuum to afford compound **13** as clear oil (251.4 mg, 63%).

^{1}H NMR (300 MHz, Chloroform-*d*) δ 4.90 (s, 1H), 3.29 – 3.07 (m, 3H), 2.77 (t, *J* = 6.6 Hz, 1H), 1.91 (ns, 2H), 1.61 (q, *J* = 6.8 Hz, 2H), 1.43 (s, 9H). **HRMS (ESI):** m/z calcd $[M+H]^+$ for $C_8H_{19}N_2O_2$ = 175.1441; found $[M+H]^+$ 175.1449.

- Synthesis of *tert*-butyl (2-(2-aminoethoxy)ethyl)carbamate (compound **14**)

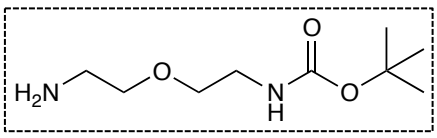

2,2'-oxydiethanamine (0.3 mL, 2.76 mmol) was dissolved in dry dioxane (3 mL) and stirred at room temperature. Di-*tert*-butylcarbonate (0.1 mL, 0.46 mmol) was added in dioxane (2 mL) dropwise to the reaction mixture. This was stirred for 12 h and concentrated under reduced pressure. The residue was dissolved in water and rinsed with DCM (3 times). The combined organics were rinsed with brine, dried over $MgSO_4$, filtered and concentrated in vacuum to afford compound **14** as clear oil (66 mg, 70%).

^{1}H NMR (300 MHz, Chloroform-*d*) δ 4.99 (s, 1H), 3.47 (m, *J* = 10.7, 5.3 Hz, 4H), 3.34 – 3.17 (m, 2H), 2.84 (t, *J* = 5.2 Hz, 2H), 1.69 – 1.46 (m, 2H), 1.41 (d, *J* = 0.9 Hz, 9H); **HRMS (ESI):** m/z calcd $[M+H]^+$ for $C_9H_{21}N_2O_3$ = 205.1547; found $[M+H]^+$ 205.1543.

- Synthesis of *tert*-butyl (2-(2-(2-aminoethoxy)ethoxy)ethyl)carbamate (compound **15**)

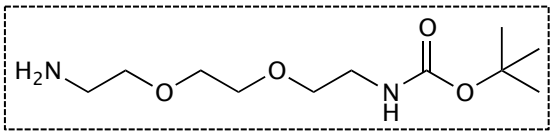

To a solution of 2,2'-(ethylenedioxy)-bis[ethylamine] (5.4 mmol, 5.9 eq), in dioxane (4 mL) was added dropwise at room temperature over 2 h a solution of di-*tert*-butyl dicarbonate (200 mg, 0.92 mmol, 1 eq) in dioxane (1 mL). The mixture was stirred for 12 h and then concentrated under reduced pressure. The residue was dissolved in water and rinsed with DCM (3 times). The combined organic layers were rinsed with brine, dried over $MgSO_4$, filtered and concentrated in vacuo to give **15** (139 mg, 61%) of a pale yellow oil.

^{1}H NMR (300 MHz, Chloroform-*d*) δ 5.20 (s, 1H), 3.58 (s, 4H), 3.49 (dt, *J* = 8.9, 5.2 Hz, 4H), 3.28 (d, *J* = 5.3 Hz, 2H), 2.89 – 2.77 (m, 2H), 1.74 (s, 3H), 1.40 (s, 9H). **HRMS (ESI):** m/z calcd $[M+H]^+$ for $C_{11}H_{24}N_2O_4$ = 249.1800; found $[M+H]^+$ 249.1809

VI.2.1.2.2. *Conjugation of I-BET762 with spacers (Scheme 3, p44)*

Literature basis: Chung, C.W.; Coste, H.; White, J.H.; Mirguet, O.; Wilde, J.; Gosmini, R.L.; Delves, C.; Magny, S.M.; Woodward, R.; Hughes, S.A.; Boursier E.V.; Flynn, H.; Bouillot, A.M.; Bamborough, P.;

Brusq, J.M.; Gellibert, F.J.; Jones, E.J.; Riou, A.M.; Homes, P.; Martin, S.L.; Uings, I.J.; Toum, J.; Clement, C.A.; Boullay, A.B.; Grimley, R.L.; Blandel, F.M.; Prinjha, R.K.; Lee, K.; Kirilovsky, J.; Nicodeme, E.; *J. Med. Chem*. **2011**. *54(11)*:3827

- Synthesis of compound **16**

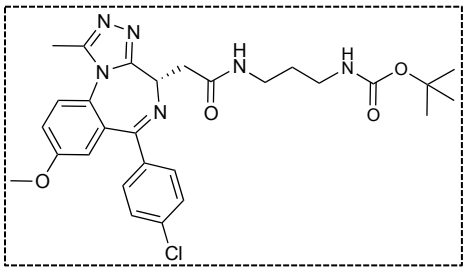

The carboxylic acid **12** (100 mg, 0.26 mmol) was degassed under vacuum and refilled with argon prior adding anhydrous THF (3 mL). To this solution was added DIPEA (87 µL, 0.52 mmol, 2 eq) and HATU (190 mg, 0.52 mmol, 2 eq). The reaction was stirred for 3 h at room temperature, time at which compound **13** (66 mg, 0.38 mmol, 1.5 eq) was added dropwise to the mixture. This was stirred 12-14 h at room temperature before being concentrated under reduced pressure. The crude material was dissolved in DCM and washed with 1N HCl. The aqueous phase was extracted twice with DCM. The combined organics were then washed with 1N NaOH followed by brine, dried in $MgSO_4$, filtered and concentrated under reduced pressure to afford compound **16** as a yellow solid (64 mg, 45%).

^{1}H NMR (300 MHz, Chloroform-*d*) δ 7.84 (s, 1H), 7.47 – 7.41 (m, 2H), 7.37 (d, *J* = 8.9 Hz, 1H), 7.31 – 7.25 (m, 2H), 7.17 (dd, *J* = 8.9, 2.9 Hz, 1H), 6.84 (d, *J* = 2.9 Hz, 1H), 5.76 (s, 1H), 4.69 (dd, *J* = 7.9, 6.0 Hz, 1H), 3.77 (s, 3H), 3.45 (m, *J* = 21.1, 14.1, 7.1 Hz, 3H), 3.15 (d, *J* = 6.0 Hz, 2H), 2.61 (s, 3H), 1.67 (p, *J* = 6.6 Hz, 2H), 1.49 (bs, 2H), 1.40 (s, 9H) signals from the PEG linker predicted to overlap. **HRMS (ESI):** m/z calcd $[M+H]^+$ for $C_{28}H_{33}ClN_6NaO_4$ = 575.2132; found $[M+H]^+$ 575.2144

- Synthesis of compound **17**

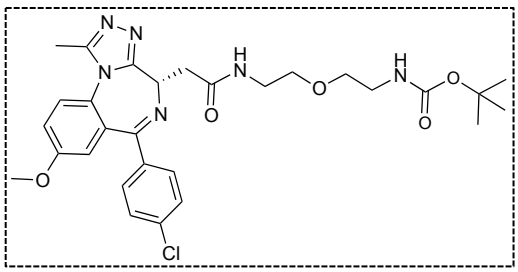

The carboxylic acid **12** (52 mg, 0.13 mmol) was degassed under vacuum and refilled with argon prior adding anhydrous THF (6 mL). To this solution was added DIPEA (45 µL, 0.26 mmol) and HBTU (98.6 mg, 0.26 mmol). The reaction was stirred for 3 h at room temperature, time at which compound **14** (40 mg, 0.19 mmol) was added dropwise to the mixture. This was stirred for 12 h before being concentrated under reduced pressure. The crude material was dissolved in ethyl acetate and washed successively with saturated $NaHCO_3$, water and brine, before drying in $MgSO_4$, filtering and concentrating under reduced pressure to afford compound **17** as a yellow solid (64 mg, 75%).

^{1}H NMR (300 MHz, Chloroform-*d*) δ 7.53 – 7.46 (m, 2H), 7.36 – 7.30 (m, 3H), 7.20 (dd, *J* = 9.0, 2.9 Hz, 1H), 6.86 (d, *J* = 2.9 Hz, 1H), 5.38 (s, 1H), 4.89 (s, 1H), 4.67 – 4.54 (m, 1H), 3.80 (s, 3H), 3.74 – 3.62

(m, 2H), 3.52 (t, *J* = 5.6 Hz, 4H), 3.34 – 3.28 (m, 4H), 3.00 (s, 2H), 2.80 (s, 1H), 2.63 (s, 3H), 1.44 (d, *J* = 1.1 Hz, 9H); signals from the PEG linker predicted to overlap. **HRMS (ESI):** m/z calcd $[M+H]^+$ for $C_{29}H_{35}ClN_6NaO_5$ = 605.2250; found $[M+H]^+$ 605.2244

- Synthesis of compound **18**

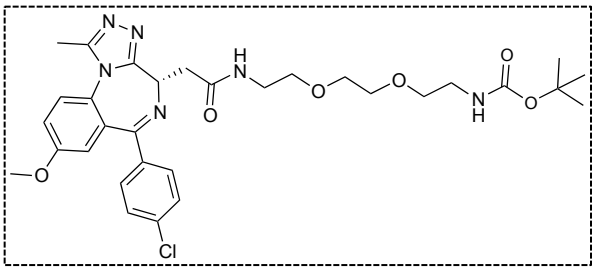

To a solution of acid **12** (100 mg, 0.26 mmol) in THF at room temperature was added diisopropylethylamine DIPEA (90 µL, 0.52 mmol, 2 equiv.) followed by HATU (197.7 mg, 0.52 mmol, 2 equiv.). The reaction mixture was stirred for 3 h at this temperature and compound **15** (0.52 mmol, 2 equiv.) was added dropwise. The mixture was stirred for 12 h before being concentrated under reduced pressure. The crude material was dissolved in DCM and washed with 1N HCl. The aqueous layer was extracted twice with DCM. The combined organics were washed with 1 N NaOH followed by brine, dried over $MgSO_4$ filtered and concentrated in vacuo. The residue was purified by flash-chromatography on silica using dichloromethane/methanol 95/5 to give compound **18** as a yellow solid (73.6 mg, 56%).

^{1}H NMR (300 MHz, Chloroform-*d*) δ 7.47 (d, *J* = 8.6 Hz, 2H), 7.36 (d, *J* = 8.9 Hz, 1H), 7.29 (d, *J* = 8.6 Hz, 2H), 7.17 (dd, *J* = 8.9, 2.9 Hz, 1H), 7.02 (s, 1H), 6.82 (d, *J* = 2.8 Hz, 1H), 5.39 – 5.29 (m, 1H), 4.61 (t, *J* = 7.0 Hz, 1H), 3.76 (s, 3H), 3.60 (s, 4H), 3.54 (t, *J* = 5.2 Hz, 4H), 3.51 – 3.44 (m, 3H), 3.33 (dq, *J* = 10.6, 6.3, 5.5 Hz, 3H), 2.58 (s, 3H), 1.39 (s, 9H). **HRMS (ESI)**: m/z calcd $[M+H]^+$ for $C_{31}H_{39}ClN_6O_6$ = 627.2692; found $[M+H]^+$ 627.2683

VI.2.1.2.3. *Conjugation with fluorescein (Scheme 3, p44)*

- Synthesis of compound **19**

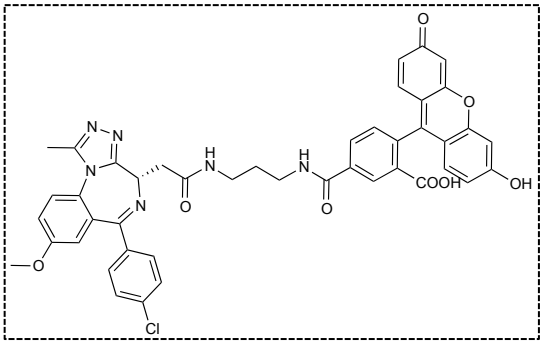

Compound **16** (58 mg, 0.1 mmol) was degassed under vacuum and refilled with argon (3 times). This was dissolved in DCM (2 mL) and TFA (1.5 mL, 19.4 mmol) was added at 0 ˚C. The reaction was left to warm to room temperature and stirred for 2 h. The reaction mixture was concentrated under reduced pressure and the crude analyzed by ^{1}H NMR. Proton peak integration revealed that the reaction was complete, since Boc was successfully removed (76.4 mg, 0.14 mmol). The TFA salt was then degassed in vacuum and refilled with argon (3 times). The solid was then dissolved in DMF (6 mL) and DIPEA was added (0.24 mL, 0.14 mmol) followed by NHS fluorescein

(65.8 mg, 0.14 mmol). The round bottom flask was covered in foil to protect the reaction mixture from light and the reaction was stirred for 12 h at room temperature before concentrating under reduced pressure. Toluene was added 3 times to aid the removal of DMF. The crude compound was purified by preparative TLC with a gradient of acetone:hexane (7:3, two runs) and acetone (100%). The product was extracted in DCM and concentrated to afford **19** as a yellow solid (26 mg; 23%). **HRMS (ESI):** m/z calcd $[M+H]^+$ for $C_{44}H_{36}ClN_6O_8$ = 811.2278; found $[M+H]^+$ 811.2267

- Synthesis of compound **20**

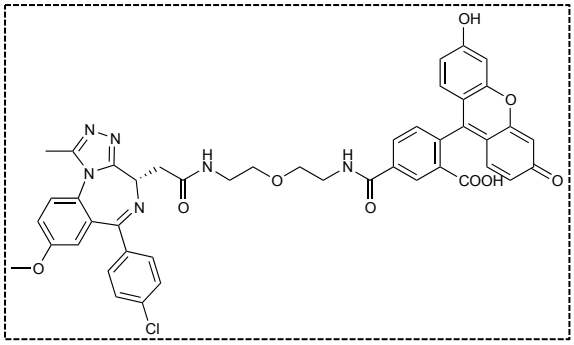

Compound **17** (57 mg, 0.098 mmol) was degassed under vacuum and refilled with argon (3 times). This was dissolved in DCM (2 mL) and TFA (1.5 mL, 19.4 mmol) was added at 0 ˚C. The reaction was left to warm to room temperature and stirred for 2 h. The reaction mixture was concentrated under reduced pressure and the crude analyzed by ^{1}H NMR. Proton peak integration revealed that the reaction was incomplete, as Boc was still present in the mixture. The crude was diluted again in DCM (2 mL) and TFA (2 mL, 25.9 mmol) was added at 0 ˚C. The reaction was stirred for an additional 5 h at room temperature before being concentrated under reduced pressure. ^{1}H NMR analysis confirmed that Boc was removed and obtain the intermediate amine in the form of TFA salt, which was used without further purification (62.3 mg, 0.11 mmol). This was then degassed in vacuum and refilled with argon (3 times). The solid was then dissolved in DMF (6 mL) and DIPEA was added (0.19 mL, 0.11 mmol) followed by NHS fluorescein (50 mg, 0.11 mmol). The round bottom flask was covered in foil to protect the reaction mixture from light and the reaction was stirred for 12 h at room temperature before concentrating under reduced pressure. Toluene was added 3 times to aid the removal of DMF. The crude product was purified by preparative TLC with a gradient of acetone:hexane (7:3, two runs) and acetone (100%). The product was extracted in DCM and concentrated to afford **17** as a yellow solid (25 mg; 27%). **HRMS (ESI):** m/z calcd $[M+H]^+$ for $C_{45}H_{38}ClN_6O_9$ = 841.2383; found $[M+H]^+$ 841.2379

- Synthesis of compound **21**

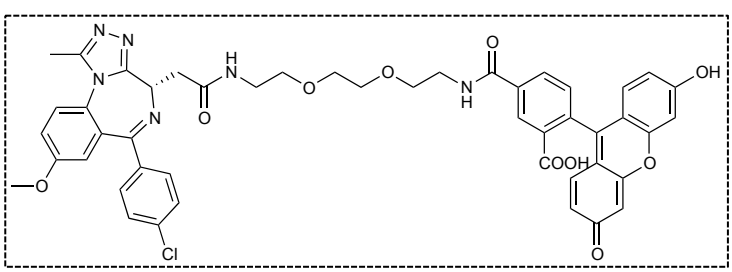

Compound **18** (96.7 mg, 0.15 mmol) was degassed under vacuum, refilled with argon two times and dissolved in DCM (3 mL). Trifluoroacetic acid (TFA)

(1 mL, 12 mmol, 80 eq) was added at 0 ˚C. The reaction was left to warm to room temperature and stirred for 12 h. The reaction crude was concentrated and Boc deprotection confirmed by ^{1}H NMR. The deprotected amine was used without further purification. This was dissolved in DMF (4 mL) and DIPEA (296 µL, 1.7 mmol) was added, followed by NHS fluorescein (80.5 mg, 0.17 mmol). The reaction was stirred at room temperature for 12-14 h before being concentrated under reduced pressure. The obtained crude (244 mg) was purified through a column chromatography on silica gel with DCM:MeOH (8:2). The fractions were pooled together and concentrated under reduced pressure to afford the fluorescent (yellow) solid **21** (118 mg, 76%). **HRMS (ESI):** m/z calcd $[M+H]^+$ for $C_{47}H_{41}ClN_6O_{10}$ = 885.2645; found $[M+H]^+$ 885.2635

- Synthesis of compound **22** (Scheme 4, p45)

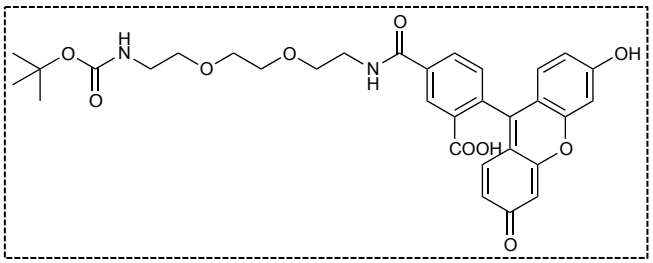

Compound **15** (95 mg, 0.38 mmol, 1.6 eq) was degassed under vacuum and refilled with argon (3 times) before dissolving in anhydrous DMF (2 mL). DIPEA (0.33 mL, 1.9 mmol, 5 eq) was added and the mixture stirred for few min. at room temperature. NHS fluorescein (117 mg, 0.24 mmol, 1 eq) was dissolved in the minimum amount of anhydrous DMF possible and added to the reaction vessel under an inert atmosphere. The reaction was stirred for 12 h at room temperature and the crude concentrated under reduced pressure. The crude was purified over a column chromatography on silica gel with DCM:MeOH (85:15). The fractions were pooled and concentrated under reduced pressure to afford compound **22** as a yellow solid (97 mg, 67%).

^{1}H NMR (300 MHz, Methanol-*d4*) δ 8.43 (d, *J* = 1.5 Hz, 1H), 7.63 (s, 1H), 7.29 (d, *J* = 8.0 Hz, 1H), 6.68 (d, *J* = 2.3 Hz, 2H), 6.62 (d, *J* = 7.4 Hz, 2H), 6.54 (dt, *J* = 8.8, 2.9 Hz, 2H), 3.64 (t, *J* = 3.8 Hz, 4H), 3.53 (ddd, *J* = 14.4, 7.8, 3.8 Hz, 5H), 3.40 (d, *J* = 5.5 Hz, 1H), 3.19 (t, *J* = 5.6 Hz, 1H), 3.11 (t, *J* = 5.6 Hz, 1H), 1.39 (s, 9H). **HRMS (ESI):** m/z calcd $[M+H]^+$ for $C_{32}H_{35}N_2O_{10}$ = 607.2286; found $[M+H]^+$ 607.2286

VI.2.1.2.4. *Conjugation with nitrobenzofurazan dye*

Literature basis: Xie, Z.; Wang, K.; Zhang, C.; Yang, Z.; Chen, Y.; Guo, Z.; Lu, G.; He, W. *New J. Chem*. **2011**. *35:*607. Cal, P.M.S.D.; Frade, R.F.M.; Chudasama, V.; Cordeiro, C.; Caddick, S.; Gois, P.M.P. *Chem. Commun*. **2014.** *50:*5261

- Synthesis of compound **24**

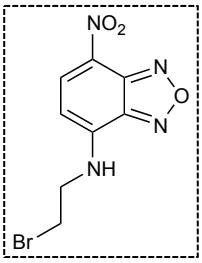

The starting material NDB-Cl **23** (100 mg, 0.5 mmol, 1 eq) was dissolved in methanol (5 mL). 2-Bromoethylamine hydrobromide (123 mg, 0.6 mmol, 1.2 eq) and DIPEA (180 µL, 1 mmol, 2 eq) were added to the solution. The reaction mixture was stirred at room temperature for 12 h. The reaction crude was concentrated and purified over a column chromatography on silica gel with EtOAc:hexane (1:1) to afford **24** as an orange solid (57 mg, 40%).

^{1}H NMR (300 MHz, Methanol-*d4*) δ 8.50 (d, *J* = 8.8 Hz, 1H), 6.41 (d, *J* = 8.8 Hz, 1H), 3.96 (s, 2H), 3.68 (d, *J* = 6.6 Hz, 2H).

- Synthesis of compound **25**

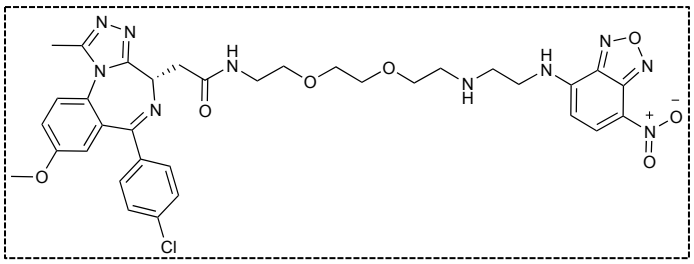

Compound **18** (26 mg, 0.04 mmol) was degassed under vacuum and refilled with argon before being dissolved in DCM (1 mL). TFA (1 mL, 12 mmol, 300 eq) was added at 0 ˚C. The reaction was left to warm to room temperature and stirred for 12-14 h. The reaction crude was concentrated thoroughly. To remove all TFA toluene was added several times followed by evaporation. When thoroughly dried, the reaction crude was placed under an argon flow to remove any traces of acid. The Boc-deprotected intermediate (0.04 mmol, assumed 100 % conversion, 1.1 eq) was diluted in methanol (1 mL) and stirred. DIPEA (50 µL, 0.21 mmol, 7 eq) was added and the reaction stirred for a further 5 min., time after which compound **24** (10.4 mg, 0.036 mmol, 1 eq) was added. The reaction was stirred for 12-14 h at room temperature. According to the TLC the starting materials did not react and more DIPEA was added (10 eq). The reaction was left for a further 24 h and the formation of a new product was observed. In an attempt to consume all the starting material, the reaction was heated at 50 ˚C and more 10 eq of DIPEA were added. Two preparative TLC (DCM:MeOH, 92.5:7.5) on silica gel were performed to isolate the pure product **25** (11.2 mg, 38%).

HRMS (ESI): m/z calcd $[M+H-CNO]^+$ for $C_{34}H_{37}ClN_{10}O_7$ = 690.2443; found $[M+H-CNO]^+$ = 690.2443 (ionization fragmentation pattern reported for oxidized NBD)

VI.2.2. Experimental details on the biophysical characterization of compounds

VI.2.2.1. AlphaScreen specific binding assay

Bromodomain screening and determination of IC_{50} values were conducted at Cerep (Celle l'Evescault, France) on a fee-for-service basis. The first domain of Bromodomain 2 (BRD2(1)), the first

domain of bromodomain3 (BRD3(1)), and the first and second domain of Bromodomain 4 (BRD4(1) and RD4(2)) were assayed as described in the Table 7. Compounds were tested at several concentrations for IC_{50} determination. Compound binding was calculated as a percentage inhibition of the binding of a radioactively labelled ligand specific for each target. Results showing an inhibition or simulation higher than 50% were considered to represent significant effects of the test compounds. The IC_{50} values and Hill coefficients (nH) were determined by non-linear regression analysis of the competition curves generated with mean replicate values using Hill equation curve fitting.

Table 7. BET-bromodomain binding assay protocols.

Assay	Source	Ligand	Incubation	Detection Method
BRD2(1) (h) bromodomain	human recombinant	Biotin-H4 tetra acetyl Lys 5/8/12/16 50 nM	30 min, r.t.	AlphaScreen
BRD3(1) (h) bromodomain	human recombinant (E. Coli)	Biotin-H4 tetra acetyl Lys 5/8/12/16 25 nM	30 min, r.t.	AlphaScreen
BRD4(1) (h) bromodomain	human recombinant	Biotin-H4 tetra acetyl Lys 5/8/12/16 50 nM	30 min, r.t.	AlphaScreen
BRD4(2) (h) bromodomain	human recombinant (E. Coli)	Biotin-H4 tetra acetyl Lys 5/8/12/16 50 nM	30 min, r.t.	AlphaScreen

Controls in compound **I-BET762 (1)** study: BRD2(1) – I-BET151: 1.5 x 10^{-8} M (nHill = 1.9); BRD3(1) – I-BET151: 2.4 x 10^{-8} M (nHill = 2.2); BRD4(1) – I-BET151: 1.3 x 10^{-8} M (nHill = 1.3); BRD4(2) – PFI-1: 1.1 x 10^{-6} M (nHill = 1.3).

Controls in compounds **19**, **20** and **21** study: BRD2(1) – JQ1: 3.7 x 10-7 M (nHill = 2.1); BRD3(1) – JQ1: 7.9 x 10-7 M (nHill > 3); BRD4(1) – JQ1: 7.9 x 10-7 M (nHill = 3); BRD4(2) – PFI-1: 3.5 x 10-6 M (nHill > 3).

VI.2.2.2. Permeability Determination

Permeability studies were conducted at Pion, Inc. (Billerica, MA, US). The PAMPA EvolutionTM instrument was used to determine permeability. The effective permeability, Pe, of each compound was measured at pH 6.8 in the donor compartment using low-binding, low UV Prisma buffer. The drug-free acceptor compartment was filled with acceptor sink buffer containing a scavenger at the start of the test. The proprietary scavenger mimics serum proteins and blood circulation, thus creating sink conditions. In

the default protocol the aqueous solutions of studied compounds were prepared by diluting and thoroughly mixing 3 µL of DMSO stock in 600 µL of Prisma HT buffer. Final concentration of organic solvent (DMSO) in aqueous buffer is 0.5% (v/v). The reference solution is identical to the donor at time zero, so that any surface adsorption effects from the plastic is compensated. The PAMPA sandwich was assembled and allowed to incubate for ~15 h. The solutions in the donor compartment were un-stirred within duration of the experiment. Thus, the thickness of the aqueous boundary layer expected to be about 1000 µm. The sandwich was then separated, and both the donor and receiver compartments were assayed for the amount of drug present by comparison with the UV spectrum obtained from reference standards. Mass balance was used to determine the amount of material remaining in the membrane filter and on the plastic (%R).

VI.2.3. Experimental details on the biological studies

VI.2.3.1. Cell culture conditions

LNCaP cells were maintained in RPMI 1640 medium supplemented with penicillin (50 IU/mL), streptomycin (50 µg/mL), 10 % (v/v) serum, and 10 % (v/v) Glutamax at 37 ˚C and 5 % CO_2. Subculture was performed once a week and the cells reseeded in constant volumes of cell suspension and medium. The split ratio used for subculture was 1:6 to 1:10. Cells were split 20 times until discarding.

VI.2.3.2. Preparation of stock compounds

All stocks of drugs used in biological assays were prepared at 50 mM in sterile DMSO. Drugs were thoroughly weighed in sterile eppendorfs, diluted in the proper amount of DMSO and stored at -80 ˚C. Before each experiment drugs were left to thaw at room temperature and a working stock was prepared in cell culture medium. Unless otherwise stated DMSO from initial stocks was diluted 1000x in each assay to prevent vehicle-induced toxicity.

VI.2.3.3. Cellular growth inhibition

LNCaP cells were seeded on flat bottom 96-well plates at a density of 2500 cells/well (optimized for 6 days of growth). The outside wells of the plate were filled with 200 µL of sterile water, minimizing the edge effect. T_0 measurements were taken the following day using Cell-Titer Blue (Promega) following the manufacturer's instructions and measured on an Infinite M200 multimode plate reader (Tecan). The remaining plates were treated with DMSO or serial dilutions of compounds and incubated for 6 days. After 6 days the plates were developed as above, with LNCaP cells being incubated with Cell-Titer Blue for 2 h. Results are background correct by subtraction of values from wells containing no cells,

expressed as percentage of the T_0 value, and plotted against compound concentration. The T_0 was normalised to 100 %, representing the number of viable cells at the time of compound addition. The cellular response was determined for each compound by using GraphPad Prism software. Growth IC_{50} (gIC_{50}) values correspond to the concentration at the mid-point of the growth window (between DMSO and T_0 values).

VI.2.3.4. Flow cytometry determination of fluorescein-positive cells

LNCaP cells were seeded in 6-well plates at 3 x 10^4 cells/cm^2 and grown for 48 h before being treated with drug or vehicle. Compounds were used at concentrations of 10 µM and 50 µM and incubated for 2 h at 37 ˚C. Cells were then harvested with trypsin and transferred to to FACS tubes and centrifuged for 4 min at 4000 x g. Supernatant was discarded and each cell pellet was resuspended thoroughly in 300 µL of 10 % (v/v) FCS in PBS. Vials were stored at 4 ˚C until analysis. The analysis of fluorescein-positive cells was performed on a FACSCalibur. A typical cell area was gated and a total of 50.000 events per sample were acquired. Results were expressed as percentage of the maximal FACS signal. Data were analyzed using FloJo software.

VI.2.3.5. Imaging studies after cell membrane permeabilization

LNCaP cells were seeded at 3 x 10^4 cells/cm^2 in 24 –well plates onto round glass cover slips and grown for 48 h. The medium was then removed and cells washed twice with PBS. At room temperature and outside the aseptic environment, cells were fixed with 100 µL of a solution of 4 % (v/v) paraformaldehyde in PBS. Cells were incubated with PFA for 20 min at room temperature with plate agitation. After the incubation PFA was removed and cells rinsed five times with PBS. At this point some of the cell membranes were permeabilized with 0.2 % (v/v) Triton X-100 while others remained untreated. The incubation with Triton was performed for 10-15 min. Triton was then removed and cells incubated with PBS for 4 times during 5 min. each. All cells (permeabilized and non-permeabilized) were treated with 10 µM compounds or vehicle control and incubated for 1 h. Cells were washed 4 times to remove unspecific binding. The glass cover slips were then carefully dried for the excess PBS and mounted on glass plates with mounting medium. The glass plates were stored at 4 ˚C until analysis by confocal microscopy. Imaging was done using a ZEISS LSM 710 with identical laser, filter and detector settings for all samples tested.

VI.2.3.6. Imaging studies in live cells

LNCaP cells were seeded at 1 x 10^4 cells/cm^2 in 24 –well plates (2 x 10^4 cells/well) onto round glass cover slips and grown for 48 h. The medium was removed and compounds at 10 µM were added at different time points. After the drug incubation period the plates were removed from the incubator, the medium containing drugs was removed and the wells were washed with PBS (3 times). The cells were then fixed with a solution of 4 % (v/v) paraformaldehyde in PBS (100 µL/well) for 15 min. PFA was discarded and the cells were washed again with PBS (4 times) before incubation with Hoescht staining reagent (dilution of 1:5000 from the stock solution) for 15 min. Upon Hoescht removal, cells were washed with PBS, the glass cover slips were then carefully dried for the excess PBS and mounted on glass plates with mounting medium. The glass plates were stored at 4 ˚C until analysis by confocal microscopy. Imaging was done using a ZEISS LSM 710 with identical laser, filter and detector settings for all samples tested.

VI.3. Experimental Section of Chapter III

VI.3.1. Experimental details on the synthesis of compounds

Synthesis of compound **I-BET762 (1)** is described in chapter VI.2.1.1, p117

VI.3.1.1. Synthesis of tertiary amine analogues

- Synthesis of compound **26** / **RT53 (**Scheme 7**,** p58**)**

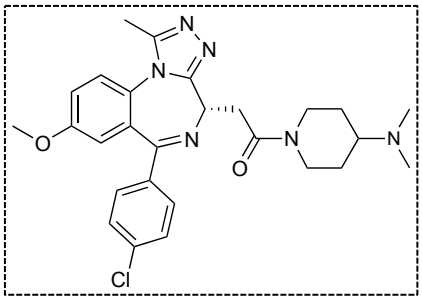

To a solution of **12** (1 eq, 0.25 mmol) in THF (3 mL) at room temperature was added DIPEA (2 eq) followed by HATU (2 eq). The reaction mixture was stirred for 3 h at room temperature and *N,N*-Dimethylpiperidin-4-amine dihydrochloride (1.5 eq) was added dropwise. The mixture was stirred for 12-14 h before being concentrated under reduced pressure. The crude material was dissolved in DCM and washed with a saturated solution of $NaHCO_3$. The aqueous layer was extracted once with DCM and the combined organics washed with brine, dried over $MgSO_4$, filtered and concentrated in vacuo. The resulting crude was purified by Combi-Flash chromatography using a gradient of 100% A (DCM with 1% triethylamine) to 10% B (MeOH with 1% triethylamine) over 20 min. to afford **RT53** as a pale yellow solid (65.1 mg, 51%).

^{1}H NMR (500 MHz, Methanol-*d4)* δ 7.73 (d, *J* = 9.0 Hz, 1H), 7.54 (t, *J* = 8.4 Hz, 2H), 7.41 (d, *J* = 9.0 Hz, 2H), 7.37 (d, *J* = 2.9 Hz, 1H), 6.91 (s, 1H), 4.69 – 4.65 (m, 1H), 4.59 (t, *J* = 11.4 Hz, 1H), 4.32 (t, *J* = 14.6 Hz, 1H), 3.82 (s, 3H), 3.66 – 3.51 (m, 2H), 3.23 (t, *J* = 13.3 Hz, 1H), 2.73 – 2.65 (m, 1H), 2.64 (s, 3H), 2.38 (s, 6H), 2.05 (t, *J* = 13.4 Hz, 1H), 1.98 – 1.89 (m, 1H), 1.72 – 1.52 (m, 1H), 1.40 (d, *J* = 12.2 Hz, 1H), 1.29 (s, 1H). **HRMS (ESI)**: m/z calcd $[M+H]^+$ for $C_{27}H_{32}ClN_6O_2$ = 507.2270; found $[M+H]^+$ 507.2271

- Synthesis of compound **27** / **RT48 (**Scheme 7**,** p58)

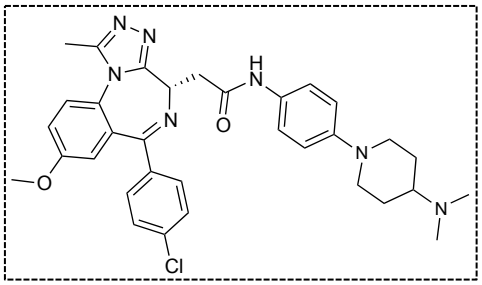

To a solution of **12** (1 eq, 0.25 mmol) in THF (3 mL) at room temperature was added DIPEA (2 eq) followed by HATU (2 eq). The reaction mixture was stirred for 3 h at room temperature and 1-(4-Aminophenyl)-*N,N*-dimethylpiperidin-4-amine (1.5 eq) was added dropwise. The mixture was stirred for 12 h before being concentrated under reduced pressure. The crude material was dissolved in DCM and washed with a saturated solution of $NaHCO_3$. The

aqueous layer was extracted once with DCM and the combined organics washed with brine, dried over $MgSO_4$, filtered and concentrated in vacuo. The resulting crude was purified by Combi-Flash chromatography using a gradient of 100% A (DCM with 1% triethylamine) to 10% B (MeOH with 1% triethylamine) over 20 min. to afford **RT48** as a pale brown solid (56 mg, 36%).

^{1}H NMR (300 MHz, Methanol-*d4*) δ 7.66 (d, *J* = 9.0 Hz, 1H), 7.49 (d, *J* = 8.6 Hz, 2H), 7.43 (d, *J* = 8.9 Hz, 2H), 7.36 – 7.27 (m, 3H), 6.91 (d, *J* = 9.1 Hz, 2H), 6.86 (d, *J* = 2.9 Hz, 1H), 4.68 – 4.58 (m, 1H), 3.76 (s, 3H), 3.71 – 3.61 (m, 2H), 3.54 (dd, *J* = 15.2, 9.0 Hz, 1H), 3.36 (dd, *J* = 15.2, 5.3 Hz, 1H), 3.27 (tq, *J* = 1.9, 0.9 Hz, 3H), 2.59 (s, 3H), 2.34 (s, 6H), 1.95 (d, *J* = 12.6 Hz, 2H), 1.59 (dd, *J* = 12.0, 3.8 Hz, 2H). **HRMS (ESI)**: m/z calcd $[M+H]^+$ for $C_{33}H_{37}ClN_7O_2$ = 598.2692; found $[M+H]^+$ 598.2892.

VI.3.1.2. Synthesis of quaternary amine analogue

Literature basis: Staben L.R.; Koenig, S. G.; Lehar, S.M.; Vandlen, R.; Zhang, D.; Chuh, J.; Yu, S.; Ng, C.; Guo, J.; Liu, Y.; Fourie-O'Donohue, A.; Go, M.; Linghu, X.; Segraves, N.L.; Wang, T.; Chen, J.; Wei, B.; Phillips, G.D.L.; Xu, K.; Kozak, K.R.; Mariathasan, S.; Flygare, J.A.; Pillow, T.H., *Nat Chem*. **2016**. *8(12)*:1112

- Synthesis of compound **28** / **RT56 (**Scheme 8**,** p58)

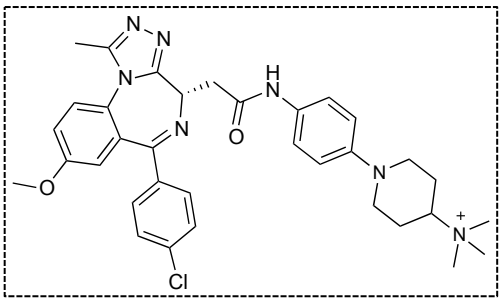

Compound **27** / **RT48** (31.5 mg, 0.05 mmol, 1 eq) and iodomethane (16.4 µL, 0.25 mmol, 5 eq) were dissolved in DMF (0.9 mL). To the reaction mixture was added TBAI (9.71 mg, 0.025 mmol, 0.5 eq) and DIPEA (22.4 µL, 0.125 mmol, 2.5 eq). The reaction was stirred at room temperature until all the starting material was consumed. The crude was purified by a semi-preparative reversed phase high-pressure liquid chromatography as indicated in the general procedures and lyophilized to afford **RT56** as a white solid (14.5 mg, 47%).

^{1}H NMR (500 MHz, Methanol-d_4) δ 7.73 (s, 1H), 7.55 (s, 2H), 7.40 (s, 1H), 7.39 (s, 1H), 7.00 (d, *J* = 7.0 Hz, 2H), 6.93 (s, 1H), 4.71 (s, 1H), 3.88 (d, *J* = 12.5 Hz, 2H), 3.83 (s, 3H), 3.56 (s, 1H), 3.53 (d, *J* = 13.0 Hz, 1H), 3.43 (d, *J* = 15.3 Hz, 1H), 3.14 (s, 9H), 2.79 (t, *J* = 12.2 Hz, 2H), 2.65 (s, 3H), 2.29 (d, *J* = 11.6 Hz, 2H), 1.94 (q, *J* = 13.1, 12.4 Hz, 2H). **HRMS (ESI)**: m/z calcd $[M+H]^+$ for $C_{34}H_{40}ClN_7O_2^+$ = 612.2848; found $[M+H]^+$ 612.2869

VI.3.2. Protein expression and purification

Plasmid DNA (BRD2: NCBI accession number NP_001106653.1, second bromodomain (BD2): E348-D455; BRD4, NCBI accession number NP_490597.1, first bromodomain (BD1): N44-E168, previously described[261]) were transformed into competent *E. coli* BL21(DE3)-R3-pRARE2 cells (phage-resistant derivative of BL21(DE3) strain), with a pRARE plasmid encoding rare codon tRNAs. Freshly grown colonies were cultured for 12 h in LB (Luria-Bertani) medium twice concentrated (2X) supplemented with 50 µg/mL kanamycin and 34 µg/mL chloramphenicol at 37 ºC. One litre of pre-warmed TB (Terrific Broth) medium was inoculated with 10 mL of the overnight culture and was incubated at 37 ºC. At an OD_{600} nm of 2.5, the culture was cooled down to 18 ºC and expression was induced for 12-14 h at 18 ºC with 0.1 mM isopropyl-β-D-thiogalactopyranoside (IPTG). Cells were then harvested by centrifugation (8700 x*g*, 15 min, 4 ºC) in a Beckman Coulter Avanti J-20 XP centrifuge, and then re-suspended in lysis buffer (50 mM HEPES, pH 7.5 at 20 °C, 500 mM NaCl, 5% Glycerol, 1 mM tris(2-carboxyethyl)phosphine (TCEP) and 1:1000 (v/v) Protease Inhibitor Cocktail III (Calbiochem)). Cells were lysed 3 times at 4 °C using a Basic Z Model Cell Disrupter (Constant Systems Ltd, UK) and DNA was removed by precipitation on ice for 30 min with 0.15% (v/v) of PEI (Polyethyleneimine). Lysates were cleared by centrifugation (16000 x*g* for 1 h at 4 °C, JA 25.50 rotor, on a Beckman Coulter Avanti J-20 XP centrifuge). Supernatants were applied to nickel-nitrilotriacetic acid agarose columns (Ni-NTA, Qiagen Ltd., 5 mL, equilibrated with 20 mL lysis buffer). The columns were washed once with 30 mL of lysis buffer, then with 20 mL of lysis buffer containing 30 mM Imidazole. Proteins were eluted using a step gradient of Imidazole in lysis buffer (50, 100, 150, 2 x 250 mM Imidazole in 50 mM HEPES, pH 7.5 at 25 ºC, 500 mM NaCl). All fractions were collected and monitored by SDS-polyacrylamide gel electrophoresis (Bio-Rad Criterion™ Precast Gels, 4-12% Bis-Tris, 1.0 mm, from Bio-Rad, CA.). Half of the eluted proteins was treated for 12-14 h at 4 ºC with Tobacco Etch Virus (TEV) protease to remove the hexa-histidine tag (for crystallography and other biophysical experiments). The other half of the proteins was kept with the hexa-histidine tag intact to be used in the SPOT assay experiments. Both tagged and untagged proteins were further purified with size exclusion chromatography on a Superdex 75 16/60 HiLoad gel filtration column (GE/Amersham Biosciences) on an ÄktaPrime™ plus system (GE/Amersham Biosciences). Recombinant BRD4 and BRD9 domains eluted as single symmetrical monomeric peaks. Samples were monitored by SDS-polyacrylamide gel electrophoresis and concentrated to 6-10 mg/mL in the gel filtration buffer, 10 mM HEPES pH 7.5, 500 mM NaCl and 5% Glycerol using Amicon® Ultra (MILLIPORE) concentrators with a 10 MWCO cut-off. Proteins were aliquoted into 100 µL fractions, flash frozen in liquid nitrogen and stored at - 80 ºC until further use. Protein handling was carried out on ice or in a cold room.

VI.3.3. Ligand binding analysis

VI.3.3.1. Differential Scanning Fluorimetry (DSF)

Thermal melting experiments were carried out using an Mx3005p Real Time PCR machine (Stratagene). Proteins were buffered in 10 mM HEPES pH 7.5, 500 mM NaCl and assayed in a 96 well plate at a final concentration of 2 µM in 20 µL volume. Compounds were added at a final concentration of 10 µM. SYPRO Orange (Molecular Probes) was added as a fluorescence probe at a dilution of 1 in 1000. Excitation and emission filters for the SYPRO-Orange dye were set to 465 nm and 590 nm, respectively. The temperature was raised with a step of 3 ˚C per minute from 25 ˚C to 96 ˚C and fluorescence readings were taken at each interval. The temperature dependence of the fluorescence during the protein denaturation process was approximated by the equation:

$$y(T) = y_F + \frac{y_U - y_F}{1 + e^{\Delta uG_{(T)}/RT}}$$

where ΔuG is the difference in unfolding free energy between the folded and unfolded state, R is the gas constant and yF and yU are the fluorescence intensity of the probe in the presence of completely folded and unfolded protein respectively. The baselines of the denatured and native state were approximated by a linear fit. The observed temperature shifts, ΔT_m^{obs}, were recorded as the difference between the transition midpoints of sample and reference wells containing protein without ligand in the same plate and determined by non-linear least squares fit.

VI.3.3.2. Isothermal Titration Calorimetry (ITC)

Experiments were carried out on an ITC200 titration microcalorimeter from MicroCal™, LLC (GE Healthcare) equipped with a Washing module, with a cell volume of 0.2003 mL and a 40 µL microsyringe. Experiments were carried out at 15 ˚C while stirring at 1000 rpm, in ITC buffer (20 mM HEPES pH 7.5 (at 25 °C), 200 mM NaCl). The microsyringe was loaded with a solution of protein sample (340 - 400 µM, in ITC buffer) and was carefully inserted into the calorimetric cell which was filled with an amount of the protein (0.2 mL, 27-33 µM in ITC buffer). Following baseline equilibration an additional delay of 60 seconds was applied. All titrations were conducted using an initial control injection of 0.3 µL followed by 38 identical injections of 1 µL with a duration of 2 seconds (per injection) and a spacing of 120 seconds between injections. The titration experiments were designed in such a fashion, as to ensure complete saturation of the proteins before the final injection. The heat of dilution for the proteins were independent of their concentration and corresponded to the heat observed from the last injection, following saturation of compound binding, thus facilitating the estimation of the baseline of each titration from the last injection. The collected data were corrected for peptide heats of dilution

(measured on separate experiments by titrating the proteins into ITC buffer) and deconvoluted using the MicroCal™ Origin software supplied with the instrument to yield enthalpies of binding (ΔH) and binding constants (K_B) in the same fashion to that previously described in detail by Wiseman and co-workers[262]. Thermodynamic parameters were calculated using the basic equation of thermodynamics ($\Delta G = \Delta H - T\Delta S = -RT\ln K_B$, where ΔG, ΔH and ΔS are the changes in free energy, enthalpy and entropy of binding respectively). In all cases a single binding site model was employed, supplied with the MicroCal™ Origin software package. Dissociation constants and thermodynamic parameters are listed in Table 4.

VI.3.3.3. AlphaScreen Detection

Bromodomain screening and determination of IC_{50} values were conducted at Cerep (Celle l'Evescault, France) on a fee-for-service basis. BRD2(1), BRD3(1), (BRD4(1) and BRD4(2) were assayed as described in chapter VI.2.2.1, Table 7.

Controls in study of compounds **26 / RT53** and **27 / RT48**: BRD2(1) – I-BET151: 1.5 x 10^{-8} M (nHill = 1.9); BRD3(1) – I-BET151: 2.4 x 10^{-8} M (nHill = 2.2); BRD4(1) – I-BET151: 1.3 x 10^{-8} M (nHill = 1.3); BRD4(2) – PFI-1: 1.1 x 10^{-6} M (nHill =1.3).

Controls in study of compound **28 / RT56**: BRD2(1) – I-BET151: 1.1 x 10^{-8} M (nHill = 1.7); BRD3(1) – I-BET151: 1.9 x 10^{-8} M (nHill = 2.4); BRD4(1) – I-BET151: 1.2 x 10^{-8} M (nHill = 1.9); BRD4(2) – PFI-1: 7.0 x 10^{-7} M (nHill =2.2).

VI.3.4. Crystallization and structure of BRD2(2) and BRD4(1) in complex with analogues

VI.3.4.1. Crystallization

Aliquots of the purified proteins were set up for crystallization in complex with compounds using a mosquito® crystallization robot (TTP Labtech, Royston UK). Coarse screens were typically setup onto Greiner 3-well plates using three different drop ratios of precipitant to protein per condition (100+50 nL, 75+75 nL and 50+100 nL). Initial hits were optimized further using Greiner 1-well plates and scaling up the drop sizes in steps. Crystallizations were carried out using the sitting drop vapour diffusion method at 4 °C. Crystals of BRD2/BD2 in complex with RT53 (1 mM final concentration) were grown by mixing 100 nL of the protein (5.7 mg/mL in 10 mM HEPES pH 7.5, 500 mM NaCl, 5% Glycerol) with 200 nL of reservoir solution containing 30% PEG1000 and 0.1 M MMT pH 7.0. Crystals of BRD2/BD2 in complex with RT56 (1 mM final concentration) were grown by mixing 150 nL of the protein (5.7 mg/mL in 10 mM HEPES pH 7.5, 500 mM NaCl, 5% Glycerol) with an equal volume of reservoir solution containing 30%

PEG1000 and 0.1 M MMT pH 7.0. Crystals of BRD4/BD1 in complex with RT53 (1 mM final concentration) were grown by mixing 150 nL of protein (5.7 mg/mL in 10 mM HEPES pH 7.5, 500 mM NaCl, 5% Glycerol) with an equal volume of reservoir solution containing 20% PEG3350, 10% ethylene glycol, 0.1 M bis-tris-propane pH 8.5 and 0.02 M Na/K phosphate. Crystals of BRD4/BD1 in complex with RT56 (1 mM final concentration) were grown by mixing 200 nL of protein (5.7 mg/mL in 10 mM HEPES pH 7.5, 500 mM NaCl, 5% Glycerol) with 100 nL of reservoir solution containing 20% PEG3350, 10% ethylene glycol, 0.1 M bis-tris-propane pH 7.5 and 0.2 M Na_2SO_4. In all cases crystals appeared within several days from sitting drop plates at 4 ˚C. Prior to data collection, all crystals were transferred to a solution consisting of the precipitation buffer supplemented with ethylene glycol and subsequently flash frozen in liquid nitrogen.

VI.3.4.2. Data collection and structure determination

Prior to data collection, all crystals were transferred to a solution consisting of the precipitation buffer supplemented with ethylene glycol and subsequently flash frozen in liquid nitrogen. Data were collected at Diamond Lightsource on beamline I04.1 at a wavelength of 0.92819 Å. Data were integrated with XDS[263] and scaled with SCALA or AIMLESS[264]. Automated model building with ARP/wARP[265] or BUCCANEER[266] resulted in a more than 90% complete models. Refinement was carried out with REFMAC[267] after several rounds of manual rebuilding with COOT[268]. The quality of the final models was validated with MOLPROBITY[269]. Hydrogen atoms were included in late refinement cycles. Data collection and refinement statistics can be found in Table 8.

Table 8. Structural data collection and refinement data statistics.

Data Collection				
PDB ID	6I7X	6I7Y	6I80	6I81
Protein/Ligand	BRD2/BD2 **RT53**	BRD2/BD2 **RT56**	BRD4/BD1 **RT53**	BRD4/BD1 **RT56**
Space group	$C222_1$	$I4_122$	$P2_12_12_1$	$P2_12_12_1$
Cell dimensions: a, b, c (Å)	64.41 66.72 129.61	127.30 127.30 40.59	37.67 44.79 79.55	37.74 44.74 79.56
α, β, γ (deg)	90.00 90.00 90.00	90.00 90.00 90.00	90.00 90.00 90.00	90.00 90.00 90.00
Resolution* (Å)	1.14 (1.20-1.14)	1.74 (1.83-1.74)	1.20 (1.26-1.20)	1.00 (1.05-1.00)
Unique observations*	101581 (14271)	17453 (2499)	42878 (6124)	73523 (10583)

Completeness* (%)	99.5 (96.9)	100.0 (99.9)	99.9 (99.3)	99.9 (99.7)
Redundancy*	5.6 (3. 5)	10.6 (11.1)	5.8 (4.2)	5.8 (4.0)
Rmerge*	0.043 (0.435)	0.059 (0.486)	0.038 (0.062)	0.036 (0.263)
I/ σI*	16.1 (2.4)	23.6 (4.6)	32.9 (17.5)	22.8 (4.6)
Refinement				
Resolution (Å)	1.14	1.74	1.20	1.00
R_{work} / R_{free} (%)	13.1/14.3	17.3/19.6	11.9/13.7	12.5/13.1
Number of atoms (protein/other/water)	1868/76/349	907/60/93	1092/48/207	1093/52/192
B-factors (Å²) (protein/other/water)2 1.85	15.79/15.08/ 30.05	25.56/25.52/ 32.87	9.41/10.27/ 23.38	10.05/13.72 / 23.54
r.m.s.d bonds (Å)	0.016	0.015	0.015	0.016
r.m.s.d angles (°)	1.757	1.978	1.744	1.906
Ramachadran				
Favoured (%)	99.52	100.00	96.52	96.49
Allowed (%)	0.48	0.00	3.48	3.51
Disallowed (%)	0.00	0.00	0.00	0.00

*Values in parentheses correspond to the highest resolution shell.

VI.3.5. Molecular Dynamics Simulations

The structure crystal structures of BRD2(2) and BRD(4) in complex with **RT53** and **RT56** were used as starting structures in our MD simulations. Parameters for **RT53** and **RT56** were generated with the antechamber module of Amber16[270], using the general Amber force field (GAFF)[271], with partial charges set to fit the electrostatic potential generated with HF/6-31G(d) by RESP[272]. The charges are calculated according to the Merz-Singh-Kollman scheme using Gaussian 09[273]. Each protein was immersed in a water box with a 10 Å buffer of TIP3P[274] water molecules. The system was neutralized by adding explicit counter ions (Cl^-). All subsequent simulations were performed using the ff14SB force field, which is an evolution of the Stony Brook modification of the Amber 99 force field force field (ff99SB)[275]. A two-stage geometry optimization approach was performed. The first stage minimizes only the positions of solvent molecules and ions, and the second stage is an unrestrained minimization of all the atoms in the simulation cell. The systems were then gently heated by incrementing the temperature from 0 to 300 K under a constant pressure of 1 atm and periodic boundary conditions. Harmonic restraints of 30

kcal/mol were applied to the solute, and the Andersen temperature coupling scheme[276] was used to control and equalize the temperature. The time step was kept at 1 fs during the heating stages, allowing potential inhomogeneities to self-adjust. Water molecules are treated with the SHAKE algorithm such that the angle between the hydrogen atoms is kept fixed. Long-range electrostatic effects are modelled using the particle-mesh-Ewald method [277]. An 8 Å cutoff was applied to Lennard-Jones and electrostatic interactions. Each system was equilibrated for 2 ns with a 2 fs time step at a constant volume and temperature of 300 K. Production trajectories were then run for additional 200 ns under the same simulation conditions.

VI.4. Experimental Section of Chapter IV

VI.4.1. Experimental details of the synthesis of compounds

VI.4.1.1. Synthesis of the photoreactive probe (Scheme 10, p79)

- Synthesis of compound **29**

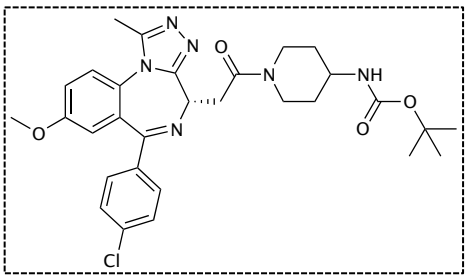

To a solution of acid **12** (102 mg, 0.25 mmol) in THF (3 mL) at room temperature was added DIPEA (90 µL, 0.5 mmol, 2 equiv.) followed by HATU (190 mg, 0.5 mmol, 2 equiv.). The reaction mixture was stirred for 3 h at room temperature. 4-(*N*-Boc-amino)piperidine (100 mg, 0.5 mmol, 2 equiv.) was added. The mixture was stirred for 12-14 h at room temperature before being concentrated under reduced pressure. The crude material was dissolved in DCM and washed with a saturated solution of $NaHCO_3$. The aqueous layer was extracted once with DCM. The combined organics were washed with brine, dried over Na_2SO_4 filtered and concentrated in vacuo. The crude was purified by Combi-Flash chromatography with a gradient of DCM/MeOH (100/0 to 90/10%) to afford 105 mg of **29** (70% yield).

^{1}H NMR (500 MHz, Chloroform-*d*) δ 7.47 (dd, *J* = 8.5, 2.4 Hz, 2H), 7.37 (d, *J* = 8.7 Hz, 1H), 7.32 (dd, *J* = 8.6, 2.8 Hz, 2H), 7.18 (dd, *J* = 9.0, 2.9 Hz, 1H), 6.85 (t, *J* = 2.0 Hz, 1H), 4.76 (t, *J* = 6.7 Hz, 1H), 4.60 – 4.44 (m, 2H), 4.30 – 4.13 (m, 1H), 3.78 (s, 3H), 3.62 (ddd, *J* = 36.2, 26.3, 17.4 Hz, 3H), 3.25 (ddd, *J* = 14.5, 11.9, 2.9 Hz, 1H), 2.86 – 2.75 (m, 1H), 2.60 (s, 3H), 2.06 (d, *J* = 13.7 Hz, 1H), 2.03 – 1.91 (m, 1H), 1.45 (d, *J* = 8.0 Hz, 9H), 1.36 – 1.22 (m, 1H). **HRMS (ESI):** m/z calcd $[M+H]^+$ for $C_{30}H_{35}ClN_6O_4$ = 579.2481; found $[M+H]^+$ 579.2457

- Synthesis of compound **30**

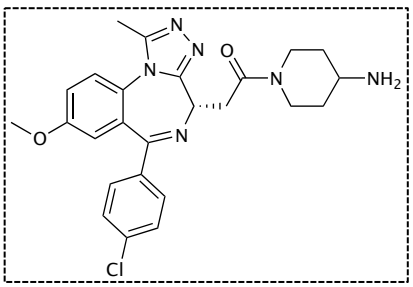

The Boc-intermediate **29** (40 mg, 0.07 mmol) was deprotected using a mixture of DCM:TFA (1:1) for 2 h at room temperature to afford compound **30** as pale yellow solid (33.5 mg, 100%).

^{1}H NMR (500 MHz, Methanol-*d4*) δ 7.71 (d, *J* = 9.2 Hz, 1H), 7.55 – 7.50 (m, 2H), 7.41 (s, 2H), 7.38 – 7.34 (m, 1H), 6.90 (s, 1H), 4.66 (t, 1H), 4.46 (t, *J* = 11.5 Hz, 1H), 4.21 (t, *J* = 15.1 Hz, 1H), 3.81 (s, 3H), 3.63 – 3.48 (m, 2H), 2.93 (d, *J* = 10.7 Hz, 1H), 2.82 – 2.73 (m, 1H), 2.62 (s, 3H), 1.98 (d, *J* = 13.0 Hz, 1H), 1.86 (d, *J* = 10.3 Hz, 1H), 1.56

– 1.38 (m, 1H), 1.27 (s, 1H). **LRMS (ESI):** m/z calcd $[M+H]^+$ for $C_{25}H_{27}ClN_6O_2$ = 479.19; found $[M+H]^+$ 479.47

- Synthesis of compound **32**

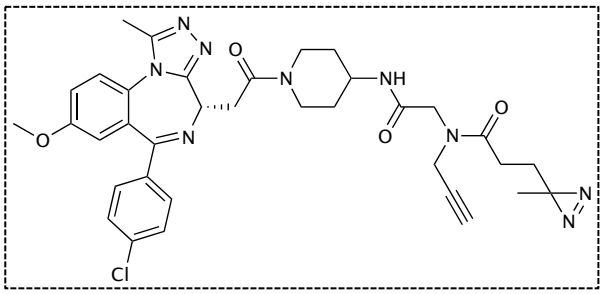

To a solution of the carboxylic acid **31** (37.5 mg, 0.2 mmol, 1.08 eq) in DMF (1.5 mL) was added DIPEA (70 µL, 0.39 mmol, 2 eq) and HATU (148.2 mg, 0.39 mmol, 2 eq). The reaction was stirred for 3 h at room temperature. To this was added compound **30** and the reaction stirred for 12-14 h at room temperature. The crude was then concentrated, diluted in DCM and washed 1 time with a saturated solution of $NaHCO_3$. The aqueous phase was extracted with DCM, the organics combined, dried over brine and Na_2SO_4, filtered and concentrated. The obtained crude was then diluted in DCM and purified over a gradient of DCM:MeOH (2.5 to 10%) to get the pure product **32** (56.8 mg, 46%).

^{1}H NMR (500 MHz, Methanol-*d*$_4$) δ 7.73 (d, *J* = 9.0 Hz, 1H), 7.54 (d, *J* = 8.3 Hz, 2H), 7.46 – 7.33 (m, 3H), 6.91 (s, 1H), 4.68 (d, *J* = 7.6 Hz, 1H), 4.48 – 4.37 (m, 1H), 4.25 (s, 2H), 4.20 (s, 2H), 4.11 (s, 1H), 4.00 (d, *J* = 13.7 Hz, 1H), 3.82 (s, 3H), 3.57 (d, *J* = 19.1 Hz, 2H), 3.35 (t, *J* = 11.8 Hz, 3H), 2.89 (d, *J* = 12.4 Hz, 1H), 2.64 (s, 3H), 2.44 (t, *J* = 7.6 Hz, 1H), 2.24 (t, *J* = 7.8 Hz, 1H), 2.04 (d, *J* = 15.2 Hz, 1H), 1.93 (d, *J* = 16.4 Hz, 1H), 1.68 (d, *J* = 8.3 Hz, 2H), 1.45 (t, *J* = 11.9 Hz, 1H), 1.34 (d, *J* = 27.5 Hz, 1H), 1.02 (d, *J* = 10.6 Hz, 3H). **HRMS (ESI):** m/z calcd $[M]^+$ for $C_{35}H_{38}ClN_9O_4$ = 684.2808; found $[M]^+$ 684.2785

VI.4.2. Experimental details on the biological studies

Compound stock solutions were made as in VI.2.3.2 (p128) and membrane permeability performed as described in chapter VI.2.2.2 (p127).

VI.4.2.1. Cell culture conditions

LNCaP and PC3 cells were maintained in RPMI 1640 medium supplemented with penicillin (50 IU/mL), streptomycin (50 µg/mL), 10% (v/v) serum, and 10% (v/v) Glutamax at 37 ˚C and 5% CO_2. Subculture was performed once a week and the cells reseeded in constant volumes of cell suspension and medium. The split ratio used for subculture was 1:6 to 1:10. Cells were split 20 times until discarding. For the cancer cell line viability screening all cells were recovered from liquid nitrogen and splitted at least once befor experimentation. These were cultured with either RPMI 1640 or Dulbecco's

modified eagle medium according to the supplier, and supplemented with penicillin (50 IU/mL), streptomycin (50 µg/mL) and 10% (v/v) serum.

VI.4.2.2. Small-Molecule sensitivity screening assay

Compound activity was profiled against a panel of 26 human cancer cell lines from different tissues in a 384-well format, opaque white assay plates at 500 – 1,000 cells per well using a semi-automated system. Cells were incubated at 37˚C/5% CO_2. Compound stocks were plated in 384-well format in 11-point and 2-fold concentration ranges. Compounds were pin-transferred into duplicate assay plates and incubated for 96 h. ATP levels were measured using Cell-Titer GLO (Promega) as a surrogate for cell viability.

VI.4.2.3. Cellular viability and proliferation

For cellular viability cells were seeded in white, opaque-bottom 96-well plates at 5000 cells/well (LNCaP) or 2500 cells/well (PC3) in a total volume of 100 µL of culture media. Serial diluted compounds (2-fold) in 100 µL media were added to the cells 24 h later. After 96 h incubation cellular viability was assessed by Cell-Titer GLO (Promega). The values were normalized to vehicle and IC_{50} was calculated using GraphPad Prism software. For proliferation assay LNCaP cells were seeded at 5000 cells/well in white, clear bottom 96-well plates in a total volume of 100 µL media. Serial diluted compounds in 100 µL media were added to the cells 12 h later and the percentage of confluence in each well measured by IncuCyte ZOOM. Cell growth was monitored by recording phase images with 10x objective at 3 h time intervals for a period of 7 days. IncuCyte ZOOM's Confluence Processing analysis tool was used to calculate cell confluence as surrogate for cellular proliferation.

VI.4.2.4. Cellular Thermal Shift Assay (CETSA)

The compounds or a DMSO vehicle were incubated with 4 x 10^6 cells for 1 h at 37 ˚C. Cells were then washed 1 x and harvested with cold PBS. After transferring to falcon tubes these were spun down for 5 min at 200 x g, and the supernatant discarded. The cell pellet was resuspended in 100 µL of PBS and transferred to PCR tubes. These were then centrifuged and the supernatant removed leaving approximately 5 µL supernatant in each tube. Cells were heat shocked in a thermal cycler at 48.5 ˚C for 3 min to denature proteins and allowed to cool down at room temperature for another 3 min. The pellet was then resuspended in 35 µL lysis buffer (50 mM Tris-HCl, pH 7.5, 5% glycerol, 100 mM NaCl, 2.5 mM $MgCl_2$, 0.2% NP40 and 1 x halt protease inhibitor cocktail). The cell suspensions were then subjected to three freeze-thaw cycles with liquid nitrogen to lyse cells. For a uniform thawing this step

was performed in a thermal cycler at 25 ˚C. Lysates were spun at 20,000 x g for 20 min at 4 ˚C to clarify and pellet aggregated protein. The tubes were carefully handled after this step to avoid disturbing the pellet. The supernatant (approximately 35 – 40 µL) containing the soluble protein fraction was transferred to a new tube. Samples were then boiled with loading buffer (1 x Laemmli Sample Buffer), spun down 3 min at 12,000 x g and split in two samples for immunoblotting.

VI.4.2.5. Diazirine photoreactive cross-linking and click chemistry

Compounds or DMSO were incubated with 4 x 10^6 cells for 1 h at 37 ˚C. After 1 h media was aspirated and plates were placed on ice and UV-irradiated for 10 min. Cells were then washed 1 x and harvested in cold PBS to falcon tubes. These were spun at 300 x g for 3 min. at 4 ˚C. The supernatant was removed and the pellet resuspended in lysis buffer with a 1:3 pellet to buffer ratio (approximately 150 µL buffer). Cells were lysed on ice for 25 min. and then centrifuged at 12,000 x g for 10 min. at 4 ˚C. BCA assay (Pierce) was used to quantify protein concentration and each sample diluted in PCR tubes to 4 mg/mL in a 50 µL final volume. Click reagents (1 mM TCEP; 100 µM TBTA, 1 mM $CuSO_4$, final concentrations) were then added followed by the bifunctional tag. These were either Alexa Fluor 647 azide or Biotin-PEG-azide. Reactions were stirred at room temperature for 1 h, while being protected from light. Samples were then boiled in loading buffer (1 x Laemmli sample buffer), centrifuged at 12,000 x g for 3 min. and run on SDS-PAGE gel. When using AlexaFluor Azide as functional tag in gel fluorescence scanning was performed using an OdysseyCLxImager (LI-COR). When using Biotin-PEG-azide as functional tag the gel was transferred to a membrane, blocked and detected with an anti-biotin antibody conjugated with HRP as in standard immunoblotting procedures.

VI.4.2.6. Affinity-based compound-anchored agarose beads

VI.4.2.6.1. *Coupling of amine-functionalized compounds to Affi-Gel® 10*

Affi-Gel® 10 Gel was purchased from Bio-rad, supplied as a ~50% solution in anhydrous isopropyl alcohol (IPA). A uniform suspension was created and 400 µL of the solution was transferred to a 2 mL microcentrifuge tube. The gel was pelleted by (400 x g, 2 min) and the IPA supernatant was removed. The pellet (~100 µL) was washed 3 times with anhydrous DMSO, followed by repeated centrifugation (400 x g, 2 min, 25 ºC). The gel was made into a ~50% suspension by addition of 100 µL anhydrous DMSO. Amine stock solution (10 mM in DMSO, 18 µL, 12% loading) or 5 µL ethanolamine (for blocked beads) was added, followed by Et_3N (2.1 µL), and the resultant mixture was shielded from light and incubated on an overhead rotator at room temperature for 16 h. Ethanolamine (5 µL) was added and the mixture was incubated for a further 4 h at room temperature on an end-over-end rotator. The gel

was pelleted (400 x g, 2 min) and the supernatant was removed. The amine-modified gel pellet (~200 µL) was washed 3 times with anhydrous DMSO, followed by repeated centrifugation (400 x g, 2 min). The modified gel was then washed 3 times with cold PBS, and used as a 50% suspension in PBS.

VI.4.2.6.2. *Compound anchored pull-downs*

LNCaP cells were plated at $4x10^6$ cells in 60 mm petri dishes and left for 12 h to adhere. The next day media was aspirated and cells were washed once with cold PBS, following by collection in cold PBS. Cells were centrifuged (300 x g, 3 min, 4 ˚C) and the supernatant was removed. Pellets were resuspended in modified lysis buffer (with protease inhibitor) approximately 3 times the size of the pellet (150 µL). Lysis was performed on ice for 20 min and the samples centrifuged at 14000 x g for 10 min. The supernatant was collected and protein concentration determined by the Pierce BCA Portein Assay as before. For each pull down-condition, 500 µg of protein was diluted in the same lysis buffer (PBS) to a final volume of 450 µL. For the soluble completion condition, 4 µL of a 50 mM stock of free compound was added and allowed to incubate for 1 h at room temperature. Compound anchored beads (50 µL) were added to each sample, followed by DMSO to achieve a concentration of 2% (10 µL in bead-only conditions, 6 µL for soluble competition). Lysates were incubated with compound-anchored beads at 4 ˚C with end-over-end rotation for 12-14 h. Samples were gently centrifuged (200 x g) to remove flow-through (collected for blot) and rinsed with PBS thrice prior to resuspension of beads in 2 x SDS loading buffer (50 µL). Samples were boiled for 10 min at 95 ˚C and centrifuged (200 x g) to allow transfer of eluted proteins to fresh tubes for SDS-page and western blot analysis.

VI.4.2.7. Immunoblotting

Cells were lysed with RIPA buffer supplemented with halt protease inhibitor cocktail on ice bath for 20 min. The lysates were spun at 14000 x g for 10 min at 4 ˚C. A BCA assay (Pierce) was used to quantify protein concentration. The following antibodies were used: BRD4 (Bethyl Labs, A301-985A, 1:5000 dilution); BRD2 (Bethyl Labs, A302-582A, 1:1,000 dilution), c-MYC (Santa Cruz, sc-40, 1:500 dilution), Parp (Cell Signalling, 9532, 1:1000 dilution), GAPDH (Cell Signaling, 2118, 1:1000 dilution) and Actin (Cell Signallling, 4970S, 1:1000 dilution). Blots were imaged after incubating with HRP-conjugated secondary antibodies anti-mouse IgG (Cell Signaling, 7076S, 1:2000 dilution), anti-rabbit IgG (Cell Signaling, 7074S 1:2000 dilution) and anti-biotin (Cell Signaling, 7075S, 1:2000). Detection of secondaries was performed with Thermo Scientific™ SuperSignal™ West Pico PLUS Chemiluminescent Substrate (34580) according to manufacturer's instructions. For concentration- and time-dependent analysis of protein content LNCaP cells were plated in 6-well plates at 35000 cells/well in a volume of 2 mL/well. After 12 h they were either treated with increasing concentration of

compounds (dose-dependent) or single–dose (0.5 and 1.0 μM, time-dependent) experiments. In the former cells were incubated for 48 h prior harvesting and immunoblotting.

VI.4.2.8. Cell Cycle Analysis

LNCaP cells were seeded in 6-well plates at 1.0 x 10^5 cells/well in a total volume of 2 mL media and treated with different concentrations of compounds 24 h later. Cells were washed 2 times with PBS 48 h post-treatment and fixed in 70% ethanol by diluting first in 600 μL cold PBS followed by adding drop-wise while vortexing 1400 μL of ice-cold 100% ethanol. Samples were vortexed immediately and fixed at 4 ˚C for 12 h. At the day of experiment the samples were diluted 1:2 in PBS and centrifuged prior dissolving in a solution of PBS with 5% (v/v) FCS containing 50 μg/mL of PI and 100 μg/mL RNAse. Cells were incubated at 37 ˚C for 30 min. and stored in the dark at 4 ˚C until analysis by flow cytometry using a BD FACSCelesta cytometer and running BD FACSDiva software. Data was analysed with ModFit software.

VI.4.2.9. RNA extraction and gene expression quantitation

LNCaP cells and PC3 cells were plated in 6 well plates and treated in quadruplicates with vehicle (DMSO), I-BET762 or RT53 at 1.0 μM for 24 h. After treatment cells were collected and washed once with PBS. Total RNA was extracted and purified using Qiagen® RNeasy Mini Kit according to the manufacturer's instruction. RNA samples were quantified and quality assessed using an Advanced Analytical Fragment Analyzer. 20 ng of totalRNA was used for library preparation with ERCC Spike-in control Mix A (Ambion 10^{-6} final dilution). All steps are performed on a Tecan EVO150. 3'DGE-custom primers 3V6NEXT-bmc#1-24 are added to a final concentration of 1.2 μM. (5'-/5Biosg/ACACTCTTTCCCTACACGACGCTCTTCCGATCT[BC_6]$N_{10}T_{30}$VN-3' where 5Biosg = 5' biotin, [BC6] = 6bp barcode specific to each sample/well, N10 = Unique Molecular Identifiers, Integrated DNA technologies). After addition of the oligonucleotides, samples are denatured at 72 ˚C for 2 min. followed by addition of SMARTScribe RT per manufacturer's recommendations with Template-Switching oligo5V6NEXT -(12 μM, [5V6NEXT : 5'-iCiGiCACACTCTTTCCCTACACGACGCrGrGrG-3' where iC: iso-dC, iG: iso-dG, rG: RNA G]) and incubation at 42 ˚C for 90 min followed by inactivation at 72 ˚C for 10 min. Following the template switching reaction, cDNA from 24 wells containing unique well identifiers are pooled together and cleaned using RNA Ampure beads at 1.0X. cDNA is eluted with 90 μL of water followed by digestion with Exonuclease I at 37˚C for 45 min., inactivation at 80˚C for 20 min. Single stranded cDNA is then cleaned using RNA Ampure beads at 1.0X and eluted in 50 μL of water. Second strand synthesis and

PCR amplification was done using the Advantage 2 Polymerase Mix (Clontech) and the SINGV6 primer (10 pmol, Integrated DNA Technologies 5'-/5Biosg/ACACTCTTTCCCTACACGACGC-3'). 12 cycles of PCR was performed followed by clean up using regular SPRI beads at 1.0X, and was eluted with 20 µl of EB. Successful amplification of cDNA was confirmed using the Fragment Analyzer. Illumina libraries are then produced using standard Nextera tagmentation substituting P5NEXTPT5-bmc primer (25 µM, Integrated DNA Technologies, (5'-AATGATACGGCGACCACCGAGATCTACACTCTTTCCCTACACGACGCTCTTCCG*A*T*C*T*-3' w here * = phosphorothioate bonds.)in place of the normal N500 primer. Final libraries were cleaned using SPRI beads at 0.8X and quantified using the Fragment Analyzer and qPCR before being loaded for paired-end sequencing using the Illumina NextSeq500.

VI.4.2.10. Sequencing data analysis

Post-sequencing, quality-control on each of the libraries was performed to assess coverage depth, enrichment for messenger RNA (exon/intron and exon/intergenic density ratios), fraction of rRNA reads and number of detected genes using bespoke scripts. Sequences were aligned against the human genome GRCh38/hg38 ENSEMBL 89 using STAR, with parameters --runThreadN 8 --runMode alignReads --outFilterType BySJout --outFilterMultimapNmax 20 --alignSJoverhangMin 8 --alignSJDBoverhangMin 1 --outFilterMismatchNmax 999 --alignIntronMin 10 --alignIntronMax 1000000 --alignMatesGapMax 1000000 --outSAMtype BAM SortedByCoordinate --quantMode TranscriptomeSAM, pointing to a Suffix Array assembly containing exon-exon junctions for 75 nucleotide reads. Gene expression was estimated based on reads mapping near the 3' end of transcripts using ESAT [278] based on the hg38 Refseq annotation, with flags java -Xmx128G -task score3p -wLen 50 -wExt 5000 -wOlap 0 -sigTest 0.01 -multimap ignore. Results were summarized as counts per million mapped reads (CPMs), merged across samples, log-transformed and subjected to hierarchical clustering and visualization [279-281]. Differential expression analysis was conducted for each cell line independently against the corresponding DMSO control. Fold change and significance were determined using the glmFit and glmLRT functions in the edgeR statistical analysis package [282].

VI.5. Experimental Section of Chapter V

VI.5.1. Experimental details of the synthesis of compounds

Literature basis - Kularatne, S.A.; Zhou, Z.; Yang, J.; Post, C.B.; Low, P.S.. *Mol. Pharm.*; **2009**. *6(3)*:790-800

Synthesis of compound **26** (RT53) is described in VI.3.1.1, (p131)

Synthesis of compounds **35**, **36**, **37** and **38** was performed by WuXi AppTec on a fee-for-service basis.

- Syntehsis of compound **35**

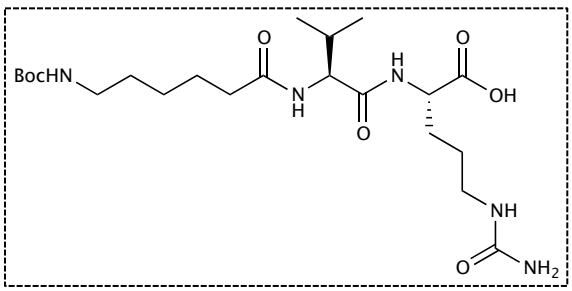

To a vessel containing CTC Resin (15 mmol, 15 g, 1.0 mmol/g) and Fmoc-Cit-OH (5.95 g, 15 mmol, 1 eq) was added DCM under nitrogen atmosphere. DIPEA (4.0 eq) was added dropwise and the solution stirred for 2 h. MeOH was then added and stirred for 30 min., followed by washing with DMF (5 x). A mixture of 20% piperidine/DMF was used for Fmoc deprotection for 30 min, followed by DMF washes (5 x). Fmoc-Cit-OH (1.0 eq) was added and mixed for 30 seconds, before adding activation buffer under nitrogen for about 1 h, time after which the mixture was drained and washed with DMF (5 x). A mixture of 20% Piperidine/DMF was again left to react for 30 min., then washed with DMF (5 x). The protected amino acid Fmoc-Val-OH (3 eq) was added and stirred for 30 sec. Activation buffer was added with nitrogen flow and the mixture stirred for 1 h. Cleavage buffer (20% HFIP/DCM) was added to the flask containing the protected peptide at room temperature, and stirred for 30 min twice. The solvent was removed under vacuum to afford the crude product. The mixture was purified by Prep-FLASH (A: H_2O, B: ACN) and lyophilized to give the final product **35** (5 g, 68.4%).

LRMS (ESI): m/z calcd $[M+H]^+$ for $C_{22}H_{41}N_5O_7$ = 488.3; found $[M+H]^+$ 488.2

- Synthesis of compound **36**

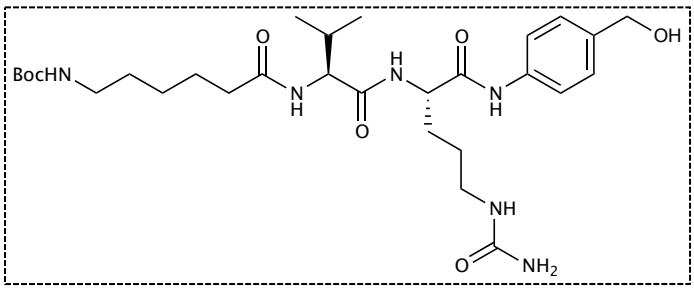

To a solution of compound **35** (1 g, 2.05 mmol) and (4-aminophenyl)methanol (758 mg, 6.15 mmol) in DMF (10 mL) was added HOBt (831 mg, 6.15 mmol) and DIC (776 mg, 6.15 mmol), stirred at room

temperature (23 °C) for 3 h. TLC and LC-MS indicated that the reactants had been consumed and that the product emerged. The reaction mixture was added dropwise to MTBE (100 mL), filtered and concentrated in vacuum. The crude product was purified by column chromatography on silica gel (100-200 mesh size) using DCM/MeOH (150:1-6:1) as eluent to give compound **36** (0.9 g, 67% yield) as a white solid.

MS (ESI): m/z calcd $[M+H]^+$ for $C_{29}H_{48}N_6O_7$ = 593.4; found $[M+H]^+$ 593.2

- Synthesis of compound **37**

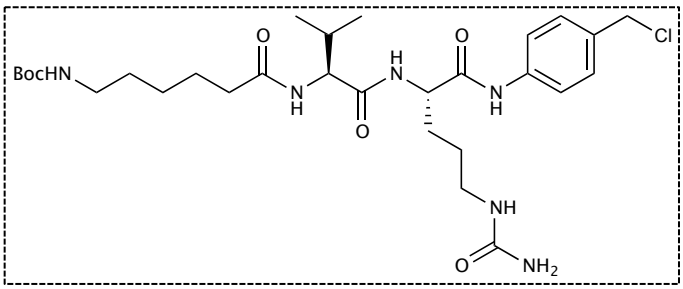

Compound **36** (0.5 g, 844 umol) was suspended in DMF (5 mL) and heated to dissolve all solids. After cooling to 0 °C, $SOCl_2$ (151 mg, 1.27 mmol) was added dropwise. Following the addition, the reaction was held at 0 °C for 5 h. LC-MS showed the reaction was complete. The reaction mixture was treated slowly with water (10 mL) to precipitate a yellow solid, which was collected by filtration. The solid was washed sequentially with water (10 mL) and MTBE (20 mL). The product was dried in vacuum to give compound **37** (0.39 g, 76% yield) as a yellow solid.

LRMS (ESI): m/z calcd $[M+H]^+$ for $C_{29}H_{47}ClN_6O_6$ = 611.3; found $[M+H]^+$ 611.2

- Synthesis of compound **38** / **VC – PABQ – RT53**

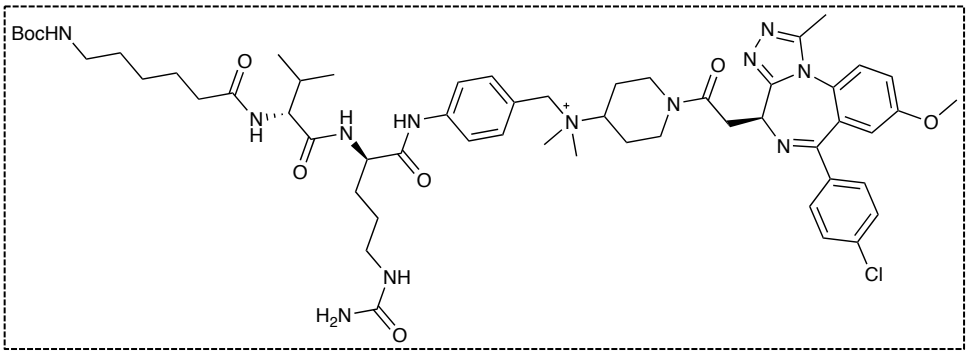

Compound **37** (156 mg, 254 μmol) and compound **26** (**RT53)** (86 mg, 170 μmol) were combined in DMF (0.5 mL) at room temperature (25 °C). To the solution was added TBAI (31.3 mg, 84.8 μmol) followed by DIPEA (54.8 mg, 424 μmol, 2.5 eq) and the mixture stirred at 25 °C for 16 h. LC-MS showed the reaction was complete. The residue was purified by prep-HPLC (formic acid condition) to give compound **VC-PABQ-RT53** (0.16 g, 79% yield) as a white solid.

^{1}H NMR: (400 MHz DMSO-*d_6*) 10.39 (s, 1H), 8.55 (s, 1H), 8.05-8.35 (m, 1H), 7.70-7.93 (m, 3H), 7.17-7.62 (m, 6H), 6.82-6.93 (m, 1H), 6.74 (s, 1H), 6.02-6.24 (m, 1H), 5.35-5.55 (m, 2H), 4.31-4.66 (m, 5H),

4.18 (t, *J* = 7.7 Hz, 1H), 3.80 (s, 2H), 3.54-3.75 (m, 2H), 3.17 (d, *J* = 13.1 Hz, 2H), 2.83-3.02 (m, 8H), 2.53-2.71 (m, 4H), 2.04-2.39 (m, 5H), 1.80-2.03 (m, 2H), 1.55-1.78 (m, 3H), 1.33-1.53 (m, 14H), 1.17-1.26 (m, 2H), 0.85 (dd, *J* = 11.8, 6.8 Hz, 6H).

LRMS (ESI): m/z calcd $[M+H]^+$ for $C_{56}H_{78}ClN_{12}O_8^+$ = 1081.6; found $[M+H]^+$ 1081.4

- Synthesis of compound **41**

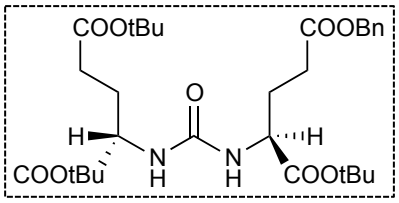

Triphosgene (33.6 mg, 11.3 mmol) and compound **39** (100 mg, 0.34 mmol) were suspended in DCM (5 mL) at 0 ˚C under argon and stirred for 5 min. Et_3N (103.6 µL, 0.74 mmol) was then added dropwise and the mixture stirred at 0 ˚C for 2 h. Compound **40** (122.6 mg, 0.37 mmol) in Et_3N (67.2 µL, 0.48 mmol) in DCM (1 mL) were added and the mixture stirred at room temperature for 12 h. The reaction was then quenched with 1 M HCl (10 mL), and the organic layer concentrated to give the crude product as yellow oil. The crude was purified by Combi-Flash chromatography using a gradient of 70% A (hexane) to 100% B (ethyl acetate) over 20 min. to obtain the pure product **41** as a clear oil (41 mg, 21%).

^{1}H NMR (400 MHz, Chloroform-*d*) δ 7.34 (s, 5H), 5.11 (s, 3H), 4.34 (d, J = 18.9 Hz, 2H), 2.50 – 2.40 (m, 2H), 2.35 – 2.25 (m, 2H), 2.20 – 2.01 (m, 2H), 1.99 – 1.81 (m, 2H), 1.48 – 1.40 (m, 27H)

- Synthesis of compound **42**

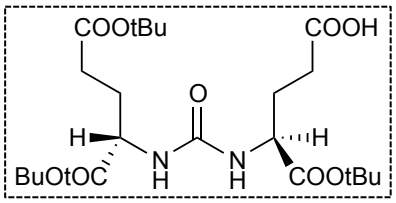

Compound **41** (67.8 mg, 0.11 mmol) was diluted in DCM and the mixture degassed under argon for 5 min. To the mixture was then added 10% palladium on activated charcoal (10 mg), and degassed for another 5 min. The reaction was stirred for 48 h at room temperature under hydrogen, time after which was filtered through a celite pad and concentrated to obtain the product **42** as a colorless oil (55 mg, 100%).

^{1}H NMR (300 MHz, Chloroform-*d*) δ 5.84 (d, *J* = 8.4 Hz, 1H), 5.45 (s, 1H), 4.48 – 4.38 (m, 1H), 4.36 – 4.28 (m, 1H), 2.44 – 2.37 (m, 2H), 2.36 – 2.26 (m, 2H), 2.19 – 1.98 (m, 2H), 1.92 – 1.82 (m, 2H), 1.48 (s, 9H), 1.46 (s, 9H), 1.43 (s, 9H)

- Synthesis of compound **43**

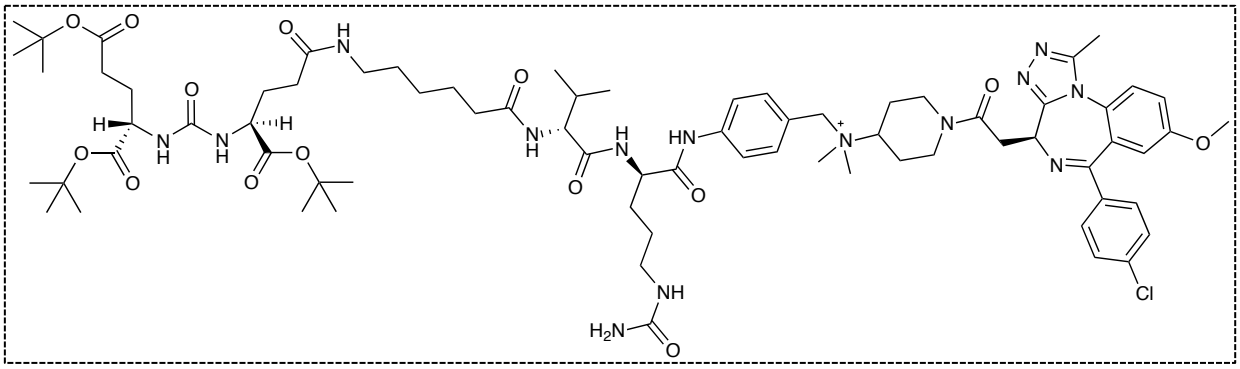

Compound **38 / VC-PABQ-RT53** (44 mg, 0.041 mmol) was dissolved in 2 mL of DCM and TFA (400 µL) was then added. After 1 h, no starting material was detected by MALDI-TOF and the reaction mixture was concentrated at reduced pressure, co-evaporating with toluene. Crude product NH_2-compound **38** was used with no further purification in the next step. Compound **42** (24 mg, 0.049 mmol) was dissolved in 2 mL of DMF, and HBTU (17 mg, 0.045 mmol) and DIPEA (25 µL, 0.14 mmol) were added. The resulting solution was stirred for 15 min at room temperature and it was then added to crude NH_2-compound **38** dissolved in 1 mL of DMF. After 16 h reaction, the mixture was purified directly by semi-preparative HPLC on Phenomenex Luna C18(2) column (10 µ, 250 mm × 21.2 mm) at a flow rate of 10 mL/min using the following gradient: water+0.1% TFA/acetonitrile 55:45 to 30:70 in 25 min.. Fractions containing product by mass (t_R=12.9) were collected and lyophilized to give pure **43** (34 mg, 0.024 mmol, 58% yield).

HRMS (ESI+): m/z: calcd. $[M+H]^+$ for $C_{74}H_{108}ClN_{14}O_{14}^+$ 1451.7852, found $[M+H]^+$ 1451.7829.

- Synthesis of Compound **44** / **DUPA – VC –PABQ – RT53**

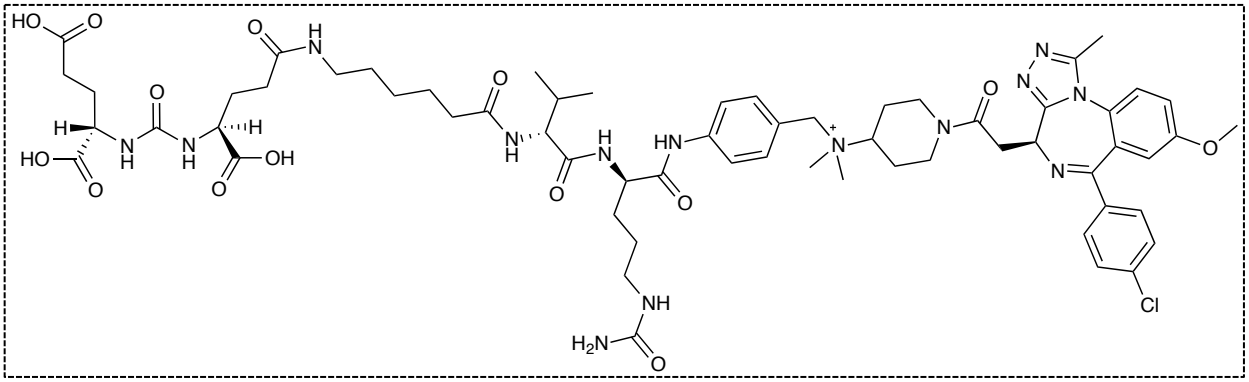

Compound **43** (28 mg, 0,019 mmol) was dissolved in 2 mL of DCM and TFA (500 µL) was then added. After 1.5 h no starting material was detected by MALDI-TOF and the reaction mixture was concentrated, co-evaporating with toluene. Crude product was diluted in a 1:1 mixture CH_3CN and H_2O and purified by HPLC on a Phenomenex Luna C18(2) column (10 µ, 250 mm × 21.2 mm) at a flow rate of 10 mL/min using the following gradient: water+0.1% TFA/acetonitrile 80:20 to 60:40 in 40 min.. Fractions containing

product by mass (t_R=32.0) were collected and lyophilized to give pure **44** / **DUPA-VC-PABQ-RT53** (12 mg, 0.0098 mmol, 51% yield).

^{1}H-NMR (400 MHz, Methanol-*d*$_4$) δ ppm 7.79-7.72 (m, 3H), 7.54-7.51 (m, 4H), 7.41-7.37 (m, 3H), 6.91-6.90 (m, 1H), 4.78-4.69 (m, 2H), 4.52-4.49 (m, 4H), 4.30-4.23 (m, 2H), 4.13 (d, *J* = 7.5 Hz, 1H), 3.01 (s, 3H), 3.76-3.51 (m, 3H), 3.35 (m, 1H), 3.22-3.11 (m, 4H), 2.98 (bs, 6H), 2.74-2.65 (m, 4H), 2.40-2.23 (m, 9H), 2.14-2.04 (m, 4H), 1.92-1.74 (m, 5H), 1.64-1.47 (m, 6H), 1.35-1.31 (m, 2H), 0.97 (d, *J* = 6.8 Hz, 3H), 0.96 (d, *J* = 6.8 Hz, 3H). **HRMS (ESI+):** m/z: calcd. [M+] for $C_{62}H_{84}ClN_{14}O_{14}^+$ 1283.5974, found [M+] 1283.5912.

VI.5.2. Cathepsin cleavage assay for linker-drug conjugate

Cathepsin B from human liver (18.3 µM stock in 50 mM sodium acetate, pH 5.0 with 1 mM EDTA) was activated by incubation at ambient temperature for 15 min with 30 mM dithiothreitol and 15 mM EDTA at pH 5.0. The activated enzyme at a final concentration of 0.14 µM was added to a mixture containing the linker-drug conjugate at a final concentration of 100 µM in the reaction buffer (50 mM sodium acetate, pH 5.0 with 1 mM EDTA and 2.5 % DMF). The solution was incubated at 37 ˚C with agitation and aliquots were taken at multiple time points for LC-MS analysis. Each aliquot was immediately quenched by adding E-64 protease inhibitor (Sigma E3132) at a final concentration of 0.14 µM (1:1 enzyme to inhibitor ratio). A reaction without enzyme was included as enzyme blank. The rate of free drug release was estimated from peak area (mAU*s) divided by the sum of free drug and linker-drug conjugates.

VI.5.3. Experimental details on the biological studies

Preparation of drug stocks was performed as described in chapter VI.2.3.2 (p128) and cell culture conditions as in VI.4.2.1 (p140).

VI.5.3.1. Cellular viability assay

Cells were seeded in white, opaque-bottom 96-well plates at 5000 cells/well (LNCaP) or 2000 cells/well (PC3) in a total volume of 100 µL of culture media. Serial diluted compounds (2-fold) in 100 µL media were added to the cells 24 h later. After 96 h incubation cellular viability was assessed by Cell-Titer GLO (Promega) according to the manufacture's instructions. The values were normalized to vehicle and IC_{50} was calculated using GraphPad Prism software.

VI.5.3.2. Dose – and time-dependent analysis of Myc expression

LNCaP cells were plated in 6-well plates at 35000 cells/well in a volume of 2 mL/well and left to adhere for 12 h. These were then treated with increasing concentration of compounds (dose-dependent) or single–dose (2.5 μM, time-dependent) experiments. In the dose-dependent assay cells were incubated for 48 h prior harvesting and immunoblotting, while in time-dependent cells were lysed at the indicated time points and stored in lysis buffer at -20 ˚C until the day of analysis. Cell lysis was performed with RIPA buffer supplemented with halt protease inhibitor cocktail on ice bath for 20 min. The lysates were spun at 14000 x g for 10 min at 4 ˚C. A BCA assay (Pierce) was used to quantify protein concentration. Myc protein levels were examined using a c-MYC (Santa Cruz, sc-40, 1:500 dilution) antibody and either Vinculin (Cell Signaling, 4650, 1:1000) or GAPDH (Cell Signaling, 2118, 1:1000 dilution) as loading controls. Blots were imaged after incubating with HRP-conjugated secondary antibodies anti-mouse IgG (Cell Signaling, 7076S, 1:2,000 dilution) and anti-rabbit IgG (Cell Signaling, 7074S 1:2000 dilution). Detection of secondaries was performed with Thermo Scientific™ SuperSignal™ West Pico PLUS Chemiluminescent Substrate (34580) according to manufacturer's instructions.

VI.5.3.3. Development of prostate cancer mice model and drug administration

Sub-cutaneous tumors were induced in male NOD SCID mice (Charles River Laboratories International, 6 weeks, n=5) by injection of 1.5 x 10^6 LNCaP prostate cancer cells, suspended in 50 μL of sterile 1x PBS solution and 50 μL of Matrigel® Matrix (Corning). For determination of tumor growth, individual tumors were measured (2-3 times per week) using calliper and tumor volume was calculated by the formula: Tumor volume (mm^3) = width x ($length^2$)/2. Treatments began when tumor volume reached 100 mm^3, by injecting intravenously (tail-vein injection) 12 mg/kg of each compound during 7 consecutive days. Measurement of animal weight was performed 3 times per week. At the end of the trial, all tumors were weighted and collected along with major organs (kidneys, spleen, liver, lungs, heart, and intestines) for histology and pathology analysis. All experimental protocols were approved by the IMM Animal Care and Use Committee and follow the European guidelines for animal use.

References

References

1 Tessarz, P. & Kouzarides, T. Histone core modifications regulating nucleosome structure and dynamics. *Nature reviews. Molecular cell biology* **15**, 703-708, doi:10.1038/nrm3890 (2014).

2 Jones, P. A., Issa, J. P. & Baylin, S. Targeting the cancer epigenome for therapy. *Nature reviews. Genetics* **17**, 630-641, doi:10.1038/nrg.2016.93 (2016).

3 Filippakopoulos, P. & Knapp, S. Targeting bromodomains: epigenetic readers of lysine acetylation. *Nature Reviews Drug Discovery* **13**, 337-356, doi:10.1038/nrd4286 (2014).

4 Bannister, A. J. & Kouzarides, T. Regulation of chromatin by histone modifications. *Cell Research* **21**, 381, doi:10.1038/cr.2011.22 (2011).

5 Kouzarides, T. Chromatin modifications and their function. *Cell* **128**, 693-705, doi:10.1016/j.cell.2007.02.005 (2007).

6 Dawson, Mark A. & Kouzarides, T. Cancer Epigenetics: From Mechanism to Therapy. *Cell* **150**, 12-27, doi:10.1016/j.cell.2012.06.013 (2012).

7 Beck, S. *et al.* A blueprint for an international cancer epigenome consortium. A report from the AACR Cancer Epigenome Task Force. *Cancer research* **72**, 6319-6324, doi:10.1158/0008-5472.can-12-3658 (2012).

8 Kundaje, A. *et al.* Integrative analysis of 111 reference human epigenomes. *Nature* **518**, 317-330, doi:10.1038/nature14248 (2015).

9 Rando, O. J. & Chang, H. Y. Genome-wide views of chromatin structure. *Annual review of biochemistry* **78**, 245-271, doi:10.1146/annurev.biochem.78.071107.134639 (2009).

10 Weinstein, J. N. *et al.* The Cancer Genome Atlas Pan-Cancer analysis project. *Nature genetics* **45**, 1113-1120, doi:10.1038/ng.2764 (2013).

11 Morin, R. D. *et al.* Frequent mutation of histone-modifying genes in non-Hodgkin lymphoma. *Nature* **476**, 298-303, doi:10.1038/nature10351 (2011).

12 Figueroa, M. E. *et al.* Leukemic IDH1 and IDH2 mutations result in a hypermethylation phenotype, disrupt TET2 function, and impair hematopoietic differentiation. *Cancer cell* **18**, 553-567, doi:10.1016/j.ccr.2010.11.015 (2010).

13 Lu, C. *et al.* IDH mutation impairs histone demethylation and results in a block to cell differentiation. *Nature* **483**, 474-478, doi:10.1038/nature10860 (2012).

14 Turcan, S. *et al.* IDH1 mutation is sufficient to establish the glioma hypermethylator phenotype. *Nature* **483**, 479-483, doi:10.1038/nature10866 (2012).

15 Johnstone, R. W. & Licht, J. D. Histone deacetylase inhibitors in cancer therapy: is transcription the primary target? *Cancer cell* **4**, 13-18 (2003).

16 Falkenberg, K. J. & Johnstone, R. W. Histone deacetylases and their inhibitors in cancer, neurological diseases and immune disorders. *Nature reviews. Drug discovery* **13**, 673-691, doi:10.1038/nrd4360 (2014).

17 Doroshow, D. B., Eder, J. P. & LoRusso, P. M. BET inhibitors: a novel epigenetic approach. *Ann Oncol* **28**, 1776-1787, doi:10.1093/annonc/mdx157 (2017).

18 Kaminskas, E. *et al.* Approval summary: azacitidine for treatment of myelodysplastic syndrome subtypes. *Clinical cancer research : an official journal of the American Association for Cancer Research* **11**, 3604-3608, doi:10.1158/1078-0432.ccr-04-2135 (2005).

19 Kaminskas, E., Farrell, A. T., Wang, Y. C., Sridhara, R. & Pazdur, R. FDA drug approval summary: azacitidine (5-azacytidine, Vidaza) for injectable suspension. *The oncologist* **10**, 176-182, doi:10.1634/theoncologist.10-3-176 (2005).

20 Ball, B., Zeidan, A., Gore, S. D. & Prebet, T. Hypomethylating agent combination strategies in myelodysplastic syndromes: hopes and shortcomings. *Leukemia & lymphoma* **58**, 1022-1036, doi:10.1080/10428194.2016.1228927 (2017).

21 Chun, P. Histone deacetylase inhibitors in hematological malignancies and solid tumors. *Archives of pharmacal research* **38**, 933-949, doi:10.1007/s12272-015-0571-1 (2015).

22 Duvic, M. *et al.* Phase 2 trial of oral vorinostat (suberoylanilide hydroxamic acid, SAHA) for refractory cutaneous T-cell lymphoma (CTCL). *Blood* **109**, 31-39, doi:10.1182/blood-2006-06-025999 (2007).

23 Olsen, E. A. *et al.* Phase IIb multicenter trial of vorinostat in patients with persistent, progressive, or treatment refractory cutaneous T-cell lymphoma. *Journal of clinical oncology : official journal of the American Society of Clinical Oncology* **25**, 3109-3115, doi:10.1200/jco.2006.10.2434 (2007).

24 Shu, S. & Polyak, K. BET Bromodomain Proteins as Cancer Therapeutic Targets. *Cold Spring Harbor symposia on quantitative biology* **81**, 123-129, doi:10.1101/sqb.2016.81.030908 (2016).

25 Fujisawa, T. & Filippakopoulos, P. Functions of bromodomain-containing proteins and their roles in homeostasis and cancer. *Nature reviews. Molecular cell biology* **18**, 246-262, doi:10.1038/nrm.2016.143 (2017).

26 Haynes, S. R. *et al.* The bromodomain: a conserved sequence found in human, Drosophila and yeast proteins. *Nucleic acids research* **20**, 2603 (1992).

27 Filippakopoulos, P. & Knapp, S. The bromodomain interaction module. *FEBS Letters* **586**, 2692-2704, doi:10.1016/j.febslet.2012.04.045 (2012).

28 Bannister, A. J. & Kouzarides, T. The CBP co-activator is a histone acetyltransferase. *Nature* **384**, 641-643, doi:10.1038/384641a0 (1996).

29 Ogryzko, V. V., Schiltz, R. L., Russanova, V., Howard, B. H. & Nakatani, Y. The transcriptional coactivators p300 and CBP are histone acetyltransferases. *Cell* **87**, 953-959 (1996).

30 Xu, Y. & Vakoc, C. R. Targeting Cancer Cells with BET Bromodomain Inhibitors. *Cold Spring Harbor perspectives in medicine* **7**, doi:10.1101/cshperspect.a026674 (2017).

31 Liu, W. *et al.* Brd4 and JMJD6-associated anti-pause enhancers in regulation of transcriptional pause release. *Cell* **155**, 1581-1595, doi:10.1016/j.cell.2013.10.056 (2013).

32 Shen, C. *et al.* NSD3-Short Is an Adaptor Protein that Couples BRD4 to the CHD8 Chromatin Remodeler. *Molecular cell* **60**, 847-859, doi:10.1016/j.molcel.2015.10.033 (2015).

33 Denis, G. V. *et al.* Identification of transcription complexes that contain the double bromodomain protein Brd2 and chromatin remodeling machines. *Journal of proteome research* **5**, 502-511, doi:10.1021/pr050430u (2006).

34 Denis, G. V., Vaziri, C., Guo, N. & Faller, D. V. RING3 kinase transactivates promoters of cell cycle regulatory genes through E2F. *Cell growth & differentiation : the molecular biology journal of the American Association for Cancer Research* **11**, 417-424 (2000).

35 Belkina, A. C. & Denis, G. V. BET domain co-regulators in obesity, inflammation and cancer. *Nature reviews. Cancer* **12**, 465-477, doi:10.1038/nrc3256 (2012).

36 Jiang, Y. W. *et al.* Mammalian mediator of transcriptional regulation and its possible role as an end-point of signal transduction pathways. *Proceedings of the National Academy of Sciences of the United States of America* **95**, 8538-8543 (1998).

37 Sinha, A., Faller, D. V. & Denis, G. V. Bromodomain analysis of Brd2-dependent transcriptional activation of cyclin A. *The Biochemical journal* **387**, 257-269, doi:10.1042/bj20041793 (2005).

38 Loven, J. *et al.* Selective inhibition of tumor oncogenes by disruption of super-enhancers. *Cell* **153**, 320-334, doi:10.1016/j.cell.2013.03.036 (2013).

39 Dey, A., Chitsaz, F., Abbasi, A., Misteli, T. & Ozato, K. The double bromodomain protein Brd4 binds to acetylated chromatin during interphase and mitosis. *Proceedings of the National Academy of Sciences of the United States of America* **100**, 8758-8763, doi:10.1073/pnas.1433065100 (2003).

40 Dey, A. *et al.* A bromodomain protein, MCAP, associates with mitotic chromosomes and affects G(2)-to-M transition. *Molecular and cellular biology* **20**, 6537-6549 (2000).

41 Dey, A., Nishiyama, A., Karpova, T., McNally, J. & Ozato, K. Brd4 marks select genes on mitotic chromatin and directs postmitotic transcription. *Molecular biology of the cell* **20**, 4899-4909, doi:10.1091/mbc.E09-05-0380 (2009).

42 Mochizuki, K. *et al.* The bromodomain protein Brd4 stimulates G1 gene transcription and promotes progression to S phase. *J Biol Chem* **283**, 9040-9048, doi:10.1074/jbc.M707603200 (2008).

43 Yang, Z., He, N. & Zhou, Q. Brd4 recruits P-TEFb to chromosomes at late mitosis to promote G1 gene expression and cell cycle progression. *Molecular and cellular biology* **28**, 967-976, doi:10.1128/mcb.01020-07 (2008).

44 You, J. *et al.* Regulation of aurora B expression by the bromodomain protein Brd4. *Molecular and cellular biology* **29**, 5094-5103, doi:10.1128/mcb.00299-09 (2009).

45 Huang, B., Yang, X. D., Zhou, M. M., Ozato, K. & Chen, L. F. Brd4 coactivates transcriptional activation of NF-kappaB via specific binding to acetylated RelA. *Molecular and cellular biology* **29**, 1375-1387, doi:10.1128/mcb.01365-08 (2009).

46 Nicodeme, E. *et al.* Suppression of inflammation by a synthetic histone mimic. *Nature* **468**, 1119-1123, doi:10.1038/nature09589 (2010).

47 Bamborough, P. *et al.* Fragment-based discovery of bromodomain inhibitors part 2: optimization of phenylisoxazole sulfonamides. *Journal of medicinal chemistry* **55**, 587-596, doi:10.1021/jm201283q (2012).

48 Schweiger, M. R., You, J. & Howley, P. M. Bromodomain protein 4 mediates the papillomavirus E2 transcriptional activation function. *Journal of virology* **80**, 4276-4285, doi:10.1128/jvi.80.9.4276-4285.2006 (2006).

49 Wu, S. Y. *et al.* Brd4 links chromatin targeting to HPV transcriptional silencing. *Genes & development* **20**, 2383-2396, doi:10.1101/gad.1448206 (2006).

50 You, J., Croyle, J. L., Nishimura, A., Ozato, K. & Howley, P. M. Interaction of the bovine papillomavirus E2 protein with Brd4 tethers the viral DNA to host mitotic chromosomes. *Cell* **117**, 349-360 (2004).

51 You, J. *et al.* Kaposi's sarcoma-associated herpesvirus latency-associated nuclear antigen interacts with bromodomain protein Brd4 on host mitotic chromosomes. *Journal of virology* **80**, 8909-8919, doi:10.1128/jvi.00502-06 (2006).

52 Friborg, J., Jr., Kong, W., Hottiger, M. O. & Nabel, G. J. p53 inhibition by the LANA protein of KSHV protects against cell death. *Nature* **402**, 889-894, doi:10.1038/47266 (1999).

53 Radkov, S. A., Kellam, P. & Boshoff, C. The latent nuclear antigen of Kaposi sarcoma-associated herpesvirus targets the retinoblastoma-E2F pathway and with the oncogene Hras transforms primary rat cells. *Nature medicine* **6**, 1121-1127, doi:10.1038/80459 (2000).

54 Huether, R. *et al.* The landscape of somatic mutations in epigenetic regulators across 1,000 paediatric cancer genomes. *Nature communications* **5**, 3630, doi:10.1038/ncomms4630 (2014).

55 Cleary, S. P. *et al.* Identification of driver genes in hepatocellular carcinoma by exome sequencing. *Hepatology (Baltimore, Md.)* **58**, 1693-1702, doi:10.1002/hep.26540 (2013).

56 Network, C. G. A. R. Comprehensive genomic characterization of squamous cell lung cancers. *Nature* **489**, 519-525, doi:10.1038/nature11404 (2012).

57 Liu, J. *et al.* Genome and transcriptome sequencing of lung cancers reveal diverse mutational and splicing events. *Genome research* **22**, 2315-2327, doi:10.1101/gr.140988.112 (2012).

58 Network, C. G. A. R. Comprehensive molecular profiling of lung adenocarcinoma. *Nature* **511**, 543-550, doi:10.1038/nature13385 (2014).

59 Liu, L. *et al.* Identification of hallmarks of lung adenocarcinoma prognosis using whole genome sequencing. *Oncotarget* **6**, 38016-38028, doi:10.18632/oncotarget.5697 (2015).

60 Peifer, M. *et al.* Integrative genome analyses identify key somatic driver mutations of small-cell lung cancer. *Nature genetics* **44**, 1104-1110, doi:10.1038/ng.2396 (2012).

61 Grunwald, C. *et al.* Expression of multiple epigenetically regulated cancer/germline genes in nonsmall cell lung cancer. *International journal of cancer* **118**, 2522-2528, doi:10.1002/ijc.21669 (2006).

62 Odejide, O. *et al.* A targeted mutational landscape of angioimmunoblastic T-cell lymphoma. *Blood* **123**, 1293-1296, doi:10.1182/blood-2013-10-531509 (2014).

63 Okosun, J. *et al.* Integrated genomic analysis identifies recurrent mutations and evolution patterns driving the initiation and progression of follicular lymphoma. *Nature genetics* **46**, 176-181, doi:10.1038/ng.2856 (2014).

64 Ojesina, A. I. *et al.* Landscape of genomic alterations in cervical carcinomas. *Nature* **506**, 371-375, doi:10.1038/nature12881 (2014).

65 Oh, H. R., An, C. H., Yoo, N. J. & Lee, S. H. Somatic mutations of amino acid metabolism-related genes in gastric and colorectal cancers and their regional heterogeneity--a short report. *Cellular oncology (Dordrecht)* **37**, 455-461, doi:10.1007/s13402-014-0209-1 (2014).

66 Segura, M. F. *et al.* BRD4 sustains melanoma proliferation and represents a new target for epigenetic therapy. *Cancer research* **73**, 6264-6276, doi:10.1158/0008-5472.can-13-0122-t (2013).

67 Zhang, P. *et al.* BRD4 promotes tumor growth and epithelial-mesenchymal transition in hepatocellular carcinoma. *International journal of immunopathology and pharmacology* **28**, 36-44, doi:10.1177/0394632015572070 (2015).

68 Pastori, C. *et al.* BET bromodomain proteins are required for glioblastoma cell proliferation. *Epigenetics* **9**, 611-620, doi:10.4161/epi.27906 (2014).

69 Patel, A. J. *et al.* BET bromodomain inhibition triggers apoptosis of NF1-associated malignant peripheral nerve sheath tumors through Bim induction. *Cell reports* **6**, 81-92, doi:10.1016/j.celrep.2013.12.001 (2014).

70 Baratta, M. G. *et al.* An in-tumor genetic screen reveals that the BET bromodomain protein, BRD4, is a potential therapeutic target in ovarian carcinoma. *Proceedings of the National Academy of Sciences of the United States of America* **112**, 232-237, doi:10.1073/pnas.1422165112 (2015).

71 Delmore, Jake E. *et al.* BET Bromodomain Inhibition as a Therapeutic Strategy to Target c-Myc. *Cell* **146**, 904-917, doi:10.1016/j.cell.2011.08.017 (2011).

72 Chapuy, B. *et al.* Discovery and characterization of super-enhancer-associated dependencies in diffuse large B cell lymphoma. *Cancer cell* **24**, 777-790, doi:10.1016/j.ccr.2013.11.003 (2013).

73 Shi, J. *et al.* Disrupting the interaction of BRD4 with diacetylated Twist suppresses tumorigenesis in basal-like breast cancer. *Cancer cell* **25**, 210-225, doi:10.1016/j.ccr.2014.01.028 (2014).

74 Roe, J. S., Mercan, F., Rivera, K., Pappin, D. J. & Vakoc, C. R. BET Bromodomain Inhibition Suppresses the Function of Hematopoietic Transcription Factors in Acute Myeloid Leukemia. *Molecular cell* **58**, 1028-1039, doi:10.1016/j.molcel.2015.04.011 (2015).

75 Alekseyenko, A. A. *et al.* The oncogenic BRD4-NUT chromatin regulator drives aberrant transcription within large topological domains. *Genes & development* **29**, 1507-1523, doi:10.1101/gad.267583.115 (2015).

76 Filippakopoulos, P. *et al.* Selective inhibition of BET bromodomains. *Nature* **468**, 1067-1073, doi:10.1038/nature09504 (2010).

77 Vidler, L. R., Brown, N., Knapp, S. & Hoelder, S. Druggability analysis and structural classification of bromodomain acetyl-lysine binding sites. *Journal of medicinal chemistry* **55**, 7346-7359, doi:10.1021/jm300346w (2012).

78 Brand, M. *et al.* Small molecule inhibitors of bromodomain-acetyl-lysine interactions. *ACS chemical biology* **10**, 22-39, doi:10.1021/cb500996u (2015).

79 Tetsuya Tahara, M. M., Kenji Chiba, Shunichi Manabe, Masanori Shindo, Takashi Nakagawa, Takeshi Nakamura Therapeutic agent for osteoporosis and diazepine compound. (1998).

80 Shinji Miyoshi, S. O., Kazunori Iwata, Hidemasa Hikawa, Kunio Sugahara Antitumor agent. (2009).

81 Mirguet, O. *et al.* Discovery of epigenetic regulator I-BET762: lead optimization to afford a clinical candidate inhibitor of the BET bromodomains. *Journal of medicinal chemistry* **56**, 7501-7515, doi:10.1021/jm401088k (2013).

82 Mirguet, O. *et al.* From ApoA1 upregulation to BET family bromodomain inhibition: discovery of I-BET151. *Bioorganic & medicinal chemistry letters* **22**, 2963-2967, doi:10.1016/j.bmcl.2012.01.125 (2012).

83 Riveiro, M. E. *et al.* OTX015 (MK-8628), a novel BET inhibitor, exhibits antitumor activity in non-small cell and small cell lung cancer models harboring different oncogenic mutations. *Oncotarget* **7**, 84675-84687, doi:10.18632/oncotarget.13181 (2016).

84 Zhang, G. *et al.* Down-regulation of NF-kappaB transcriptional activity in HIV-associated kidney disease by BRD4 inhibition. *J Biol Chem* **287**, 28840-28851, doi:10.1074/jbc.M112.359505 (2012).

85 Khmelnitsky, Y. L. *et al.* In vitro biosynthesis, isolation, and identification of predominant metabolites of 2-(4-(2-hydroxyethoxy)-3,5-dimethylphenyl)-5,7-dimethoxyquinazolin-4(3H)-one (RVX-208). *European journal of medicinal chemistry* **64**, 121-128, doi:10.1016/j.ejmech.2013.03.062 (2013).

86 Fish, P. V. *et al.* Identification of a chemical probe for bromo and extra C-terminal bromodomain inhibition through optimization of a fragment-derived hit. *Journal of medicinal chemistry* **55**, 9831-9837, doi:10.1021/jm3010515 (2012).

87 Hewings, D. S. *et al.* Optimization of 3,5-dimethylisoxazole derivatives as potent bromodomain ligands. *Journal of medicinal chemistry* **56**, 3217-3227, doi:10.1021/jm301588r (2013).

88 Gosmini, R. *et al.* The discovery of I-BET726 (GSK1324726A), a potent tetrahydroquinoline ApoA1 up-regulator and selective BET bromodomain inhibitor. *Journal of medicinal chemistry* **57**, 8111-8131, doi:10.1021/jm5010539 (2014).

89 Wyce, A. *et al.* Inhibition of BET bromodomain proteins as a therapeutic approach in prostate cancer. *Oncotarget* **4**, 2419-2429, doi:10.18632/oncotarget.1572 (2013).

90 Lucas, X. *et al.* 4-Acyl pyrroles: mimicking acetylated lysines in histone code reading. *Angewandte Chemie (International ed. in English)* **52**, 14055-14059, doi:10.1002/anie.201307652 (2013).

91 Norbert Schmees, J. K., Bernard Haendler, Roland Neuhaus, Pascale Lejeune, Stephan Siegel, Martin Kruger, Amaury Ernesto Fernandez-Montalvan, Hermann Kunzer, Daniel Gallenkamp. BET Protein-inhibiting 5-aryl triazole azepines. WO/2014/048945 (2014).

92 Picaud, S. *et al.* RVX-208, an inhibitor of BET transcriptional regulators with selectivity for the second bromodomain. *Proceedings of the National Academy of Sciences* **110**, 19754 (2013).

93 Schulz, M. N. & Hubbard, R. E. Recent progress in fragment-based lead discovery. *Current opinion in pharmacology* **9**, 615-621, doi:10.1016/j.coph.2009.04.009 (2009).

94 Gehling, V. S. *et al.* Discovery, Design, and Optimization of Isoxazole Azepine BET Inhibitors. *ACS Medicinal Chemistry Letters* **4**, 835-840, doi:10.1021/ml4001485 (2013).

95 Allen, B. K. *et al.* Large-Scale Computational Screening Identifies First in Class Multitarget Inhibitor of EGFR Kinase and BRD4. *Scientific reports* **5**, 16924, doi:10.1038/srep16924 (2015).

96 Ciceri, P. *et al.* Dual kinase-bromodomain inhibitors for rationally designed polypharmacology. *Nature chemical biology* **10**, 305-312, doi:10.1038/nchembio.1471 (2014).

97 Ember, S. W. *et al.* Acetyl-lysine binding site of bromodomain-containing protein 4 (BRD4) interacts with diverse kinase inhibitors. *ACS chemical biology* **9**, 1160-1171, doi:10.1021/cb500072z (2014).

98 Martin, M. P., Olesen, S. H., Georg, G. I. & Schonbrunn, E. Cyclin-dependent kinase inhibitor dinaciclib interacts with the acetyl-lysine recognition site of bromodomains. *ACS chemical biology* **8**, 2360-2365, doi:10.1021/cb4003283 (2013).

99 Chaidos, A., Caputo, V. & Karadimitris, A. Inhibition of bromodomain and extra-terminal proteins (BET) as a potential therapeutic approach in haematological malignancies: emerging preclinical and clinical evidence. *Therapeutic advances in hematology* **6**, 128-141, doi:10.1177/2040620715576662 (2015).

100 Lockwood, W. W., Zejnullahu, K., Bradner, J. E. & Varmus, H. Sensitivity of human lung adenocarcinoma cell lines to targeted inhibition of BET epigenetic signaling proteins. *Proceedings of the National Academy of Sciences of the United States of America* **109**, 19408-19413, doi:10.1073/pnas.1216363109 (2012).

101 Sahai, V., Redig, A. J., Collier, K. A., Eckerdt, F. D. & Munshi, H. G. Targeting BET bromodomain proteins in solid tumors. *Oncotarget* **7**, 53997-54009, doi:10.18632/oncotarget.9804 (2016).

102 Bradner, J. E., Hnisz, D. & Young, R. A. Transcriptional Addiction in Cancer. *Cell* **168**, 629-643, doi:10.1016/j.cell.2016.12.013 (2017).

103 Stathis, A. *et al.* Clinical Response of Carcinomas Harboring the BRD4–NUT Oncoprotein to the Targeted Bromodomain Inhibitor OTX015/MK-8628. *Cancer Discovery* **6**, 492 (2016).

104 Dawson, M. A. *et al.* Inhibition of BET recruitment to chromatin as an effective treatment for MLL-fusion leukaemia. *Nature* **478**, 529-533, doi:10.1038/nature10509 (2011).

105 Mertz, J. A. *et al.* Targeting MYC dependence in cancer by inhibiting BET bromodomains. *Proceedings of the National Academy of Sciences of the United States of America* **108**, 16669-16674, doi:10.1073/pnas.1108190108 (2011).

106 Ott, C. J. *et al.* BET bromodomain inhibition targets both c-Myc and IL7R in high-risk acute lymphoblastic leukemia. *Blood* **120**, 2843-2852, doi:10.1182/blood-2012-02-413021 (2012).

107 Zuber, J. *et al.* RNAi screen identifies Brd4 as a therapeutic target in acute myeloid leukaemia. *Nature* **478**, 524-528, doi:10.1038/nature10334 (2011).

108 Dawson, M. A. *et al.* Recurrent mutations, including NPM1c, activate a BRD4-dependent core transcriptional program in acute myeloid leukemia. *Leukemia* **28**, 311-320, doi:10.1038/leu.2013.338 (2014).

109 Picaud, S. *et al.* PFI-1, a highly selective protein interaction inhibitor, targeting BET Bromodomains. *Cancer research* **73**, 3336-3346, doi:10.1158/0008-5472.can-12-3292 (2013).

110 Roderick, J. E. *et al.* c-Myc inhibition prevents leukemia initiation in mice and impairs the growth of relapsed and induction failure pediatric T-ALL cells. *Blood* **123**, 1040 (2014).

111 Chaidos, A. *et al.* Potent antimyeloma activity of the novel bromodomain inhibitors I-BET151 and I-BET762. *Blood* **123**, 697-705, doi:10.1182/blood-2013-01-478420 (2014).

112 Boi, M. *et al.* The Brd-Inhibitor OTX015 Shows Pre-Clinical Activity in Anaplastic Large T-Cell Lymphoma (ALCL). *Blood* **120**, 4872 (2012).

113 Nagarajan, S. *et al.* Bromodomain protein BRD4 is required for estrogen receptor-dependent enhancer activation and gene transcription. *Cell reports* **8**, 460-469, doi:10.1016/j.celrep.2014.06.016 (2014).

114 Feng, Q. *et al.* An epigenomic approach to therapy for tamoxifen-resistant breast cancer. *Cell Res* **24**, 809-819, doi:10.1038/cr.2014.71 (2014).

115 Bihani, T. *et al.* Resistance to everolimus driven by epigenetic regulation of MYC in ER+ breast cancers. *Oncotarget* **6**, 2407-2420, doi:10.18632/oncotarget.2964 (2015).

116 Stuhlmiller, T. J. *et al.* Inhibition of Lapatinib-Induced Kinome Reprogramming in ERBB2-Positive Breast Cancer by Targeting BET Family Bromodomains. *Cell reports* **11**, 390-404, doi:10.1016/j.celrep.2015.03.037 (2015).

117 Shu, S. *et al.* Response and resistance to BET bromodomain inhibitors in triple-negative breast cancer. *Nature* **529**, 413-417, doi:10.1038/nature16508 (2016).

118 Lehmann, B. D. *et al.* Identification of human triple-negative breast cancer subtypes and preclinical models for selection of targeted therapies. *The Journal of clinical investigation* **121**, 2750-2767, doi:10.1172/jci45014 (2011).

119 Vazquez, R. *et al.* The bromodomain inhibitor OTX015 (MK-8628) exerts anti-tumor activity in triple-negative breast cancer models as single agent and in combination with everolimus. *Oncotarget* **8**, 7598-7613, doi:10.18632/oncotarget.13814 (2017).

120 Asangani, I. A. *et al.* Therapeutic targeting of BET bromodomain proteins in castration-resistant prostate cancer. *Nature* **510**, 278-282, doi:10.1038/nature13229 (2014).

121 Asangani, I. A. *et al.* BET Bromodomain Inhibitors Enhance Efficacy and Disrupt Resistance to AR Antagonists in the Treatment of Prostate Cancer. *Molecular cancer research : MCR* **14**, 324-331, doi:10.1158/1541-7786.mcr-15-0472 (2016).

122 Shimamura, T. *et al.* Efficacy of BET bromodomain inhibition in Kras-mutant non-small cell lung cancer. *Clinical cancer research : an official journal of the American Association for Cancer Research* **19**, 6183-6192, doi:10.1158/1078-0432.ccr-12-3904 (2013).

123 Jauset, T. *et al.* BET inhibition is an effective approach against KRAS-driven PDAC and NSCLC. *Oncotarget* **9**, 18734-18746, doi:10.18632/oncotarget.24648 (2018).

124 Govindan, R. *et al.* Genomic landscape of non-small cell lung cancer in smokers and never-smokers. *Cell* **150**, 1121-1134, doi:10.1016/j.cell.2012.08.024 (2012).

125 Garcia, P. L. *et al.* The BET bromodomain inhibitor JQ1 suppresses growth of pancreatic ductal adenocarcinoma in patient-derived xenograft models. *Oncogene* **35**, 833-845, doi:10.1038/onc.2015.126 (2016).

126 Mazur, P. K. *et al.* Combined inhibition of BET family proteins and histone deacetylases as a potential epigenetics-based therapy for pancreatic ductal adenocarcinoma. *Nature medicine* **21**, 1163-1171, doi:10.1038/nm.3952 (2015).

127 McCleland, M. L. *et al.* CCAT1 is an enhancer-templated RNA that predicts BET sensitivity in colorectal cancer. *The Journal of clinical investigation* **126**, 639-652, doi:10.1172/jci83265 (2016).

128 Li, G. Q. *et al.* Suppression of BRD4 inhibits human hepatocellular carcinoma by repressing MYC and enhancing BIM expression. *Oncotarget* **7**, 2462-2474, doi:10.18632/oncotarget.6275 (2016).

129 Cheng, Z. *et al.* Inhibition of BET bromodomain targets genetically diverse glioblastoma. *Clinical cancer research : an official journal of the American Association for Cancer Research* **19**, 1748-1759, doi:10.1158/1078-0432.ccr-12-3066 (2013).

130 Henssen, A. *et al.* BET bromodomain protein inhibition is a therapeutic option for medulloblastoma. *Oncotarget* **4**, 2080-2095, doi:10.18632/oncotarget.1534 (2013).

131 Berthon, C. *et al.* Bromodomain inhibitor OTX015 in patients with acute leukaemia: a dose-escalation, phase 1 study. *The Lancet. Haematology* **3**, e186-195, doi:10.1016/s2352-3026(15)00247-1 (2016).

132 Amorim, S. *et al.* Bromodomain inhibitor OTX015 in patients with lymphoma or multiple myeloma: a dose-escalation, open-label, pharmacokinetic, phase 1 study. *The Lancet. Haematology* **3**, e196-204, doi:10.1016/s2352-3026(16)00021-1 (2016).

133 Abramson, J. S. *et al.* BET Inhibitor CPI-0610 Is Well Tolerated and Induces Responses in Diffuse Large B-Cell Lymphoma and Follicular Lymphoma: Preliminary Analysis of an Ongoing Phase 1 Study. *Blood* **126**, 1491 (2015).

134 Stathis, A. & Bertoni, F. BET Proteins as Targets for Anticancer Treatment. *Cancer Discov* **8**, 24-36, doi:10.1158/2159-8290.cd-17-0605 (2018).

135 Massard, C. *et al.* A phase Ib trial with MK-8628/OTX015, a small molecule inhibitor of bromodomain (BRD) and extra-terminal (BET) proteins, in patients with selected advanced solid tumors. *European Journal of Cancer* **69**, S2-S3, doi:10.1016/S0959-8049(16)32609-0 (2016).

136 Shapiro, G. I. *et al.* Abstract A49: Clinically efficacy of the BET bromodomain inhibitor TEN-010 in an open-label substudy with patients with documented NUT-midline carcinoma (NMC). *Molecular cancer therapeutics* **14**, A49 (2015).

137 O'Dwyer, P. J. *et al.* Abstract CT014: GSK525762, a selective bromodomain (BRD) and extra terminal protein (BET) inhibitor: results from part 1 of a phase I/II open-label single-agent study in patients with NUT midline carcinoma (NMC) and other cancers. *Cancer research* **76**, CT014 (2016).

138 Hottinger, A. F. *et al.* P08.63 Dose optimization of MK-8628 (OTX015), a small molecule inhibitor of bromodomain and extra-terminal (BET) proteins, in patients with recurrent glioblastoma. *Neuro-Oncology* **18**, iv56-iv56, doi:10.1093/neuonc/now188.196 (2016).

139 Postel-Vinay, S. *et al.* First-in-human phase I dose escalation study of the Bromodomain and Extra-Terminal motif (BET) inhibitor BAY 1238097 in subjects with advanced malignancies. *European Journal of Cancer* **69**, S7-S8, doi:10.1016/S0959-8049(16)32620-X (2016).

140 Andrieu, G., Belkina, A. C. & Denis, G. V. Clinical trials for BET inhibitors run ahead of the science. *Drug discovery today. Technologies* **19**, 45-50, doi:10.1016/j.ddtec.2016.06.004 (2016).

141 Bisgrove, D. A., Mahmoudi, T., Henklein, P. & Verdin, E. Conserved P-TEFb-interacting domain of BRD4 inhibits HIV transcription. *Proceedings of the National Academy of Sciences of the United States of America* **104**, 13690-13695, doi:10.1073/pnas.0705053104 (2007).

142 Banerjee, C. *et al.* BET bromodomain inhibition as a novel strategy for reactivation of HIV-1. *Journal of leukocyte biology* **92**, 1147-1154, doi:10.1189/jlb.0312165 (2012).

143 Lu, P. *et al.* The BET inhibitor OTX015 reactivates latent HIV-1 through P-TEFb. *Scientific reports* **6**, 24100, doi:10.1038/srep24100 (2016).

144 Wang, X., Helfer, C. M., Pancholi, N., Bradner, J. E. & You, J. Recruitment of Brd4 to the human papillomavirus type 16 DNA replication complex is essential for replication of viral DNA. *Journal of virology* **87**, 3871-3884, doi:10.1128/jvi.03068-12 (2013).

145 Ren, K. *et al.* An Epigenetic Compound Library Screen Identifies BET Inhibitors That Promote HSV-1 and -2 Replication by Bridging P-TEFb to Viral Gene Promoters through BRD4. *PLoS pathogens* **12**, e1005950, doi:10.1371/journal.ppat.1005950 (2016).

146 Francisco, J. C. *et al.* Transcriptional Elongation Control of Hepatitis B Virus Covalently Closed Circular DNA Transcription by Super Elongation Complex and BRD4. *Molecular and cellular biology* **37**, doi:10.1128/mcb.00040-17 (2017).

147 Bolden, J. E. *et al.* Inducible in vivo silencing of Brd4 identifies potential toxicities of sustained BET protein inhibition. *Cell reports* **8**, 1919-1929, doi:10.1016/j.celrep.2014.08.025 (2014).

148 Di Micco, R. *et al.* Control of embryonic stem cell identity by BRD4-dependent transcriptional elongation of super-enhancer-associated pluripotency genes. *Cell reports* **9**, 234-247, doi:10.1016/j.celrep.2014.08.055 (2014).

149 Korb, E., Herre, M., Zucker-Scharff, I., Darnell, R. B. & Allis, C. D. BET protein Brd4 activates transcription in neurons and BET inhibitor Jq1 blocks memory in mice. *Nature neuroscience* **18**, 1464-1473, doi:10.1038/nn.4095 (2015).

150 Sullivan, J. M. *et al.* Autism-like syndrome is induced by pharmacological suppression of BET proteins in young mice. *The Journal of experimental medicine* **212**, 1771-1781, doi:10.1084/jem.20151271 (2015).

151 Raux, B. *et al.* Exploring Selective Inhibition of the First Bromodomain of the Human Bromodomain and Extra-terminal Domain (BET) Proteins. *Journal of medicinal chemistry* **59**, 1634-1641, doi:10.1021/acs.jmedchem.5b01708 (2016).

152 Bhadury, J. *et al.* BET and HDAC inhibitors induce similar genes and biological effects and synergize to kill in Myc-induced murine lymphoma. *Proceedings of the National Academy of Sciences* **111**, E2721 (2014).

153 Hyun, L. D. *et al.* Synergistic effect of JQ1 and rapamycin for treatment of human osteosarcoma. *International journal of cancer* **136**, 2055-2064, doi:doi:10.1002/ijc.29269 (2015).

154 Ramadoss, M. & Mahadevan, V. Targeting the cancer epigenome: synergistic therapy with bromodomain inhibitors. *Drug discovery today* **23**, 76-89, doi:10.1016/j.drudis.2017.09.011 (2018).

155 Siegel, M. B. *et al.* Small molecule inhibitor screen identifies synergistic activity of the bromodomain inhibitor CPI203 and bortezomib in drug resistant myeloma. *Oncotarget* **6**, 18921-18932, doi:10.18632/oncotarget.4214 (2015).

156 Chan, K. H., Zengerle, M., Testa, A. & Ciulli, A. Impact of Target Warhead and Linkage Vector on Inducing Protein Degradation: Comparison of Bromodomain and Extra-Terminal (BET) Degraders Derived from Triazolodiazepine (JQ1) and Tetrahydroquinoline (I-BET726) BET Inhibitor Scaffolds. *Journal of medicinal chemistry* **61**, 504-513, doi:10.1021/acs.jmedchem.6b01912 (2018).

157 Saenz, D. T. *et al.* Novel BET protein proteolysis-targeting chimera exerts superior lethal activity than bromodomain inhibitor (BETi) against post-myeloproliferative neoplasm secondary (s) AML cells. *Leukemia* **31**, 1951-1961, doi:10.1038/leu.2016.393 (2017).

158 Sun, B. *et al.* BET protein proteolysis targeting chimera (PROTAC) exerts potent lethal activity against mantle cell lymphoma cells. *Leukemia* **32**, 343-352, doi:10.1038/leu.2017.207 (2018).

159 Winter, G. E. *et al.* DRUG DEVELOPMENT. Phthalimide conjugation as a strategy for in vivo target protein degradation. *Science (New York, N.Y.)* **348**, 1376-1381, doi:10.1126/science.aab1433 (2015).

160 Srinivasarao, M. & Low, P. S. Ligand-Targeted Drug Delivery. *Chemical reviews* **117**, 12133-12164, doi:10.1021/acs.chemrev.7b00013 (2017).

161 Chari Ravi, V. J., Miller Michael, L. & Widdison Wayne, C. Antibody–Drug Conjugates: An Emerging Concept in Cancer Therapy. *Angewandte Chemie International Edition* **53**, 3796-3827, doi:10.1002/anie.201307628 (2014).

162 Poon, K. A. *et al.* Preclinical safety profile of trastuzumab emtansine (T-DM1): mechanism of action of its cytotoxic component retained with improved tolerability. *Toxicology and applied pharmacology* **273**, 298-313, doi:10.1016/j.taap.2013.09.003 (2013).

163 Doronina, S. O. *et al.* Development of potent monoclonal antibody auristatin conjugates for cancer therapy. *Nature biotechnology* **21**, 778-784, doi:10.1038/nbt832 (2003).

164 Senter, P. D. & Sievers, E. L. The discovery and development of brentuximab vedotin for use in relapsed Hodgkin lymphoma and systemic anaplastic large cell lymphoma. *Nature biotechnology* **30**, 631-637, doi:10.1038/nbt.2289 (2012).

165 Srinivasarao, M., Galliford, C. V. & Low, P. S. Principles in the design of ligand-targeted cancer therapeutics and imaging agents. *Nature reviews. Drug discovery* **14**, 203-219, doi:10.1038/nrd4519 (2015).

166 Lambert, J. M. & Chari, R. V. Ado-trastuzumab Emtansine (T-DM1): an antibody-drug conjugate (ADC) for HER2-positive breast cancer. *Journal of medicinal chemistry* **57**, 6949-6964, doi:10.1021/jm500766w (2014).

167 LoRusso, P. M., Weiss, D., Guardino, E., Girish, S. & Sliwkowski, M. X. Trastuzumab emtansine: a unique antibody-drug conjugate in development for human epidermal growth factor receptor 2-positive cancer. *Clinical cancer research : an official journal of the American Association for Cancer Research* **17**, 6437-6447, doi:10.1158/1078-0432.ccr-11-0762 (2011).

168 Kantarjian, H. M., Vandendries, E. & Advani, A. S. Inotuzumab Ozogamicin for Acute Lymphoblastic Leukemia. *The New England journal of medicine* **375**, 2100-2101, doi:10.1056/NEJMc1612040 (2016).

169 Uy, N., Nadeau, M., Stahl, M. & Zeidan, A. M. Inotuzumab ozogamicin in the treatment of relapsed/refractory acute B cell lymphoblastic leukemia. *Journal of blood medicine* **9**, 67-74, doi:10.2147/jbm.s136575 (2018).

170 Baron, J. & Wang, E. S. Gemtuzumab ozogamicin for the treatment of acute myeloid leukemia. *Expert review of clinical pharmacology* **11**, 549-559, doi:10.1080/17512433.2018.1478725 (2018).

171 Beck, A., Goetsch, L., Dumontet, C. & Corvaia, N. Strategies and challenges for the next generation of antibody-drug conjugates. *Nature reviews. Drug discovery* **16**, 315-337, doi:10.1038/nrd.2016.268 (2017).

172 Hanahan, D. & Weinberg, Robert A. Hallmarks of Cancer: The Next Generation. *Cell* **144**, 646-674, doi:10.1016/j.cell.2011.02.013 (2011).

173 Younes, A. *et al.* Brentuximab vedotin (SGN-35) for relapsed CD30-positive lymphomas. *The New England journal of medicine* **363**, 1812-1821, doi:10.1056/NEJMoa1002965 (2010).

174 Krall, N., Scheuermann, J. & Neri, D. Small targeted cytotoxics: current state and promises from DNA-encoded chemical libraries. *Angewandte Chemie (International ed. in English)* **52**, 1384-1402, doi:10.1002/anie.201204631 (2013).

175 Krall, N. *et al.* A small-molecule drug conjugate for the treatment of carbonic anhydrase IX expressing tumors. *Angewandte Chemie (International ed. in English)* **53**, 4231-4235, doi:10.1002/anie.201310709 (2014).

176 Kularatne, S. A. *et al.* Synthesis and biological analysis of prostate-specific membrane antigen-targeted anticancer prodrugs. *Journal of medicinal chemistry* **53**, 7767-7777, doi:10.1021/jm100729b (2010).

177 Kularatne, S. A., Zhou, Z., Yang, J., Post, C. B. & Low, P. S. Design, synthesis, and preclinical evaluation of prostate-specific membrane antigen targeted (99m)Tc-radioimaging agents. *Molecular pharmaceutics* **6**, 790-800, doi:10.1021/mp9000712 (2009).

178 Leamon, C. P. *et al.* Folate-vinca alkaloid conjugates for cancer therapy: a structure-activity relationship. *Bioconjugate chemistry* **25**, 560-568, doi:10.1021/bc400441s (2014).

179 Vlahov, I. R. & Leamon, C. P. Engineering folate-drug conjugates to target cancer: from chemistry to clinic. *Bioconjugate chemistry* **23**, 1357-1369, doi:10.1021/bc2005522 (2012).

180 Reddy, J. A. *et al.* Rational combination therapy of vintafolide (EC145) with commonly used chemotherapeutic drugs. *Clinical cancer research : an official journal of the American Association for Cancer Research* **20**, 2104-2114, doi:10.1158/1078-0432.ccr-13-2423 (2014).

181 Reddy, J. A. *et al.* Preclinical evaluation of EC145, a folate-vinca alkaloid conjugate. *Cancer research* **67**, 4434-4442, doi:10.1158/0008-5472.can-07-0033 (2007).

182 van Dam, G. M. *et al.* Intraoperative tumor-specific fluorescence imaging in ovarian cancer by folate receptor-alpha targeting: first in-human results. *Nature medicine* **17**, 1315-1319, doi:10.1038/nm.2472 (2011).

183 Chung, C.-W. *et al.* Discovery and characterization of small molecule inhibitors of the BET family bromodomains. *Journal of medicinal chemistry* **54**, 3827-3838, doi:10.1021/jm200108t (2011).

184 Zhao, Y., Yang, C. Y. & Wang, S. The making of I-BET762, a BET bromodomain inhibitor now in clinical development. *Journal of medicinal chemistry* **56**, 7498-7500, doi:10.1021/jm4014407 (2013).

185 Mirguet, O. *et al.* Discovery of Epigenetic Regulator I-BET762: Lead Optimization to Afford a Clinical Candidate Inhibitor of the BET Bromodomains. *Journal of medicinal chemistry* **56**, 7501-7515, doi:10.1021/jm401088k (2013).

186 Eglen, R. M. *et al.* The Use of AlphaScreen Technology in HTS: Current Status. *Current Chemical Genomics* **1**, 2-10, doi:10.2174/1875397300801010002 (2008).

187 Leopoldo, M., Lacivita, E., Berardi, F. & Perrone, R. Developments in fluorescent probes for receptor research. *Drug discovery today* **14**, 706-712, doi:10.1016/j.drudis.2009.03.015 (2009).

188 Hegener, O., Jordan, R. & Haberlein, H. Dye-labeled benzodiazepines: development of small ligands for receptor binding studies using fluorescence correlation spectroscopy. *Journal of medicinal chemistry* **47**, 3600-3605, doi:10.1021/jm021009+ (2004).

189 Bernardes, G. J. *et al.* A traceless vascular-targeting antibody-drug conjugate for cancer therapy. *Angewandte Chemie (International ed. in English)* **51**, 941-944, doi:10.1002/anie.201106527 (2012).

190 Casi, G., Huguenin-Dezot, N., Zuberbuhler, K., Scheuermann, J. & Neri, D. Site-specific traceless coupling of potent cytotoxic drugs to recombinant antibodies for pharmacodelivery. *J Am Chem Soc* **134**, 5887-5892, doi:10.1021/ja211589m (2012).

191 Dragovich, P. S. *et al.* Conjugation of Indoles to Antibodies through a Novel Self-Immolating Linker. *Chemistry (Weinheim an der Bergstrasse, Germany)* **24**, 4830-4834, doi:10.1002/chem.201800859 (2018).

192 Zhang, D. *et al.* Immolation of p-Aminobenzyl Ether Linker and Payload Potency and Stability Determine the Cell-Killing Activity of Antibody-Drug Conjugates with Phenol-Containing Payloads. *Bioconjugate chemistry* **29**, 267-274, doi:10.1021/acs.bioconjchem.7b00576 (2018).

193 Chari, R. V., Miller, M. L. & Widdison, W. C. Antibody-drug conjugates: an emerging concept in cancer therapy. *Angewandte Chemie (International ed. in English)* **53**, 3796-3827, doi:10.1002/anie.201307628 (2014).

194 Adem, Y. T. *et al.* Auristatin antibody drug conjugate physical instability and the role of drug payload. *Bioconjugate chemistry* **25**, 656-664, doi:10.1021/bc400439x (2014).

195 Zhao, R. Y. *et al.* Synthesis and Evaluation of Hydrophilic Linkers for Antibody–Maytansinoid Conjugates. *Journal of medicinal chemistry* **54**, 3606-3623, doi:10.1021/jm2002958 (2011).

196 Xiao, J., Burn, A. & Tolbert, T. J. Increasing Solubility of Proteins and Peptides by Site-Specific Modification with Betaine. *Bioconjugate chemistry* **19**, 1113-1118, doi:10.1021/bc800063k (2008).

197 Rodrigues, T. & Bernardes, G. J. Antibody-drug conjugates: The missing link. *Nature chemistry* **8**, 1088-1090, doi:10.1038/nchem.2685 (2016).

198 Rodrigues, T. & Bernardes, G. J. L. Development of Antibody-Directed Therapies: Quo Vadis? *Angewandte Chemie (International ed. in English)* **57**, 2032-2034, doi:10.1002/anie.201712185 (2018).

199 Staben, L. R. *et al.* Targeted drug delivery through the traceless release of tertiary and heteroaryl amines from antibody-drug conjugates. *Nature chemistry* **8**, 1112-1119, doi:10.1038/nchem.2635 (2016).

200 Lehar, S. M. *et al.* Novel antibody–antibiotic conjugate eliminates intracellular S. aureus. *Nature* **527**, 323, doi:10.1038/nature16057 (2015).

201 Pillow, T. H. Novel linkers and connections for antibody-drug conjugates to treat cancer and infectious disease. *Pharmaceutical patent analyst* **6**, 25-33, doi:10.4155/ppa-2016-0032 (2017).

202 Niesen, F. H., Berglund, H. & Vedadi, M. The use of differential scanning fluorimetry to detect ligand interactions that promote protein stability. *Nature protocols* **2**, 2212-2221, doi:10.1038/nprot.2007.321 (2007).

203 Seal, J. *et al.* Identification of a novel series of BET family bromodomain inhibitors: binding mode and profile of I-BET151 (GSK1210151A). *Bioorganic & medicinal chemistry letters* **22**, 2968-2972, doi:10.1016/j.bmcl.2012.02.041 (2012).

204 Wang, L. *et al.* Fragment-Based, Structure-Enabled Discovery of Novel Pyridones and Pyridone Macrocycles as Potent Bromodomain and Extra-Terminal Domain (BET) Family Bromodomain Inhibitors. *Journal of medicinal chemistry* **60**, 3828-3850, doi:10.1021/acs.jmedchem.7b00017 (2017).

205 De Vivo, M., Masetti, M., Bottegoni, G. & Cavalli, A. Role of Molecular Dynamics and Related Methods in Drug Discovery. *Journal of medicinal chemistry* **59**, 4035-4061, doi:10.1021/acs.jmedchem.5b01684 (2016).

206 Wang, C. Y. & Filippakopoulos, P. Beating the odds: BETs in disease. *Trends in biochemical sciences* **40**, 468-479, doi:10.1016/j.tibs.2015.06.002 (2015).

207 Morse, M. A. *et al.* BET bromodomain inhibitors show anti-papillomavirus activity in vitro and block CRPV wart growth in vivo. *Antiviral research* **154**, 158-165, doi:10.1016/j.antiviral.2018.03.012 (2018).

208 Herrmann, H. *et al.* Small-molecule inhibition of BRD4 as a new potent approach to eliminate leukemic stem- and progenitor cells in acute myeloid leukemia AML. *Oncotarget* **3**, 1588-1599, doi:10.18632/oncotarget.733 (2012).

209 Da Costa, D. *et al.* BET inhibition as a single or combined therapeutic approach in primary paediatric B-precursor acute lymphoblastic leukaemia. *Blood cancer journal* **3**, e126, doi:10.1038/bcj.2013.24 (2013).

210 Leal, A. S. *et al.* Bromodomain inhibitors, JQ1 and I-BET 762, as potential therapies for pancreatic cancer. *Cancer letters* **394**, 76-87, doi:10.1016/j.canlet.2017.02.021 (2017).

211 Zhang, H. P. *et al.* Upregulation of Mcl-1 inhibits JQ1-triggered anticancer activity in hepatocellular carcinoma cells. *Biochemical and biophysical research communications* **495**, 2456-2461, doi:10.1016/j.bbrc.2017.12.153 (2018).

212 Lenhart, R. *et al.* Sensitivity of Small Cell Lung Cancer to BET Inhibition Is Mediated by Regulation of ASCL1 Gene Expression. *Molecular cancer therapeutics* **14**, 2167-2174, doi:10.1158/1535-7163.mct-15-0037 (2015).

213 Gabay, M., Li, Y. & Felsher, D. W. MYC activation is a hallmark of cancer initiation and maintenance. *Cold Spring Harbor perspectives in medicine* **4**, doi:10.1101/cshperspect.a014241 (2014).

214 Coude, M. M. *et al.* BET inhibitor OTX015 targets BRD2 and BRD4 and decreases c-MYC in acute leukemia cells. *Oncotarget* **6**, 17698-17712, doi:10.18632/oncotarget.4131 (2015).

215 Donato, E. *et al.* Compensatory RNA polymerase 2 loading determines the efficacy and transcriptional selectivity of JQ1 in Myc-driven tumors. *Leukemia* **31**, 479-490, doi:10.1038/leu.2016.182 (2017).

216 Sahai, V. *et al.* BET bromodomain inhibitors block growth of pancreatic cancer cells in three-dimensional collagen. *Molecular cancer therapeutics* **13**, 1907-1917, doi:10.1158/1535-7163.mct-13-0925 (2014).

217 Dong, X., Hu, X., Chen, J., Hu, D. & Chen, L. F. BRD4 regulates cellular senescence in gastric cancer cells via E2F/miR-106b/p21 axis. *Cell death & disease* **9**, 203, doi:10.1038/s41419-017-0181-6 (2018).

218 Zhang, Z. *et al.* Preclinical Efficacy and Molecular Mechanism of Targeting CDK7-Dependent Transcriptional Addiction in Ovarian Cancer. *Molecular cancer therapeutics* **16**, 1739-1750, doi:10.1158/1535-7163.mct-17-0078 (2017).

219 Ghosh, A. & Heston, W. D. Tumor target prostate specific membrane antigen (PSMA) and its regulation in prostate cancer. *Journal of cellular biochemistry* **91**, 528-539, doi:10.1002/jcb.10661 (2004).

220 Jafari, R. *et al.* The cellular thermal shift assay for evaluating drug target interactions in cells. *Nature protocols* **9**, 2100-2122, doi:10.1038/nprot.2014.138 (2014).

221 Axelsson, H., Almqvist, H., Seashore-Ludlow, B. & Lundback, T. in *Assay Guidance Manual* (eds G. S. Sittampalam *et al.*) (Eli Lilly & Company and the National Center for Advancing Translational Sciences, 2004).

222 Schurmann, M., Janning, P., Ziegler, S. & Waldmann, H. Small-Molecule Target Engagement in Cells. *Cell chemical biology* **23**, 435-441, doi:10.1016/j.chembiol.2016.03.008 (2016).

223 Tanaka, M. *et al.* Design and characterization of bivalent BET inhibitors. *Nature chemical biology* **12**, 1089-1096, doi:10.1038/nchembio.2209 (2016).

224 Smith, E. & Collins, I. Photoaffinity labeling in target- and binding-site identification. *Future medicinal chemistry* **7**, 159-183, doi:10.4155/fmc.14.152 (2015).

225 Chaitanya, G. V., Alexander, J. S. & Babu, P. P. PARP-1 cleavage fragments: signatures of cell-death proteases in neurodegeneration. *Cell Communication and Signaling : CCS* **8**, 31-31, doi:10.1186/1478-811X-8-31 (2010).

226 Davies, D. & Allen, P. in *Flow Cytometry: Principles and Applications* (ed Marion G. Macey) 165-179 (Humana Press, 2007).

227 Yang, J., Chen, H., Vlahov, I. R., Cheng, J. X. & Low, P. S. Evaluation of disulfide reduction during receptor-mediated endocytosis by using FRET imaging. *Proceedings of the National Academy of Sciences of the United States of America* **103**, 13872-13877, doi:10.1073/pnas.0601455103 (2006).

228 Jones, L. R. *et al.* Releasable Luciferin−Transporter Conjugates: Tools for the Real-Time Analysis of Cellular Uptake and Release. *Journal of the American Chemical Society* **128**, 6526-6527, doi:10.1021/ja0586283 (2006).

229 Mohamed, M. M. & Sloane, B. F. Cysteine cathepsins: multifunctional enzymes in cancer. *Nature reviews. Cancer* **6**, 764-775, doi:10.1038/nrc1949 (2006).

230 Sanderson, R. J. *et al.* In vivo drug-linker stability of an anti-CD30 dipeptide-linked auristatin immunoconjugate. *Clinical cancer research : an official journal of the American Association for Cancer Research* **11**, 843-852 (2005).

231 Cazzamalli, S. *et al.* Enhanced Therapeutic Activity of Non-Internalizing Small-Molecule-Drug Conjugates Targeting Carbonic Anhydrase IX in Combination with Targeted Interleukin-2. *Clinical cancer research : an official journal of the American Association for Cancer Research*, doi:10.1158/1078-0432.ccr-17-3457 (2018).

232 Gebleux, R., Stringhini, M., Casanova, R., Soltermann, A. & Neri, D. Non-internalizing antibody-drug conjugates display potent anti-cancer activity upon proteolytic release of monomethyl auristatin E in the subendothelial extracellular matrix. *International journal of cancer* **140**, 1670-1679, doi:10.1002/ijc.30569 (2017).

233 Caculitan, N. G. *et al.* Cathepsin B Is Dispensable for Cellular Processing of Cathepsin B-Cleavable Antibody-Drug Conjugates. *Cancer research* **77**, 7027-7037, doi:10.1158/0008-5472.can-17-2391 (2017).

234 Gikanga, B., Adeniji, N. S., Patapoff, T. W., Chih, H. W. & Yi, L. Cathepsin B Cleavage of vcMMAE-Based Antibody-Drug Conjugate Is Not Drug Location or Monoclonal Antibody Carrier Specific. *Bioconjugate chemistry* **27**, 1040-1049, doi:10.1021/acs.bioconjchem.6b00055 (2016).

235 Perrino, E. *et al.* Curative properties of noninternalizing antibody-drug conjugates based on maytansinoids. *Cancer research* **74**, 2569-2578, doi:10.1158/0008-5472.can-13-2990 (2014).

236 Seshadri, R. *et al.* Clinical significance of HER-2/neu oncogene amplification in primary breast cancer. The South Australian Breast Cancer Study Group. *Journal of clinical oncology : official journal of the American Society of Clinical Oncology* **11**, 1936-1942, doi:10.1200/jco.1993.11.10.1936 (1993).

237 Brune, V. *et al.* Origin and pathogenesis of nodular lymphocyte-predominant Hodgkin lymphoma as revealed by global gene expression analysis. *The Journal of experimental medicine* **205**, 2251-2268, doi:10.1084/jem.20080809 (2008).

238 Eckerle, S. *et al.* Gene expression profiling of isolated tumour cells from anaplastic large cell lymphomas: insights into its cellular origin, pathogenesis and relation to Hodgkin lymphoma. *Leukemia* **23**, 2129-2138, doi:10.1038/leu.2009.161 (2009).

239 Scheller, J., Chalaris, A., Garbers, C. & Rose-John, S. ADAM17: a molecular switch to control inflammation and tissue regeneration. *Trends in immunology* **32**, 380-387, doi:10.1016/j.it.2011.05.005 (2011).

240 Stivarou, T., Stellas, D., Vartzi, G., Thomaidou, D. & Patsavoudi, E. Targeting highly expressed extracellular HSP90 in breast cancer stem cells inhibits tumor growth in vitro and in vivo. *Cancer biology & therapy* **17**, 799-812, doi:10.1080/15384047.2016.1195041 (2016).

241 Chavakis, T., Willuweit, A. K., Lupu, F., Preissner, K. T. & Kanse, S. M. Release of soluble urokinase receptor from vascular cells. *Thrombosis and haemostasis* **86**, 686-693 (2001).

242 Kufe, D. W. Mucins in cancer: function, prognosis and therapy. *Nature reviews. Cancer* **9**, 874-885, doi:10.1038/nrc2761 (2009).

243 O'Shannessy, D. J., Somers, E. B., Maltzman, J., Smale, R. & Fu, Y. S. Folate receptor alpha (FRA) expression in breast cancer: identification of a new molecular subtype and association with triple negative disease. *SpringerPlus* **1**, 22, doi:10.1186/2193-1801-1-22 (2012).

244 Wustemann, T., Haberkorn, U., Babich, J. & Mier, W. Targeting prostate cancer: Prostate-specific membrane antigen based diagnosis and therapy. *Medicinal research reviews*, doi:10.1002/med.21508 (2018).

245 Liu, H. *et al.* Constitutive and antibody-induced internalization of prostate-specific membrane antigen. *Cancer research* **58**, 4055-4060 (1998).

246 Chittasupho, C. Multivalent ligand: design principle for targeted therapeutic delivery approach. *Therapeutic delivery* **3**, 1171-1187 (2012).

247 Nagy, A. & Schally, A. V. Targeting cytotoxic conjugates of somatostatin, luteinizing hormone-releasing hormone and bombesin to cancers expressing their receptors: a "smarter" chemotherapy. *Current pharmaceutical design* **11**, 1167-1180 (2005).

248 Sun, L. C. & Coy, D. H. Somatostatin receptor-targeted anti-cancer therapy. *Current drug delivery* **8**, 2-10 (2011).

249 Chen, S. *et al.* Mechanism-Based Tumor-Targeting Drug Delivery System. Validation of Efficient Vitamin Receptor-Mediated Endocytosis and Drug Release. *Bioconjugate chemistry* **21**, 979-987, doi:10.1021/bc9005656 (2010).

250 Xia, W. & Low, P. S. Folate-Targeted Therapies for Cancer. *Journal of medicinal chemistry* **53**, 6811-6824, doi:10.1021/jm100509v (2010).

251 Emons, G. *et al.* Dose escalation and pharmacokinetic study of AEZS-108 (AN-152), an LHRH agonist linked to doxorubicin, in women with LHRH receptor-positive tumors. *Gynecologic Oncology* **119**, 457-461, doi:10.1016/j.ygyno.2010.08.003 (2010).

252 Sundaram, S., Durairaj, C., Kadam, R. & Kompella, U. B. Luteinizing hormone-releasing hormone receptor–targeted deslorelin-docetaxel conjugate enhances efficacy of docetaxel in prostate cancer therapy. *Molecular cancer therapeutics* **8**, 1655 (2009).

253 Jayaprakash, S., Wang, X., Heston Warren , D. & Kozikowski Alan , P. Design and Synthesis of a PSMA Inhibitor–Doxorubicin Conjugate for Targeted Prostate Cancer Therapy. *ChemMedChem* **1**, 299-302, doi:10.1002/cmdc.200500044 (2006).

254 Tolcher, A. *et al.* P1.05A ph 1 study of 2 different schedules of the PSMA-tubulysin small-molecule drug conjugate EC1169 in pts with rec Met Cast-Resist PC (MCRPC). *Annals of Oncology* **26**, ii17-ii17, doi:10.1093/annonc/mdv090.5 (2015).

255 Morris, M. *et al.* 793PDPhase 1 study of the PSMA-targeted small-molecule drug conjugate EC1169 in patients with metastatic castrate-resistant prostate cancer (mCRPC). *Annals of Oncology* **28**, mdx370.010-mdx370.010, doi:10.1093/annonc/mdx370.010 (2017).

256 Dubowchik, G. M. *et al.* Cathepsin B-labile dipeptide linkers for lysosomal release of doxorubicin from internalizing immunoconjugates: model studies of enzymatic drug release and antigen-specific in vitro anticancer activity. *Bioconjugate chemistry* **13**, 855-869 (2002).

257 Roy, J. *et al.* DUPA conjugation of a cytotoxic indenoisoquinoline topoisomerase I inhibitor for selective prostate cancer cell targeting. *Journal of medicinal chemistry* **58**, 3094-3103, doi:10.1021/jm5018384 (2015).

258 Wang, X. *et al.* Targeted treatment of prostate cancer. *Journal of cellular biochemistry* **102**, 571-579, doi:10.1002/jcb.21491 (2007).

259 Xu, L. *et al.* Targetable BET proteins- and E2F1-dependent transcriptional program maintains the malignancy of glioblastoma. *Proceedings of the National Academy of Sciences of the United States of America* **115**, E5086-e5095, doi:10.1073/pnas.1712363115 (2018).

260 Enomoto, K. *et al.* Targeting MYC as a Therapeutic Intervention for Anaplastic Thyroid Cancer. *The Journal of clinical endocrinology and metabolism* **102**, 2268-2280, doi:10.1210/jc.2016-3771 (2017).

261 Filippakopoulos, P. *et al.* Histone recognition and large-scale structural analysis of the human bromodomain family. *Cell* **149**, 214-231, doi:10.1016/j.cell.2012.02.013 (2012).

262 Wiseman, T., Williston, S., Brandts, J. F. & Lin, L. N. Rapid Measurement of Binding Constants and Heats of Binding Using a New Titration Calorimeter. *Analytical Biochemistry* **179**, 131-137, doi:10.1016/0003-2697(89)90213-3 (1989).

263 Kabsch, W. XDS. *Acta Crystallographica Section D Biological Crystallography* **66**, 125-132, doi:10.1107/S0907444909047337 (2010).

264 Evans, P. R. & Murshudov, G. N. How good are my data and what is the resolution? *Acta Crystallographica Section D Biological Crystallography* **69**, 1204-1214, doi:10.1107/S0907444913000061 (2013).

265 Perrakis, A., Morris, R. & Lamzin, V. S. Automated protein model building combined with iterative structure refinement. *Nat Struct Biol* **6**, 458-463 (1999).

266 Cowtan, K. The Buccaneer software for automated model building. 1. Tracing protein chains. *Acta Crystallographica Section D Biological Crystallography* **62**, 1002-1011, doi:10.1107/S0907444906022116 (2006).

267 Murshudov, G. N. *et al.* REFMAC5 for the refinement of macromolecular crystal structures. *Acta Crystallographica Section D Biological Crystallography* **67**, 355-367, doi:10.1107/S0907444911001314 (2011).

268 Emsley, P., Lohkamp, B., Scott, W. G. & Cowtan, K. Features and development of Coot. *Acta Crystallographica Section D Biological Crystallography* **66**, 486-501, doi:10.1107/S0907444910007493 (2010).

269 Chen, V. B. *et al.* MolProbity: all-atom structure validation for macromolecular crystallography. *Acta Crystallographica Section D Biological Crystallography* **66**, 12-21, doi:10.1107/S0907444909042073 (2010).

270 Amber (2016).

271 Wang, J., Wolf, R. M., Caldwell, J. W., Kollman, P. A. & Case, D. A. Development and testing of a general amber force field. *Journal of computational chemistry* **25**, 1157-1174, doi:10.1002/jcc.20035 (2004).

272 Bayly, C. I., Cieplak, P., Cornell, W. & Kollman, P. A. A well-behaved electrostatic potential based method using charge restraints for deriving atomic charges: the RESP model. *The Journal of Physical Chemistry* **97**, 10269-10280, doi:10.1021/j100142a004 (1993).

273 Frisch, M. J. *Gaussian 09*, 2009).

274 Jorgensen, W. L. C., J.; Madura, J.D.; Impey, R.W.; Klein,M.L. Comparison of simple potential functions for simulating liquid water. *The Journal of chemical physics* **79**, 9 (1983).

275 Hornak, V. *et al.* Comparison of multiple Amber force fields and development of improved protein backbone parameters. *Proteins* **65**, 712-725, doi:10.1002/prot.21123 (2006).

276 Andrea, T. A. S., W.C.; Andersen, H.C. The role of long ranged forces in determining the structure and properties of liquid water. *Journal of Chemical Physics* **79** (1983).

277 Darden, T. Y., D.; Pedersen, L. Particle mesh Ewald: An Nslog(N) method for Ewald sums in large systems. *The Journal of chemical physics* **98**, 3 (1993).

278 Derr, A. *et al.* End Sequence Analysis Toolkit (ESAT) expands the extractable information from single-cell RNA-seq data. *Genome research* **26**, 1397-1410, doi:10.1101/gr.207902.116 (2016).

279 Dobin, A. *et al.* STAR: ultrafast universal RNA-seq aligner. *Bioinformatics (Oxford, England)* **29**, 15-21, doi:10.1093/bioinformatics/bts635 (2013).

280 Li, H. *et al.* The Sequence Alignment/Map format and SAMtools. *Bioinformatics (Oxford, England)* **25**, 2078-2079, doi:10.1093/bioinformatics/btp352 (2009).

281 Soumillon, M., Cacchiarelli, D., Semrau, S., van Oudenaarden, A. & Mikkelsen, T. S. Characterization of directed differentiation by high-throughput single-cell RNA-Seq. *bioRxiv* (2014).

282 Robinson, M. D., McCarthy, D. J. & Smyth, G. K. edgeR: a Bioconductor package for differential expression analysis of digital gene expression data. *Bioinformatics (Oxford, England)* **26**, 139-140, doi:10.1093/bioinformatics/btp616 (2010).